UNIVERSITÉ DU QUÉBEC

THÈSE

PRÉSENTÉE À

L'UNIVERSITÉ DU QUÉBEC À CHICOUTIMI

COMME EXIGENCE PARTIELLE

DU DOCTORAT EN RESSOURCES MINÉRALES

PAR

NADÈGE TOLLARI

SATURATION DES MINÉRAUX PHOSPHATÉS DANS LES MAGMAS SILICATÉS – IMPLICATIONS SUR LA GENÈSE DES ROCHES RICHES EN FE-TI-P

Août 2007

Bibliothèque
Paul-Émile-Boulet

UQAC
Université du Québec
à Chicoutimi

Mise en garde/Advice

Afin de rendre accessible au plus grand nombre le résultat des travaux de recherche menés par ses étudiants gradués et dans l'esprit des règles qui régissent le dépôt et la diffusion des mémoires et thèses produits dans cette Institution, **l'Université du Québec à Chicoutimi (UQAC)** est fière de rendre accessible une version complète et gratuite de cette œuvre.

Motivated by a desire to make the results of its graduate students' research accessible to all, and in accordance with the rules governing the acceptation and diffusion of dissertations and theses in this Institution, the **Université du Québec à Chicoutimi (UQAC)** is proud to make a complete version of this work available at no cost to the reader.

L'auteur conserve néanmoins la propriété du droit d'auteur qui protège ce mémoire ou cette thèse. Ni le mémoire ou la thèse ni des extraits substantiels de ceux-ci ne peuvent être imprimés ou autrement reproduits sans son autorisation.

The author retains ownership of the copyright of this dissertation or thesis. Neither the dissertation or thesis, nor substantial extracts from it, may be printed or otherwise reproduced without the author's permission.

RÉSUMÉ

La compréhension de la formation des intrusions litées et des gisements qui y sont associés est extrêmement importante du fait de leurs concentrations économiques en Cr, V, Ti, P et PGE ainsi que pour le développement des outils d'exploration pour ces éléments. Pour cela il est nécessaire de connaître quels sont les processus de formation à l'origine des roches des intrusions litées. Parmi les différents types de roches concernées, on trouve des roches atypiques nommées nelsonites. Les nelsonites sont des roches principalement formées d'apatite et d'oxydes de Fe et Ti que l'on retrouve aussi associées aux complexes anorthositiques.

Deux modèles de formation sont proposés pour expliquer la genèse des nelsonites : (i) le modèle d'immiscibilité de deux liquides et, (ii) le modèle de cristallisation fractionnée suivit par accumulation de l'apatite et des oxydes. Aucun élément n'a, jusqu'ici, permis de trancher entre ces deux processus et le sujet est encore très discuté.

Nous avons abordé le problème en trois temps :

- Tout d'abord par une approche expérimentale qui nous a permis dans un premier temps de mettre au point une équation permettant de prédire la composition magmatique lors de la saturation en phosphate d'un magma silicaté et ceci pour une large gamme de composition (10 à 80% molaire de SiO_2 incluant les liquides péralumineux) et de température (≈ 800-1400°C).

$$M_{P_2O_5}^{liq-sat} = \exp\left[T\left(\frac{-0.8579}{139.00 - M_{SiO_2}^{liq}} + 0.0165\right) - 3.3333\ln\left(M_{CaO}^{liq}\right)\right]$$

Où M représente la concentration molaire et T la température en K.

Dans ces expériences sans volatiles nous avons cristallisé de la whitlockite comme minéral phosphaté et non de l'apatite.

- Dans un second temps une deuxième série d'expériences, couplée à des modélisations de cristallisation fractionnée, nous a permis de définir les champs d'immiscibilité de deux liquides dans le système SiO_2-TiO_2+FeO+P_2O_5+MgO+CaO-Al_2O_3+Na_2O+K_2O. Dans ces nouvelles expériences nous avons ajouté à nos compositions H_2O et F pour permettre la saturation de fluoroapatite. Cette partie de ce travail de recherche montre qu'un magma mafique est saturé en apatite avant de traverser les champs d'immiscibilité de deux liquides.
- Pour finir nous avons travaillé sur des échantillons naturels de nelsonites et de roches associées riches en apatite. Ces échantillons proviennent de la Suite Intrusive de Sept-Îles au Canada et de la « Rustenburg Layered Suite » dans le complexe du Bushveld en Afrique du Sud. L'analyse des éléments traces dans les apatites de ces roches couplées à un bilan de masse indique que l'apatite contrôle la distribution des éléments du groupe des terres rares, de l'U, du Th, du Cl, du Ca et du Sr dans ces roches. Les compositions des magmas parents des nelsonites ont étaient calculées par inversion et comparées à des roches naturelles. Nous avons par la suite modélisé la cristallisation fractionnée des roches naturelles concordantes dans le but de vérifier si il est possible d'obtenir des nelsonites, ou du moins des roches riches en apatite et oxydes de Fe et Ti, avec ce processus. Les résultats des modélisations indiquent qu'il est possible de former des roches similaires aux troctolites de la Suite Intrusive de Sept-Îles et à la ferrodiorite de la « Rustenburg Layered Suite » par cristallisation fractionnée.

Nos expériences, appuyées pas nos modélisations, indiquent que le modèle de cristallisation fractionnée suivit par une accumulation des grains d'apatite et d'oxydes de Fe et Ti est le plus raisonnable pour expliquer la formation des nelsonites et des roches associées riches en apatite.

ABSTRACT

Understanding the genesis of layered intrusions and their associated ore-deposits is crucial due to economic concentrations of Cr, V, Ti, P and PGE, and for the developments of exploration tools for these elements. To provide constraints on how Fe-Ti-P rich rocks form, it would be helpful to understand the processes by which the various lithologies of layered intrusions form. Among the various types of rocks found in layered intrusions, nelsonites are very unusual, as they are mainly made up of apatite and Fe-Ti oxides. Nelsonites are also encountered in association with anorthositic complexes.

Two models for the formation of nelsonites have been proposed: (i) two-liquid immiscibility and (ii) fractional crystallisation followed by apatite and oxide accumulation. This issue is highly debated and no clear argument has been found to favour either of these two hypotheses.

In order to provide further constraints on the formation processes of the nelsonites, we have considered the problem in tree parts:

- Firstly, we performed experiments controlling $fO2$, without volatiles. Our results allowed us to predict the magmatic composition at the phosphate saturation point of a silicate magma according to the following equation:

$$M_{P_2O_5}^{liq-sat} = \exp\left[T\left(\frac{-0.8579}{139.00 - M_{SiO_2}^{liq}} + 0.0165\right) - 3.3333\ln\left(M_{CaO}^{liq}\right)\right]$$

Where M is the molar concentration and T the temperature in Kelvin.

This equation can be used for magma with a large spectrum of compositions (10-18% mol. SiO_2, including per-aluminous liquids) over a large range of temperature (≈800-1400°C). In these experiments without volatiles we crystallized whitlockite and no apatite.

- A second set of buffered experiments with H_2O and F added were performed. The results were compared to fractional crystallisation modeling and allow us to clearly constrain the two-liquid immiscibility fields in a SiO_2-TiO_2+FeO+P_2O_5+MgO+CaO-Al_2O_3+Na_2O+K_2O system. We concluded that mafic magma would become saturated in apatite before reaching the two-liquid immiscibility fields.

- Finally, we determined the trace elements in the apatite of nelsonites and associated apatite-rich rocks from the Sept-Îles intrusive complex (Quebec, Canada) and from the Rustenberg Layered Suite of the Bushveld Complex (South Africa). The trace element data in the apatites and whole-rock indicate that apatite is controlling the whole-rock budget of the rare earth elements; U, Th, Cl, Ca and Sr. We calculated the composition of the parent magma of the nelsonites by inversion and compared our modeling to the natural rock data. We also modeled fractional crystallisation in magmas assumed to be similar in composition to the marginal rocks of the layered intrusion in order to consider whether nelsonites and apatite and oxide-rich rocks could have formed through fractional crystallisation. Our calculations demonstrate that rocks similar to the Sept-Îles intrusive suite as well as the Rustenberg Layered Suite could form by fractional crystallisation.

Our experiments and modeling, suggest that fractional crystallisation and crystal accumulation of apatite and Fe-Ti oxides is the most likely process to generate nelsonites and apatite-rich rocks associated with the nelsonites.

REMERCIEMENTS

Je remercie en premier lieu ma directrice de thèse, le Dr. Sarah-Jane Barnes ainsi que les membres de mon comité le Dr. Mike Toplis et le Dr. Richard Cox, qui ont été là tout au long de ce travail de recherche pour éviter que je ne me perde dans les méandres de la rédaction et de la recherche. Je remercie ces trois personnes pour leur patience et leurs conseils tout au long de mon cheminement (du début, lors de mon apprentissage de la langue anglaise jusqu'aux corrections finales de la thèse).

Un gros merci pour le Dr. Don Baker qui a su m'endurer au sein de son laboratoire. Je veux le remercier tout particulièrement pour son sens de l'humour et pour sa patience face à toutes mes questions.

Un merci bien particulier pour toutes les personnes qui sont souvent nommés « la clique de français » mais qui sont bien plus que ça (et d'ailleurs pas tous français) : Fabien Solgadi, Bélinda Godel, Nicolas Vinet, Tommy Desbiens, Ambre Luguet, Stéphanie Lavaure, Claude Pilote, Véronique Hounsell, Tafadzwa Gomwe, Carlos Oré et tous les autres que je ne cite pas mais que je n'oublie pas. Toutes ces personnes ont été présentes aussi bien dans les bons moments (et oui il y en a au cours d'un doctorat) que dans les mauvais. Je les remercie pour leur soutien, leurs conseils, pour toutes les discussions que nous avons pu avoir (scientifiques ou non) et pour toutes ces petites choses qui ne s'expliquent pas mais qui font que la vie étudiantes est plus facile et plus enrichissante grâce à eux.

Je n'oublie pas bien entendu toutes les personnes qui m'ont aidé par leurs conseils et leur expertise. Je citerais donc ces personnes sans aucun ordre particulier en m'excusant

pour ce que j'oublie sûrement : Liping Bail (Université McGill, Montréal), Laurent Tissandier (CRPG, Nancy), Mickael Higgins (UQAC, Suite Intrusive de Sept-Îles), L-Paul Bédard (UQAC; géochimie, minéralogie)

Merci à tout les gens rencontrés dans les divers congrès avec qui j'ai eu des discussions sur divers aspects du projet. Merci à Candide Girard et Anna Boivin qui sont toujours là pour les étudiants.

Un gros merci à mes parents qui ont toujours était là sans conditions, et ceux, malgré la durée de mes études et les contraintes liées à la distance. Sans eux je ne serais pas là et je le sais.

Un très très grand merci aussi à ma famille québécoise. Si je dois un jour « blâmer » quelqu'un pour mon amour du Québec ce sera eux sans aucun doute. Je remercie la famille Girard-Gagnon, Thérèse, Jean-Marie, Catherine, Élise, Adoum et Mistrigri pour m'avoir accueilli comme personne ne saurait le faire.

Un tendre merci à celui qui n'a pas connu tout mon cheminement mais qui a vécu la fin de ma thèse (et c'est pas la partie la plus facile) et qui, malgré mon stress, mes doutes et mes larmes est toujours resté à mes coté et m'a enduré de son mieux....Merci David.

TABLE DES MATIÈRES

LISTE DES FIGURES

LISTE DES TABLEAUX

LISTE DES ANNEXES

CHAPITRE 1

INTRODUCTION

Les minéraux phosphatés sont très fréquents dans certains types de roches magmatiques (les compositions de ces roches pouvant aller de granitiques jusqu'aux derniers stades des systèmes mafiques). Parmi ces minéraux, le plus fréquent sur notre planète est l'apatite ($Ca_5(PO_4)_3(OH, F, Cl)$). La présence de ce minéral dans une roche est intéressante car elle implique certaines contraintes quant aux conditions de formation et de mise en place (teneurs en certains éléments traces du liquide résiduel, pression et température) de la roche en question.

De plus, l'apatite est un des principaux composants des roches riche en Fe-Ti-P. Ces roches peuvent avoir des noms et des compositions variables. Elles sont fréquentes dans les complexes anorthositiques et les intrusions litées (Von Gruenewaldt, 1993; McLelland et al., 1994; Cimon, 1998; Dymek and Owens, 2001). La roche la plus insolite de cette famille de roche est la nelsonite. Watson (1907) a introduit ce terme pour décrire des dykes composés d'apatite et d'oxydes de Fe-Ti associés à de l'anorthosite dans les comtés de Nelson et d'Amherst en Virginie. D'après Philpotts (1967) et Kolker (1982), les nelsonites ont le plus souvent une texture homogène, i. e- équigranulaire à grains fins (Fig. 1. 1). Elles se trouvent sous la forme de dykes ou de lits associées à des oxydes tels que le magnétite et/ou l'ilménite (Dymek and Owens, 2001). Ces roches sont le plus souvent associées à des anorthosites (Owens and Dymek, 1992).

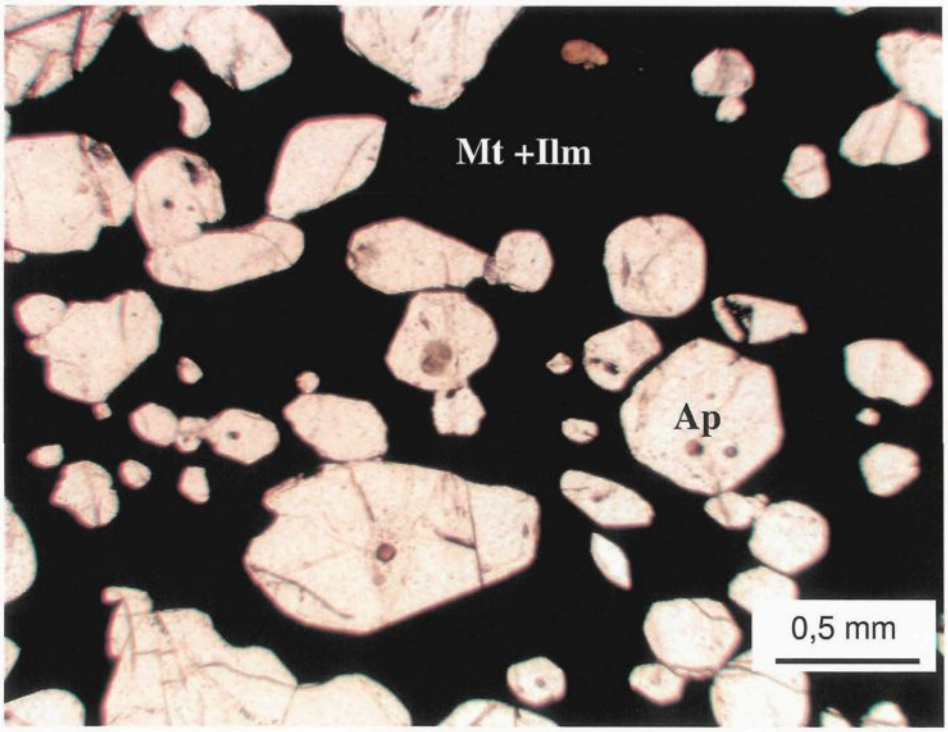

Figure 1. 1 : Nelsonite. Photographie au microscope optique d'une lame mince en lumière analysée polarisée. Échantillons HN-99-46 de la Suite Intrusive de Sept-Îles.

apatite = Ap; magnétite = Mt; ilménite = Ilm

Cependant, il est possible de les trouver associées à des roches volcaniques alcalines à calco-alcalines (Frietsch and Perdahl, 1995), à des plutons alcalins-calco-alcalins (Hildebrand, 1986) ou aux stades tardifs d'intrusions litées (voir paragraphes précédents). D'un point de vu économique ces roches peuvent représenter une source importante de phosphore et de Fe-Ti (Kolker, 1982).

La formation de ce type de roche est toujours sujet à discussion et dépend fortement de la saturation en apatite qui est un de ces composants majeurs. Afin d'expliquer la formation des nelsonites de nombreux processus pétrogénétiques ont été proposés (métasomatisme, immiscibilité, cristallisation fractionnée). Malgré des résultats intéressants, aucun des modèles proposés ne s'applique à l'ensemble des nelsonites (Nabil, 2003).

Certains auteurs proposent que ces roches soient des cumulas formés par cristallisation fractionnée et accumulation d'apatite et d'oxydes de Fe et Ti à partir d'un magma mafique (Emslie, 1975; Goldberg, 1984; McLelland et al., 1994; Eales and Cawthorn, 1996; Dymek and Owens, 2001; Barnes et al., 2004; Tegner et al., 2006). Dans les chapitres 2 et 3 nous montrerons expérimentalement qu'un magma tholéitique peut évoluer en un magma dioritique saturé en phosphate et en oxydes de Fe-Ti par cristallisation fractionnée. L'accumulation des oxydes et de l'apatite dans la pile cristalline peut, supposément, conduire à la formation des nelsonites et des gabbronorites ou des troctolites nelsonitiques.

Cependant, d'autre auteurs (Philpotts, 1967; Naslund, 1983; Jakobsen et al., 2005), proposent l'immiscibilité de deux liquides comme processus de formation de ce type de roche. D'après eux, un magma silicaté riche en Fe se sépare en deux liquides : un liquide

dioritique riche en Si et un liquide riche en Fe-P. Dans ce modèle les nelsonites correspondent au résultat de la cristallisation du liquide riche en Fe-P.

De nombreuses études ont été menées afin de mieux comprendre quels sont les facteurs influençant la saturation en phosphate d'un liquide magmatique. Pour les granites péralcalins et subalumineux, ainsi que pour des compositions péralumineuses, il existe différentes équations capables de modéliser la cristallisation des minéraux phosphatés dans ces systèmes (Bea *et al.,* 1992; Harrison et Watson, 1984; Pichavant *et al.,* 1992; Watson, 1979; Wolf et London, 1994). Malgré le grand nombre de ces études, les systèmes mafiques ont été peu étudiés (Sha, 2000).

Afin d'affiner la stratégie d'exploitation des intrusions litées à travers le monde il est intéressant de connaître les processus de cristallisation qui ont lieu en leur sein. C'est pourquoi, une étude approfondie sur la saturation en phosphate des liquides ferrobasaltiques dans des conditions correspondant aux stades tardifs de la différenciation des intrusions litées est primordiale.

Dans le but de tester l'influence de la composition du magma, de la température, de la pression et de la fugacité d'oxygène (qui agit sur la teneur en Fe^{3+} du magma) sur la stabilité des minéraux phosphatés, nous avons réalisé deux séries d'expériences (Chapitre 2 et 3). La première série d'expériences de cristallisation a été exécutées à un atmosphère en utilisant deux compositions initiales différentes (compositions ferrobasaltiques avec 8 ou 15 %pds FeO*) auxquelles du phosphore est ajouté (sous la forme P_2O_5) en quantité suffisante pour atteindre la saturation en un minéral phosphaté. Nous avons travaillé dans une gamme de température variant de 1030°C à 1070°C.

La deuxième série d'expériences a aussi été réalisée a partir de deux compositions initiales auxquelles nous avons ajouté 1 % pds d'H_2O et 1 % pds de Fluor (F). La première

composition est la même que celle utilisée dans les expériences précédentes (avec 15 % pds de FeO*). La deuxième composition est similaire à la composition de dykes mafiques provenant de la Suite Intrusive de Sept-Îles (Hounsell, 2003). Ce ferrobasalte contient plus d'alcalins. Ces dykes sont considérés comme le magma parent possible des nelsonites de cette intrusion (Hounsell, 2003; Tollari et al., submitted-b). Cette série d'expérience a été réalisée à 5 kbar dans une gamme de température variant de 1000°C à 1050°C. Ces expériences contenait de l'apatite contrairement aux premières. Elles ont permis de mieux comprendre dans quelles conditions ces minéraux sont cristallisés, et, plus globalement, ont permis de mieux comprendre l'évolution que subit un magma lors de la formation d'une intrusion litée.

Dans un second temps, nous avons testé les deux modèles proposés pour expliquer la formation des roches riches en apatite et en oxydes de Fe et Ti. Nous avons travaillé sur des échantillons naturels provenant de la Suite Intrusive de Sept-Îles et du complexe du Bushveld (Fig. 1. 2 et 1. 3). Nous avons analysé les éléments traces et majeurs dans les apatites de ces roches (nelsonites, ferrodiorite et nelsonites troctolitiques). Grâce à ces analyses nous avons recalculé la composition du liquide magmatique à l'équilibre avec les apatites contenues dans nos échantillons. Nous avons par la suite, simulé l'évolution de ces deux magmas à l'aide de codes numériques. Tout ceci afin de vérifier lequel des deux modèles de formations proposées est à l'origine des roches riches en Fe, Ti et P.

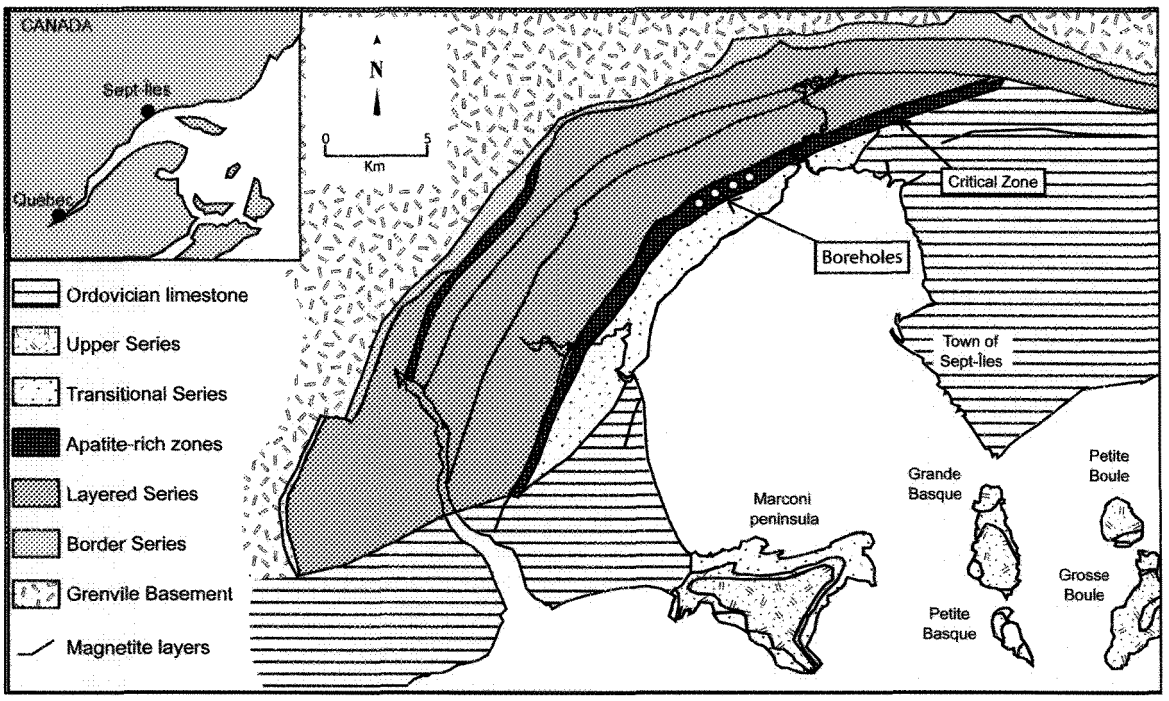

Figure 1. 2 : Carte géologique simplifiée de la Suite Intrusive de Sept-Îles montrant la position des forages d'où proviennent les échantillons.

(modifiée d'après Cimon, 1998; Higgins, 2005)

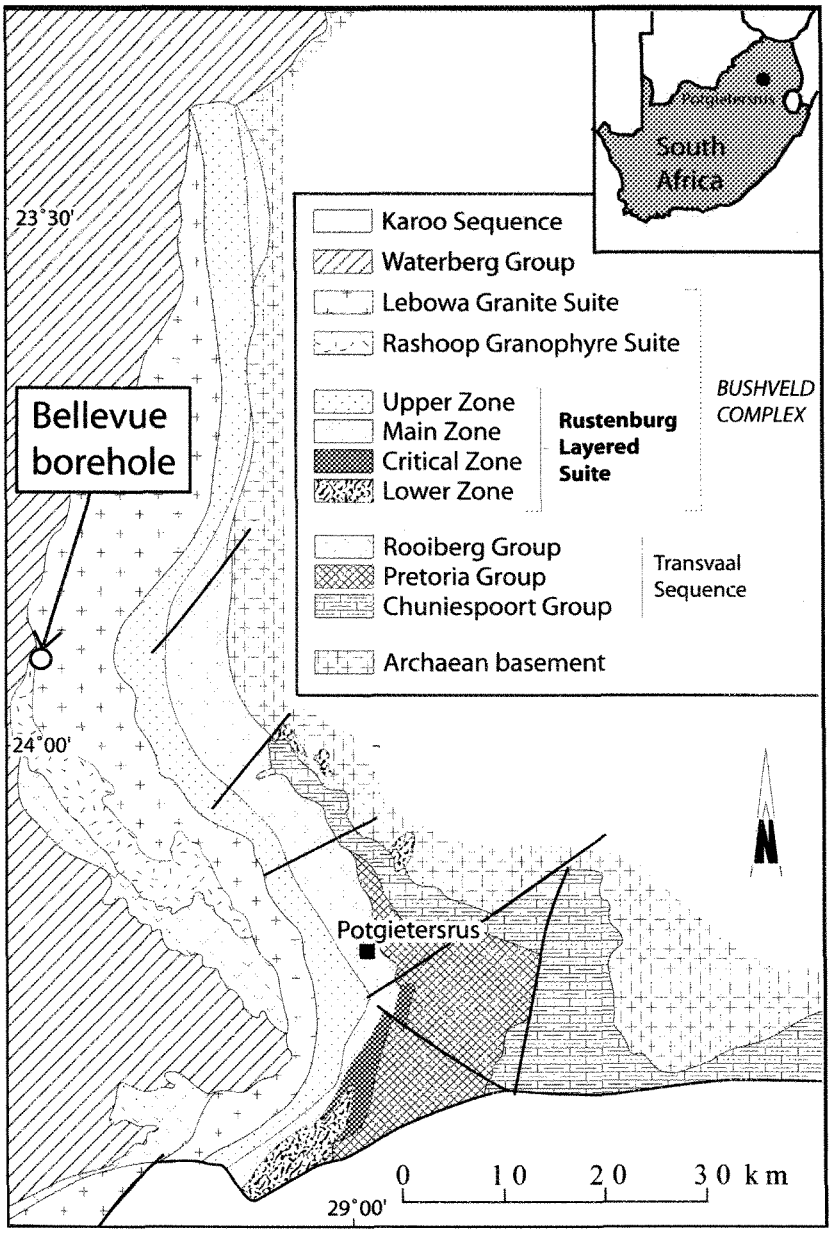

Figure 1. 3 : Carte géologique du « Northern Limb » de la Suite Litée de Rustenburg du complexe du Bushveld montrant la position du forage de Bellevue (BV-1).

(modifiée d'après Von Gruenewaldt et al., 1986; Von Gruenewaldt et al., 1989)

1.1 PROBLÉMATIQUE

1.1.1 L'apatite dans les intrusions litées et les anorthosites

L'apatite est fréquemment présente dans la partie supérieure des intrusions litées (Wager, 1960; Morse, 1979b; Reynolds, 1985a; Hunter and Sparks, 1987; Cimon, 1998) (Fig. 1. 4) ou est associée à des anorthosites (Owens and Dymek, 1992; Bachari, 2005; Fredette, 2006) (le plus souvent sous la forme fluorapatite).

Généralement, l'apatite se rencontre de façon disséminée dans la roche (exemple de l'intrusion de Skaergaard). Elle peut cependant constituer des lits massifs composés essentiellement d'oxydes de Fe-Ti et d'apatite (exemple du Lac à Paul (Fredette, 2006), Lac St Jean (Bachari, 2005); du « Layer Q » du complexe du Bushveld (Eales and Cawthorn, 1996), du complexe du Duluth (Nabil, 2003) ou de la Suite Intrusive de Sept-Îles (Cimon, 1998)) (Fig. 1. 4). Ces roches sont nommées nelsonites (Watson, 1907).

Le cas de l'apatite dans les intrusions litées et dans les complexes anorthositiques sera donc discuté dans les paragraphes suivants puis je parlerais des nelsonites.

- Cas des intrusions litées -

Étant donné l'importance économique des intrusions litées, nous avons choisit comme terrain d'étude pour ce projet de recherche, deux des principales intrusions dans le monde : la Suite Intrusive de Sept-Îles et le complexe du Bushveld (Fig. 1. 2 et 1. 3). Ces intrusions seront présentées plus en détails dans la partie traitant de la provenance des échantillons.

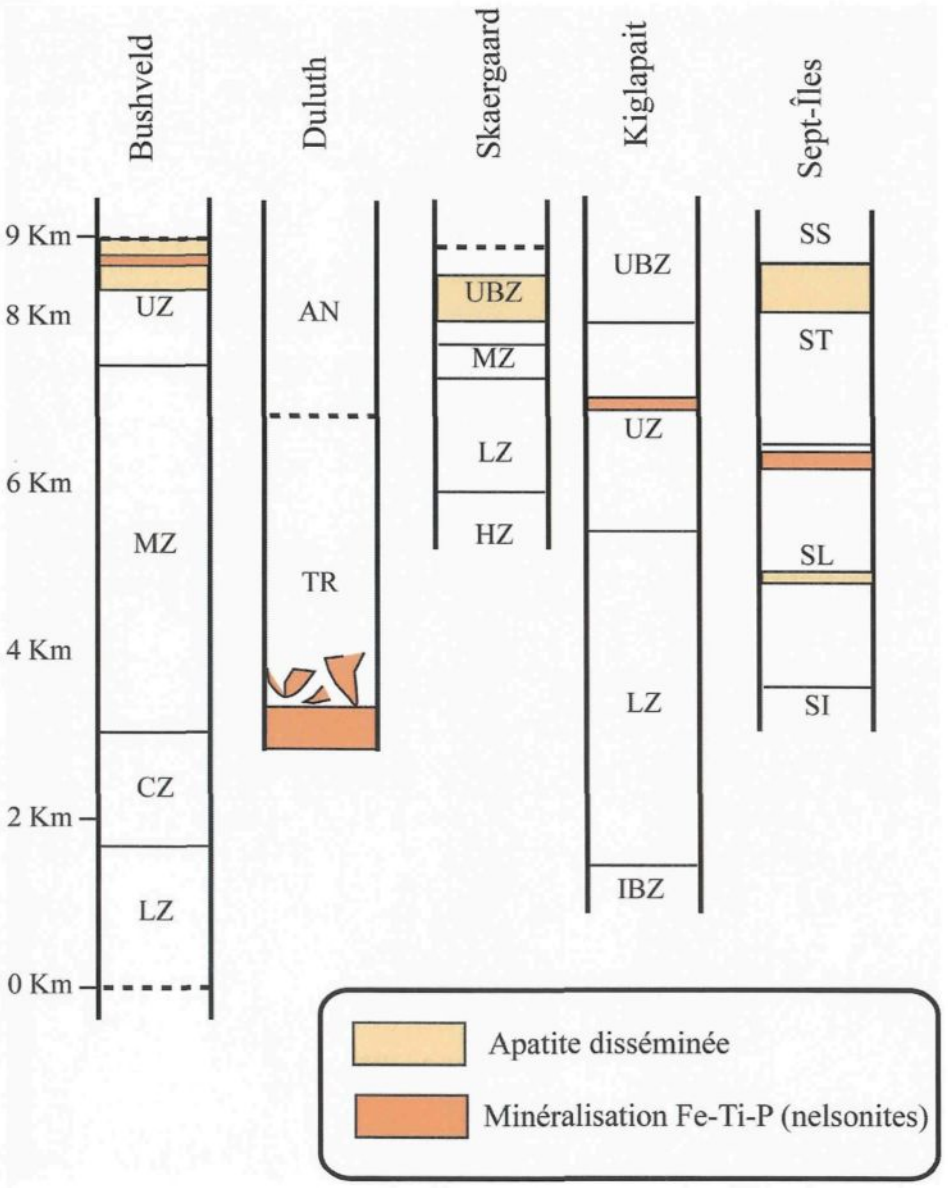

Figure 1. 4 : Localisation stratigraphique des unités à apatite ou nelsonites dans quelques intrusions et complexe mafiques stratifiés dans le monde.

(UZ, Zone supérieure; MZ, Zone principale; CZ, Zone critique; LZ, Zone inférieure; AN, Anorthosite; TR, Troctolite; UBZ, Zone de bordure supérieure; HZ, Zone cachée; IBZ, Zone de bordure interne; SS, Série supérieure; ST, Série transitionnelle; SL, Série litée; SI, Série inférieure) (modifiée d'après Wager, 1960; Morse, 1979a; Severson, 1994; Cimon, 1998; Barnes et al., 2004).

Dans les intrusions litées, l'apatite ne devient, en générale, une phase majeure que dans les stades les plus tardifs de l'évolution magmatique (Fig. 1. 4). Ceci est dû à la nécessité d'enrichir le magma en éléments incompatibles (P et F par exemple). Les roches les plus enrichis en minéraux phosphatés sont nommées nelsonites. Elles contiennent très peu, ou pas du tout, de minéraux silicatés. Cependant, il existe toute une gamme de noms donnés aux roches riches en Fe-Ti et P en fonction de leur teneur en apatite et en minéraux silicatés (exemple, gabbro-nelsonites, nelsonites troctolitiques, ferrodiorite).

Le complexe du Duluth fait exception à cette règle. En effet, les formations contenant l'apatite sous forme massive (notées « oxide-bearing ultramafic intrusions », OUI) dans cette intrusion se trouvent en discordance à la base de l'intrusion. Ce phénomène a été expliqué par Nabil (2003). Ce dernier, explique dans son modèle que les couches enrichies en oxydes et apatites qui se forment dans la partie supérieure de la chambre magmatique sont très denses. Ces dernières sont si denses par rapport aux roches sous jacentes non consolidées, qu'elles peuvent se déstabiliser, se fragmenter et chuter dans la chambre magmatique. Ce modèle explique la position particulière ainsi que la forme des roches enrichies en oxydes de Fe - Ti et P dans le complexe du Duluth.

- Cas des anorthosites -

L'apatite est considérée comme une des phases accessoires présentes dans certains complexes anorthositiques. Elle peut même y devenir une phase majeure : plutons de Labrieville et de St Urbain, Québec (Owens and Dymek, 1992); Secteur de St Charles dans la Suite Intrusive du Saguenay-Lac-St-Jean (Bachari, 2005); Secteur du Lac à Paul au Lac

St-Jean (Fredette, 2006). Dans tous les cas, elle est associée à la cristallisation de magma très fractionné ferrodiorite.

Concernant les roches dans lesquelles l'apatite est une phase majeure, le magma parent des faciès anorthositiques et des faciès plus mafiques est actuellement interprété comme ayant la composition d'un basalte alumineux évolué (Ashwal, 1993). Les minéralisations en Fe-Ti sont, quand à elles, associées à des ferrodiorites.

Comme dans le cas des intrusions litées, les roches dans lesquelles l'apatite est considérée comme une phase majeure, sont nommées de différentes manières en fonction de leurs compositions (pourcentages d'apatite et d'oxydes de Fe-Ti). Ces roches sont associées à des faciès plus mafiques possédant des enrichissements variables en oxydes de Fe-Ti et en apatite. Les jotunites, l'équivalent des monzonorites enrichis légèrement en Fe, Ti et P, correspondent à certains de ces faciès (Hargraves, 1962; Carter, 1982; Owens and Dymek, 1992).

Les nelsonites forment le plus souvent des boudins montrant des contacts discordant ou progressifs avec l'anorthosite ou les jotunites encaissantes (Owens and Dymek, 1992). Les jotunites peuvent aussi former des dykes au sein des anorthosites. La forme en lobe des nelsonites est interprété comme étant le résultat du boudinage des lits enrichis en oxydes de Fe-Ti-P à l'état semi-solide (Barnes, communication personnelle).

1.1.2 Provenance des échantillons

Comme exposé précédemment, nous avons choisis comme terrain d'étude pour ce projet de recherche, deux des principales intrusions litées dans le monde : la Suite Intrusive de Sept-Îles et le complexe du Bushveld (Figs. 1. 2 et 1. 3).

- La Suite Intrusive de Sept-Îles -

La Suite Intrusive de Sept-Îles, Québec, est centrée à 30 km au sud de la ville de Sept Îles. De taille beaucoup plus modeste que le complexe du Bushveld, elle a un diamètre de 80 km et occupe une superficie de 4000 km^2. La plus grande partie de l'intrusion étant sous le fleuve St-Laurent, seulement 5% de cette superficie affleure. Cette intrusion était initialement divisée en quatre séries : la série inférieure, la série litée, la série transitionnelle et la série supérieure (Cimon, 1998). De nouvelles interprétations quant à la structure de cette intrusion nous indique qu'elle correspond en fait à plusieurs intrusions différentes et non à une intrusion unique (Higgins, 2005). Quatre intrusions sont ainsi reconnues : L'intrusion Mafique de Sept-Îles, l'intrusion Sept-Îles Border, l'intrusion de la Pointe du Criarde et l'intrusion de Sept-Îles Late Gabbro.

L'apatite en tant que phase majeure se retrouve dans l'intrusion Mafique de Sept-Îles à la limite supérieure de la série litée (Higgins and Doig, 1981; Cimon, 1998). Plus précisément, elle est présente à l'intérieur d'une séquence hybride appelée zone critique (ZCR) (Cimon, 1998). Cette zone a une épaisseur d'environ 250 m et est subdivisée en quatre sous-zones identifiées de la base au sommet par : sous-zone à magnétite, sous-zone à nelsonite, sous-zone à nelsonite-gabbro et sous-zone à microtroctolite (Fig. 1. 5).

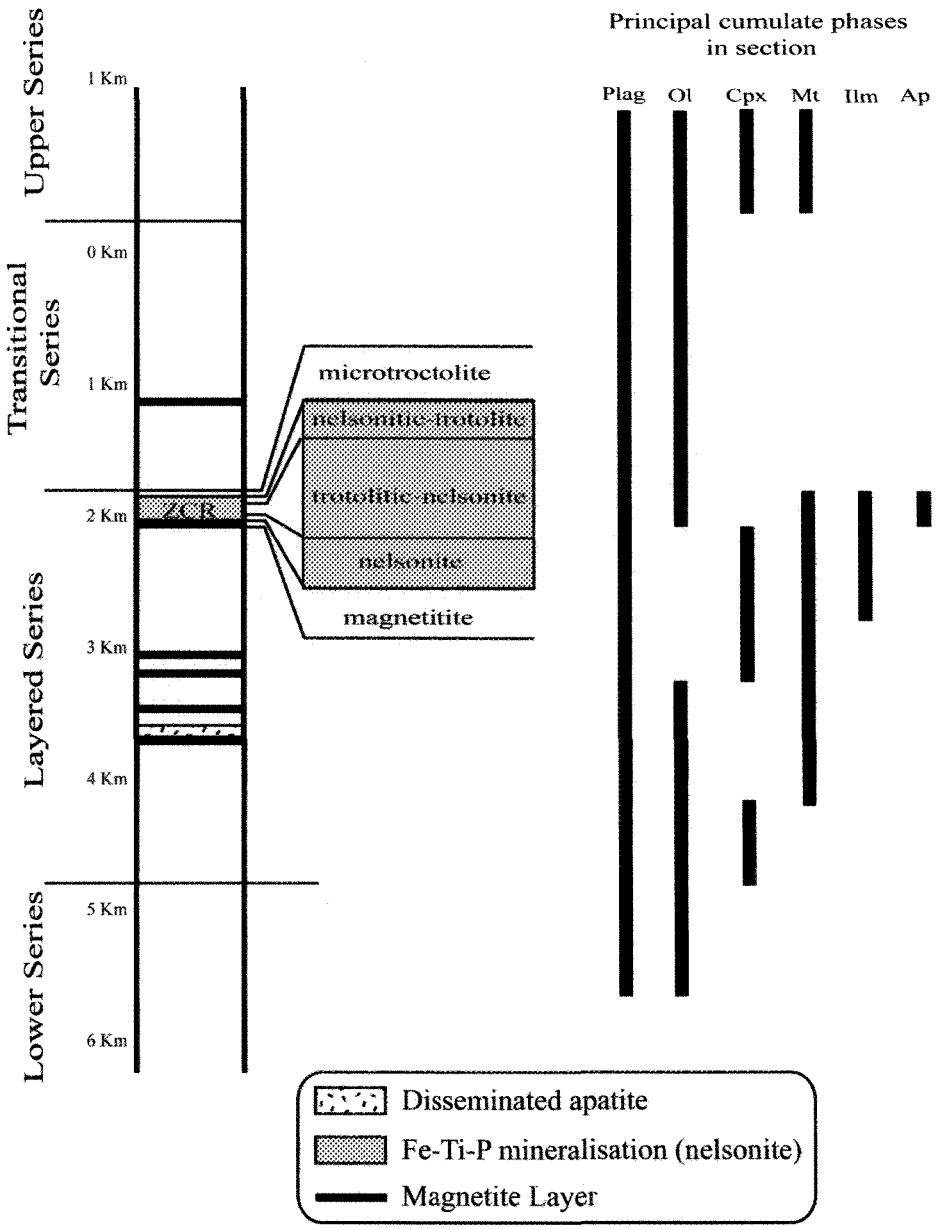

Figure 1. 5: Coupe stratigraphique simplifiées de la Suite Intrusive de Sept-Îles montrant la position de la ZCR, Zone Critique d'où proviennent nos échantillons.

(modifiée d'après Cimon, 1998; Nabil, 2003)

Plag = plagioclase, Ol = olivine, Cpx = clinopyroxene, Mt = magnétite, Ilm= ilménite and Ap = apatite

La figure 1. 5 est une coupe de l'intrusion. Cette figure souligne le fait que les roches enrichies en phosphore sont confinées à l'intérieur de séquences bien.

L'enrichissement le plus bas dans la colonne, localisé à l'intérieur de la ZGT, est interprété comme étant le résultat d'un fractionnement très localisé produit par une cellule de différenciation indépendante (Higgins, 2005). Comme mentionné précédemment, les teneurs les plus élevées (jusqu'à plus de 9% de P_2O_5 dans la roche totale) se retrouvent dans la ZCR. Elles correspondent aux nelsonites et gabbro-nelsonites.

Nabil (2003) et Higgins (2005) suggère que la formation de ces nelsonites soit le résultat de la différenciation magmatique. D'après cet auteur, les magmas tardifs, très enrichis en phosphore du fait de la cristallisation fractionnée, précipiteraient de grande quantité d'apatite à la suite de la cristallisation de la magnétite.

- Le complexe du Bushveld -

Le complexe du Bushveld (Afrique du Sud) est la plus vaste intrusion au monde (450 km de long sur 270 km de large).

Le complexe du Bushveld comprend la "Rustenburg Layered Suite" et la "Granite and Granophyre Suite ». Nos échantillons proviennent de la partie nord du complexe, plus exactement du forage Bellevue situé dans la partie nord de la « Rustenburg Layered Suite » (Fig. 1. 3). La "Rustenburg Layered Suite" est divisée en cinq zones: la Marginal, la Lower, la Critical, la Main et l'Upper Zones (Hall, 1932). L'Upper Zone est définie par l'apparition de la magnétite comme phase majeur du cumulât. L'Upper Zone contient 26 à 32 couches de magnétite dépendant de la localité (Cawthorn and Lee, 1998). Ces unités cycliques sont constituées d'une couche de magnétite surmontée par une couche de gabbronorite ou de

diorite et d'anorthosite. L'Upper Zone est divisée en trois sous-zones (Sack et al., 1980) basées sur les minéraux composant le cumulât (Fig. 1. 6). Les 1000m les plus bas de cette zone, la sub-zone A, est un cumulât de plagioclase, pyroxène et magnétite. Au dessus on retrouve approximativement 400 m dans lesquels l'olivine devient une phase du cumulât (subzone B). L'apatite devient une phase du cumulât dans les derniers 600 m de la coupe (subzone C). Dans le forage de Bellevue, une couche de nelsonite est présente à 305 m et, est nommée couche R (Barnes et al., 2004).

Nos deux échantillons proviennent de cette nelsonite et de la diorite nelsonitique située au dessus (Fig. 1. 6). Des nelsonites dans des positions similaires ont été rapportés dans le « Western Limb » et sur dans la coupe de Villa Nora dans le complexe du Bushveld (Von Gruenewaldt, 1993; Cawthorn, 2006).

D'après Reynolds (1985b), la formation de cet horizon est dû à la séparation par immiscibilité d'un liquide enrichi en Fe-Ti-Mn-Ca-P-ETR à partir d'un magma résiduel dioritique très évolué. D'autres auteurs au contraire, considèrent que la formation de ces litages est due à un phénomène de cristallisation fractionnée (Barnes et al., 2004; Tegner et al., 2006).

1.2 PROCESSUS DE CRISTALLISATION DES MINÉRAUX PHOSPHATÉS

Comme cela a été dit dans l'introduction, l'apatite est un minéral commun sur notre planète. Malgré cela, ce minéral, dans les systèmes mafiques, n'a fait l'objet que de peu d'études jusqu'à aujourd'hui.

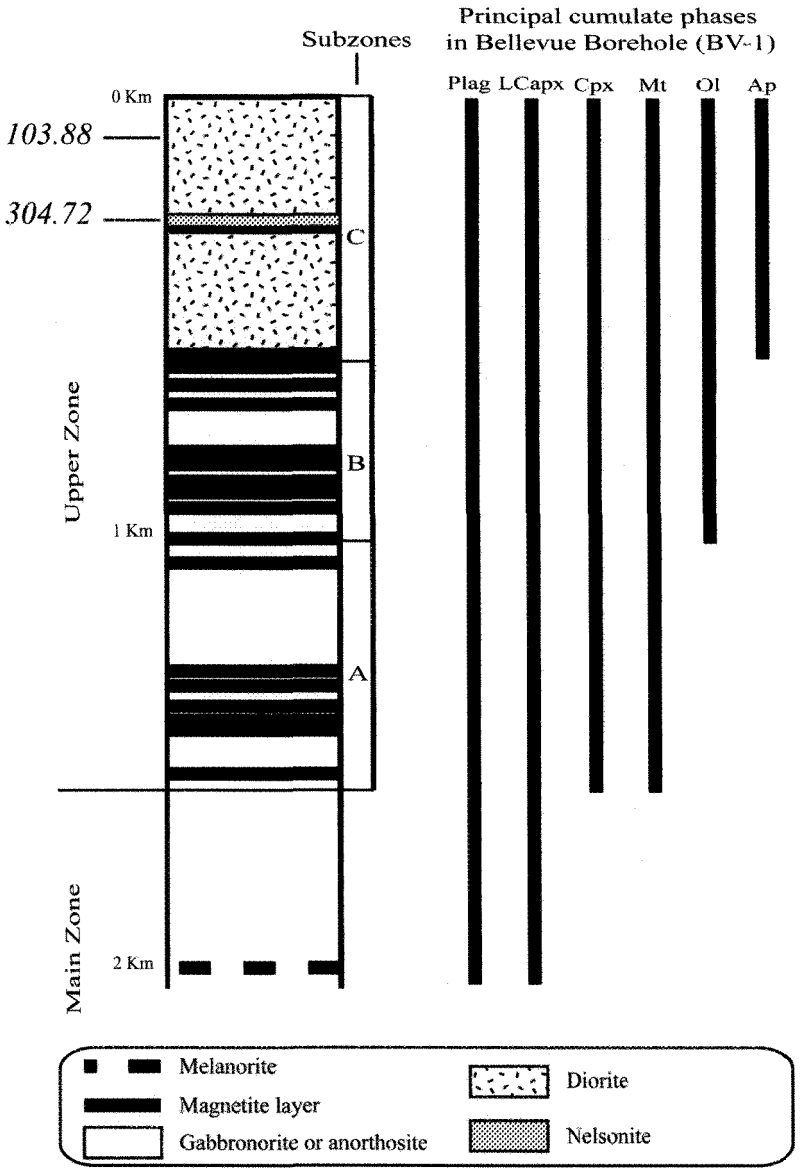

Figure 1. 6 : Coupe stratigraphique simplifiée du forage Bellevue (BV-1) de l'Upper Zone de la partie nord du complexe du Bushveld montrant la position de nos échantillons. (modifié d'après Barnes et al., 2004; Ashwal et al., 2005) Plag = plagioclase, LCapx = pyroxène pauvre en Ca, Cpx = clinopyroxène, Mt = magnétite, Ol = olivine and Ap = apatite

Un des problèmes abordés dans cette thèse est la détermination des conditions de saturations des phosphates, et plus particulièrement de l'apatite, dans les systèmes mafiques. Pour répondre à cela, il est important de bien comprendre quelle est l'évolution d'un magma lors de sa mise en place (Fig. 1. 7).

La première étape est l'injection d'un liquide basaltique mafique dans une chambre magmatique où il commence à se refroidir et à cristalliser. La cristallisation est de type cristallisation fractionnée : les cristaux formés et le liquide résiduel se séparent par densité.

Le liquide résiduel évolue lors de la cristallisation fractionnée et les teneurs en silice, en phosphore (P) ainsi qu'en éléments incompatibles augmentent dans le système. En effet, durant la cristallisation d'un magma basaltique, le P_2O_5 n'est pas incorporé dans les phases cristallines qui précipitent précocement. Il se comporte comme un élément incompatible (Wager and Brown, 1967) jusqu'à ce qu'il soit suffisamment enrichi dans le liquide silicaté pour causer, soit la précipitation des minéraux phosphatés auxquels il est incorporé, soit la formation d'un liquide riche en Fe-Ti-P. C'est à ce stade que les opinions divergent et que les auteurs ne s'accordent pas en ce qui concerne la suite du scénario.

Différents auteurs s'accordent pour dire que les nelsonites précipitent à partir d'un liquide fortement enrichis en Fe, Ti et P. Cependant, deux possibilités ont été proposées dans la littérature pour expliquer la formation de ces liquides : (i) l'immiscibilité de deux liquides (Philpotts, 1967; Jakobsen et al., 2005); (ii) la différentiation magmatique (Nabil, 2003; Barnes et al., 2004; Tegner et al., 2006). Nous traiterons ces deux hypothèses et décrirons l'évolution supposée du magma suivant chacun de ces deux cas.

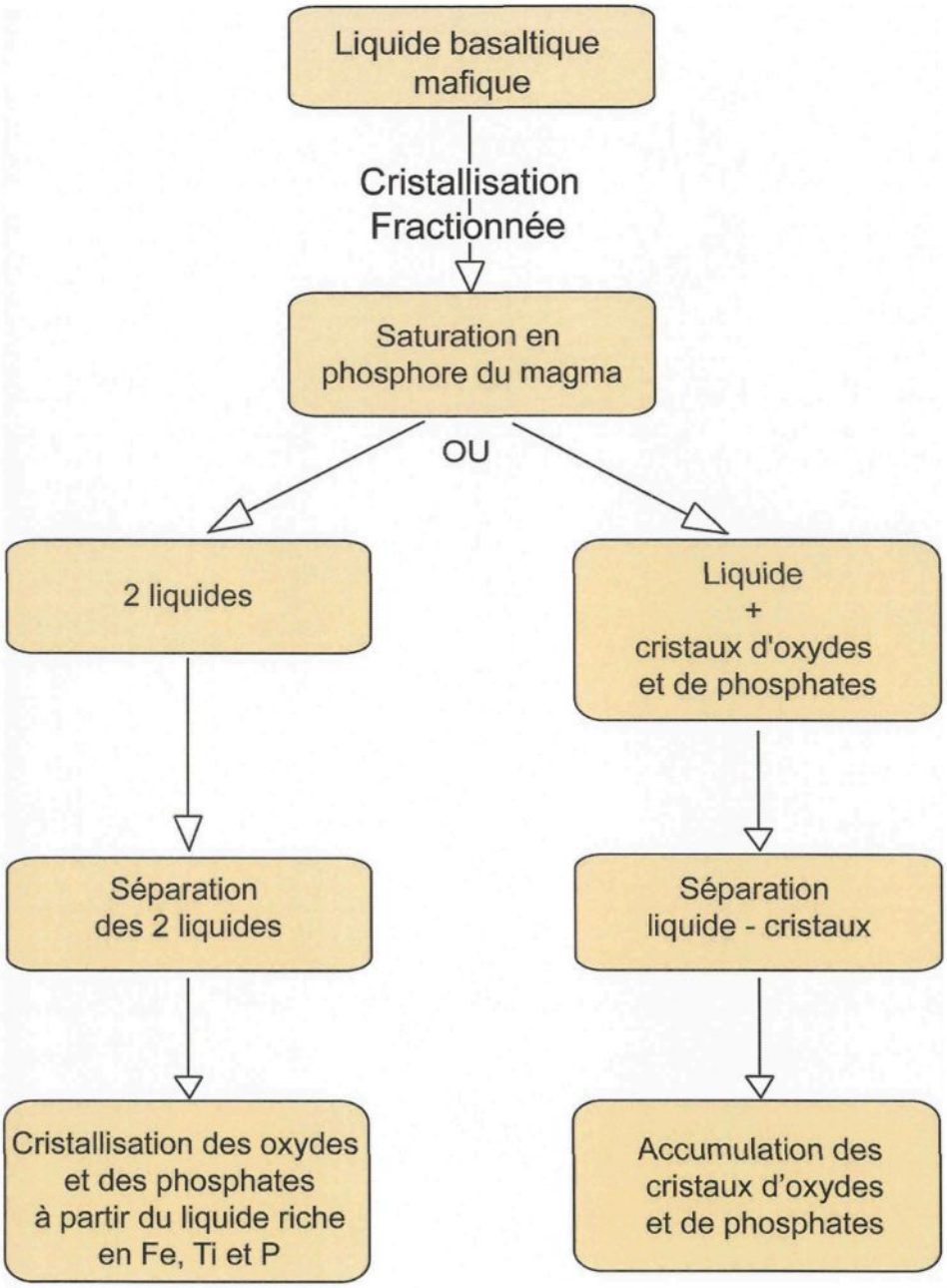

Figure 1. 7 : Schéma récapitulatif des deux scénarios possibles pour l'évolution d'un magma basaltique mafique.

1.2.1 L'immiscibilité de deux liquides

- Le modèle -

Le processus de cristallisation fractionnée peut éventuellement mener à l'immiscibilité de liquides dans les stades tardifs de l'évolution de certains basaltes. Suite à cette constatation certaines questions doivent être posées :

- Quels sont les processus qui ont lieu au sein d'un magma permettant la formation de deux liquides?
- Quels sont les éléments qui peuvent favoriser la formation et la stabilité de ces deux liquides coexistants?

Pour répondre à la première question il est important de regarder plus en détail les liquides formés par immiscibilité. Les produits typiques de l'immiscibilité de deux liquides sont (Roedder, 1978):

- Un liquide felsique, alcalin ou alumino-silicaté riche en Si
- Un liquide riche en Fe, Mg, Ca, Ti et P

La polymérisation du liquide joue un rôle important dans la formation de ces deux liquides coexistants. Mais avant d'aller plus loin il est important de rappeler ce qu'est la polymérisation d'un magma. Le taux de polymérisation d'un magma correspond en fait au nombre de liaisons Si-O-Si ou Si-O-Al dans le magma en question. La silice et l'oxygène s'associent et forment ainsi des chaînes. Un magma très polymérisé contient ce type de liaison en grand nombre et inversement un magma peu polymérisé en contient peu. Certains cations peuvent briser ce type de liaisons et donc dépolymériser le magma. Lors de l'augmentation de la concentration de ces cations dans le magma, il est possible de

provoquer une forte dépolymérisation qui peut conduire à l'immiscibilité (séparation de deux liquides).

Pour vérifier l'effet de certains cations sur l'état de polymérisation d'un magma, un grand nombre d'études ont été réalisées (Roedder, 1951; Philpotts, 1967; Rutherford et al., 1974; Roedder, 1978; Visser and Kostervangroos, 1979b; a; Wood and Hess, 1980; Philpotts, 1982). D'après Irvine (1976), Naslund (1976; 1983) et Philpotts (1982) Na_2O, CaO et MgO causent une diminution de l'immiscibilité; ajoutés en grandes quantités ces éléments peuvent même la supprimer totalement. Les résultats de Wood et Hess (1977) indiquent que Al_2O_3 limite aussi l'immiscibilité en agissant comme un agent homogénéisant qui rend les deux liquides plus compatibles. Par contre, Ti, Cr et P élargissent le champ d'immiscibilité (Hess, 1977; Wood and Hess, 1980) en accentuant les différences structurales entre les deux liquides. Naslund (1983) résume en disant que les cations avec un fort potentiel ionique (Fe^{3+}, Ti^{4+}, P^{5+}) causent une augmentation du champ d'immiscibilité alors que les cations avec un faible potentiel ionique (Ca^{2+}, Mg^{2+}) ont tendance à le réduire.

Pour reprendre l'évolution du magma basaltique qui nous intéresse, il faut revenir à la formation des deux liquides immiscibles. Des gouttelettes de liquides riches en Fe-Ti-P et d'autres riches en Si vont tout d'abord se former (Fig. 1. 8). Les gouttelettes riches en Fe-Ti-P, très denses, vont chuter dans la pile magmatique et se rejoindre pour former une couche de liquide riche en Fe-Ti-P à la base de la stratigraphie. Le liquide plus riche en Si quand a lui va « flotter » au dessus du précédent. On a ainsi deux liquides distincts qui vont se séparer par densité. Les minéraux phosphatés et les oxydes précipiteront à partir du liquide enrichi en P et Fe pouvant ainsi former des lits de nelsonites.

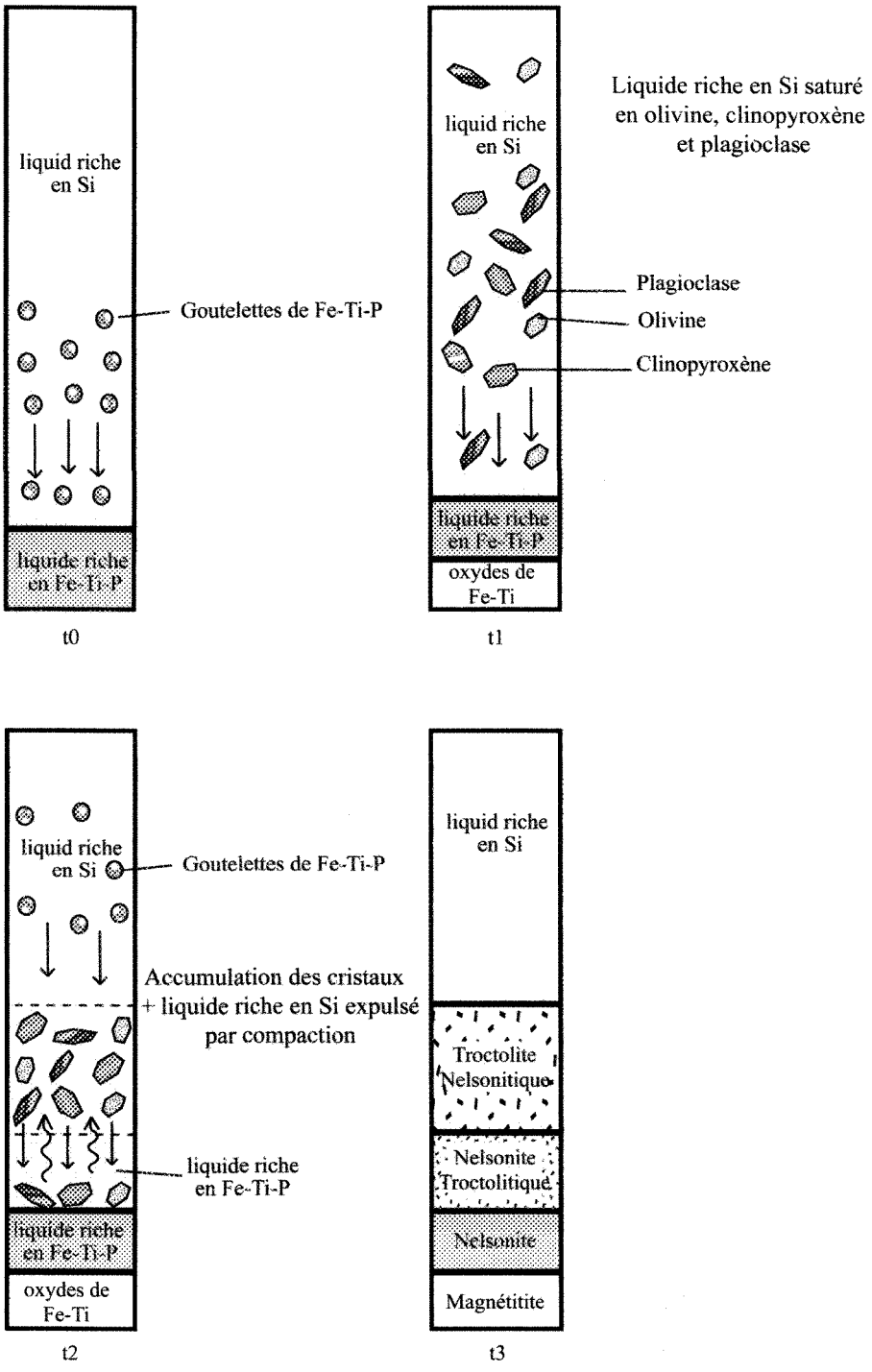

Figure 1. 8 : Évolution schématique des rapports entre le refroidissement et les différentes unités dans la section stratigraphique de la partie supérieure d'une intrusion litée (modifié d'après Usselman et al., 1979). (t0 = temps initiale, deux liquides immiscibles, t1, t2 et t3 = cristallisation)

- Critique du modèle -

Comme cela a été dit précédemment deux hypothèses sont proposées pour expliquer la formation des liquides riches en Fe, Ti et P parents des nelsonites. D'après Philpotts (1967) et Naslund (1983), le modèle d'immiscibilité est le seul mécanisme valable pour former les nelsonites, car il permet l'enrichissement nécessaire à la formation de ces roches (30% apatite et 60% oxydes de Fe et Ti). Les résultats des expériences de Philpotts (1967) montrent, en effet, que la formation de deux liquides immiscibles dans le système magnétite-apatite-diorite est possible. Cependant, Philpotts a réalisé ses expériences à des températures supérieures ou égales à 1400°C (à 1 atm), alors qu'il affirme que les températures de formation des nelsonites varient entre 850°C et 1000°C. Il note aussi que les conditions de fugacité d'oxygène dans ses expériences ne sont pas représentatives d'un système naturel. En effet, Kolker (1982) confirme cela en affirmant que, pour les couples d'oxydes (magnétite-ilménite) présents dans les nelsonites, les températures d'équilibre et les fugacités d'oxygène estimées sont de l'ordre de 600°C à 1000°C et de 10^{-20} à 10^{-11} atm fO_2. Les travaux de Pasteris (1985), de Sassani (1992) et de Nabil (2003), sur les nelsonites du complexe du Duluth, donnent les mêmes résultats (Fig. 1. 9). Nabil a aussi obtenus des résultats similaires pour la Suite Intrusive de Sept-Îles (Fig. 1. 10). Les températures et les fugacités d'oxygène, ainsi obtenues, donnent une trajectoire proche de celle de la courbe du tampon QFM (Fig. 1. 11). D'autres études, (Toplis et al., 1994b) ont montré que les températures nécessaires pour obtenir un minéral phosphaté était de l'ordre de 1050°C à 1100°C.

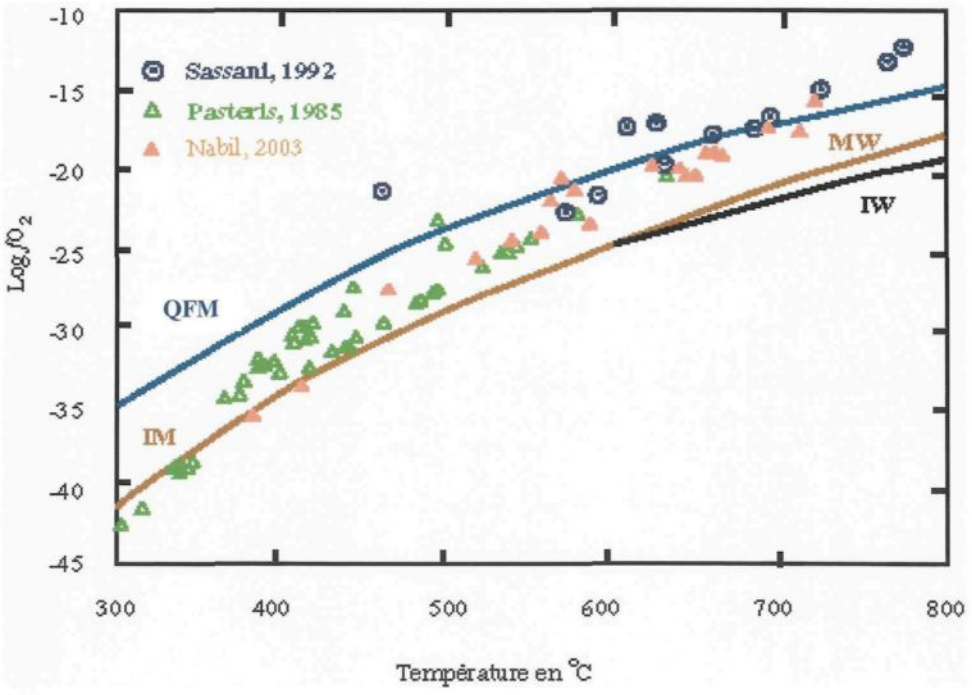

Figure 1. 9 : Diagramme de température versus Log de la fugacité d'oxygène dans les différentes régions du Complexe de Duluth.

(d'après Pasteris, 1985; Sassani, 1992; Nabil, 2003)

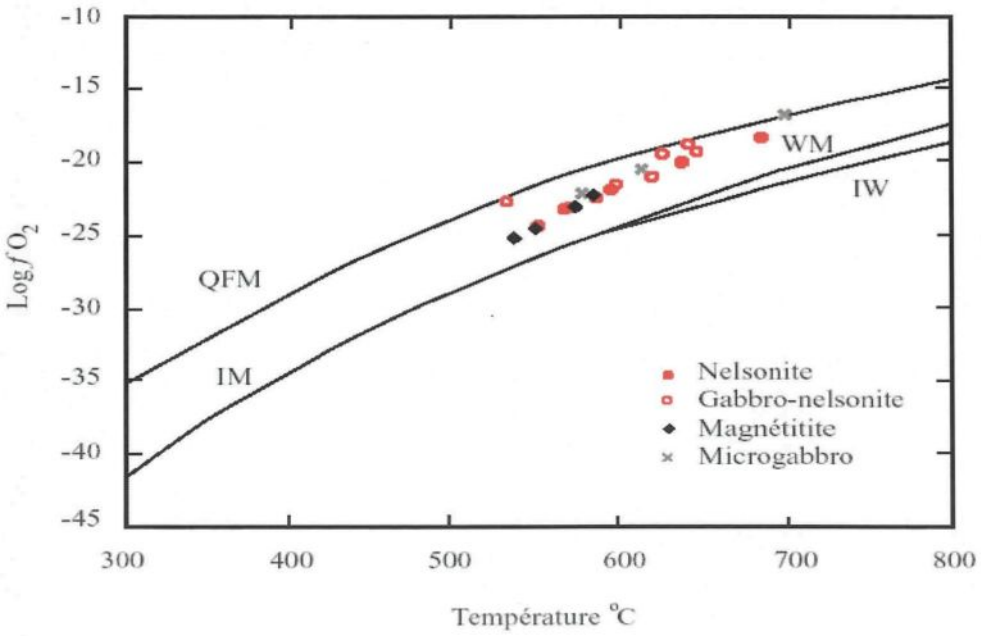

Figure 1. 10 : Diagramme de Température versus Log de la fugacité d'oxygène illustrant les conditions dans lesquelles certaines paires d'oxydes (ilménite-titanomagnétite) de Sept-îles ont été rééquilibrées durant le refroidissement sub-solidus.

Les courbes représentent les tampons de référence. (F=fayalite, M=magnétite, Q=quartz, I=fer, W=wustite) (d'après Nabil, 2003)

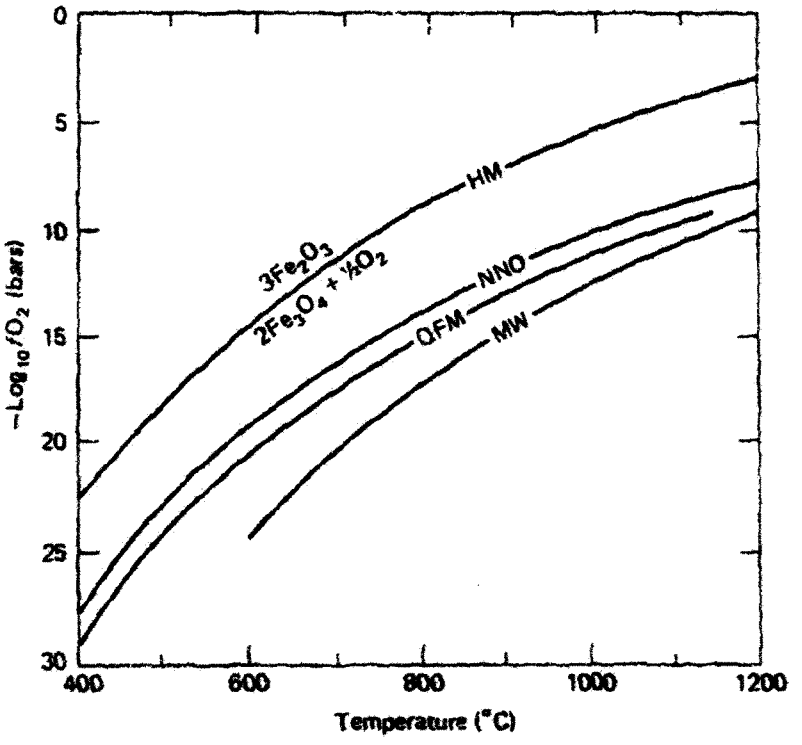

Figure 1. 11 : Fugacité d'oxygène des tampons les plus communs en fonction de la température. Hématite-magnétite (HM), nickel-oxyde de nickel (NNO), quartz-fayalite-magnétite (QFM), et magnétite-wüstite (MW). (d'après Philpotts, 1969)

Watson (1979), quand à lui, a travaillé sur la cristallisation de l'apatite à plus haute température mais ne dépassant jamais 1350°C et n'obtient jamais d'immiscibilité dans ses expériences. De plus, d'autres auteurs, tel que Roedder (1956) et Freestone (1978) ont travaillé sur l'immiscibilité. Ils ont positionnés sur un diagramme ternaire le champ d'immiscibilité dans un système (fayalite-leucite-silicate) (Fig. 1. 12). En y plaçant les compositions de roches contenant de l'apatite et même des nelsonites (exemples des roches de la Suite Intrusive de Sept-Îles, (Nabil, 2003)) on remarque qu'aucune de ces roches ne tombent dans le champs d'immiscibilité.

A partir de ces observations certaines questions peuvent être posées et devront être résolues avant d'écarter ou de choisir le modèle d'immiscibilité de deux liquide: (i) Les conditions d'expérimentation utilisées lors de ces études correspondent-elles aux conditions naturelles? (ii) Est-ce que les liquides riches en Fe, Ti et P obtenus lors de ces expériences ressemblent aux nelsonites?

1.2.2 Différenciation magmatique

- Le modèle -

Pour parler de ce scénario, il faut revenir un peu en arrière dans l'évolution du magma basaltique, au moment où la concentration en Fe, Ti et P dans le liquide devient importante. La cristallisation des oxydes de Fe et Ti va provoquer l'augmentation de la concentration en phosphore du magma et, ainsi, provoquer la saturation du liquide en apatite (Toplis et al., 1994a) (Fig. 1. 13).

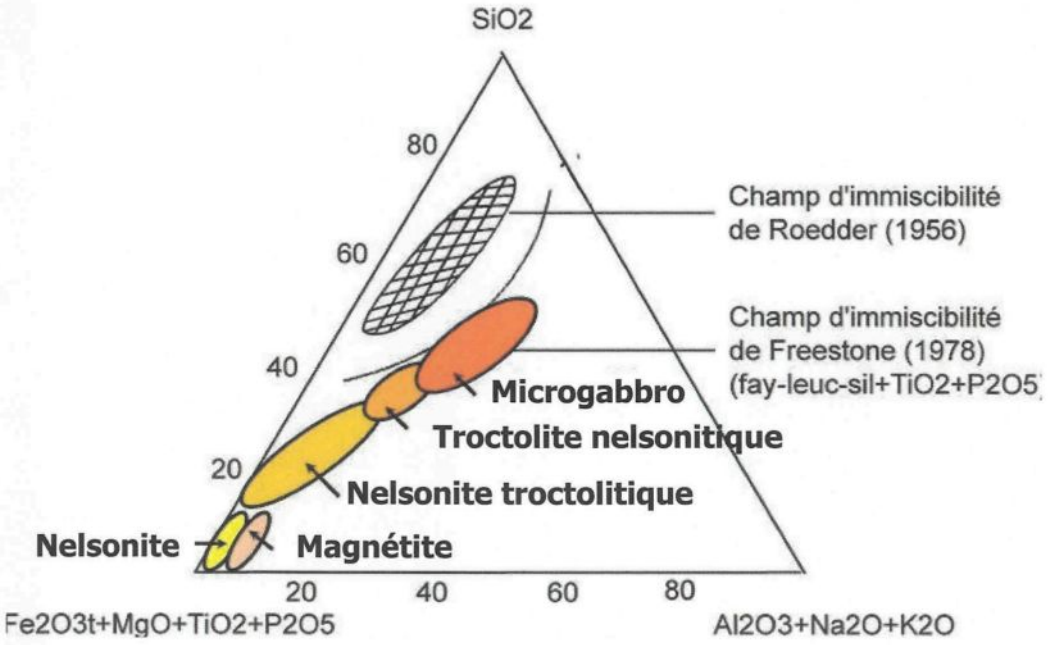

Figure 1. 12 : diagramme ternaire de Roedder (1956) et son extension de Freestone (1978) qui résulte de l'addition de 3% TiO_2 et 1% P_2O_5. Analyses et classification des roches Nabil (2003).

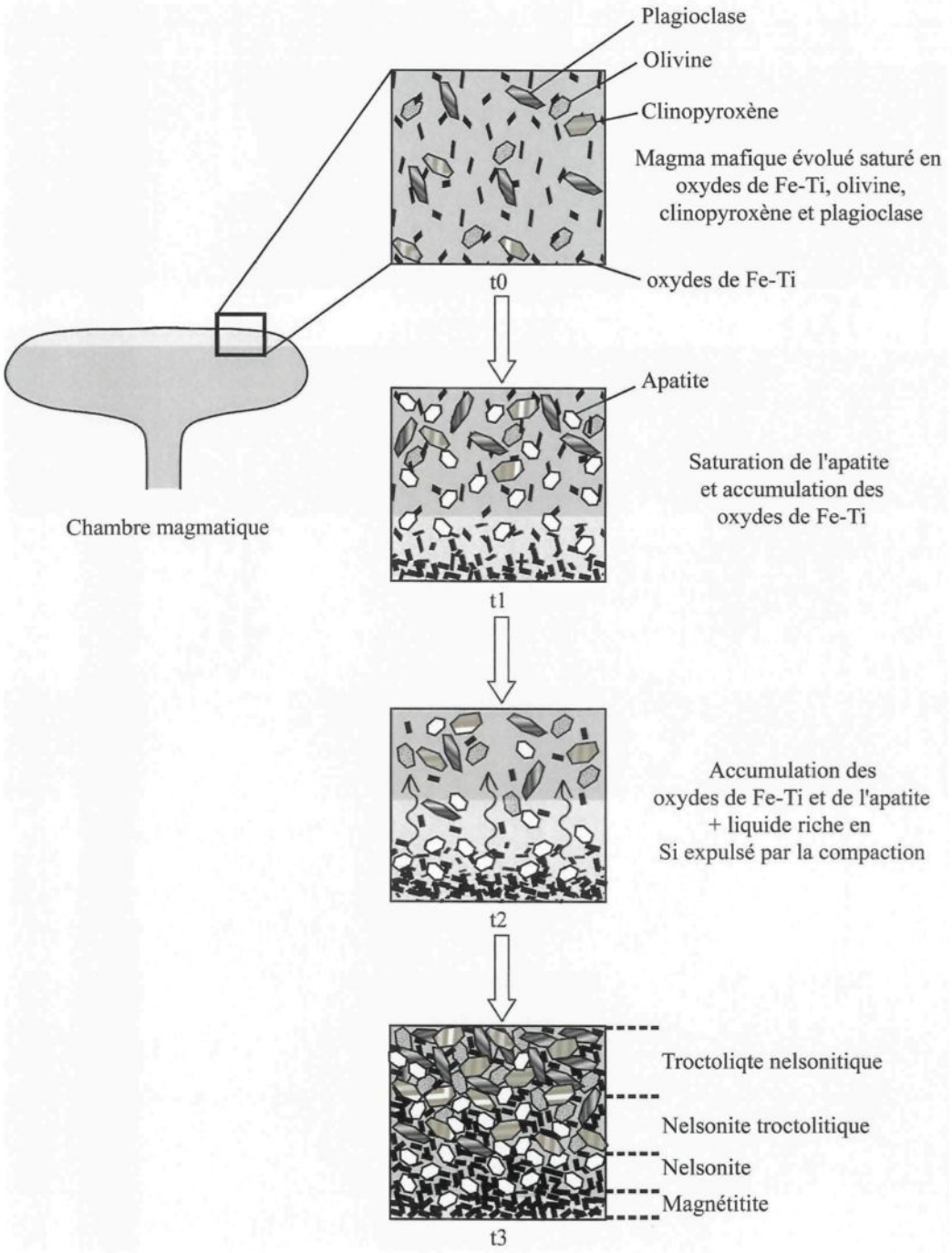

Figure 1. 13 : Modèle de formation des nelsonites et des roches associées par cristallisation fractionnée et accumulation dans la partie supérieure des intrusions litées. (t0 = temps initial, t1, t2 et t3 = refroidissement du magma)

Les minéraux phosphatés et les oxydes de Fe-Ti cristallisent donc presque simultanément. A ce stade, on a présence d'un liquide riche en Si et d'un cumulât d'oxydes de Fe-Ti et d'apatite. Par gravité, le liquide et les cristaux se séparent : le liquide plus léger va avoir tendance à rester en surface alors que les cristaux, plus lourds, vont chuter (Wager and Brown, 1967). Grâce au poids de la pile de cristaux, le liquide est expulsé au fur et à mesure de l'accumulation. Le cumulât va ainsi former des lits composés essentiellement d'oxydes de Fe-Ti et d'apatite (si les proportions sont respectées ce cumulât donnera des nelsonites).

- Critique du modèle -

Philpotts (1967) et Naslund (1983) affirment que le modèle de différenciation magmatique ne permet pas l'enrichissement nécessaire à la formation des nelsonites (30% d'apatite et 60% oxydes de Fe et Ti). En effet, dans les expériences de Toplis et Carroll (1995), les oxydes de Fe-Ti, les minéraux phosphatés et les minéraux silicatés ne sont pas présents dans les proportions cotectiques 1/3 phosphates – 2/3 oxydes. De plus, les auteurs n'ont pas observé plus de 15 wt% d'oxydes de Fe et Ti dans les résultats de leurs expériences. Il faut donc impliquer un mécanisme pour expliquer la séparation des oxydes et des phosphates d'avec les minéraux silicatés. Le processus proposé est la séparation par densité permettant l'accumulation des oxydes et des minéraux phosphatés dans la pile magmatique. Cependant, Philpotts (1967) et Naslund (1983) considèrent qu'une certaine quantité de minéraux silicatés doit rester emprisonnée dans le cumulât. D'ailleurs la séparation de certains de ces minéraux avec les minéraux phosphatés reste un problème. En effet, l'apatite a une densité de 3,15 – 3,2 et les clinopyroxènes ont des densités variant de 3,2 à

3,5 selon leur composition (Augite 3,2 – 3,5; Diopside 3,2 – 3,3), il est donc difficile d'expliquer leur séparation par gravité. Le modèle par différenciation magmatique présente aussi certains problèmes :

- Comment les clinopyroxènes et l'apatite, qui ont des densité proche et qui cristallisent en même temps, peuvent être séparés dans la pile de cumulât pour permettre un enrichissement en minéraux phosphatés ?
- Est-ce que le cumulât ressemble aux nelsonites d'un point de vue texturale et compositionnelle (proportions un tiers d'apatite et deux tiers d'oxydes de Fe-Ti) ?

1.2 CONCLUSIONS ET REMARQUES

Comme nous venons de le montrer l'apatite et, plus particulièrement, les formations enrichies en apatite et oxydes de Fe-Ti (nelsonites), sont associées, le plus souvent, à la partie supérieure des intrusions litées ou des complexes anorthositiques. Cette constatation aboutit à certaines questions : i) Quels sont les facteurs influençant la saturation en phosphate et en minéraux phosphatés (apatite) dans un magma? ii) En quoi la position particulière de l'apatite nous renseigne-elle sur ces facteurs? iii) Une fois la saturation en phosphate atteinte, comment expliquer l'enrichissement en apatite et oxydes de Fe-Ti nécessaire à la formation des nelsonites?

L'état actuel des connaissances ne permet pas de trancher entre les deux processus proposés pour la genèse des liquides parentaux des roches riches en apatites et oxydes de Fe et Ti. Ce travail de recherche se propose d'essayer de résoudre ce problème. Pour cela il faudra répondre aux nombreuses questions énoncées dans la problématique.

1.3 OBJECTIFS

Les principaux facteurs influençant la saturation en apatite d'un magma mafique sont encore peu connus. De plus, malgré un grand nombre d'études antérieures, aussi bien expérimentales que de terrain, les deux principaux modèles proposés pour expliquer la formation des roches enrichies en apatite et oxydes de Fe et Ti sont toujours débattus. Le but de cette thèse est donc de déterminer quels sont les facteurs influençant la saturation en apatite d'un magma mafique et de quantifier l'effet de chacun de ces facteurs. Ceci afin de mieux comprendre les processus de cristallisation qui ont lieu dans les stades tardifs des intrusions litées et, plus tard, de mieux comprendre les processus à l'origine des nelsonites. Ce but global se divise en différents objectifs plus spécifiques : Le premier objectif de cette thèse est de préciser sous quelles conditions cristallisent les minéraux phosphatés en déterminant quels sont les facteurs qui influencent la saturation en phosphore des systèmes ferrobasaltiques. L'information recueillie lors de cette étape permettra de déterminer les conditions de formation (pression, température et composition magmatique) de ces minéraux. Ces résultats permettront ainsi de limiter le champ de formation des nelsonites. Le second objectif est de trouver des indices, en étudiant des échantillons naturels, nous renseignant sur les processus pétrogénétiques et géochimiques à l'origine des roches contenant de l'apatite dans la partie supérieure des intrusions litées. Ceci nous permettra d'obtenir des renseignements essentiels sur les compositions magmatiques à l'origine des roches riches en apatites et oxydes de Fe et Ti. Enfin, le but final est de tenter de trancher entre le modèle d'immiscibilité et le modèle de cristallisation fractionnée pour expliquer la formation des nelsonites.

1.4 PLAN DE LA THÈSE

Cette thèse se présente sous la forme d'un recueil de manuscrits d'articles dont, lors de la rédaction finale de la thèse, un fut publié, un accepté et un soumis. Les trois manuscrits constituent les chapitres 2, 3 et 4 de la thèse. Les chapitres 2 et 3 traitent des objectifs liés à la détermination des facteurs influençant la saturation en apatite d'un ferrobasalt. Le chapitre 4 traite des études réalisées sur les échantillons naturels. Une section « résumé et conclusions » a été ajoutée à la suite des trois manuscrits (chapitre 5). Les idées principales présentées dans les chapitres 2, 3 et 4 y sont reprises et le modèle de formation des nelsonites, choisit en fonction de nos résultats, y est présenté.

RÉFÉRENCES

Ashwal, L.D. 1993. Anorthosites. Springer, Berlin Heidelberg New York.

Ashwal, L.D., Webb, S.J., and Knoper, M.W. 2005. Magmatic stratigraphy in the Bushveld Northern Lobe: continuous geophysical and mineralogical data from the 2950 m Bellevue drillcore. South African Journal of Geology, **108**: 199-232.

Bachari, H. 2005. La genèse des dépôts d'oxydes de Fer, Titane et Vanadium associès aux anorthosites massives de la région du Lac-St-Jean (St Charles et Lac Élan) et de la région de Havre St-Pierre (Massif de la Rivière-au-Tonnerre, Massif de la Rivière Romaine et Massif du Lac Allard), Québec, Canada. Mémoire de maîtrise ès sciences, Université du Québec à Chicoutimi, Chicoutimi.

Barnes, S.-J., Maier, W.D., and Ashwal, L.D. 2004. Platinum-group element distribution in the Main Zone and Upper Zone of the Bushveld Complex, South Africa. Chemical Geology, **208**: 293-317.

Carter, B.A. 1982. Field trip number 5; Geology and structural setting of the San Gabriel anorthosite-syenite body and adjacent rocks of the western San Gabriel Mountains, Los Angeles County, California. In Geologic excursions in the Transverse Ranges, southern California; guidebook. Edited by Geological Society of America, United States. p. 1-53.

Cawthorn, R.G. 2006. personal communication.

Cawthorn, R.G., and Lee, C. 1998. Field excursion guide to the Bushveld Complex, 8'th International Platinum Symposium, Geological Survey of South Africa, South Africa. p. 113.

Cimon, J. 1998. L'unité à apatite de rivière des rapides, Complexe de Sept îles. Localisation stratigraphique et facteurs à l'origine de sa formation. In Proceedings of the 33rd forum on the Geology of industrial minerals--Actes du 33 ème forum sur la Geologie des mineraux industriels Special Volume. Canadian Institute of Mining and Metallurgy, Canada, **50**: 75-96.

Dymek, R.F., and Owens, B.E. 2001. Petrogenesis of apatite-rich rocks (nelsonites and oxide-apatite gabbronorites) associated with massif anorthosites. Economic Geology, **96**: 797-815.

Eales, H.V., and Cawthorn, R.G. 1996. The Bushveld Complex. In Layered Intrusions. Edited by Cawthorn R.G.. Elsevier, Amsterdam. p. 181-229.

Emslie, R.F. 1975. Nature and origin of anorthositic suites. Geoscience Canada, **2**: 99-104.

Fredette, J. 2006. Pétrographie, géochimie et potentiel économique en Fe-Ti-P du secteur de Lac à Paul, Parte Nord de le Suite Anorthositique du Lac-Saint-Jean, Province du Grenville, Québec. Mémoire de maîtrise ès sciences, Université du Québec à Chicoutimi, Chicoutimi.

Freestone, I.C. 1978. Liquid immiscibility in alkali-rich magmas. Chemical Geology, **23**: 115-123.

Frietsch, R., and Perdahl, J.-H. 1995. Rare earth elements in apatite and magnetite in Kiruna-type iron ores and some other iron types. Ore Geology Reviews. **9**: p. 489-510.

Goldberg, S.A. 1984. Geochemical relationships between anorthosite and associated iron-rich rocks, Laramie Range, Wyoming. Contributions to Mineralogy and Petrology. **87**: 376-387.

Hall, A.L. 1932. The Bushveld Igneous Complex in the central Transvaal. Geological Survey of South Africa, South Africa Memoir **28**: 544.

Hargraves, R.B. 1962. Petrology of the Allard Lake anorthosite suite, Quebec. In Petrologic studies--A volume in honor of .. F. Buddington. Geological Society of America. p. 163-189.

Hess, P.C. 1977. Structure of silicate melts. Canadian Mineralogist. **15**: 162-178.

Higgins, M.D. 2005. A new interpretation of the structure of the Sept Iles Intrusive suite, Canada. Lithos. **83**: 199-213.

Higgins, M.D., and Doig, R. 1981. The Sept-Iles Anorthosite Complex - Field relationships, geochronology, and petrology. Canadian Journal of Earth Sciences, **18**: 561-573.

Hildebrand, R.S. 1986. Kiruna-type deposits: Their origin and relationship to intermediate subvolcanis plutons in the Great Bear magmatic zone, Northwest Canada. Economic Geology, **81**: p. 640-659.

Hounsell, V. 2003. Géochimie des dykes mafiques et composés de la suite intrusives de Sept-Îles, Québec. Projet de fin d'études, Université du Québec à Chicoutimi, Chicoutimi.

Hunter, R.H., and Sparks, R.S.J. 1987. The differentiation of the Skaergaard Intrusion. Contributions to Mineralogy and Petrology. **95**: 451-461.

Irvine, T.N. 1976. Metastable liquid immiscibility and MgO-FeO-SiO2 fractionation patterns in the system Mg2SiO4-Fe2SiO4-CaAl2Si2O8-SiO2. Carnegie Institution of Washington, Year Book. **75**: 597-611.

Jakobsen, J.K., Veksler, I.V., Tegner, C., and Brooks, C.K. 2005. Immiscible iron- and silica-rich melts in basalt petrogenesis documented in the Skaergaard intrusion. Geology. **33**: 885-888.

Kolker, A. 1982. Mineralogy and geochemistry of Fe-Ti oxide and apatite (nelsonite) deposits and evaluation of the liquid immiscibility hypothesis. Economic Geology. **77**: 1146-1158.

McLelland, J., Ashwal, L., and Moore, L. 1994. Composition and petrogenesis of oxide-rich, apatite-rich gabbronorites associated with Proterozoic anorthosite massifs - Examples from the Adirondack Mountains, New-York. Contributions to Mineralogy and Petrology. **116**: 225-238.

Morse, S.A. 1979a. Kiglapait geochemistry .1. Systematics, sampling, and density. Journal of Petrology, **20**: 555-590.

Morse, S.A. 1979b. Kiglapait geochemistry .2. Petrography. Journal of Petrology. **20**: 591-624.

Nabil, H. 2003. Genèse des dépôts de Fe-Ti-P associés aux intrusions litées (exemples: intrusion mafique de Sept-Îles, au Québec; Complexe de Duluth aux États-Unis). Mémoire de Philosophae doctor, Université du Québec à Chicoutimi, Chicoutimi.

Naslund, H.R. 1976. Liquid immiscibility in the system KAl-Si3O8-NaAlSi3O8-FeO-Fe2O3 and its applications to natural magmas. Carnegie Institution of Washington, Year Book. **75**: 592-596.

Naslund, H.R. 1983. The effect of oxygen fugacity on liquid immiscibility in iron-bearing silicate melts. American Journal of Science. **283**: 1034-1059.

Owens, B.E., and Dymek, R.F. 1992. Fe-Ti-P-rich rocks and massif anorthosite - problems of interpretation illustrated from the Labrieville and St-Urbain-plutons, Quebec. Canadian Mineralogist. **30**: 163-190.

Pasteris, J.D. 1985. Relationships between temperature and oxygen fugacity among Fe-Ti oxides in 2 regions of the Duluth Complex. Canadian Mineralogist. **23**: 111-127.

Philpotts, A.R. 1967. Origin of certain iron-titanium oxide and apatite rocks. Economic Geology. **62**: 303-315.

Philpotts, A.R. 1982. Compositions of immiscible liquids in volcanic-rocks. Contributions to Mineralogy and Petrology. **80**: 201-218.

Reynolds, I.M. 1985a. The nature and origin of titaniferous magnetite-rich layers in the Upper Zone of the Bushveld Complex - a review and synthesis. Economic Geology **80**: 1089-1108.

Reynolds, I.M. 1985b. Contrasted mineralogy and textural relationships in the uppermost titaniferous magnetite layers of the Bushveld Complex in the Bierkraal Area North of Rustenburg. Economic Geology. **80**: 1027-1048.

Roedder, E. 1951. Low temperature liquid immiscibility in the system K2O-FeO-Al2O3-SiO2. American Mineralogist. **36**: 282-286.

Roedder, E. 1956. The role of liquid immiscibility in igneous petrogenesis: a discussion. Journal of Geology. **64**: 84-88.

Roedder, E. 1978. Silicate liquid immiscibility in magmas and in system K2O-FeO-Al2O3-SiO2 - Example of serendipity. Geochimica et Cosmochimica Acta. **42**: 1597-1617.

Rutherford, M.J., Hess, P.C., and Garland, H.D. 1974. Experimental liquid line of descent and liquid immiscibility for basalt 70017. In Proceedings of the Fifth Lunar Science

Conference; mineralogy and petrology. Pergamon Press, Inc., New York, N.Y., United States. **5**: 569-583.

Sack, R.O., Carmichael, I.S.E., Rivers, M., and Ghiorso, M.S. 1980. Ferric-ferrous equilibria in natural silicate liquids at 1bar. Contributions to Mineralogy and Petrology. **75**: 369-376.

Sassani, D.C. 1992. Petrologic and thermodynamic investigation of the aqueous transport of platinium-group elements during alteration of mafic intrusive rocks. Memoty of Philosophae .Doctor, Washington University, St Louis, MO.

Severson, M.J. 1994. Igneous stratigraphy and mineralization in the partridge river intrusion, South Kawishiwi Intrusion and South Complex Area of the Duluth Complex, Northeastern Minnesota - Report, University of Minnesota, Duluth.

Tegner, C., Cawthorn, R.G., and Kruger, F.J. 2006. Cyclicity in the Main and Upper Zones of the Bushveld Complex, South Africa: crystallization from a Zoned Magma Sheet. Journal of petrology: 1-23.

Tollari, N., Barnes, S.-J., Nabil, H., and Cox, R.A. submitted. Trace elements concentrations in apatites from the Intrusive Suite of Sept-Îles, Canada and the Bushveld Complex, South Africa - Implications for the genesis of nelsonites.

Toplis, M.J., and Carroll, M.R. 1995. An experimental-study of the influence of oxygen fugacity on Fe-Ti oxide stability, phase-relations, and mineral-melt equilibria in ferro-basaltic systems. Journal of Petrology. **36**: 1137-1170.

Toplis, M.J., Libourel, G., and Carroll, M.R. 1994a. The role of phosphorus in crystallization processes of basalt - an experimental-study. Geochimica et Cosmochimica Acta. **58**: 797-810.

Toplis, M.J., Dingwell, D.B., and Libourel, G. 1994b. The effect of phosphorus on the iron redox ratio, viscosity, and density of an evolved ferro-basalt. Contributions to Mineralogy and Petrology. **117**: 293-304.

Usselman, T.M., Hodge, D.S., Naldrett, A.J., and Campbell, I.H. 1979. Physical constraints on the characteristics of nickel-sulfide ore in ultramafic lavas. Canadian Mineralogist. **17**: 361-372.

Visser, W., and Kostervangroos, A.F. 1979a. Effects of P2O5 and TiO2 on liquid-liquid equilibria in the system K2O-FeO-Al2O3-SiO2. American Journal of Science. **279**: 970-988.

Visser, W., and Kostervangroos, A.F. 1979b. Effect of pressure on liquid immiscibility in the system K2O-FeO-Al2O3-SiO2-P2O5. American Journal of Science. **279**: 1160-1175.

Von Gruenewaldt, G. 1993. Ilmenite-apatite enrichments in the Upper Zone of the Bushveld Complex: A major titanium-rock phosphate resource. International Geology Review. **35**: 987-1000.

Von Gruenewaldt, G., Hulbert, L.J., and Naldrett, A.J. 1989. Contrasting platinum-group element concentration patterns in cumulates of the Bushveld Complex. Mineralium Deposita. **24**: 219-229.

Von Gruenewaldt, G., Hatton, C.J., Merkle, R.K.W., and Gain, S.B. 1986. Platinum-group element-chromite associations in the Bushveld Complex. Economic Geology. **81**: 1067-1079.

Wager, L.R. 1960. The major element variation of the layered series of the Skaergaard Intrusion and a Re-estimation of the average composition of the Hidden Layered Series and of the successive residual magmas. Journal of Petrology. **1**: 364-398.

Wager, L.R., and Brown, G.M. 1967. Layered Igneous Rocks. Oliver and Boyd, Edinburgh.

Watson, E.B. 1979. Apatite saturation in basic to intermediate magmas. Geophysical Research Letters. **6**: 937-940.

Watson, T.L. 1907. Mineral resources of Virginia, J. P. Bell Company, Lynchburg.

Wood, M.I., and Hess, P.C. 1977. Role of Al2O3 in immiscible silicate melts. Transactions-American Geophysical Union. **58**: 520-520.

Wood, M.I., and Hess, P.C. 1980. The structural role of Al2O3 and TiO2 in immiscible silicate liquids in the system SiO2-MgO-CaO-FeO-TiO2-Al2O3. Contributions to Mineralogy and Petrology. **72**: 319-328.

CHAPITRE 2

PREDICTING PHOSPHATE SATURATION IN SILICATE MAGMAS AN EXPERIMENTAL STUDY OF THE EFFECTS OF THE MELT COMPOSITION AND TEMPERATURE

N. Tollari, M.J. Toplis, S-J. Barnes, publié dans Geochimica Cosmochimica Acta, 03/06

2.1 RÉSUMÉ

Une série d'expérience a été réalisée à une atmosphère afin de tester l'influence de la teneur en Fer et de l'état d'oxydation sur la saturation en minéraux phosphatés dans des systèmes magmatiques. Le but étant, de connaître et de comprendre qu'elles sont les conditions de saturation en phosphate durant les stades tardifs de la différentiation des intrusions litées mafiques. Quatre compositions avec des contenus en Fer différents ont été utilisées. Les expériences couvrent une gamme de température allant de 1030°C à 1070°C et de fugacité d'oxygène de 1,5 unités log au-dessous, jusqu'à 1,5 unités log au-dessus du tampon Fayalite-Magnétite-Quartz. Les résultats démontrent que ni le contenu en Fer, ni l'état d'oxydation du système joue un rôle significatif sur la saturation en phosphate. D'autre

part, la teneur en SiO_2 et en CaO exerce un contrôle sur l'apparition des minéraux phosphatés. Nous résultats ont été combinés avec ceux de la littérature pour définir une équation qui prédit quelle teneur en P_2O_5 est nécessaire pour saturer, en whitlockite ou apatite, un liquide silicaté :

$$X_{P_2O_5}^{liq-SAT} = \exp\left[\left(T\left\{\frac{-4.653}{123.5 - X_{SiO_2}^{liq}} + 0.1207\right\}\right) - 3.333 \ln\left(X_{CaO}^{liq}\right)\right]$$

Où M représente la concentration molaire et T la température en K. Cette équation est valide à travers un éventail très large de composition et de température (par exemple valable de 10 à 80% molaire de SiO_2), incluant les liquides péralumineux. L'équation est utilisée pour illustrer les effets relatifs de la composition chimique du magma et de la température sur la saturation en phosphate; ceci d'une façon générale, puis, plus particulièrement pour le cas des systèmes ferrobasaltiques. La conclusion est que les liquides magmatiques peuvent atteindrent des concentrations en phosphore et en Fer très élevées avant d'atteindre la saturation en phosphate. Cependant ce processus ne se fera par l'association du Fer ferrique et du phosphore comme prévu à l'origine, mais plutôt par suite des variations des teneurs en SiO_2 et CaO du liquide, qui est une fonction de la différentiation magmatique. Ces résultats peuvent aider à expliquer la pétrogenèse des nelsonites, bien que davantage de travail soit exigé.

2.2 INTRODUCTION

Apatite is a common mineral in many plutonic rocks, ranging from granites (e.g. Bea *et al.*, 1992) to the late stage cumulates of mafic systems (e.g. Wager and Brown, 1967; Von Gruenewaldt, 1993). Furthermore, volatile free phosphates, for example whitlockite, are present in igneous rocks of extraterrestrial origin, such as lunar samples (Griffen *et al.*, 1972) and achondrite meteorites (Delaney *et al.*, 1984; Lundberg *et al.*, 1988). The presence of a crystalline phosphate in such rocks is of interest because it provides a potential constraint on the composition of the liquid with which the minerals were in equilibrium and/or the conditions of temperature and pressure. For example, the work of Watson (1979) and Harrison and Watson (1984) showed that temperature and liquid composition, in particular SiO_2 content, are important factors affecting how much P_2O_5 is required to saturate silicate melts. The model proposed by Harrison and Watson (1984) has been shown to work well for peralkaline and subaluminous granites, although modification is required when predicting apatite saturation in peraluminous compositions (Bea *et al.*, 1992; Pichavant *et al.*, 1992; Wolf and London, 1994). Furthermore, it has been suggested that SiO_2 concentration is not the only compositional factor affecting apatite saturation in granitic systems and that CaO content may also play a role (Bea *et al.*, 1992).

Mafic systems have received less attention than felsic systems, a notable exception being the study of Sha (2000) who considered both apatite and whitlockite saturation in a wide range of liquid compositions at temperatures in the range 1200-1400°C. However, the fact remains that few experimental data exist for phosphate saturation in ferrobasaltic liquids at the temperatures corresponding to the late stage differentiation of layered intrusions such as the Skaergaard (e.g. Wager, 1960) or the Bushveld (Harney and Von Gruenewaldt, 1995) and it is with these systems in mind that the present study was initiated.

One potentially important characteristic of evolved mafic systems is the high FeO* content of the liquids (total iron expressed as FeO) which may reach ~18wt% (Brooks *et al.,* 1991; Toplis and Carroll, 1995), or possibly even more (McBirney and Naslund, 1990). Such high iron contents may affect phosphate saturation because of association of P^{5+} and Fe^{3+} in the liquid (Mysen, 1992; Gwinn and Hess, 1993; Toplis *et al.,* 1994a ; 1994b). For example, the existence of P-Fe^{3+} complexes has been held responsible for the fact that small additions of P_2O_5 dramatically influence the stability field of magnetite (Toplis *et al.,* 1994a). This is also consistent with the general finding that P^{5+} is associated with trivalent cations in silicate liquids, for example, rare earth elements (Ryerson and Hess, 1978), and Al^{3+} (Toplis and Schaller, 1998; Schaller *et al.,* 1999).

A strong interaction of P^{5+} and Fe^{3+} in silicate liquids may therefore retard the saturation of both crystalline phosphates and iron-titanium oxides during magmatic differentiation, leading to extremely high concentrations of Fe and P in the liquid. A further consequence of this interaction may be that once either magnetite or apatite finally appears on the liquidus, the other phase will precipitate in abundance. This in turn may potentially explain the petrogenesis of enigmatic rock-types dominated by apatite and iron-titanium oxides such as nelsonites found at the highest stratigraphic levels of certain layered intrusions and anorthosites (Barnes *et al.,* 2004; Cimon, 1998; Davies et Cawthorn, 1984; Nabil, 2003; Philpotts, 1967; Vermark and Von Gruenewaldt, 1986; Dymek and Owens, 2001).

In order to test the influence of melt composition on phosphate saturation, in particular the role of ferric iron, we have experimentally saturated ferrobasaltic compositions of variable iron content over a wide range of oxygen fugacity (fO_2) at 1 atmosphere. Our new data are combined with the literature data base of liquid compositions

coexisting with crystalline phosphate to construct a predictive model for saturation of apatite ($Ca_5(PO_4)_3(OH, F, Cl)$) and whitlockite ($(Ca, Mg, Fe^{2+})_3(PO_4)_2$) valid over extremely wide ranges of liquid composition. Some applications to natural systems are briefly discussed.

2.3 EXPERIMENTAL APPROACH AND METHODS

2.3.1 Starting materials and compositions studied

The starting materials used for these experiments were synthetic glass powders prepared from mixtures of reagent grade oxides (SiO_2, TiO_2, Al_2O_3, Fe_2O_3, MgO) and carbonates ($CaCO_3$, Na_2CO_3, K_2CO_3). Two different P-free compositions were prepared: SC4, the ferrobasaltic composition studied by Toplis *et al.* (1994a) which contains ~15 wt% FeO*, and SC4-8, a composition which maintains the same relative proportions of all oxides as SC4 with the exception of FeO*, which is present at a level of only ~8 wt% (Table 2. 1). These compositions, representative of natural liquids, were chosen because the phase relations of SC4 are known as a function of temperature and oxygen fugacity (Toplis and Carroll, 1995) and because the effects of adding P_2O_5 have been quantified at 1072°C (Toplis *et al.,* 1994a).

Two different amounts of P_2O_5 (5 and 10 wt%) were added to each base composition to ensure saturation in a crystalline phosphate. Glasses SC4(5) and SC4(10) (where the number in parentheses is the P_2O_5 content) are those whose density was measured by Toplis *et al.* (1994b), while glasses SC4-8(5) and SC4-8(10) were synthesised for this study. The P-free base compositions were prepared in thin-walled platinum crucibles heated above their liquidus in air for 1h.

Table 2. 1: Starting compositions. All concentrations in wt%.

	SC4-B	**SC4-8**
SiO_2	49.5	54.41
TiO_2	4.3	4.80
Al_2O_3	11.5	12.85
FeO*	14.6	8.07
MgO	4.8	5.14
CaO	10.0	10.84
Na_2O	2.9	3.35
K_2O	0.48	0.54

The liquids were quenched by pouring onto a metal plate, then crushed and remelted for another hour to ensure chemical homogeneity. Phosphorous was incorporated as P_2O_5 through addition of NH_4PO_3 (for composition SC4) and H_3PO_4 (for composition SC4-8). The P-bearing compositions were then remelted and crushed two further times. In this way four bulk compositions have been studied, although it should be appreciated that the liquids present at the end of each experiment are variable in composition because of the different phase relations as a function of temperature and fO_2 as detailed below.

2.3.2 Experimental techniques

All experiments were carried out in a vertical rapid quench gas mixing furnace at atmospheric pressure (described by Toplis *et al.,* 1994a).Although working at 1 bar has the drawback that whitlockite rather than apatite crystallizes in this volatile free system it has the advantage that oxygen fugacity may be carefully controlled and monitored, an essential consideration when assessing the effect of ferric iron on phosphate saturation. Oxygen fugacity was controlled using CO-CO_2 gas mixtures (Deines *et al.,* 1974) and measured using a yttrium-stabilised zirconia probe. Experiments were carried out at 4 different fO_2 from 1.5 $\log_{10}$ units below the Fayalite-Magnetite-Quartz buffer (FMQ -1.5) to approximately 1.5 $\log_{10}$ units above (FMQ +1.5), as summarised in Table 2. 2.

For each experiment ~100 mg of starting material was pressed onto a loop of 0.2 mm diameter platinum wire, using polyvinyl alcohol as a binder. Before each formal experiment the Pt loops were presaturated in Fe by equilibration with composition SC4 for 12 hours at 1300°C at the relevant fO_2 before cleaning in warm HF.

Table 2. 2: Cooling history and run products

Run no.	cooling history				Final conditions		Run products
	D1[a] (h)	Ramp[b] (°C/h)	D2[c] (h)	Tf[d] (°C)	$log_{10}fO_2$	ΔFMQ[e]	Phases[f]
FMQ -1,5							
6-sc4-b5	8	3	132	1055	-11.795	-1.51	Wht, Gl, Pl, Ilm,Cpx
6-sc4-b10	8	3	132	1055	-11.795	-1.51	Wht, Gl, Pl, Mt, Ilm, Qtz, LoCaPx
6-sc4-85	8	3	132	1055	-11.795	-1.51	Wht, Gl, Pl, Ilm, Psd, Cpx
6-sc4-810	8	3	132	1055	-11.795	-1.51	Wht, Gl, Pl, Mt, Psd, Qtz, LoCaPx
FMQ -0,5							
7-sc4-b5	8	3	179	1032	-11.186	-0.57	Wht, Gl, Pl, Ilm, Cpx
7-sc4-b10	8	3	179	1032	-11.186	-0.57	Wht, Gl, Pl, Mt, Ilm, Qtz, Cpx
7-sc4-85	8	3	179	1032	-11.186	-0.57	Wht, Gl, Pl, Mt, Ilm, Qtz, Cpx
7-sc4-810	8	3	179	1032	-11.186	-0.57	Wht, Gl, Pl, Mt, Ilm, Qtz, LoCaPx, (Mg,Ca)phos
2-sc4-b5	8	3	86,5	1054	-10.815	-0.51	Wht, Gl
2-sc4-b10	8	3	86,5	1054	-10.815	-0.51	Wht, Gl, Mt, Ilm, Qtz
2-sc4-85	8	3	86,5	1054	-10.815	-0.51	Wht, Gl, Pl, Ilm, Psd, Cpx
2-sc4-810	8	3	86,5	1054	-10.815	-0.51	Wht, Gl, Pl, Mt, Ilm
3-sc4-b5	8	3	72	1075	-10.472	-0.47	Wht, Gl, Pl
3-sc4-b10	8	3	72	1075	-10.472	-0.47	Wht, Gl, Pl, Mt, Qtz
3-sc4-85	8	3	72	1075	-10.472	-0.47	Wht, Gl, Pl, Psd, Cpx
3-sc4-810	8	3	72	1075	-10.472	-0.47	Wht, Gl, Pl, Mt, Ilm, Qtz
FMQ +0,5							
4-sc4-b5	8	3	99	1056	-9.736	0.54	Wht, Gl, Pl, Ilm, Cpx
4-sc4-b10	8	3	99	1056	-9.736	0.54	Wht, Gl, Pl, Mt, Ilm, Qtz
4-sc4-85	8	3	99	1056	-9.36	0.54	Wht, Gl, Pl, Ilm, Qtz, Cpx
4-sc4-810	8	3	99	1056	-9.736	0.54	Wht, Gl, Pl, Mt, Ilm, Cpx, (Mg,Ca)phos
FMQ +1,5							
5-sc4-b5	8	3	82	1056	-8.690	1.58	Wht, Gl, Pl, Mt, Ilm, Qtz, Cpx
5-sc4-b10	8	3	82	1056	-8.690	1.58	Wht, Gl, Pl, Mt, Ilm, Qtz, Cpx, (Mg,Ca)phos
5-sc4-85	8	3	82	1056	-8.690	1.58	Wht, Gl, Pl, Mt, Psd, Qtz, Cpx
5-sc4-810	8	3	82	1056	-8.690	1.58	Wht, Gl, Pl, Mt, Ilm, Qtz, Cpx, (Mg,Ca)phos
FMQ +5,5							
8-sc4-b5	8	3	140,5	1055	-4.950	5.34	Wht, Gl, Pl, Mt, Ilm, Qtz, Cpx

[a] D1: duration above the liquidus to allow the equilibration of the iron redox ratio, before cooling
[b] Ramp: ramp of cooling in degrees Celsius by hour
[c] D2: duration at the final temperature
[d] Tf : final temperature of the experiment
[e] ΔFMQ: represents log fo_2 (experiment)- log fo_2 (FMQ buffer)
[f] phases: Wht, whitlockite; Gl, glass; Pl, plagioclase; Cpx, clinopyroxene; LoCaPx, low-Ca pyroxene; Mt, magnetite-ulvöspinel solid solution; Ilm, ilmenite-haematite solid solution; Psd, pseubroockite-Fe_2TiO_5 solid solution; Qtz, quartz; (Mg,Ca)phos, Mg-rich phosphate.

A Pt basket, to which 4 Pt loops were attached (one for each bulk composition), was suspended in the hot spot of the furnace. The furnace temperature was controlled using a Eurotherm 818 controller and measured by an independent Pt-$Pt_{10}Rh$ thermocouple located less than 1cm from the samples. Thermocouple calibration was checked against the melting point of gold (1064°C). The samples were maintained above their liquidus at 1130°C for 8 hours (D_1) in order to equilibrate the Fe^{3+}/Fe^{2+} ratio of the liquid, then cooled at a constant rate of 3°C/h to the final temperature (1030°C, 1055°C or 1070°C). This temperature was maintained for a duration D_2 to allow equilibration between crystalline phases and coexisting melts (see Table 2. 2). All experimental charges were drop-quenched into water.

2.3.3 Analytical techniques

Quenched samples were lightly crushed and mounted as chips in polished sections for petrographic and electron-microprobe analyses. The electron-microprobe analyses were performed using a Cameca SX100 (Université Henri Poincaré, Nancy, France), operated at 15kV and 15 nA beam current. Standards used were albite for Na and Al, orthoclase for Si and K, hematite for Fe, wollastonite for Ca, olivine for Mg, $MnTiO_3$ for Ti and chloroapatite for P. Counting times of 20s on the peak and 10s on the background were typically employed. Incident-beam diameter was 5 μm on glass (where space permitted) to minimize alkali volatility under the electron beam. A focused beam (1-2 μm) was used in all other cases.

2.3.4 Attainment of equilibrium

At the studied temperatures experiments of bulk composition SC4(5) and SC4(10) contain liquid proportions typically in excess of 50% (Fig. 2. 1a, b), a fact which promotes the rate of solid-liquid reactions. In this respect it may be noted that experiments of similar melt fraction, duration and temperature (Toplis *et al.,* 1994a) were demonstrated to be in equilibrium based upon reversal experiments. Furthermore, in the experiments described here, minerals are generally unzoned (as evidenced from back-scattered electron images) and the standard deviations of multiple analyses on glass and phosphate are typically small (Table 2. 3). All these lines of evidence point to a good approach to equilibrium for these samples. On the other hand, experiments on bulk compositions SC4-8(5) and SC4-8(10) contained considerably less glass, typically on the order of 20%. In these cases some extent of mineral zoning could be observed in backscattered electron images, particularly for pyroxenes (e.g. Fig. 2. 1c) and the standard deviations of multiple analyses of glasses are greater than for the bulk composition SC4, although those of whitlockite remain small (Table 2. 3). However, although the approach to equilibrium at the sample scale would not appear to be as complete for experiments using SC4-8 we have reason to believe that local equilibria between phosphate and adjacent liquid were reached, as discussed further below.

2.4 RESULTS

2.4.1 Phase equilibria

The observed phase relations are listed in Tables 2. 2 and 2. 3 and illustrated in Fig. 2. 1. All experiments contain whitlockite (Wht) and glass (Gl).

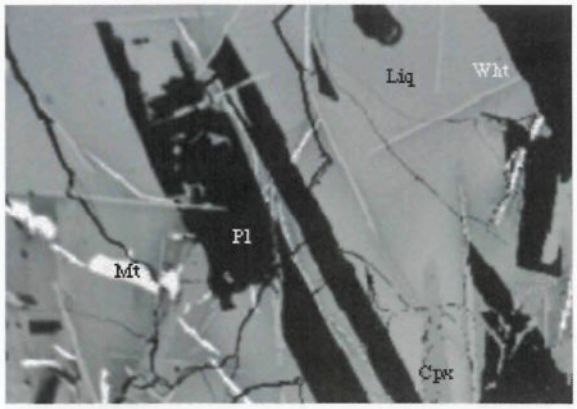

50.µ m

1)

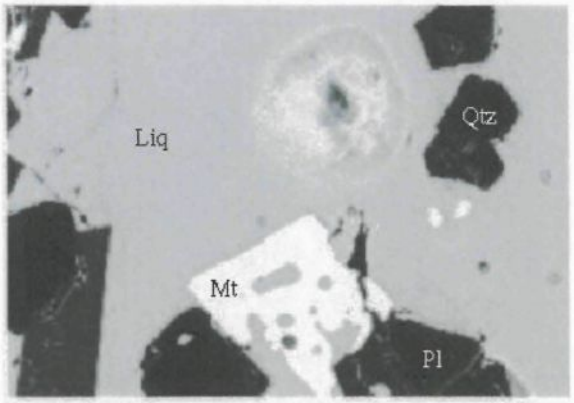

50.µ m

2)

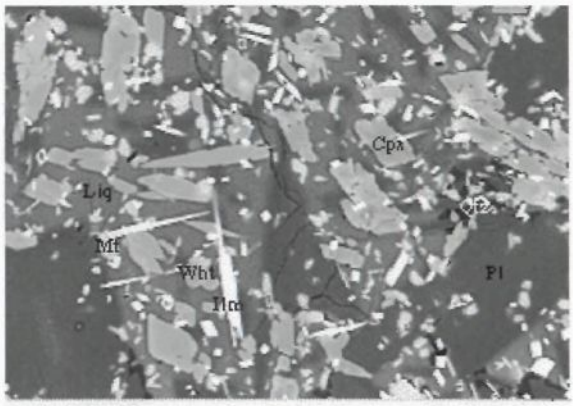

50.µ m

3)

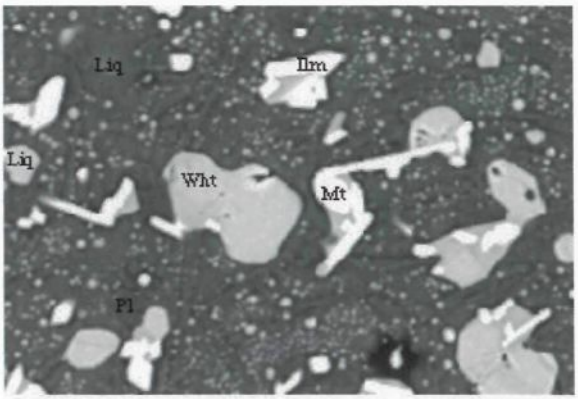

50.µ m

4)

Figure 2. 1. Back-scattered electron images of the FMQ +1.5 run products quenched from 1055°C. 1) sample SC4-B-5: Liq + Wht + Pl + Mt + Ilm + Qtz + Cpx, 2) sample SC4-B-10: Liq + Wht + Pl+ Mt +Ilm + Qtz + Cpx + (Mg,Ca)phos, 3) sample SC4-8-5: Liq + Wht + Pl + Mt + Psd + Qtz +Cpx, 4) sample SC4-8-10: Liq + Wht + Pl + Mt + Ilm + Qtz + Cpx + (Mg,Ca)phos.

Table 2. 3 : Electron microprobe analyses (wt %) of run products

Run no.	Phase[a]	% modal	number of analyses	SiO_2	TiO_2	AL_2O_3	FeO	MgO	CaO	Na_2O	K_2O	P_2O_5	Total
FMQ -1.5													
6-sc4-b5	Wht	5	9	0.18 (0.06)	0.05 (0.02)	0.04 (0.03)	3.80 (0.16)	3.07 (0.08)	47.17 (0.42)	0.25 (0.03)	0.02 (0.01)	44.79 (0.37)	99.37
	Liq	60	8	51.01 (1.22)	3.62 (0.17)	10.51 (0.45)	16.95 (0.64)	2.86 (0.20)	8.65 (0.3)	1.95 (0.12)	0.77 (0.06)	3.06 (0.25)	99.38
	Plag	20	1	57.84	0.15	26.69	0.54	0.17	9.07	5.53	0.28	0.05	100.31
	Ilm	5	1	0.09	52.37	0.19	42.52	3.35	0.23	0.03	0.01	0.01	98.79
	Cpx	10	1	50.71	1.06	1.26	21.99	17.68	6.77	0.07	0.00	0.06	99.59
6-sc4-b10	Wht	8	6	0.32 (0.31)	0.08 (0.03)	0.08 (0.07)	3.83 (0.19)	4.07 (0.10)	44.92 (0.19)	0.20 (0.03)	0.02 (0.01)	43.48 (0.64)	97.00
	Liq 1	25	4	31.56 (1.34)	3.78 (0.18)	7.42 (0.52)	21.30 (0.28)	8.57 (0.48)	10.41 (0.59)	1.12 (0.03)	0.25 (0.03)	14.68 (0.77)	99.09
	Liq 2	25	7	69.19 (0.86)	1.39 (0.1)	13.20 (1.03)	6.17 (0.29)	1.53 (0.14)	2.79 (0.61)	1.08 (0.25)	1.71 (0.14)	1.44 (0.14)	98.49
	Plag	20	1	59.00	0.41	24.68	2.10	0.34	8.64	4.66	0.55	0.41	100.78
	Mt	5	1	0.20	16.46	3.74	71.50	3.31	0.10	0.00	0.02	0.00	95.33
	Ilm	3	1	0.04	44.33	0.59	47.88	3.91	0.61	0.00	0.01	0.04	97.39
	Qtz	8	1	97.50	0.43	2.37	0.44	0.00	0.22	0.27	0.03	0.03	101.29
	Lpx	6	1	52.19	0.65	1.65	22.83	22.64	1.05	0.03	0.00	0.12	101.17
6-sc4-85	Wht	22	5	0.99 (0.39)	0.11 (0.04)	0.27 (0.13)	3.27 (0.15)	3.19 (0.08)	46.70 (0.68)	0.35 (0.02)	0.03 (0.02)	42.92 (0.59)	97.83
	Liq	15	7	72.31 (1.77)	2.02 (0.14)	11.72 (0.28)	4.62 (0.82)	0.90 (0.07)	3.28 (0.51)	0.75 (0.21)	1.24 (0.05)	0.70 (0.37)	97.54
	Plag	20	1	57.20	0.21	26.92	0.89	0.16	10.06	5.19	0.11	0.01	100.75
	Ilm	5	1	0.20	50.78	0.19	41.85	3.90	0.49	0.01	0.04	0.01	97.47
	Psd	8	1	0.13	67.30	1.58	22.39	5.88	0.33	0.02	0.01	0.01	97.65
	Cpx	30	1	50.12	1.57	2.13	17.94	17.22	10.59	0.20	0.02	1.03	100.81
6-sc4-810	Wht	12	8	0.43 (0.27)	0.09 (0.02)	0.10 (0.08)	2.96 (0.12)	4.78 (0.05)	44.55 (0.48)	0.23 (0.04)	0.03 (0.02)	47.01 (0.23)	100.16
	Liq	25	6	71.73 (0.91)	0.95 (0.09)	12.96 (1.08)	3.21 (0.24)	1.12 (0.18)	2.27 (0.64)	1.20 (0.43)	1.35 (0.11)	1.63 (0.41)	96.42
	Plag	30	1	56.07	0.17	26.87	1.34	0.16	9.67	4.87	0.15	0.27	99.57

	Mt	10	1	6.27	5.04	4.95	73.19	4.04	0.72	0.07	0.18	0.38	94.84
	Psd	5	1	3.88	43.28	2.75	39.21	3.24	2.52	0.15	0.05	2.18	97.26
	Qtz	10	1	91.50	0.39	5.41	0.23	0.03	0.90	0.53	0.02	0.02	99.02
	Lpx	8	8	52.10 (1.28)	0.59 (0.20)	2.95 (0.47)	15.17 (0.44)	27.49 (0.63)	1.14 (0.59)	0.04(0.03)	0.03 (0.022)	1.00 (0.69)	100.510
FMQ -0.5													
7-sc4-b5	Wht	12	7	1.42 (1.37)	0.13 (0.06)	0.31 (0.17)	4.33 (0.15)	2.64 (0.12)	45.39 (0.88)	0.26 (0.03)	0.07 (0.05)	45.15 (0.69)	99.70
	Liq	35	6	67.20 (1.92)	1.43 (0.09)	11.46 (0.27)	9.21 (1.49)	0.77 (0.08)	3.98 (0.63)	1.24 (0.19)	1.99 (0.09)	0.70 (0.21)	97.98
	Plag	24	1	59.08	0.18	26.29	0.64	0.14	8.82	5.34	0.25	0.06	100.81
	Ilm	5	1	0.16	48.05	0.28	45.97	1.91	0.32	0.16	0.04	0.00	96.89
	Cpx	24	1	48.55	1.05	1.32	32.20	12.14	4.38	0.09	0.01	0.09	99.83
7-sc4-b10	Wht	30	8	0.16 (0.07)	0.05 (0.01)	0.16 (0.11)	4.66 (0.18)	3.89 (0.06)	44.26 (0.29)	0.20 (0.03)	0.01 (0.02)	45.56 (0.35)	98.96
	Liq1	5	5	12.78 (0.83)	2.17 (0.53)	3.10 (0.24)	22.86 (0.55)	11.14 (0.48)	14.50 (0.48)	0.62 (0.12)	0.14 (0.03)	31.33 (1.02)	98.65
	Liq2	8	7	71.86 (1.47)	0.99 (0.09)	12.85 (0.27)	4.32 (0.25)	0.78 (0.06)	1.43 (0.12)	0.76 (0.06)	2.54 (0.08)	1.22 (0.13)	96.75
	Plag	22	1	57.47	0.11	26.65	1.16	0.07	9.16	5.40	0.35	0.13	100.51
	Mt	7	1	0.15	16.79	4.04	71.85	2.70	0.10	0.02	0.01	0.01	95.67
	Ilm	3	1	0.143	44.631	0.343	47.969	3.134	0.133	0.000	0.000	0.025	96.379
	Qtz	10	1	94.89	0.39	2.57	0.41	0.00	0.23	0.25	0.03	0.07	98.83
	Lpx	20	1	50.63	0.52	1.71	25.28	20.13	0.88	0.02	0.01	0.10	99.27
7-sc4-85	Wht	11	5	0.90 (0.47)	0.14 (0.02)	0.20 (0.10)	2.75 (0.10)	3.49 (0.04)	46.99 (0.65)	0.36 (0.04)	0.04 (0.02)	44.40 (0.27)	99.26
	Liq	14	4	75.96 (4.33)	1.57 (1.17)	10.85 (0.70)	0.57 (0.12)	0.31 (0.18)	2.74 (1.75)	1.27 (0.99)	0.81 (0.81)	1.17 (0.98)	95.25
	Plag	32	4	56.26 (0.47)	0.30 (0.17)	25.36 (1.55)	1.47 (0.35)	0.23 (0.07)	9.88 (0.55)	5.27 (0.18)	0.24 (0.18)	0.51 (0.49)	99.51
	Mt	3	1	0.18	11.63	1.80	77.19	2.46	0.28	0.00	0.04	0.01	93.58
	Ilm	6	1	0.72	51.08	1.10	37.68	3.01	0.42	0.01	0.04	0.00	94.05
	Qtz	5	1	91.84	0.57	3.75	0.37	0.10	0.69	0.44	0.02	0.30	98.07
	Cpx	29	1	51.30	1.05	1.80	19.57	20.26	4.40	0.13	0.07	0.47	99.06

Run no.	Phase[a]	% modal	number of analyses	SiO_2	TiO_2	AL_2O_3	FeO	MgO	CaO	Na_2O	K_2O	P_2O_5	Total
7-sc4-810	Wht	6	7	0.69 (0.37)	0.11 (0.05)	0.22 (0.07)	3.15 (0.08)	4.59 (0.09)	46.00 (0.91)	0.27 (0.04)	0.04 (0.03)	44.00 (0.33)	99.09
	Liq1	30	2	17.65 (3.31)	1.16 (0.15)	4.50 (0.17)	12.10 (0.76)	14.28 (0.55)	17.18 (0.63)	1.34 (0.31)	0.31 (0.12)	33.91 (0.63)	102.42
	Liq2	10	4	71.83 (0.99)	0.78 (0.06)	12.14 (0.63)	2.60 (0.20)	1.35 (0.41)	2.34 (0.89)	1.05 (0.22)	1.82 (0.14)	2.17 (0.54)	96.09
	Plag	30	1	60.55	0.20	23.37	1.36	0.27	8.00	5.16	0.28	0.64	99.81
	Mt	3	1	0.28	6.22	3.80	76.45	3.73	0.38	0.03	0.04	0.00	90.93
	Ilm	5	1	3.18	44.87	3.18	38.69	3.84	1.47	0.15	0.00	1.40	96.77
	Qtz	7	1	86.52	0.34	7.20	0.33	0.06	1.48	1.20	0.08	0.16	97.36
	Lpx	6	4	48.11 (1.36)	2.07 (1.49)	3.49 (0.51)	16.63 (0.84)	24.75 (1.98)	2.37 (1.09)	0.12 (0.14)	0.10 (0.15)	2.55 (0.70)	100.17
	Phmg	3	4	2.27 (1.28)	0.13 (0.02)	0.57 (0.53)	7.23 (0.28)	17.59 (0.51)	26.35 (0.55)	0.14 (0.08)	0.06 (0.02)	45.04 (1.04)	99.38
2-sc4-b5	Wht	5	5	0.48 (0.67)	0.07 (0.04)	0.11 (0.17)	3.03 (0.19)	3.57 (0.15)	47.26 (0.33)	0.39 (0.09)	0.04 (0.05)	44.32 (0.65)	99.28
	Liq	95	8	47.66 (0.38)	4.62 (0.10)	11.18 (0.15)	14.65 (0.15)	4.69 (0.12)	10.17 (0.19)	2.12 (0.18)	0.52 (0.02)	4.63 (0.10)	100.24
2-sc4-b10	Wht	20	12	0.16 (0.08)	0.08 (0.03)	0.08 (0.04)	3.21 (0.09)	4.40 (0.07)	45.60 (0.45)	0.18 (0.04)	0.02 (0.02)	47.32 (1.10)	101.05
	Liq1	35	8	60.28 (2.12)	1.86 (0.10)	13.46 (0.15)	8.53 (0.61)	3.51 (0.35)	5.01 (0.42)	2.33 (0.41)	0.63 (0.06)	3.88 (0.64)	99.49
	Liq2	30	8	40.13 (1.40)	3.10 (0.09)	10.71 (0.43)	15.79 (0.41)	8.20 (0.49)	9.33 (0.26)	1.45 (0.10)	0.20 (0.02)	11.33 (0.86)	100.24
	Mt	10	5	0.12 (0.03)	9.84 (0.22)	5.41 (0.34)	75.22 (1.11)	4.11 (0.16)	0.17 (0.04)	0.02 (0.03)	0.011 (0.01)	0.03 (0.04)	94.93
	Qtz	5	7	96.67 (0.56)	0.44 (0.04)	2.62 (0.23)	0.40 (0.08)	0.01 (0.01)	0.28 (0.02)	0.40 (0.07)	0.03 (0.04)	0.02 (0.03)	100.87
2-sc4-85	Wht	10	9	0.28 (0.06)	0.09 (0.05)	0.08 (0.04)	2.87 (0.15)	3.39 (0.06)	46.57 (0.26)	0.23 (0.03)	0.03 (0.01)	47.36 (0.56)	100.90
	Liq	25	10	66.52 (1.00)	2.92 (0.14)	11.91 (0.28)	7.11 (0.90)	1.80 (0.13)	5.11 (0.34)	2.14 (0.14)	1.01 (0.05)	1.19 (0.15)	99.71
	Plag	30	5	58.15 (0.46)	0.23 (0.04)	25.95 (0.31)	0.64 (0.09)	0.19 (0.03)	9.60 (0.30)	5.40 (0.13)	0.12 (0.03)	0.12 (0.06)	100.39
	Ilm	4	2	0.06 (0.01)	53.03 (0.01)	0.23 (0.02)	39.71 (0.02)	4.79 (0.04)	0.21 (0.00)	0.01 (0.02)	0.01 (0.00)	0 (0)	98.05
	Psd	4	5	0.13 (0.14)	67.37 (0.41)	1.42 (0.12)	24.48 (0.73)	5.14 (0.13)	0.23 (0.02)	0.01 (0.02)	0.02 (0.01)	0.03 (0.04)	98.83
	Cpx	27	4	51.80 (0.89)	1.92 (0.14)	1.96 (0.33)	13.34 (0.91)	20.15 (1.19)	10.79 (1.45)	0.15 (0.02)	0.01 (0.01)	0.39 (0.44)	100.51
2-sc4-810	Wht	10	10	1.07 (1.46)	0.13 (0.11)	0.25 (0.30)	2.56 (0.66)	5.22 (0.68)	44.56 (1.63)	0.24 (0.06)	0.02 (0.03)	46.92 (1.99)	100.97
	Liq1	10	5	22.80 (1.77)	2.02 (0.22)	4.43 (0.37)	12.87 (0.34)	16.62 (0.78)	14.59 (1.42)	0.82 (0.10)	0.08 (0.03)	26.79 (1.31)	101.03

	Liq2	32	7	69.98 (1.68)	1.07 (0.13)	11.89 (0.52)	4.27 (0.71)	2.77 (1.14)	2.90 (0.58)	0.84 (0.25)	1.18 (0.07)	2.27 (0.94)	97.17
	Plag	40	3	60.22 (0.22)	0.38 (0.07)	22.90 (0.79)	1.87 (0.35)	0.88 (0.42)	8.19 (0.28)	4.82 (0.35)	0.38 (0.09)	1.10 (0.60)	100.74
	Mt	3	2	0.16 (0.01)	4.40 (0.14)	4.09 (0.27)	76.14 (1.12)	5.93 (0.16)	0.23 (0.03)	0.00 (0.01)	0.01 (0.01)	0.05 (0.01)	91.01
	Ilm	5	1	0.63	46.21	2.46	42.23	4.11	0.87	0.01	0.05	0.53	97.10
3-sc4-b5	Wht	5	4	0.31 (0.24)	0.07 (0.03)	0.10 (0.12)	3.02 (0.11)	3.68 (0.01)	46.99 (0.33)	0.27 (0.02)	0.01 (0.01)	45.43 (0.94)	99.89
	Liq	80	3	46.65 (0.25)	4.81 (0.11)	10.85 (0.06)	15.42 (0.09)	4.95 (0.60)	10.05 (0.14)	2.12 (0.06)	0.51 (0.02)	4.36 (0.07)	99.71
	Plag	15	4	57.19 (0.23)	0.16 (0.01)	27.28 (0.16)	0.70 (0.07)	0.51 (0.50)	9.91 (0.20)	5.42 (0.13)	0.18 (0.01)	0.06 (0.02)	101.40
3-sc4-b10	Wht	15	10	0.11 (0.04)	0.07 (0.02)	0.08 (0.03)	2.45 (0.20)	5.09 (0.08)	45.49 (0.21)	0.18 (0.02)	0.02 (0.02)	46.43 (0.36)	99.92
	Liq1	15	8	17.52 (0.45)	2.03 (0.09)	4.11 (0.14)	12.04 (0.55)	17.81 (0.46)	15.10 (0.58)	0.81 (0.13)	0.09 (0.03)	29.78 (0.69)	99.28
	Liq2	20	7	66.62 (1.26)	1.08 (0.05)	12.57 (0.18)	4.35 (0.45)	2.25 (0.34)	2.79 (0.52)	0.84 (0.11)	1.43 (0.14)	1.85 (0.59)	93.78
	Plag	35	6	52.86 (0.35)	0.13 (0.01)	26.87 (0.60)	1.46 (0.09)	0.27 (0.13)	10.46 (0.25)	4.84 (0.14)	0.19 (0.01)	0.42 (0.24)	97.50
	Mt	10	5	0.05 (0.02)	21.65 (0.37)	1.27 (0.04)	66.76 (0.59)	3.28 (0.22)	0.29 (0.06)	0.01 (0.01)	0.01 (0.01)	0.01 (0.02)	93.33
	Qtz	5	4	92.15 (0.24)	0.49 (0.03)	2.5 (0.32)	0.41 (0.05)	0.01 (0.02)	0.20 (0.03)	0.26 (0.10)	0.03 (0.01)	0.04 (0.01)	96.10
3-sc4-85	Wht	5	7	1.06 (0.81)	0.12 (0.04)	0.21 (0.18)	2.60 (0.09)	3.67 (0.05)	46.14 (0.38)	0.29 (0.05)	0.02 (0.01)	44.53 (0.63)	98.64
	Liq	36	8	60.00 (1.51)	2.69 (0.15)	11.73 (0.08)	8.13 (0.46)	2.28 (0.17)	5.71 (0.44)	2.06 (0.36)	0.88 (0.07)	1.44 (0.26)	94.93
	Plag	28	4	52.58 (0.63)	0.19 (0.02)	26.32 (0.43)	1.27 (0.17)	0.21 (0.02)	10.27 (0.42)	5.05 (0.19)	0.12 (0.00)	0.13 (0.14)	96.15
	Psd	3	3	3.25 (3.09)	57.89 (1.47)	1.85 (0.30)	29.49 (0.88)	5.02 (0.10)	0.7 (0.18)	0.05 (0.04)	0.06 (0.06)	0.08 (0.04)	98.39
	Cpx	28	3	50.18 (1.01)	1.06 (0.25)	1.63 (0.32)	13.01 (1.03)	23.68 (1.57)	6.95 (1.94)	0.13 (0.08)	0.03 (0.02)	0.13 (0.12)	96.81
3-sc4-810	Wht	6	8	0.19 (0.14)	0.09 (0.04)	0.13 (0.08)	1.83 (0.09)	5.32 (0.07)	45.31 (0.27)	0.20 (0.02)	0.02 (0.01)	45.11 (0.24)	98.18
	Liq1	6	8	21.29 (1.47)	1.74 (0.24)	4.51 (0.39)	10.96 (0.63)	19.09 (1.44)	13.42 (1.24)	0.81 (0.06)	0.08 (0.02)	26.26 (1.19)	98.16
	Liq2	28	8	67.41 (1.16)	1.02 (0.05)	12.51 (0.34)	3.90 (0.15)	2.51 (0.33)	2.85 (0.40)	2.10 (0.67)	1.23 (0.07)	1.78 (0.36)	95.32
	Plag	40	3	53.53 (2.09)	0.17 (0.07)	25.93 (0.77)	1.81 (0.22)	0.52 (0.46)	9.87 (0.27)	5.04 (0.37)	0.12 (0.02)	0.70 (0.70)	97.68
	Mt	5	2	0.10 (0.01)	3.15 (0.09)	4.39 (0.02)	77.46 (0.14)	7.62 (0.07)	0.21 (0.04)	0.03 (0.01)	0.01 (0.02)	0.01 (0.02)	92.98
	Ilm	5	2	0.11 (0.03)	42.34 (0.14)	2.00 (0.00)	45.10 (0.69)	2.95 (0.02)	0.31 (0.03)	0.00 (0.00)	0.01 (0.01)	0.01 (0.01)	92.83
	Qtz	10	3	89.67 (1.68)	0.41 (0.03)	3.80 (0.27)	0.35 (0.09)	0.01 (0.02)	0.42 (0.05)	0.26 (0.05)	0.02 (0.01)	0.04 (0.02)	94.98
FMQ +0.5													
4-sc4-b5	Wht	5	7	0.98 (1.52)	0.07 (0.04)	0.54 (0.74)	3.19 (0.22)	3.46 (0.17)	45.68 (1.51)	0.21 (0.11)	0.02 (0.03)	43.46 (0.77)	97.60

	Liq	65	10	48.98 (1.53)	4.38 (0.18)	11.08 (0.45)	15.43 (0.70)	4.32 (0.19)	9.23 (0.32)	2.09 (0.13)	0.64 (0.04)	3.80 (0.36)	99.94
	Plag	17	1	58.03	0.14	26.63	0.81	0.13	9.36	5.88	0.24	0.03	101.25
	Ilm	3	3	0.03 (0.01)	48.48 (0.92)	0.32 (0.01)	44.55 (0.94)	3.91 (0.33)	0.27 (0.03)	0.01 (0.02)	0.03 (0.03)	0.01 (0.02)	97.61
	Cpx	10	1	52.00	0.80	1.00	23.39	19.16	4.96	0.08	0.02	0.06	101.46
4-sc4-b10	Wht	5	6	0.09 (0.03)	0.04 (0.04)	0.05 (0.02)	3.78 (0.13)	4.02 (0.12)	45.54 (0.37)	0.20 (0.01)	0.00 (0.01)	44.45 (0.51)	98.17
	Liq1	29	8	34.38 (0.46)	3.79 (0.04)	7.80 (0.15)	20.58 (0.25)	8.39 (0.21)	10.31 (0.14)	1.27 (0.04)	0.21 (0.03)	13.16 (0.36)	99.89
	Liq2	29	8	61.22 (1.32)	1.96 (0.06)	13.36 (0.17)	9.33 (0.50)	2.61 (0.38)	4.45 (0.22)	1.52 (0.07)	1.26 (0.06)	3.09 (0.31)	98.80
	Plag	10	1	58.12 (0.13)	0.14 (0.01)	27.04 (0.07)	1.00 (0.06)	0.03 (0.01)	9.71 (0.07)	5.15 (0.70)	0.19 (0.02)	0.12 (0.02)	101.49
	Mt	5	3	0.03 (0.02)	16.44 (0.35)	3.34 (0.03)	71.49 (0.68)	3.64 (0.13)	0.10 (0.05)	0.02 (0.03)	0.00 (0.01)	0 (0)	95.07
	Ilm	2	1	0.83	48.72	1.86	39.45	3.72	0.40	0.02	0.00	0.04	95.03
4-sc4-85	Wht	10	7	0.78 (0.83)	0.12 (0.05)	0.10 (0.13)	3.09 (0.16)	3.33 (0.07)	46.12 (0.50)	0.28 (0.04)	0.03 (0.03)	44.74 (0.68)	98.58
	Liq	30	8	68.27 (1.27)	1.70 (0.06)	11.62 (0.19)	5.47 (0.56)	0.99 (0.10)	3.14 (0.28)	1.73 (0.14)	1.50 (0.06)	0.52 (0.08)	94.95
	Plag	30	4	54.93 (0.85)	0.24 (0.06)	25.63 (0.63)	1.30 (0.26)	0.22 (0.05)	9.57 (0.47)	4.54 (0.13)	0.16 (0.07)	0.09 (0.03)	96.69
	Ilm	5	3	1.62 (0.43)	54.99 (1.19)	1.83 (0.65)	31.41 (2.07)	4.03 (0.90)	0.55 (0.05)	0.10 (0.11)	0.02 (0.02)	0.03 (0.02)	94.58
	Qtz	5	2	90.02 (1.97)	0.61 (0.08)	2.95 (0.05)	0.57 (0.35)	0.06 (0.06)	0.52 (0.15)	0.42 (0.11)	0.06 (0.07)	0.08 (0.08)	95.29
	Cpx	20	3	47.49 (0.15)	1.81 (0.07)	2.48 (0.14)	10.91 (0.43)	19.15 (0.97)	14.33 (1.13)	0.27 (0.06)	0 (0)	0.91 (0.21)	97.34
4-sc4-810	Wht	10	7	0.22 (0.06)	0.09 (0.01)	0.02 (0.04)	2.96 (0.13)	4.79 (0.13)	45.18 (0.41)	0.22 (0.03)	0.02 (0.03)	46.21 (0.29)	99.70
	Liq1	9	8	67.95 (1.92)	1.06 (0.17)	12.05 (1.45)	3.66 (0.17)	1.37 (0.76)	2.57 (1.66)	1.00 (0.46)	1.36 (0.12)	1.93 (1.41)	92.95
	Liq2	20	3	14.17 (1.39)	1.75 (0.28)	3.36 (0.32)	16.65 (0.71)	15.74 (1.85)	14.54 (1.52)	0.71 (0.08)	0.08 (0.01)	32.25 (1.52)	99.23
	Plag	45	2	55.96 (0.20)	0.21 (0.04)	25.07 (0.11)	1.40 (0.05)	0.17 (0.01)	8.77 (0.03)	5.18 (0.01)	0.26 (0.07)	0.43 (0.14)	97.45
	Mt	3	4	1.05 (1.69)	6.72 (0.20)	4.21 (0.22)	76.77 (0.70)	4.13 (0.37)	0.35 (0.15)	0.06 (0.10)	0.02 (0.02)	0.07 (0.06)	93.36
	Ilm	5	1	0.83	48.72	1.86	39.45	3.72	0.40	0.02	0.00	0.04	95.03
	Lpx	5	8	50.03 (0.83)	0.69 (0.13)	3.01 (0.35)	15.29 (1.15)	27.44 (1.15)	0.91 (0.29)	0.04 (0.02)	0.02 (0.02)	0.81 (0.54)	98.23
	Phmg	3	3	0.35 (0.12)	0.10 (0.02)	0.01 (0.01)	6.93 (0.07)	17.95 (0.15)	26.78 (0.13)	0.08 (0.02)	0 (0)	48.24 (0.54)	100.44

Run no.	Phase[a]	% modal	number of analyses	SiO_2	TiO_2	AL_2O_3	FeO	MgO	CaO	Na_2O	K_2O	P_2O_5	Total
FMQ +1.5													
5-sc4-b5	Wht	5	7	0.23 (0.05)	0.07 (0.03)	0.01 (0.03)	3.02 (0.15)	3.46 (0.04)	46.43 (0.36)	0.17 (0.03)	0.01 (0.01)	44.94 (0.33)	98.36
	Liq	10	5	65.09 (1.35)	1.24 (0.10)	11.75 (1.11)	4.93 (0.23)	0.91 (0.09)	3.06 (0.56)	0.71 (0.24)	1.89 (0.17)	0.51 (0.08)	90.09
	Plag	43	5	53.81 (2.18)	0.16 (0.04)	25.25 (0.69)	1.83 (0.11)	0.21 (0.04)	9.84 (0.34)	2.94 (1.26)	0.20 (0.03)	0.20 (0.20)	94.44
	Mt	10	3	0.11 (0.09)	11.00 (0.44)	2.01 (0.14)	76.02 (0.40)	2.66 (0.04)	0.26 (0.11)	0 (0)	0.02 (0.01)	0.01 (0.02)	92.09
	Ilm	2	3	0.10 (0.01)	32.63 (0.31)	0.48 (0.08)	56.56 (0.97)	2.29 (0.08)	0.41 (0.08)	0.01 (0.01)	0.02 (0.02)	0.06 (0.09)	92.55
	Qtz	5	3	84.82 (0.53)	0.57 (0.31)	2.51 (0.41)	0.54 (0.17)	0.02 (0.02)	0.31 (0.09)	0.10 (0.03)	0.01 (0.01)	0.05 (0.08)	88.93
	Cpx	25	3	45.14 (0.24)	1.19 (0.10)	2.46 (0.16)	14.18 (0.70)	19.00 (0.80)	11.34 (0.47)	0.12 (0.03)	0.01 (0.01)	0.45 (0.08)	93.89
5-sc4-b10	Wht	10	9	0.21 (0.12)	0.05 (0.04)	0.15 (0.06)	2.92 (0.21)	4.91 (0.13)	44.72 (0.46)	0.23 (0.03)	0.02 (0.01)	44.02 (0.58)	97.23
	Liq1	10	8	71.59 (1.15)	0.76 (0.04)	12.75 (0.33)	4.09 (0.37)	1.69 (0.26)	2.17 (0.31)	0.88 (0.12)	1.93 (0.10)	1.31 (0.57)	97.17
	Liq2	15	7	18.79 (0.62)	1.62 (0.10)	4.08 (0.20)	14.58 (0.94)	15.83 (0.48)	14.51 (1.27)	0.81 (0.07)	0.14 (0.03)	26.74 (0.74)	97.09
	Plag	25	1	56.38	0.08	27.02	1.17	0.10	9.52	5.41	0.21	0.12	100.00
	Mt	10	3	0.56 (0.76)	9.01 (0.09)	3.98 (0.23)	72 69 (1.03)	5.41 (0.05)	0.29 (0.06)	0.01 (0.02)	0.02 (0.03)	0.02 (0.02)	92.00
	Ilm	5	2	0.05 (0.06)	29.43 (1.3)	0.65 (0.04)	57.41 (1.7)	4.07 (0.27)	0.38 (0.01)	0.02 (0.03)	0.01 (0.02)	0.08 (0.05)	92.10
	Qtz	5	1	96.22	0.29	2.44	0.43	0.03	0.20	0.29	0.07	0.00	99.97
	Lpx	15	3	51.65 (0.64)	0.46 (0.05)	3.24 (0.26)	14.16 (1.76)	28.03 (1.12)	1.18 (0.64)	0.01 (0.01)	0.01 (0.02)	1.07 (0.87)	99.81
	Phmg	5	3	0.42 (0.23)	0.04 (0.03)	0.17 (0.09)	6.86 (0.22)	17.94 (0.22)	26.33 (0.40)	0.06 (0.02)	0.01 (0.01)	45.97 (0.04)	97.80
5-sc4-85	Wht	20	5	1.66 (0.72)	0.09 (0.02)	0.46 (0.33)	2.34 (0.08)	3.74 (0.05)	46.12 (0.25)	0.34 (0.04)	0.02 (0.02)	43.71 (0.79)	98.47
	Liq	7	3	74.34 (0.68)	1.12 (0.67)	11.62 (0.76)	2.60 (0.31)	0.84 (0.15)	2.01 (0.39)	0.56 (0.26)	1.15 (0.07)	0.63 (0.47)	94.87
	Plag	35	3	56.66	0.08	25.98 (1.16)	1.74	0.19 (0.06)	9.34	5.22 (0.47)	0.10	0.15	99.47
	Mt	7	1	2.00	0.03	1.16	0.21	0.06	0.94	0.47	0.03	0.08	0.74
	Psd	3	1	7.41	38.50	2.41	38.13	2.95	0.63	0.12	0.13	0.03	90.30
	Cpx	25	1	51.06	0.43	2.17	14.58	19.54	9.52	0.25	0.01	1.34	98.89
5-sc4-810	Wht	12	7	0.51 (0.39)	0.10 (0.02)	0.15 (0.11)	2.78 (0.21)	4.69 (0.33)	44.96 (0.76)	0.25 (0.06)	0.02 (0.02)	44.39 (0.53)	97.83
	Liq1	10	3	6.71 (0.43)	1.26 (0.59)	1.29 (0.12)	12.98 (0.60)	17.72 (0.58)	17.85 (0.83)	0.79 (0.14)	0.04 (0.01)	38.52 (0.90)	97.15

	Liq2	8	6	72.18 (1.43)	0.93 (0.08)	12.47 (0.68)	3.16 (0.17)	1.42 (0.33)	2.55 (0.77)	0.94 (0.19)	1.41 (0.07)	2.35 (0.80)	97.40
	Plag	40	1	54.53	0.04	25.23	1.62	0.70	8.65	5.45	0.14	1.72	98.07
	Mt	5	1	6.12	2.50	6.15	69.77	4.69	1.28	0.17	0.03	0.40	91.09
	Ilm	8	1	0.83	38.15	2.46	40.81	3.42	0.55	0.00	0.01	0.16	86.40
	Qtz	10	1	92.74	0.38	4.06	0.21	0.01	0.46	0.35	0.01	0.05	98.28
	Lpx	8	2	53.03 (1.62)	0.69 (0.05)	2.92 (0.03)	13.78 (0.23)	28.30 (0.10)	0.72 (0.05)	0.03 (0.02)	0.03 (0.03)	0.54 (0.33)	100.04
	Phmg	4	2	0.84 (0.68)	0.08 (0.04)	0.19 (0.17)	6.27 (0.09)	18.45 (0.07)	26.26 (0.34)	0.11 (0.02)	0.01 (0.01)	45.92 (0.55)	98.13
FMQ +5.5													
8-sc4-b5	Wht	15	5	1.01 (0.67)	0.12 (0.03)	0.27 (0.28)	1.43 (0.14)	4.36 (0.05)	47.90 (0.29)	0.31 (0.04)	0.04 (0.01)	44.26 (1.04)	99.70
	Liq	5	3	74.75 (0.72)	1.20 (0.19)	11.61 (0.81)	2.99 (0.24)	1.30 (1.00)	2.54 (0.19)	1.28 (0.23)	1.64 (0.13)	0.61 (0.37)	97.91
	Plag	40	1	65.72	3.49	10.22	9.79	0.96	2.39	2.44	1.94	1.03	97.99
	Mt	13	1	0.14	17.95	0.83	66.70	3.83	0.33	0.00	0.01	0.04	89.83
	Ilm	7	1	2.99	41.02	2.03	42.63	3.51	0.66	0.02	0.08	0.27	93.20
	Qtz	5	1	86.22	0.59	5.24	1.13	0.21	2.41	0.88	0.07	1.02	97.76
	Cpx	15	1	57.95	1.15	5.74	6.08	13.46	14.38	0.38	0.43	0.83	100.39

[a] abbrevations used for the phases: Wht. whitlockite; liq. liquid; Pl. plagioclase; Cpx. clinopyroxene; Lpx. low-Ca pyroxene; Mt. magnetite-ulvöspinel solid solution; Ilm. ilmenite-haematite solid solution; Psd. pseubroockite-Fe_2TiO_5 solid solution; Qtz. quartz; Mgph. Mg-rich phosphate.

[b] numbers in parantheses indicate the ecartype.

In experiments with additions of 10 wt% P_2O_5 (but not in experiments with additions of 5 wt% P_2O_5) two coexisting liquids occur, an observation consistent with the fact that P is known to promote liquid-liquid immiscibility in silicate systems (e.g. Visser and Koster van Groos, 1979). Although the high bulk P_2O_5 concentration in these experiments precludes any direct implications for natural systems, immiscibility has the consequence that liquid compositions are extremely variable as detailed below. In addition to liquid(s) and whitlockite, a wide range of other silicate, oxide and phosphate minerals occur in these experiments. Because the exact compositions and nature of these other phases are not of primary importance in the context of the present study, the number of analyses of each is commonly restricted (Table 2. 3). Furthermore, it is also possible that certain phases were present in the experimental charges but not described, for example, because they were low in abundance and did not intersect the surface exposed for electron microprobe analysis. However, several broad generalisations can be made concerning the phase relations of the studied compositions. Crystalline silicates are ubiquitous, notably plagioclase (Pl) and at least one pyroxene, either high-Ca clinopyroxene (Cpx) or low-Ca pyroxene (LoCapx). The latter are more common at low oxygen fugacity and high P_2O_5, an observation consistent with the results of Toplis *et al.* (1994a). In addition a large number of the experiments contained quartz, generally those with additions of 10 wt% P_2O_5. This observation is consistent with the strong increase in the activity coefficient of Si caused by the incorporation of P in silicate melts (e.g. Kushiro, 1975; Gan and Hess, 1992; Toplis *et al.*, 1994a). Three different Fe-Ti oxides are described in our experiments; magnetite-ulvöspinel solid solution (Mt), ilmenite-haematite solid solution (Ilm), and pseudobrookite-Fe_2TiO_5 solid solution (Psd). Finally, in addition to whitlockite, certain experiments,

particularly those with the highest P contents, crystallise the Ca-Mg phosphate Stanfieldite ($Ca_3Mg_3(PO_4)_4$; Huminicki and Hawthorne, 2002).

2.4.2 Variability of liquid composition

The range of glass compositions observed in this study is extremely wide, covering 10-75 wt% SiO_2, 0.5-20 wt% FeO*, and 0.2-40 wt% P_2O_5 (Table 2. 3). Before interpreting these values, it is of interest to consider the internal variability of liquid composition within individual experimental charges (in particular for experiments using SC4-8 where the proportion of liquid was low, as mentioned above). First of all we note that the spread in composition between different experiments is much greater than within a single charge, as illustrated in Fig. 2 for the case of P_2O_5 in experiments using compositions SC4-8(5) and SC4-8(10). Even so, in experiments with two liquids the range in P_2O_5 concentration in the P-rich glass can reach up to 10 wt% (Fig. 2. 2b), although in terms of relative variability this remains on the order of ±15% and in this respect is no worse than the P_2O_5-poor glass. We also find that average P_2O_5 concentration shows no continuous trend as a function of fO_2 (Fig. 2. 2a) and that the difference in composition of coexisting liquids is greater at higher oxygen fugacity (Fig. 2. 2b), an observation consistent with the results of Naslund (1983).

Detailed analysis of the spread of liquid composition within a given experimental charge shows that the variability of P_2O_5 concentration is systematically correlated with several other compositional parameters. For example, in experiments with a single glass (e.g. bulk composition SC4-8(5)) the P_2O_5 content is inversely correlated with concentration of SiO_2 and positively correlated with that of FeO* and CaO (Figs. 2. 3a-c).

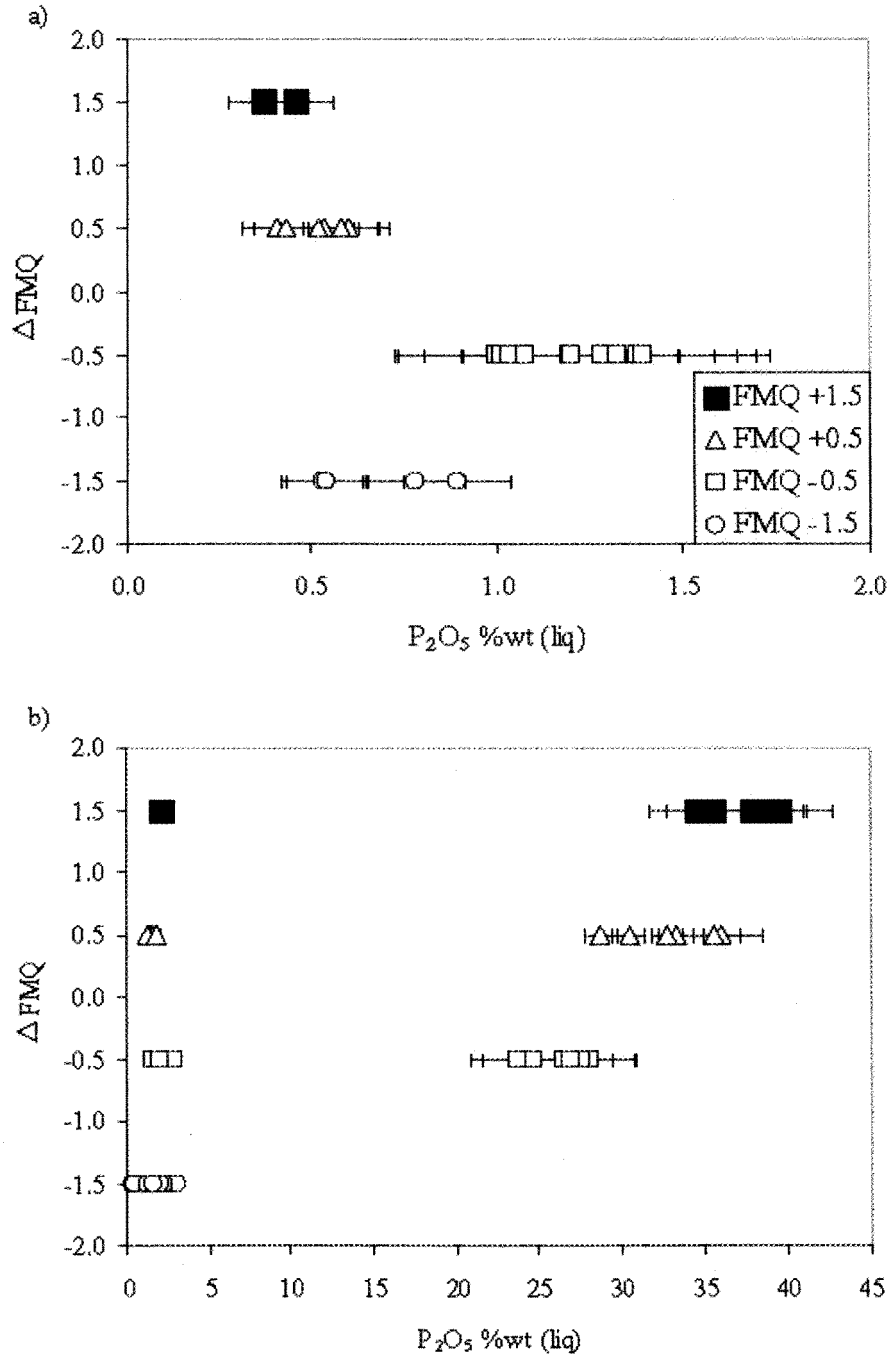

Figure 2. 2. P_2O_5 content in the glass (liquid) as a function of fO_2 in experiments performed at 1055°C. Fig. 2. 2a) composition SC4-8-5; Fig. 2. 2 b) composition SC4-8-10.

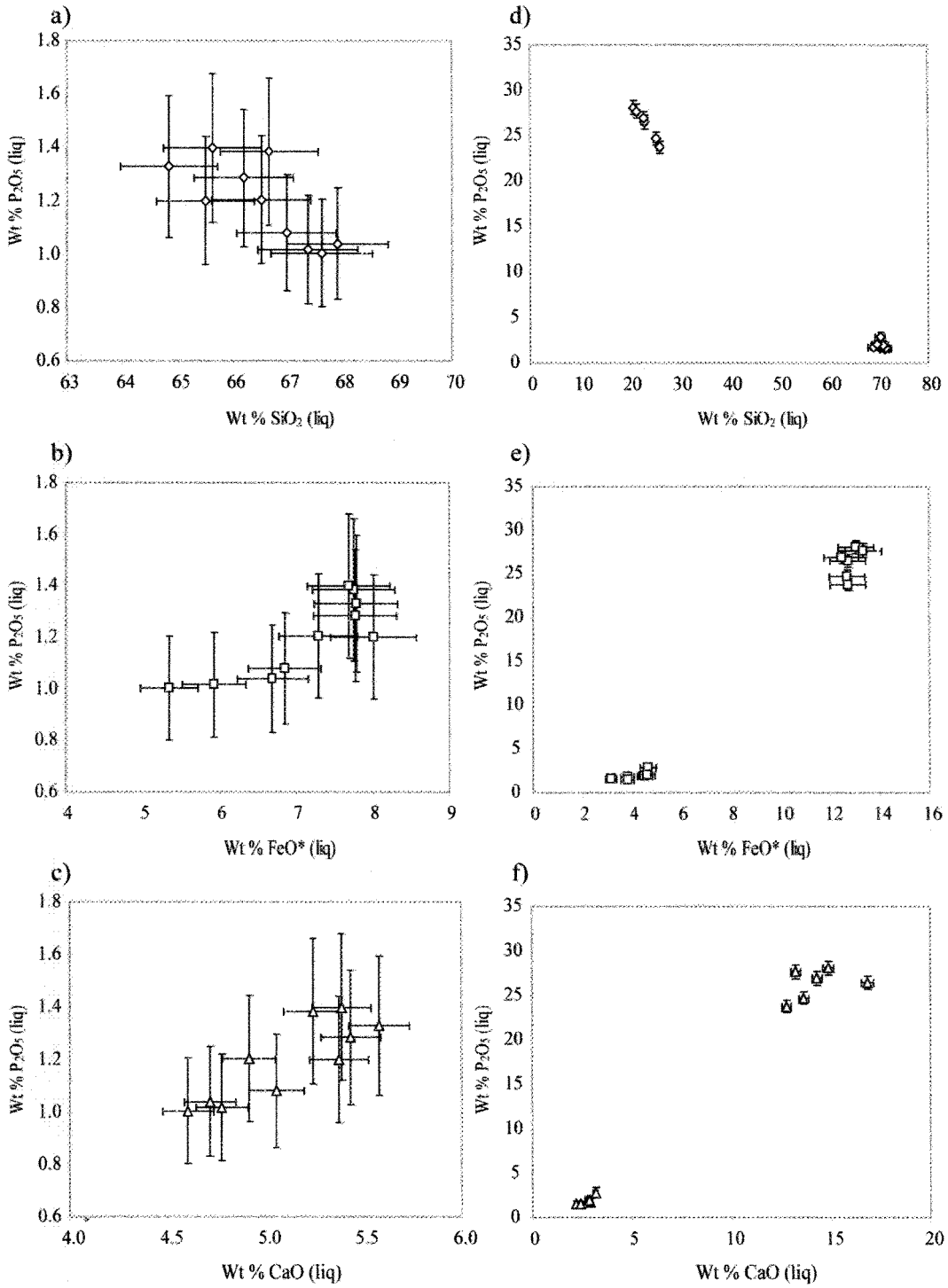

Figure 2. 3. SiO_2, and FeO* and CaO concentrations as a function of P_2O_5 in liquids of experiments 2-SC4-8-5 (Figs. 2. 3a, b, c) and 2-SC4-8-10 (Figs. 2. 3d, e, f) (experiments performed at 1055°C and ΔFMQ -0,5).

Exactly the same trends are observed in experiments with coexisting liquids (Figs. 2. 3d-f), both within each individual liquid (most prominent for the P-rich endmember) but also when comparing the P-rich and P-poor glasses. The systematic nature of these correlations, in particular the fact that the variability within one of the endmembers is identical to that observed between coexisting glasses, leads us to conclude that all liquids had reached local equilibrium with whitlockite in our experiments. For this reason, for the data treatment described below we have chosen to consider each individual analysis of liquid composition rather than averages for each experimental charge.

2.5 DISCUSSION

2.5.1 The influence of individual melt components on whitlockite saturation

- The effect of iron -

To test the hypothesis that Fe content may affect phosphate saturation, the P_2O_5 and FeO* concentrations of our liquids at 1055°C have been compared (Fig. 2. 4). Even though there is a reasonable positive correlation between these two parameters at fixed oxygen fugacity (e.g. Fig. 2. 3b, e), when all the data are considered they do not define a single trend (Fig. 2. 4), the scatter being particularly large for the bulk compositions with additions of 10 wt% P_2O_5 (Fig. 2. 4b).

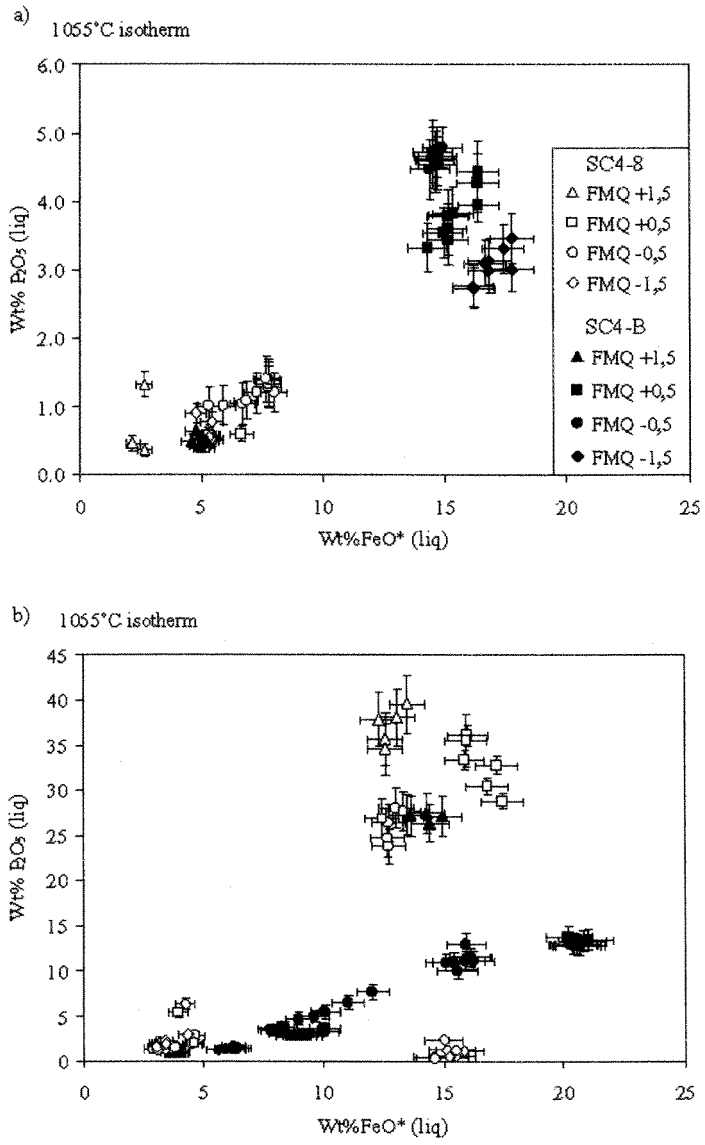

Figure 2. 4. Covariation of weight percent (wt%) P_2O_5 and wt% FeO* of phosphate saturated liquids at 1055°C. Fig. 2. 4 a) bulk compositions with 5 wt% P_2O_5. Fig.2. 4 b) bulk compositions with 10 wt% P_2O_5. Experiments at different oxygen fugacities are distinguished as shown in the key.

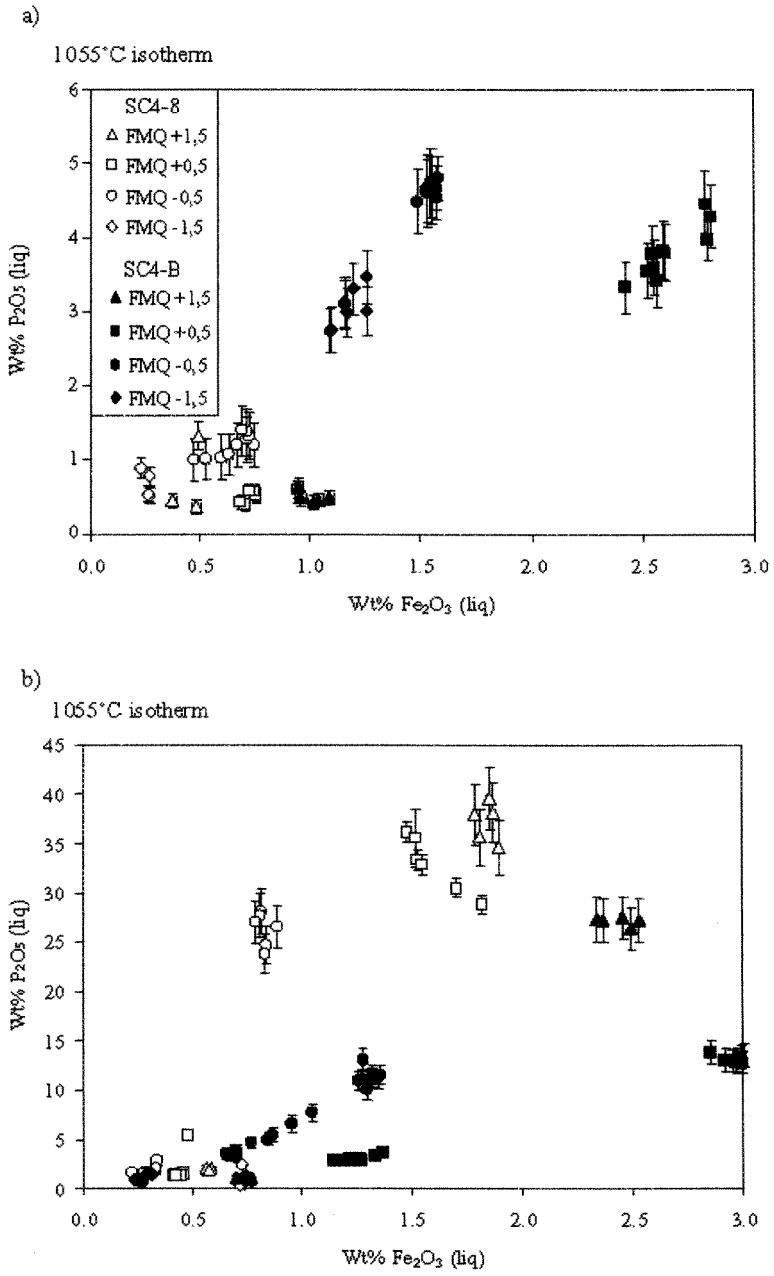

Figure 2. 5. Covariation of wt% P_2O_5 and calculated wt% Fe_2O_3 of phosphate saturated liquids at 1055°C. Fig. 2. 5 a) bulk compositions with 5 wt% P_2O_5. Fig. 2. 5 b) bulk compositions with 10 wt% P_2O_5. Experiments at different oxygen fugacities are distinguished as shown in the key.

However, such dispersion may be expected if it is ferric iron, rather than FeO*, which can stabilise P in the liquid. The Fe_2O_3 concentrations of each liquid have therefore been estimated using the calculation scheme of Kilinc *et al.* (1983), with an additional term for the effect of P_2O_5 taken from Toplis *et al.* (1994b). However, even when P_2O_5 and Fe_2O_3 concentrations in the liquids are compared no single trend is apparent (Fig. 2. 5) and there is a similar level of scatter to that observed for FeO*. It would therefore appear that ferric iron is not the dominant factor controlling phosphate stability and we conclude that some other characteristic(s) of melt composition must be considered to explain the observed variation of the P_2O_5 content of whitlockite saturated liquids.

- The effect of silica -

Previous experimental studies have concluded that the SiO_2 content of the liquid is one of the dominant factors affecting saturation of crystalline phosphates (Watson, 1979; Harrison and Watson, 1984; Sha, 2000). Our liquids cover a range of SiO_2 content even wider than those of previous studies and we too find that there is a good first order correlation of P_2O_5 and SiO_2, independent of oxygen fugacity and temperature (Fig. 2. 6a). In SiO_2-poor liquids, P_2O_5 contents are highest, but the covariation of P_2O_5 and SiO_2 is non-linear, with P_2O_5 concentration flattening off at high SiO_2 (Fig. 2. 6a). However, when one considers the data in detail it is apparent that at constant SiO_2 content there is considerable variation of P_2O_5 concentration. For example, at 50 wt% SiO_2, P_2O_5 ranges from 3 to 7 wt%, while at 70 wt% SiO_2, P_2O_5 ranges from 0.5 to 3 wt%. Furthermore, the data from experiments without immiscibility appear to define a different trend from data in experiments showing immiscibility.

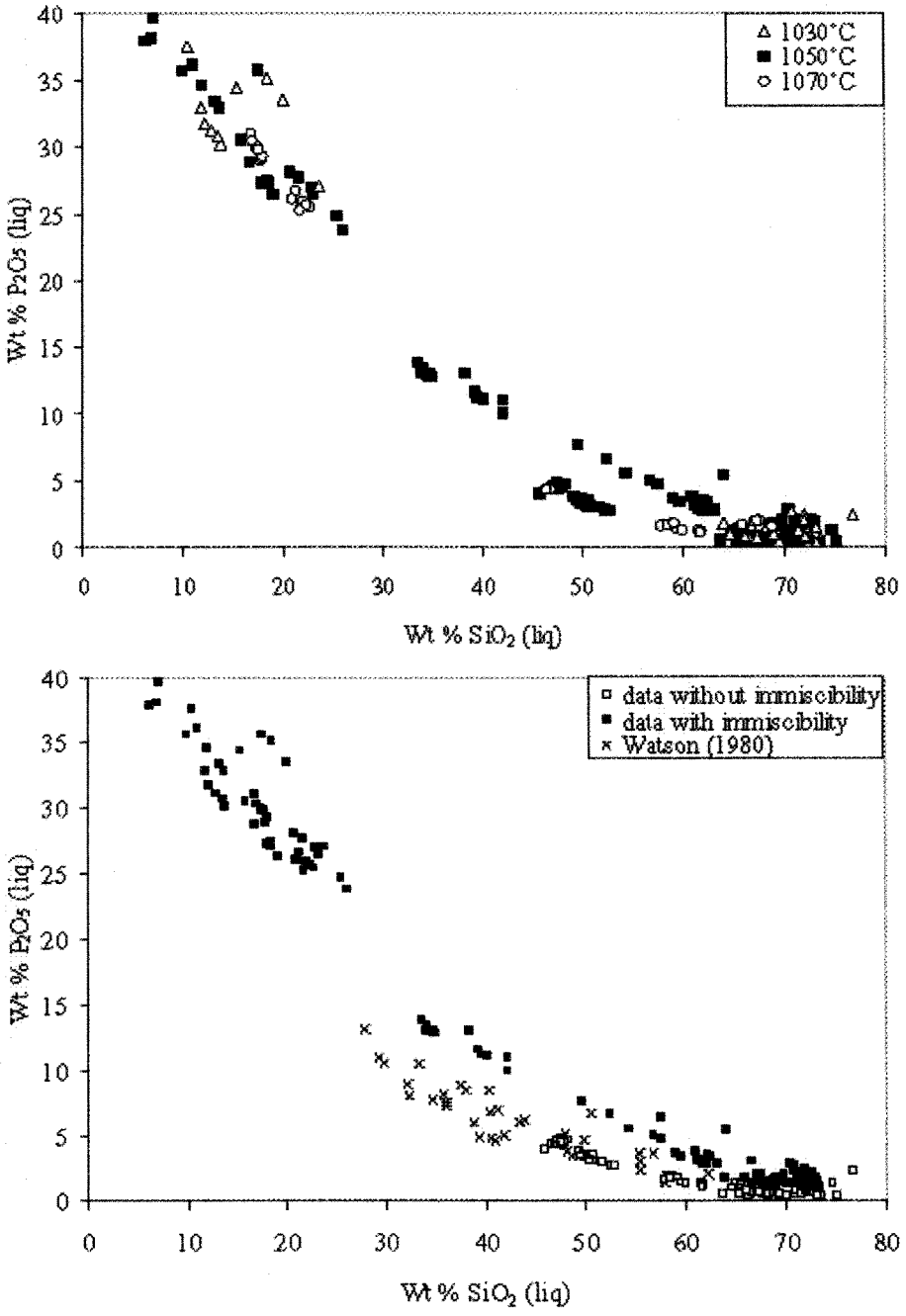

Figure 2. 6. Covariation of wt% P_2O_5 and wt% SiO_2 of phosphate saturated liquids. Liquids distinguished by temperature (Fig. 2. 6a) and by the presence or absence of immiscibility (Fig. 2. 6b).

The experiments without immiscibility are systematically lower in P-content at a given SiO_2 content (Fig. 2. 6b). The data of Watson (1979) generally overlap the trend defined by experiments containing only one liquid (Fig. 2. 6b). This is consistent with the fact that no immiscibility was described in those experiments, but is in spite of the fact that liquids of that study were saturated in apatite (rather than whitlockite) and that experiments were performed over a range of temperatures. In conclusion, even though SiO_2 content of the liquid would appear to influence phosphate saturation, the dispersion in the data leads us to infer that it is not the only factor.

- The effect of calcium -

Calcium is an essential constituent of both whitlockite and apatite and from a thermodynamic perspective the concentration of CaO may be expected to affect the saturation of these minerals. Our data show that concentrations of P_2O_5 and CaO in whitlockite saturated liquids are indeed very well correlated, increasing CaO content resulting in a highly non-linear increase of the quantity of P_2O_5 necessary to crystallise whitlockite (Fig. 2. 7). For example, for the samples without immiscibility, approximately 1 wt% P_2O_5 is necessary to saturate in whitlockite at 5 wt% CaO, while ~4.5 wt% is necessary at 10 wt% CaO (Fig. 2. 7). However, as for the case of SiO_2 previously described, the data from experiments without immiscibility define a distinct trend from data in experiments showing immiscibility, the experiments without immiscibility containing less P_2O_5 at saturation at a given CaO content (Fig. 2. 7).

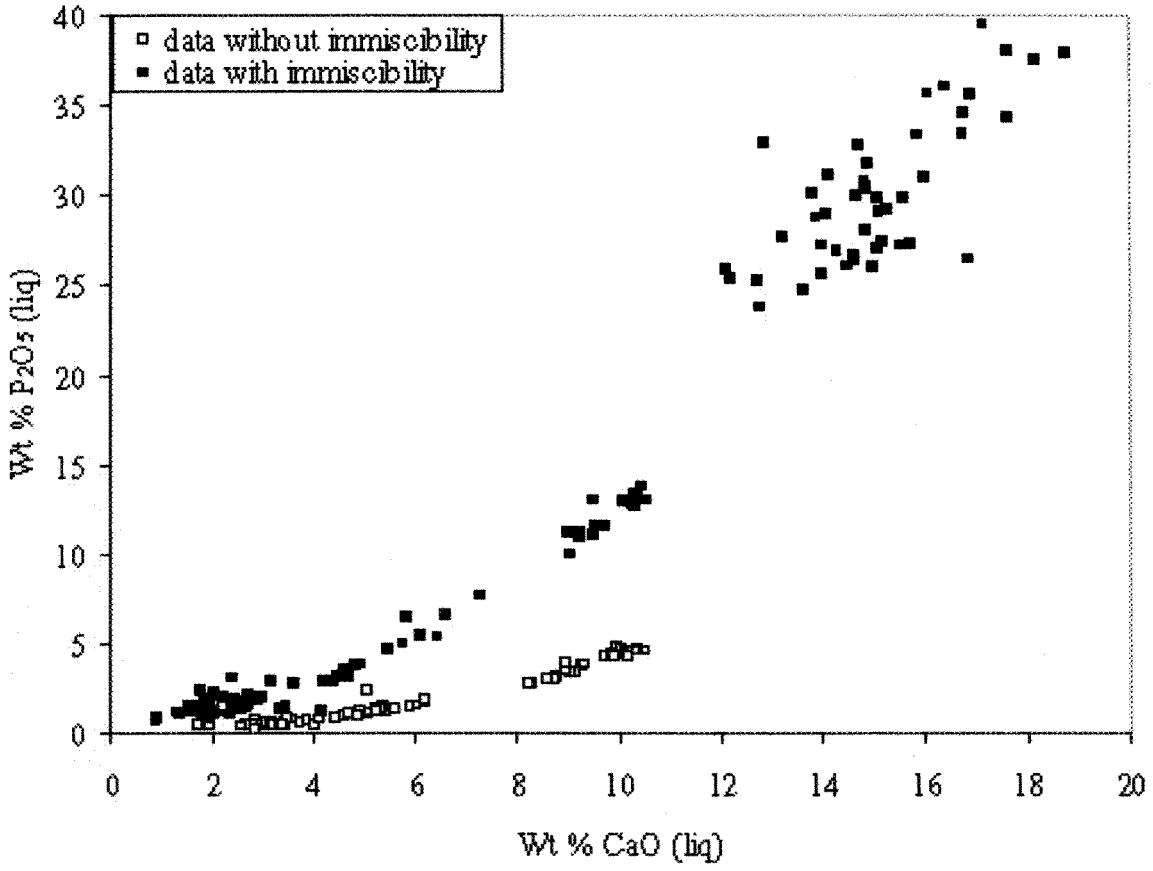

Figure 2. 7. Covariation of wt% CaO and wt% P_2O_5 in liquids at 1055°C in experiments with and without immiscibility.

2.5.2 Development of an equation to predict phosphate saturation

- Whitlockite saturation at fixed temperature -

An alternative approach to understanding the saturation of a crystalline phosphate from silicate liquids is to employ the principles of equilibrium thermodynamics, in particular the notion of an equilibrium constant (or solubility product), as detailed below. In passing we note that although the use of solubility products is widespread when describing crystallization from aqueous solutions, it is uncommon for equilibria involving silicate melts. However, this approach has been shown to be successful in rationalising solubility data for various minerals such as columbite, hafnon and zircon in granitic liquids (Linnen and Keppler 1997; 2002).

If we consider the simplified case of saturation of tricalcium phosphate (Mg-, Fe-free whitlockite), one may write the equation:

$$Ca_3(PO_4)_2^{TCP} = 3CaO^{liq} + P_2O_5^{liq} \qquad (1)$$

The equilibrium constant (K) of this reaction, which should be constant at fixed temperature, may be defined in terms of thermodynamic activities (a) in the following way:

$$K_{Ca_3(PO_4)_2} = \left(a_{CaO}^{liq}\right)^3 \times \left(a_{P_2O_5}^{liq}\right) \Big/ \left(a_{Ca_3(PO_4)_2}^{TCP}\right) \qquad (2)$$

For liquids saturated in pure tricalcium phosphate at fixed temperature, the activity of $Ca_3(PO_4)_2$ may be defined as unity, thus, expanding the activities in equation 2 in terms of mole fraction (X) and activity coefficient (γ) one obtains:

$$K_{Ca_3(PO_4)_2} = \left(X_{CaO}^{liq}\right)^3 \times \left(X_{P_2O_5}^{liq}\right) \times \left(\gamma_{CaO}^{liq}\right)^3 \times \left(\gamma_{P_2O_5}^{liq}\right) \qquad (3)$$

Quantitative application of this equation to our data is potentially compromised by two factors. The first is that the activity coefficients of CaO and P_2O_5 in silicate liquids show complex variations as a function of liquid composition (*e.g.* Libourel, 1999; Toplis and Schaller, 1998) which will be difficult to model and predict with current thermodynamic models of silicate liquids (Ghiorso et al., 1983). The second is that the phosphates in our experiments are Mg, Fe-bearing whitlockites rather than pure tri-calcium phosphate, thus it cannot be assumed that the activity of $Ca_3(PO_4)_2$ is unity.

Concerning the first of these points, the fact that activity coefficients are variable is best illustrated by coexisting immiscible liquids for which the thermodynamic activity of a given oxide component is the same in each liquid, but molar percents may be very different (Table 2. 1). Indeed, if we consider only the terms in concentration in equation 3 and calculate $K_{M\text{-}whit}$ for each of our whitlockite saturated liquids:

$$K_{M-Whit} = \left(M_{CaO}^{liq}\right)^3 \times \left(M_{P_2O_5}^{liq}\right) \qquad (4)$$

where M is the mole percent of the relevant oxide in the liquid (scale from 0 to 100), we find a variation in $K_{M\text{-}whit}$ of almost five orders of magnitude, in turn implying the same

variability in the product of activity coefficients (c.f. equation 3). However, despite this wide range, $K_{M\text{-}whit}$ is found to be a systematic function of the SiO_2 mole percent of the liquid (Fig. 2. 8). Of particular note is the fact that data from systems showing immiscibility and those not showing immiscibility define the same trend. The scatter is somewhat greater at high SiO_2 content, but remains of the same order of magnitude as uncertainties propagated from the electron microprobe analyses of CaO and P_2O_5.

To account for the influence of Mg and Fe on the activity of $Ca_3(PO_4)_2$ in our experimental phosphates we have tested various cation mixing models. However, none of these attempts provided a significantly better correlation than that observed in figure 2. 8. We thus conclude that even though the activity of $Ca_3(PO_4)_2$ is clearly not unity for the phosphates in our experiments, to a first approximation it may be assumed to be a constant. From a practical point of view the trend shown in figure 2. 8 provides a simple and powerful way to describe the compositional characteristics of our whitlockite saturated silicate liquids at 1055°C. This trend may be described by the equation:

$$\ln\left[\left(M_{CaO}^{liq}\right)^3 x\left(M_{P_2O_5}^{liq}\right)\right] = -0.0015\left(M_{SiO_2}^{liq}\right)^2 - 0.0052\left(M_{SiO_2}^{liq}\right) + 12.147 \qquad (5)$$

Mole percentages rather than mole fractions have been used here to underline the fact that although this equation is based upon the thermodynamic formalism presented above, it is not a rigorous thermodynamic expression.

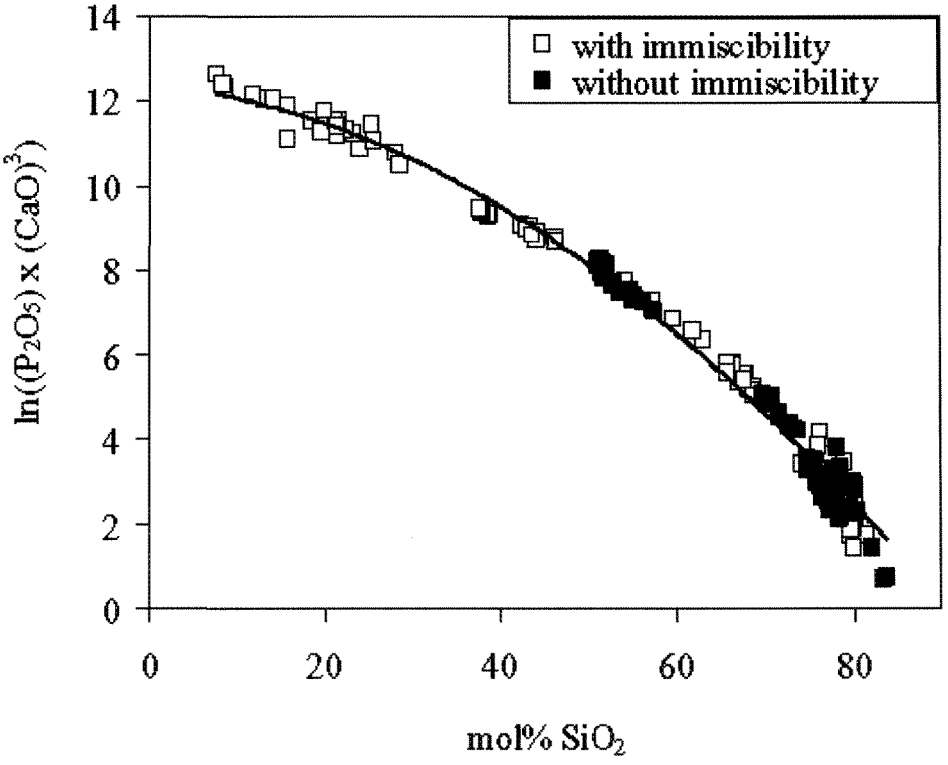

Figure 2. 8. Variation of $\ln(K_{M\text{-}Whit})$ for whitlockite saturated liquids at 1055°C (see text for details) as a function of mole% SiO_2 assuming no effect of substitutions of Mg and Fe for Ca (see text for details). Error bars are typically smaller than the size of the symbols.

The simplicity of equation 5, which requires no knowledge of how liquid composition, liquid structure and activity coefficients of CaO and P_2O_5 are related, is somewhat surprising. Indeed, it may be argued that a trend is observed in figure 2. 8 because all our experiments are multiply saturated in other mineral phases (*e.g.* systematic presence of plagioclase and a calcium-bearing pyroxene) which thus controls or at least limits the thermodynamic activities of silica and/or lime in our liquids. Below we will therefore apply the formalism developed above to experimental data from the literature which are not necessarily multiply saturated, including extension to apatite saturated liquids.

- Extension to apatite -

Apatite rather than whitlockite is the most abundant phosphate in terrestrial rocks, thus it is of interest to assess to what extent the compositional controls on apatite saturation are the same as those observed for whitlockite (c.f. figure 2. 6). In the case of apatite, the solubility product may be written:

$$K_{Ca_5(PO_4)_3(F,Cl)} = \left(a^{liq}_{CaO}\right)^5 \times \left(a^{liq}_{P_2O_5}\right)^{1.5} \times \left(a^{liq}_{F,Cl}\right) / \left(a^{apatite}_{Ca_5(PO_4)_3(F,Cl)}\right) \qquad (6)$$

Comparison of equations 2 and 6 shows that apatite saturation differs from that of whitlockite because of the presence of volatiles in the former, and because the Ca/P ratio of the crystal is different. Concerning the presence of volatiles, for the present purposes we will consider only experimental data in which liquids were saturated in flourapatite by dissolution (Watson, 1979; Sha, 2000). In this case the activity of halogens in the liquid can

be considered approximately constant, and thus should not affect the variation of the equilibrium constant as a function of melt composition. In an analogous way to $K_{M\text{-}whit}$ we define the parameter $K_{M\text{-}apatite}$, expressed as:

$$K_{M-Apatite} = \left(M^{liq}_{CaO}\right)^5 \times \left(M^{liq}_{P_2O_5}\right)^{1.5} \qquad (7)$$

The different stoichiometry of apatite and whitlockite (i.e. the different Ca/P) has the consequence that the absolute values of $K_{M\text{-}apatite}$ and $K_{M\text{-}whit}$ cannot be directly compared. One solution to this problem is to use a common basis for all liquid compositions irrespective of the crystalline phosphate in which they are saturated (i.e. consistent use of either $K_{M\text{-}apatite}$ or $K_{M\text{-}whit}$ for all liquids). In this way it may be assessed whether liquid compositions saturated in these two different phosphates are comparable or not. For this comparison we require data for whitlockite and apatite saturated liquids at the same temperature. The literature data for flourapatite saturated liquids which cover a wide range of SiO_2 content (Watson, 1979) are generally at higher temperature than our experiments. On the other hand, the data of Watson (1979) for flourapatite saturated liquids at 1200°C may be compared with those of Sha (2000) for whitlockite saturated liquids at the same temperature (Fig. 2. 9). This comparison of values of $K_{M\text{-}apatite}$ shows that a single trend is apparent as a function of SiO_2 content which, furthermore, shares many features of the trend defined by our data at lower temperature, as discussed further below.

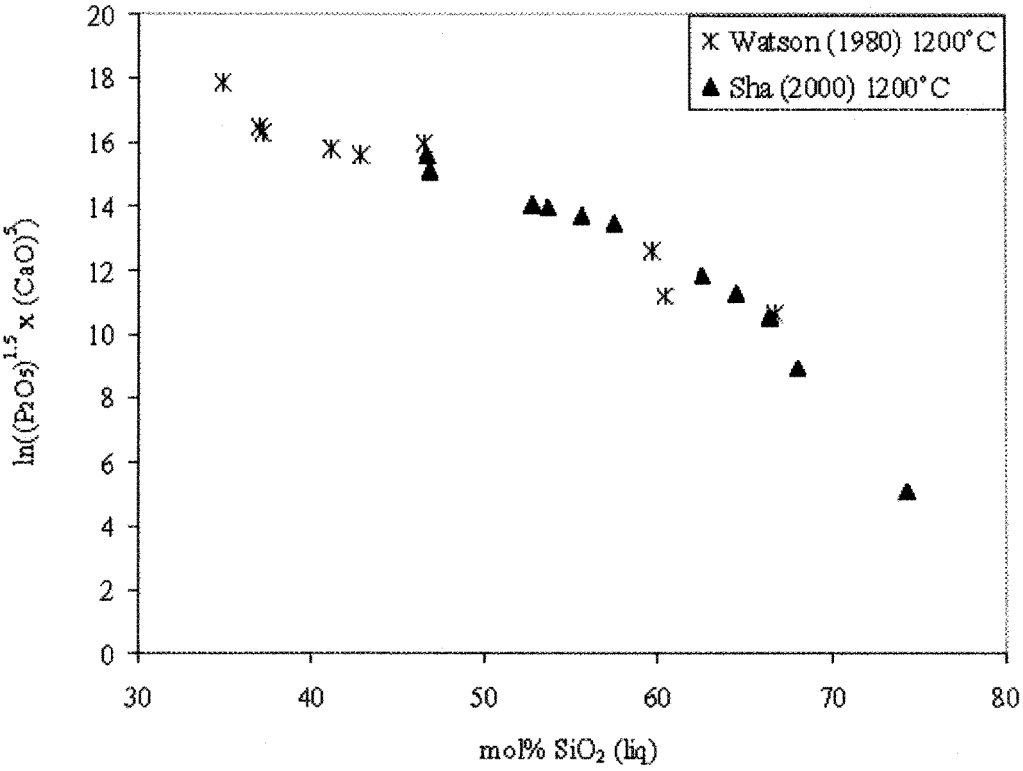

Figure 2. 9. Variation of $\ln(K_{M\text{-apatite}})$ as a function of mole% SiO_2 for whitlockite and apatite saturated liquids at 1200°C (see text for details of this comparison). Data sources as indicated in the key.

- The effect of temperature -

In addition to the importance of liquid composition, the model of Harrison and Watson (1984) implies that temperature also plays a role on apatite saturation, increasing temperature leading to higher levels of P_2O_5 in the liquid at P saturation. Although the temperature range of our experiments is not sufficient to observe this effect (Fig. 2. 6a), our data combined with those of Watson (1979), Pichavant *et al.* (1992) and Sha (2000) cover temperatures from 777°C to 1400°C. When $\ln(K_{M\text{-apatite}})$ is plotted as a function of molar percent of SiO_2, liquids from experiments at different temperatures (e.g. isothermal sections at 1055, 1200, 1300 and 1400°C) clearly define a series of parallel trends (Fig. 2. 10). Indeed, we find that when $K_{M\text{-apatite}}$ is divided by temperature, all experimental liquids considered define a single trend (Fig. 2. 11). Although this way of incorporating temperature is purely empirical, it provides a simple way to express the compositional and temperature effects that characterise liquids saturated in flourapatite and/or whitlockite and which may thus be used as the basis for a comprehensive predictive model, detailed below.

- The case of peraluminous liquids -

One notable feature of Figs. 2. 10 and 2. 11 is that the peraluminous liquids of Pichavant *et al.* (1992) follow exactly the same trend as the subaluminous and peralkaline liquids studied by other authors.

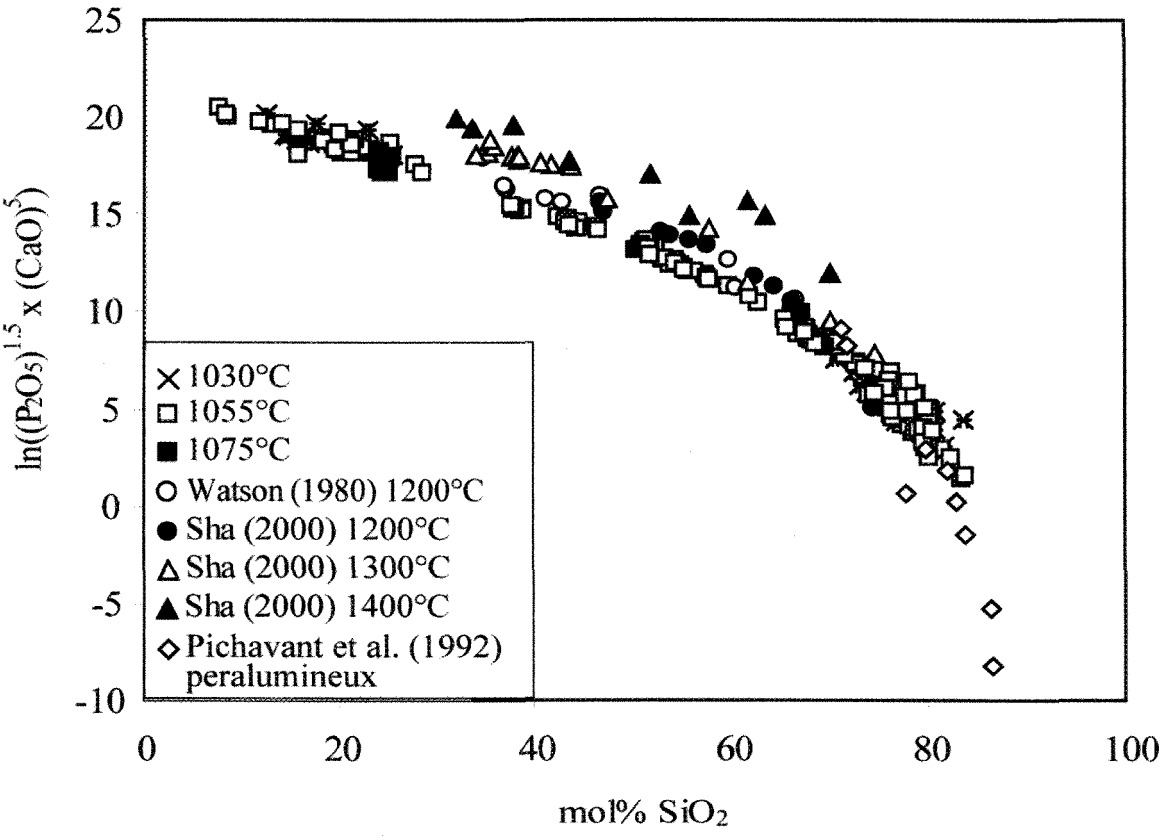

Figure 2. 10. Variation of $\ln(K_{M\text{-apatite}})$ as a function of mole% SiO_2 (see text for definition of $K_{M\text{-apatite}}$). Data sources as indicated in the key. Error bars are typically smaller than the size of the symbols.

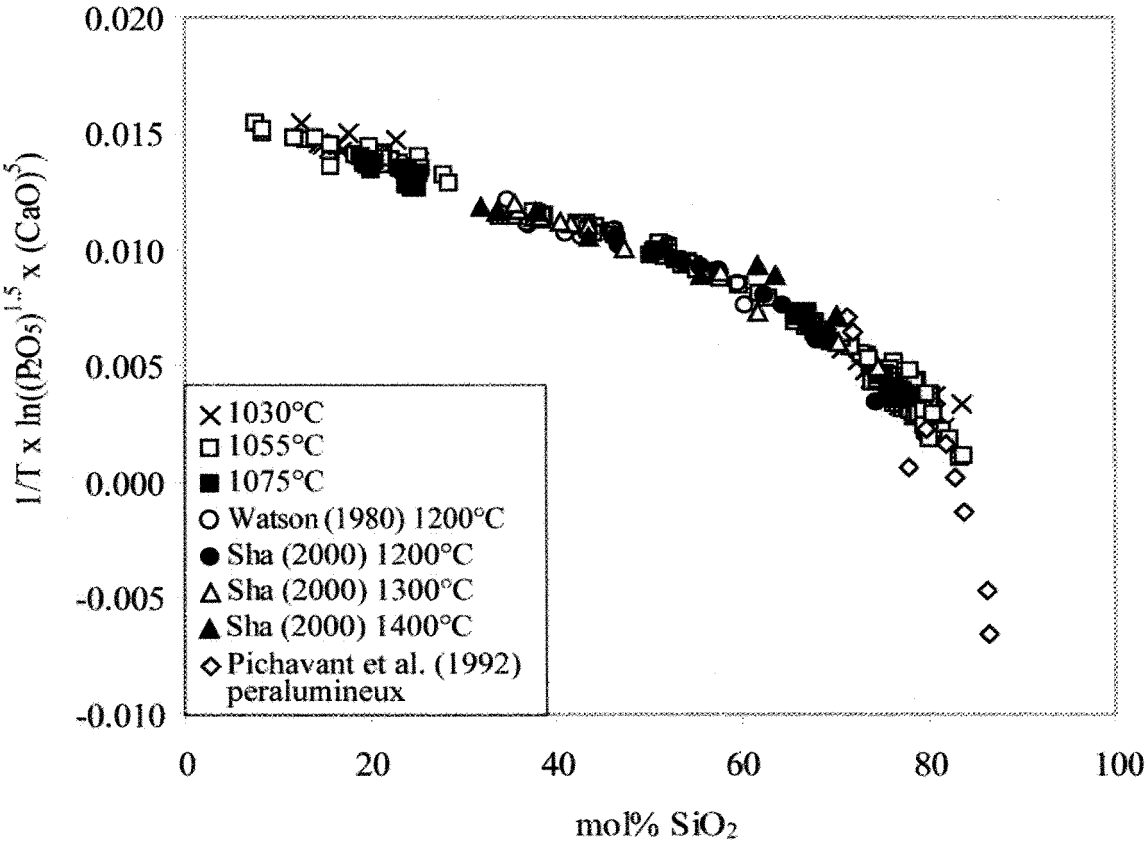

Figure 2. 11. Variation of $\ln(K_{M\text{-apatite}})/T$ as a function of mole% SiO_2. Data sources as indicated in the key. Error bars are typically smaller than the size of the symbols.

This result therefore implies that the discrepancy between the P_2O_5 content at apatite saturation measured by Pichavant *et al.* (1992) and that predicted by the model of Harrison and Watson (1984) is an indirect effect of CaO content (which is not accounted for in the model of Harrison and Watson, 1984) rather than a direct effect of the peraluminous nature of the liquids. A similar conclusion regarding the importance of CaO was proposed by Bea *et al.* (1992) based upon consideration of data from natural peraluminous granitic magmas.

2.6 A PREDICTIVE MODEL FOR PHOSPHATE SATURATION

The data shown in Fig. 2. 11 represent liquids saturated in either flourapatite, α-whitlockite (data of Sha (2000) at 1400°C) or β-whitlockite. These liquids are highly variable in composition and are not systematically saturated in other phases which may buffer the activities of certain melt components. For example, the liquids of Sha (2000) are saturated in phosphate alone, while in the study of Pichavant *et al.* (1992) corundum and andalusite are reported as accompanying phases. We therefore conclude that the correlation observed in Fig. 2. 11 may be used as the basis for a comprehensive model for calculation of the saturation of flourapatite or whitlockite from silicate magmas. Indeed, the fact that data for different phosphate minerals are not distinguished in Fig. 2. 11 implies that a given silicate liquid will either contain no phosphate, or will be saturated in one of apatite or whitlockite, crystallization of apatite presumably occurring in the presence of sufficient Cl or F, and whitlockite in volatile-free systems. Whether or not this correlation is also valid for hydroxyapatite saturated liquids remains to be established.

Quantitatively, the data of figure 2. 11 may be described as a function of silica content by the equation:

$$\frac{1}{T}\ln\left[\left(M_{CaO}^{Liq}\right)^5 \times \left(M_{P_2O_5}^{liq}\right)^{1.5}\right] = \left\{\frac{-1.2868}{139.00 - M_{SiO_2}^{liq}} + 0.0247\right\} \qquad (8)$$

The quadratic form used in equation 5 has been avoided here in order to eliminate high order terms in silica concentration of the liquid. Equation 8 may then be rearranged to define the mole% P_2O_5 of a liquid saturated in apatite/whitlockite ($M_{P_2O_5}^{liq-sat}$), as a function of temperature and the mole% SiO_2 and CaO of the liquid:

$$M_{P_2O_5}^{liq-sat} = \exp\left[\frac{2}{3}\left(T\left\{\frac{-1.2868}{139.00 - M_{SiO_2}^{liq}} + 0.0247\right\} - 5\ln\left(M_{CaO}^{liq}\right)\right)\right] \qquad (9a)$$

which may be simplified to:

$$M_{P_2O_5}^{liq-sat} = \exp\left[T\left(\frac{-0.8579}{139.00 - M_{SiO_2}^{liq}} + 0.0165\right) - 3.3333\ln\left(M_{CaO}^{liq}\right)\right] \qquad (9b)$$

2.6.1 Application to natural systems

Despite the relative simplicity of equation 9, one shortcoming of the model presented above is that concentrations are expressed in mole% rather than wt%. Not only does this render interpretation of values less intuitive than if they were in wt%, but this also has the drawback that unless the whole liquid composition is known the model cannot be used. This could be problematic in geological environments (*i.e.* layered intrusions) where the liquid is no longer present. One way around this problem is to define factors which allow conversion from wt% to mole% and *vica-versa*. To do this we have considered liquids with

SiO_2 content in the range 30 to 75 wt% (i.e. those most representative of natural compositions). For these compositions, when the mole% and wt% of each oxide are compared, it is found that the data define excellent linear correlations, which furthermore pass through the origin (Fig. 2. 12). Based upon these correlations we determine that: mole% SiO_2 = 1.11 * wt % SiO_2; mole% CaO = 1.18 * wt % CaO; mole% P_2O_5 = 0.47 * wt % P_2O_5. Using these correction factors equation 9 can be used even when only wt% analyses are known or can be assumed, although we stress that molar values should be used wherever possible.

This equation may be used in several ways, either to assess whether a given liquid is saturated in phosphate or not, or rearranged to constrain the composition and/or temperature of a system which is known to be saturated in either apatite or whitlockite. From a more general perspective it may also be used to illustrate the importance of each parameter (T, CaO, SiO_2) on wt% P_2O_5 required for phosphate saturation. For example, at fixed CaO content of the liquid equation 9 may be used to show that the effect of changing SiO_2 content dominates the effect of changing temperature (Fig. 2. 13a). Furthermore, the effect of temperature is particularly small for SiO_2 content greater than 55 mol% (Fig. 2. 13a). At fixed temperature (of 1050°C), it is predicted that the effect of CaO is negligible at high SiO_2 content, but may become extremely important at lower SiO_2 content (Fig. 2. 13b). In other words, in granitic systems the influence of CaO concentration of the liquid on wt% P_2O_5 required for phosphate saturation will be minor, but this will not be true in low-SiO_2 basaltic systems.

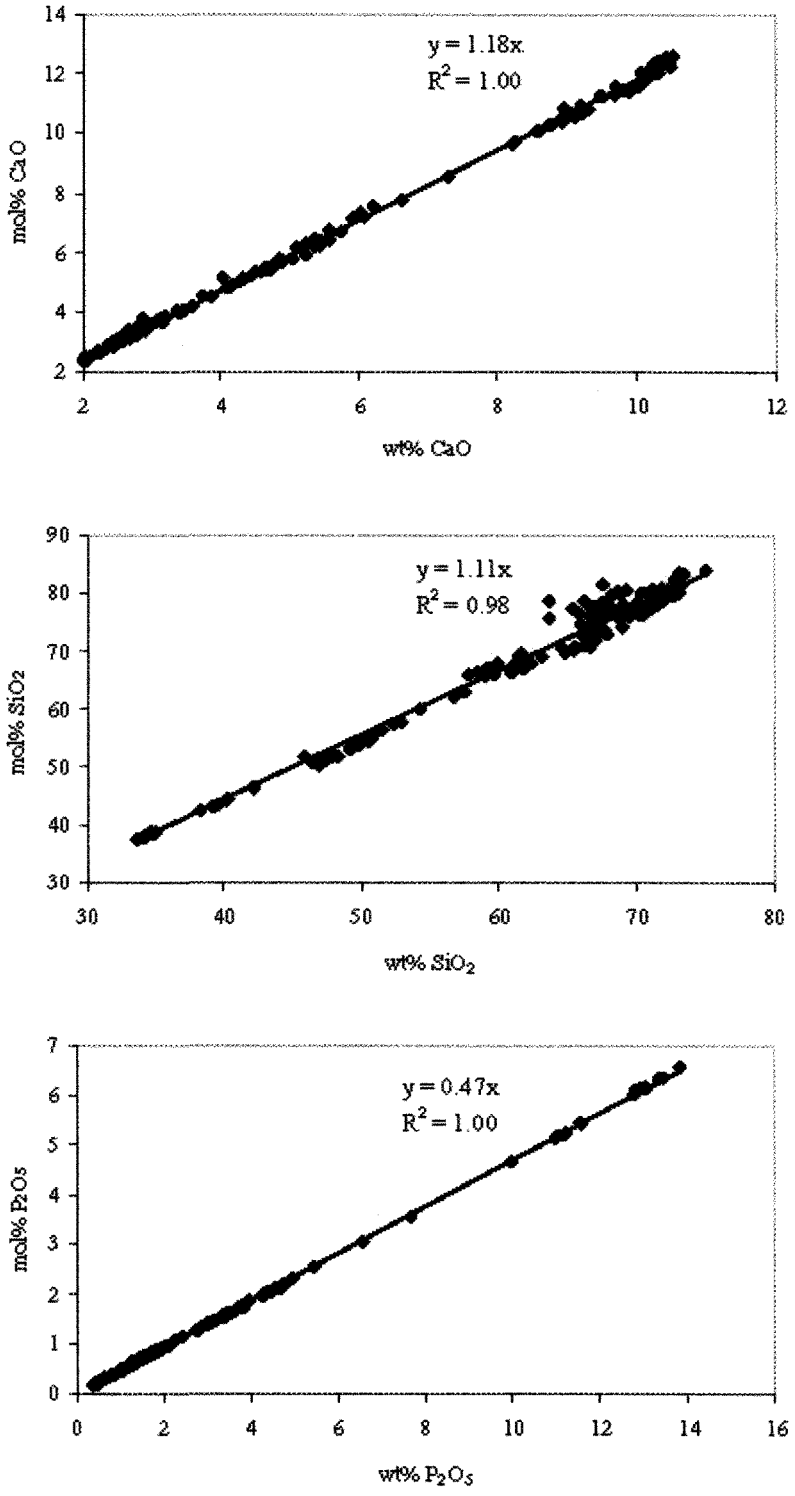

Figure 2. 12. Relations between weight percent and mole percent for components CaO, SiO_2 and P_2O_5 in typical magmatic compositions. Equations are given in the text.

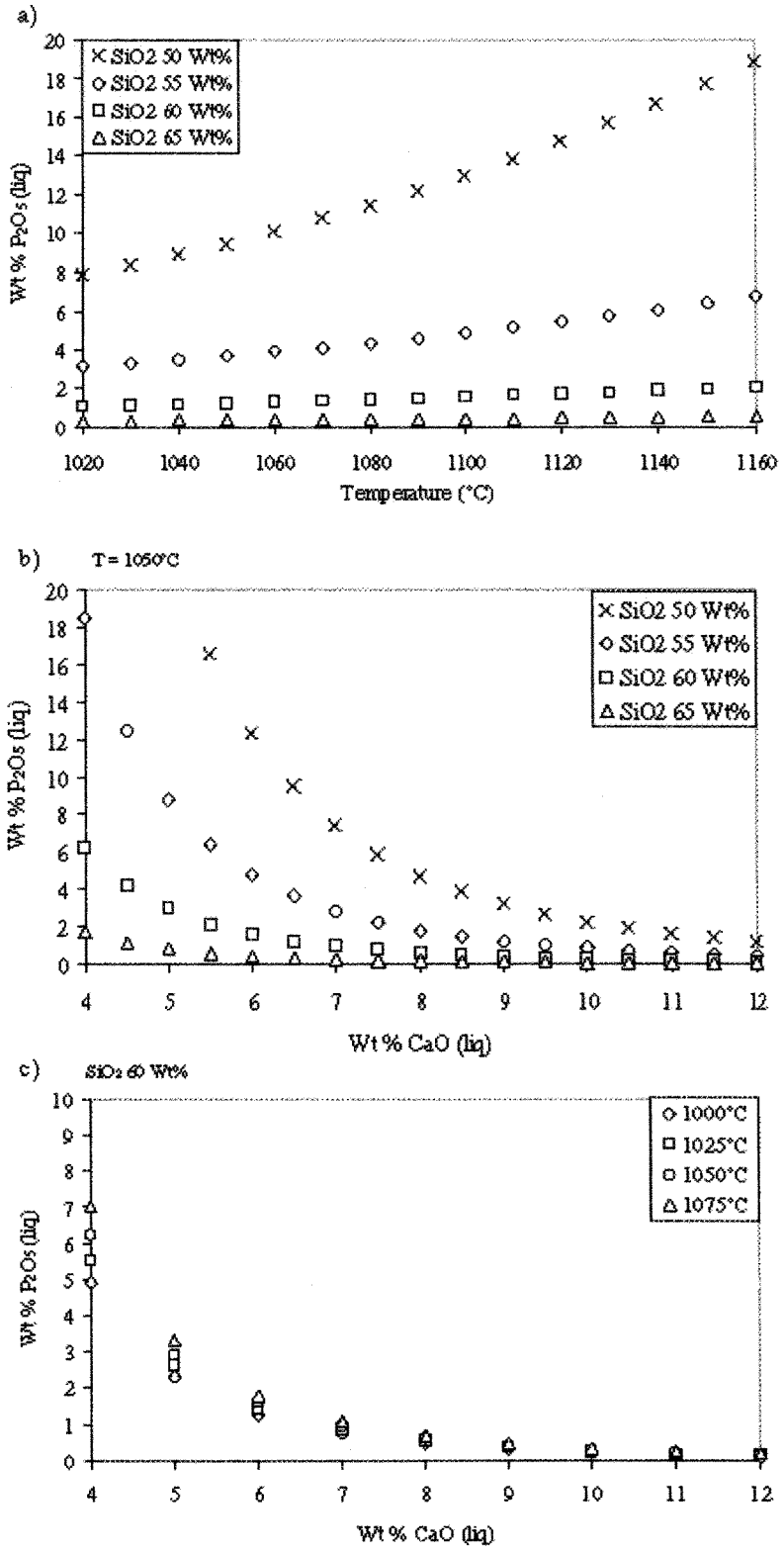

Figure 2. 13. Calculated values of wt% P_2O_5 required for phosphate saturation as a function of wt% SiO_2, CaO and temperature.

Finally, at fixed SiO_2 content, it may be appreciated that the effect of CaO dominates that of temperature, although the effect of temperature is more marked at low CaO content (Fig. 2. 13c).

Despite the fact that the effects of changing SiO_2 and CaO concentrations in the liquid dominate those of changing temperature, it is clear that there is a complex interdependence of temperature, SiO_2 and CaO concentration on wt% P_2O_5 required for phosphate saturation and that equation 9 should be used for any quantitative application.

- Illustrating saturation as a function of magmatic differentiation -

Although equation 9 may be used to calculate how temperature and melt composition affect wt% P_2O_5 required for phosphate saturation, as illustrated in Fig. 2. 13, it is not immediately obvious how this parameter will vary along the liquid line of descent of a real magmatic system. Indeed, how wt% P_2O_5 required for phosphate saturation varies in response to the changes in major element composition of the liquid caused by fractional crystallization will obviously be a key factor which will determine at which point along the liquid line of descent a phosphate will appear. The other key factor is the evolution of the phosphorus content of the liquid as differentiation progresses, saturation occurring when the P_2O_5 content of the liquid becomes greater than the wt% P_2O_5 required for phosphate saturation. This is illustrated below for the case of differentiation of a ferrobasaltic magma along the FMQ buffer using the experimentally determined liquids described by Toplis and Carroll (1995). The initial liquid used in that study has the composition of a dyke found close to the Skaergaard intrusion and which has been proposed as a possible parental magma of that intrusion (Brooks and Nielsen, 1978). A detailed account of the phase

relations and liquid compositions can be found in Toplis and Carroll (1995) although the salient features are summarised below.

For each individual liquid of Toplis and Carroll (1995) the value of wt% P_2O_5 required for phosphate saturation has been calculated and is reported as a function of temperature in Fig. 2. 14. For the different liquid compositions produced during cooling, the calculated variation of wt% P_2O_5 required for phosphate saturation defines three distinct segments. The one at highest temperature is characterised by decreasing wt% P_2O_5 required for phosphate saturation with falling temperature. In this range olivine and plagioclase are the only liquidus phases and the liquid has approximately constant CaO and SiO_2 content (Toplis and Carroll, 1995). The calculated variation in wt% P_2O_5 required for phosphate saturation can thus be attributed to the change in temperature. A marked change in the behaviour of wt% P_2O_5 required for phosphate saturation occurs at ~1130°C (Fig. 2. 14), corresponding to the appearance of clinopyroxene on the liquidus (Toplis and Carroll, 1995). In the temperature range 1130 to 1100°C, the SiO_2 content of the liquid is approximately constant, but the CaO content of the liquid is decreasing. Therefore, the marked increase in wt% P_2O_5 required for phosphate saturation can be attributed to the falling CaO content of the liquid, which dominates the effect of falling temperature. The second major change in the behaviour of wt% P_2O_5 required for phosphate saturation occurs at ~1100°C (Fig. 2. 14) when magnetite appears on the liquidus. For temperatures below 1100°C the CaO content of the liquid continues to decrease, but the SiO_2 content of the liquid increases with falling temperature.

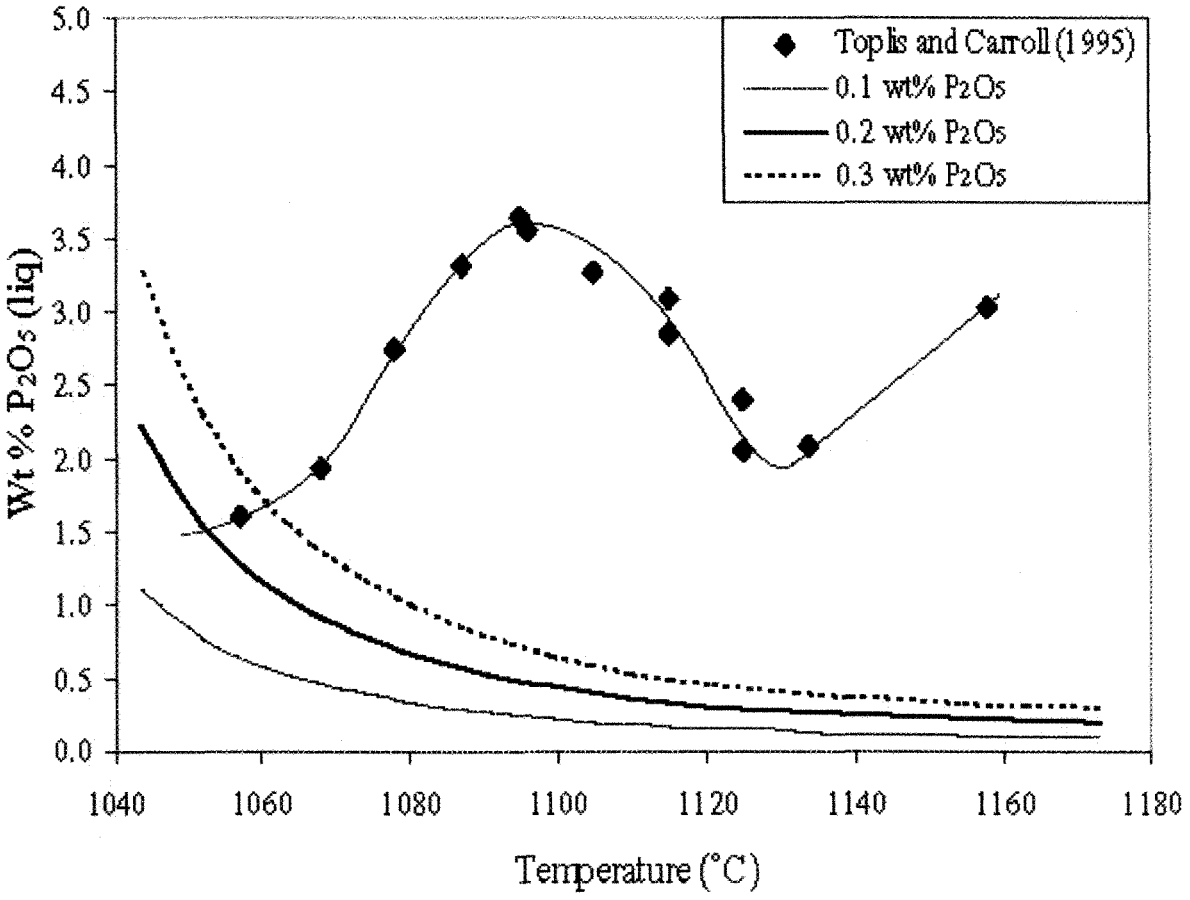

Figure 2. 14. Values of wt% P_2O_5 required to saturate experimental liquids of Toplis and Carroll (1995) in a crystalline phosphate calculated using equation 9b (diamonds). Solid and dashed curves represent wt% P_2O_5 of the liquid as a function of temperature assuming that the initial liquids contained 0.1, 0.2 and 0.3 wt% P_2O_5 (as labelled). Intersection of the curves and diamonds may be used to predict phosphate saturation as detailed in the text.

The drop in wt% P_2O_5 required for phosphate saturation with decreasing temperature can therefore be attributed to the increase in SiO_2 content, an effect which dominates those of CaO content and temperature which are both acting to increase wt% P_2O_5 required for phosphate saturation.

These values of wt% P_2O_5 required for phosphate saturation may then be compared with the theoretical evolution of P_2O_5 in the liquid to assess at what point phosphate saturation would occur. For example, assuming that phosphorous is perfectly incompatible and using the variation of percentage crystallization as a function of temperature determined by Toplis and Carroll (1995), one predicts that if the liquid at 1170°C contained 0.2 wt% P_2O_5, then phosphate saturation should occur at 1055°C when the liquid contains 1.5 wt% P_2O_5 (Fig. 2. 14). A concentration of P_2O_5 in the initial liquid of 0.1wt% P_2O_5 leads to slightly lower saturation temperatures and a concentration of P_2O_5 in the liquid at saturation of approximately 1 wt% (Fig. 2. 14). These ranges of temperature and P_2O_5 content are perfectly consistent with independent estimates proposed for the Skaergaard intrusion (McBirney and Naslund, 1990; Wager, 1960), providing evidence for the validity of the model.

- The petrogenesis of rocks dominated by association of apatite and Fe-Ti oxide -

Rocks dominated by the presence of apatite and Fe-Ti oxide may be found in diverse magmatic environments, including mafic intrusions, rocks associated with anorthosites, and ophiolites (*e.g.* Wager and Brown, 1967; Philpotts, 1967; Dymek and Owens, 2001; Mitsis and Economou-Eliopoulos, 2001). The petrogenesis of these rock types, in particular that of nelsonites, is the subject of debate. The principal proposals are: 1) that nelsonites represent

the crystallization products of an immiscible Fe-Ti oxide liquid which separated from a silicate magma (e.g. Philpotts, 1967; Ripley *et al.*, 1998), an immiscibility which may be linked to magma mixing (e.g. Clark and Kontak, 2004); 2) that apatite and oxide represent cumulates from an evolved silicate magma (e.g. Emslie, 1975; Dymek and Owens, 2001; Barnes *et al.*, 2004).

Even though the experimental results presented here show immiscibility, the bulk P_2O_5 contents of our starting compositions are unrealistically high for natural ferrobasaltic liquids and any direct application of our results to the question of nelsonite petrogenesis is probably unfounded. On the other hand the calculated variation of wt% P_2O_5 required for phosphate saturation during ferrobasaltic differentiation (Fig. 2. 14) may be used to assess whether or not extremely high levels of P and Fe may be reached in the liquid, without the need to postulate liquid immiscibility. For example, figure 2. 14 shows that during cotectic crystallization of olivine, plagioclase and clinopyroxene the wt% P_2O_5 required for phosphate saturation increases sharply, a trend which is only reversed by the appearance of magnetite. As discussed above this is the consequence of decreasing CaO content of the liquid during crystallization of olivine gabbro (Shi and Libourel, 1991; Toplis and Carroll, 1995). Thus, if the appearance of magnetite on the liquidus is displaced to lower temperature (*i.e.* the middle segment in Fig. 2. 14 extends to lower temperature, and thus higher values of wt% P_2O_5 required for phosphate saturation), the saturation temperature of phosphate will also be lowered and the concentrations of P_2O_5 in the liquid will be significantly higher when a phosphate does finally appear. We therefore conclude that retarding magnetite saturation will indeed tend to retard phosphate saturation, but not because ferric iron stabilises P in the liquid as originally postulated, but rather as a

consequence of the variations of CaO and SiO_2 content of the liquid as a function of magmatic differentiation.

The fact that the presence of P in ferrobasaltic liquids retards magnetite crystallization (Toplis *et al.*, 1994a) therefore provides a chemical mechanism to enrich magmatic liquids to high concentrations of both Fe and P. However, the extent to which this mechanism is relevant to the petrogenesis of nelsonites remains to be demonstrated. For example, nelsonites typically contain less than 10% silicate minerals, although more than 10% of such phases were present in all of our experiments. We conclude that further experimental work and petrographic study of natural nelsonites is required to understand the physical and chemical mechanisms which lead to the formation of these enigmatic rocks.

2.7 CONCLUDING REMARKS

In the light of our experimental results, and those in the literature, we conclude that it is SiO_2 and CaO concentrations of the liquid that dominate phosphate saturation in magmatic systems, any effect of iron and/or oxidation state being of secondary importance. Based upon these results we propose an equation which may be used to predict the P_2O_5 concentration of silicate liquids saturated either in whitlockite or apatite as a function of melt chemistry and temperature. Of particular note is the fact that this equation is valid over extremely wide ranges of liquid composition (e.g. SiO_2 content from 10 to 80 mol%), not only for peralkaline and subaluminous compositions, but also peraluminous liquids.

ACKNOWLEDGEMENTS

This work was supported financially by a Canada Research Chair and Natural Sciences and Engineering Council Discovery Grants to SJB and a CNRS grant (Intérieur de la Terre) to MT. The referees are thanked for giving up their valuable time to review this manuscript. This work has benefited from the help of numerous people and NT would like to acknowledge the support of Richard LeBreton, Fabien Solgadi, Tafadzwa Gomwe, Bélinda Godel, Fabien Palhol, Laurent Tissandier, and the microprobe technicians of the Service Commun de Micro-Analyse at the Université Henri Poincaré in Nancy.

REFERENCES

Barnes S. J., Maier W. D. and Ashwal L. D. (2004) Platinium-group element distribution in the Main Zone and in the Upper Zone of the Northern Limb of the Bushveld Complex. *Chem. Geol.* **208,** 293-317.

Bea F., Fershtater G., and Corretge L. G. (1992) The geochemistry of phosphorus in granite rocks and the effect of aluminium. *Lithos* **29,** 43-56.

Brooks C. K. and Nielsen T. F. D. (1978) Early stages in the differentiation of the Skaergaard magma as revealed by closely related suite of dye rocks. *Lithos* **11**, 1-14.

Brooks C. K., Larsen L. M. and Nielsen T. F. D. (1991) Importance of iron-rich tholeiitic magmas at divergent plate margins: A reappraisal. *Geology* **19,** 269-272.

Cimon J. (1998) L'unité à apatite de rivière des rapides, Complexe de Sept îles. Localisation stratigraphique et facteurs à l'origine de sa formation. *Ministère des ressources naturelles, Québec* **97**, 1-32.

Clark A. H., and Kontak D.J. (2004) Fe-Ti-P oxide melts generated through magma mixing in the Antuata Subvolcanic Center, Peru: Implications for the origin of nelsonite and iron-oxide dominated hydrothermal deposits. *Econ. Geol.* **99,** 377-395.

Davies G. and Cawthorn R. G. (1984) Mineralogical data on a multiple intrusion in the Rustenburg Layered Suite of the Bushveld Complex. *Mineral. Mag.* **48**, 469-480.

Deines P., Hafzinger R. H., Ulmer G. C. and Woermann E. (1974) Temperature-oxygen fugacity tables for selected gas mixtures in the system C-H-O at one atmosphere total pressure. *Bulletin of the Earth and Mineral Sciences Experiment Station, Pennsylvania State University* **88**, 128.

Delaney J. S., O'Neill C. and Prinz M. (1984) Phosphate minerals in eucrites. *Lunar Planet. Sci.* **XV**, 208-209 (abstr.).

Dymek R. F. and Owens B. E. (2001) Petrogenesis of apatite-rich rocks (nelsonites and oxide-apatite gabbros) associated with massif anorthosites. *Econ. Geol.* **96,** 797-815.

Emslie R. F. (1975) Major rock units of the Morin Complex, southwestern Quebec. *Geol. Survey of Canada Paper* 74-48, 37 p.

Gan H. and Hess P. C. (1992) Phosphate speciation in potassium aluminosilicate glasses *Amer. Mineral.* **77,** 495-506.

Ghiorso M.S., Carmichael I. S. E., Rivers M.L. and Sack R. O. (1983) The Gibbs free energy of mixing of natural silicate liquids; an expanded regular solution approximation for the calculation of magmatic intensive variables. *Contrib. Mineral. Petrol.* **84,** 107-145.

Griffen W. L., Amli R. and Heier K. S. (1972) Whitlockite and apatite from lunar rock 14310 and from Ödegärden, Norway. *Earth Planet. Sci. Lett.* **15**, 53-58.

Gwinn R. and Hess P. C. (1993) The role of phosphorus in rhyolitic liquids as determined from the homogenous iron redox equilibrium. *Contrib. Mineral. Petrol.* **106,** 129-141.

Harney D. M. W. and Von Gruenewaldt G. (1995) Ore-forming processes in the upper part of the Bushveld complex, South Africa. *J. African Earth Sci.* **20**, 77-89.

Harrison T. M. and Watson E. B. (1984) The behavior of apatite during crustal anatexis: equilibrium and kinetic considerations. *Geochim. Cosmochim. Acta.* **48,** 1467-1477.

Huminicki D. M. C. and Hawthorne F. C. (2002) The crystal chemistry of phosphate mineral. *In* Phosphates - Geochemical, geobiological and materials importance. *eds.* Kohn M. J., Rakovan J. and Hughes J. M. *Mineral. Soc. Am., Reviews in Mineralogy.* **48,** 123-235.

Kilinc A., Carmichael I. S. E., Rivers M. L. and Sack R. O. (1983) The ferric-ferrous ratio of natural silicate liquids equilibrated in air. *Contrib. Mineral. Petrol.* **83**, 136-140.

Kushiro I. (1975) On the nature of silicate melt and its significance in magma genesis: Regularities in the shift of the liquidus boundaries involving olivine, pyroxene, and silica minerals. *Am. J. Sci.* **275,** 411-431.

Libourel G. (1999) Systematics of calcium partitioning between olivine and silicate melt: implications for melt structure and calcium content of magmatic olivines. *Contrib. Mineral. Petrol.* **136**, 63-80.

Linnen R. L. and Keppler H. (1997) Columbite solubility in granitic melts: Consequences for the enrichment and fractionation of Nb and Ta in the Earth's crust. *Contrib. Mineral. Petrol.* **128,** 213-227.

Linnen R. L. and Keppler H. (2002) Melt composition control on Zr/Hf fractionation in magmatic processes. *Geochim. Cosmochim. Acta* **66**, 3293-3301.

Lundberg L. L, Crozaz G., McKay G. and Zinner E. (1988) Rare earth element carriers in the Shergotty meteorite and implications for its chronology. *Geochim. Cosmochim. Acta* **52**, 2147-2163.

Mitsis I. and Economou-Eliopoulos M. (2001) Occurrence of apatite associated with magnetite in an ophiolite complex. *Amer. Mineral.* **86,** 1143-1150.

McBirney A. R. and Naslund H. R. (1990) The differentiation of the Skaergaard intrusion. A discussion of Hunter R. H. and Sparks R. S. J. (*Contrib. Mineral. Petrol.* **95**, 451-461). *Contrib. Mineral. Petrol.* **104**, 235-240.

Mysen B.O. (1992) Iron and phosphorus in calcium silicate quenched melts. *Chem. Geol.* **98,** 175-202.

Nabil H. (2003) Genèse des dépôts de Fe-Ti-P associés aux intrusions litées (exemples: intrusion mafique de Sept-Îles, au Québec; Complexe de Duluth aux États-Unis). Ph. D. thesis, Université du Québec à Chicoutimi.

Naslund H. R. (1983) The effect of oxygen fugacity on liquid immiscibility in iron-bearing silicate melts. *Amer. J. Sci.* **283**, 1034-1059.

Pichavant M., Montel J. M. and Richard L. R. (1992) Apatite solubility in peraluminous liquids: experimental data and an extension of the Harrison-Watson model. *Geochim. Cosmochim. Acta* **56,** 3855-3861.

Philpotts A. R. (1967) Origin of certain iron-titanium oxide and apatite rocks. *Econ. Geol* **62**, 303-315.

Ripley E. M., Severson M. J. and Hauck S. A. (1998) Evidence for sulphide and Fe-Ti-P-rich liquid immiscibility in the Duluth Complex, Minnesota. *Econ. Geol.* **93,** 1052-1062.

Ryerson F. J. and Hess P. C. (1978) Implications of liquid-liquid distribution coefficients to mineral-liquid partitioning. *Geochim. Cosmochim. Acta* 42, 921-932.

Schaller T., Rong C., Toplis M. J. and Cho, H. (1999) TRAPDOR NMR investigations of phosphorus-bearing aluminosilicate glasses. *Journal of Non-Crystalline Solids* **248,** 19-27.

Sha L. (2000) Whitlockite solubility in silicate melts : Some insights into lunar and planetary evolution. *Geochim. Cosmochim. Acta* **64**, 3217-3236.

Shi P. and Libourel G. (1991) The effects of FeO on the system CMAS at low pressure and implications for basaltic differentiation processes. *Contrib. Mineral. Petrol.* **108,** 129-145.

Toplis M. J. and Carroll M.R. (1995) An experimental study of the influence of oxygen fugacity on Fe-Ti oxide stability, phase relations, and mineral-melt equilibria in ferro-basaltic systems. *Journal Petrol.* **36**, 1137-1170.

Toplis M. J. and Schaller T. (1998) A ^{31}P MAS NMR study of glasses in the system $x Na_2O$-$(1-x)Al_2O_3$-$2SiO_2$-yP_2O_5. *Journal of Non-Crystalline Solids* **224**, 57-68.

Toplis M. J. Libourel G. and Carroll M. R. (1994 a.) The role of phosphorus in cristallisation processes of basalt: An experimental study. *Geochim. Cosmochim. Acta* **58,** 797-810.

Toplis M. J., Dingwell D. B. and Libourel G. (1994 b.) The effect of phosphorus on the iron redox ratio, viscosity, and density of an evolved ferro-basalt. *Contrib. Mineral. Petrol.* **117**, 293-304.

Vermark C. F. and Von Gruenewaldt G. (1986) Introduction to the Bushveld Complex. *Mineral deposits of Southern Africa* **2**, 1021-1029.

Visser W. and Koster van Groos A. F. (1979) Effects of P_2O_5 and TiO_2 on liquid-liquid equilibria in the system K_2O-FeO-Al_2O_3-SiO_2. *Amer. J. Sci.* **279,** 970-988.

Von Gruenewaldt G. (1993) Ilmenite-Apatite Enrichments in the Upper Zone of the Bushveld Complex: A Major Titanium-Rock Phosphate Resource. *International Geology Review* **35**, 987-1000.

Wager L. R. (1960) The major element variation of the layered series of the Skaergaard intrusion and a re-estimation of the average composition of the hidden layered series and of the successive residual magmas. *J. Petrol.* **1,** 364-398.

Wager L. R. and Brown G. M. (1967) *Layered Igneous Rocks*. Oliver and Boyd, Edinburgh.

Watson E. B. (1979) Apatite saturation in basic to intermediate magmas. *Geophys. Res. Let.* **6**, 937-940.

Wolf M. B. and London D. (1994) Apatite dissolution into peraluminous haplogranitic melts: An experimental study of solubilities and mechanisms. *Geochim. Cosmochim. Acta* **58**, 4127-4145.

CHAPITRE 3

AN EXPERIMENTAL STUDY ON THE EFFECTS OF PRESSURE AND FLUORINE ON APATITE SATURATION IN MAFIC MAGMAS – IMPLICATIONS FOR THE FORMATION OF APATITE-RICH ROCKS IN THE EVOLUTION OF LAYERED INTRUSIONS AND MASSIF TYPE ANORTHOSITES.

N. Tollari, D. R. Baker, S-J. Barnes, soumis dans Contribution to Mineralogy and Petrology, 08/2007

3.1 RÉSUMÉ

L'apatite est une phase majeure dans la partie supérieure de certaines intrusions litées et de certains complexes anorthositiques. Nous avons étudiés l'effet de la pression et du fluor sur la saturation de l'apatite dans les magmas mafiques afin de mieux comprendre sous quelles conditions ce minéral cristallise. Il est d'autant plus important de connaître les conditions, sous lesquelles l'apatite cristallise, puisque ce minéral est un des composants principal des nelsonites (1/3 apatite et 2/3 Fe-Ti oxydes). Deux modèles de formation sont actuellement proposés pour ce type de roche : (i) le modèle de cristallisation de l'apatite et des oxydes à partir d'un magma mafique évolué et de l'accumulation de ces minéraux dans la pile magmatique et, (ii) le modèle d'immiscibilité de deux liquides dans lequel un magma

mafique se sépare en deux liquides, un riche en Si et l'autre riche en Fe, Ti et P. L'apatite et les oxydes cristallisent à partir du liquide riche en Fe, Ti et P.

Des expériences, réalisées à partir de compositions mafiques à 500 MPa, confirment certains travaux antérieurs qui indiquaient que, les facteurs les plus importants dans la saturation des minéraux phosphatés, sont les concentrations en SiO_2 et CaO du magma. Les systèmes riches en F atteignent la saturation en apatite à des teneurs plus basses en SiO_2 et plus haute en CaO que les systèmes sans F.

En combinant nos résultats antérieurs avec d'autres déjà publiés dans le diagramme pseudo ternaire SiO_2-FeO+TiO_2+MgO+CaO+P_2O_5-Al_2O_3+Na_2O+K_2O nous avons pu déterminer l'étendue du champs d'immiscibilité de deux liquides dans ce système. L'extension du champ d'immiscibilité diminue lors de l'augmentation de la pression. L'extension du champ d'immiscibilité est aussi affectée par la température. En effet, le champ d'immiscibilité semble disparaître pour des températures supérieures à 1200°C et inférieures à 1000°C environ. Donc le champ d'immiscibilité est stable pour une gamme de pression, composition et température donnée.

Les trajectoires d'évolution des liquides magmatiques de trois systèmes naturels qui contiennent des roches riches en apatite et en oxydes de Fe et Ti (La suite intrusive de Sept-Îles, le complexe anorthositique du Lac-St-Jean et l'intrusion litée de Skaergaard) ont été modélisés. Dans les trois cas la saturation en apatite a lieu avant que la trajectoire intercepte le champ d'immiscibilité. La formation des roches riches en apatite et en oxydes de Fe et Ti peut donc être expliquée par la cristallisation fractionnée suivi de l'accumulation de l'apatite et des oxydes de Fe et Ti dans les intrusions et complexe considérés.

3.2 INTRODUCTION

Apatite and Fe-Ti oxides occur as cumulate phases in the upper parts of some mafic layered intrusions (Cimon 1998; Eales and Cawthorn 1996; Huntington 1979; Morse 1980; Nabil 2003; Wager and Brown 1968) and as lenses of apatite and Fe-Ti oxide rich rocks in massive type anorthosites (Dymek and Owens 2001; Fredette 2006). The composition of the silicate liquid and intensive variables (temperature, pressure, fO_2 at the time of apatite saturation are poorly constrained in this system. Apart from modelling the formation of silicate rocks the timing of phosphate saturation is also of interest in explaining the origin of an unusual rock type, nelsonite, which consists of 1/3 apatite and 2/3 Fe-Ti oxide. Two possible origins are suggested for this rock type. One model suggests that apatite and oxide crystallize from the evolved mafic magma and accumulate on the magma pile to form the nelsonitic layers and pods (Barnes et al. 2004; Eales and Cawthorn 1996; Emslie 1975; Goldberg 1984; McLelland et al. 1994; Tegner et al. 2006). The second model suggests that nelsonites are the product of liquid immiscibility with the nelsonite and a SiO_2-rich liquid segregated from a liquid of ferrobasaltic composition (Jakobsen et al. 2005; Naslund 1983; Philpotts 1967).

Tollari et al. (2006) carried out a series of experiments on liquids of ferrobasaltic compositions similar to Skaergaard magma with 5 weight percent P_2O_5 and 10 weight percent P_2O_5 added to the liquids. The charges with 5 weight percent P_2O_5 showed a crystallization order similar to that observed at Skaergaard and none contained liquid immiscible textures. Tollari et al. (2006) concluded that the apatite and Fe-Ti oxide observed in the upper parts of layered intrusions could have crystallized from the evolved mafic magma. The charges with 10 weight percent P_2O_5 added did contain two liquids, the

Fe-Ti-P rich liquid and a SiO_2 rich liquid. However, it is not clear how these liquids could form in natural systems. Most basaltic magmas contain 0.2 to 1 weight percent P_2O_5. During initial crystal fractionation the P_2O_5 in the magma rises because P_2O_5 does not enter any of the crystalline phases. However, as shown by Tollari et al. (2006) as a magma of basaltic composition crystallizes phosphate saturation occurs at approximately 1.5 to 2 weight percent P_2O_5 and after this the content of the magma rapidly diminishes. Essentially in natural systems it appears that apatite and Fe-Ti oxide saturation occurs before the FeO, TiO_2 and P_2O_5 concentrations build up sufficiently in the magma to provoke the segregation of a Fe-Ti-P liquid.

The focus of the experiments of Tollari et al. (2006) was to consider the effect of fO_2 on phosphate and Fe-Ti oxide saturation and were run at 0.1 MPa. Thus, no volatiles such as F and H_2O were added to the charges and the phosphate that crystallized was whitlockite, rather than apatite. Whitlockite occurs in meteorites and lunar rocks, but is not common in terrestrial systems. The presence of F and H_2O in the silicate liquid could potentially change the structure of the liquid and thus influence the relative timing of apatite and Fe-Ti-P liquid saturation. For this reason we have carried out a new series of experiments using the same ferrobasalt composition as Tollari et al. (2006) but with F and H2O present. In addition a parallel series of experiments using an alkali basalt has been investigated.

3.3 EXPERIMENTAL APPROACH AND METHODS

3.3.1 Starting materials and compositions studied

For all experiments two basic rock compositions were used. The first is a ferrobasaltic composition (SC4-b) (Tollari et al. 2006). This composition corresponds to a residual liquid obtained by Toplis and Carroll (1995) during crystallization experiments which investigated a synthetic analogue of one potential parental liquid which formed the Skaergaard intrusion (Brooks and Nielsen 1978). The second composition, Dy-spt, corresponds to the composition of mafic dykes from the Sept-Îles Intrusive Suite (Hounsell 2003). This composition contains slightly more alkalies than the Sc4-b (Table 3.1).

The starting materials for all experiments were two synthetic glasses prepared from mixtures of reagent grade oxides and carbonates (SiO_2, TiO_2, Al_2O_3, Fe_2O_3, MgO, $CaCO_3$, and K_2CO_3). Fluorine in the form of 3.5 weight percent NaF (equivalent to 1 weight percent F and 3.25 weight percent Na_2O) was added to half of the starting compositions. In addition, ~5 weight percent P_2O_5, as $(NH_4)_2H_4PO_3$, was added to each base composition, and 10 weight percent P_2O_5 to two aliquots of Sc4-b. The charges were melted at 1400°C for 1h in air, and the resulting glasses were crushed. This procedure was repeated twice for each composition studied. The chemical compositions of the powders (Sc4-b and Dy-spt with and without F) are listed in Table 3. 1. The amounts of P_2O_5 (2.2 to 6.8 weight percent, Table 3. 1) found in the quenched glass in experiments which produced no crystalline phases are lower than the amounts of P_2O_5 added (5 and 10 weight percent) which we attribute this to the loss of P_2O_5 during the preparation of the starting glasses.

Table 3. 1. Nominal compositions of starting material (wt %).

	With F			Without F		
Run no.	**Dy-spt [a]**	**Sc4-b [b]**	**Sc4-b 10**	**Dy-spt**	**Sc4-b**	**Sc4-b 10**
SiO_2	44.01	46.39	44.15	44.43	46.83	44.55
TiO_2	3.76	4.09	3.89	3.79	4.13	3.93
Al_2O_3	13.37	10.58	10.43	13.50	10.68	10.52
FeO	14.65	15.43	14.69	14.79	15.58	14.82
MgO	5.21	4.38	4.17	5.26	4.42	4.21
CaO	7.90	9.24	8.79	7.97	9.33	8.87
Na_2O	3.21	2.86	2.72	3.24	2.89	2.75
K_2O	1.19	0.46	0.44	1.20	0.46	0.44
P_2O_5	4.79	4.69	8.93	4.84	4.73	9.01
H_2O	0.96 [c]	0.94 [c]	0.89 [c]	0.97 [c]	0.95 [c]	0.90 [c]
F	0.96	0.94	0.89	-	-	-
Total	**100**	**100**	**100**	**100**	**100**	**100**

Numbers in parentheses indicate standard deviations
[a] Dy-spt is from Tollari et al. (submitted)
[b] Sc4-b is from Toplis et al. (Toplis et al. 1994)
[c] H_2O was added to the initial composition in the graphite capsule.

3.3.2 Experimental method

Experiments were performed in double capsules in which the inner capsule was graphite and the outer capsule was Pt. The use of double capsules is necessary to minimize iron loss and to fix oxygen fugacity close to the carbon-carbon monoxide buffer. This buffer corresponds to an oxygen fugacity 1 to 2 log units lower than the Fayalite-Magnetite-Quartz buffer (Frost 1991).

The 3 mm-long graphite capsules were loaded with 10 to 15 mg of the starting mixture and water (1 weight percent), closed with a graphite lid and inserted into the Pt capsule. The Pt-capsule was then welded shut in a water bath to avoid water loss during welding. The capsules were dried in an oven for 1 hour to homogenize the water and rock powder and were then checked for water loss by weighing.

The experiments were performed in a piston-cylinder apparatus using 1.91 cm diameter, crushable alumina-pyrex-NaCl assemblies (Baker 2004). The temperature was controlled by type C thermocouples. The samples were maintained above their liquidus at 1250°C and 550 MPa for 1 hour, and then cooled at a constant rate of 50°C/min to temperature of either 1000°C, 1015°C, 1030°C, 1040°C, 1050°C or 1100°C, and a fixed at pressure of 500 MPa. These conditions were maintained for variable durations of between 66h to 142h, to allow equilibration between crystalline phases and coexisting melts (see Table 3. 2). At the end of each experiment the samples were quenched isobarically (500MPa) to 600°C in less than 15 s.

Table 3. 2. Cooling history and run conditions.

Cooling history and run conditions					
Run no.	cooling history [a]			Final conditions [b]	Run products [c]
	D1 (h)	Ramp (°C/min)	D2 (h)	Tf (°C)	
With 5 wt% P2O5					
With F					
McGill 1					
Dy-spt	1	50	72	1000	Gl, Fap, Plg, Low Ca px, Ilm
Sc4-b	1	50	72	1000	Gl, Fap, Low Ca px, Ilm
McGill 10					
Dy-spt	1	50	92	1015	Gl, Fap, Plg, Low Ca px, Ilm
Sc4-b	1	50	92	1015	Gl, Fap, Low Ca px, Ilm
McGill 11					
Dy-spt	1	50	73	1040	Gl, Fap, Low Ca px, Ilm
Sc4-b	1	50	73	1040	Gl, Fap, Plg, Low Ca px, Qtz, Ilm
McGill 12					
Dy-spt	1	50	142	1100	Gl, Ilm
Sc4-b	1	50	142	1100	Gl, Ilm
Without F					
McGill7					
Dy-spt	1	50	140	1000	Gl, Hap, Cpx, Low Ca px, Ilm
Sc4-b	1	50	140	1000	Gl, Hap, Plg, Cpx, Low Ca px, Ilm
McGill 8					
Dy-spt	1	50	66	1015	Gl, Hap, Plg, Cpx, Ol, Ilm
Sc4-b	1	50	66	1015	Gl, Hap, Plg, Cpx, Low Ca px, Ilm
McGill 9					
Dy-spt	1	50	69	1040	Gl, Ilm
Sc4-b	1	50	69	1040	Gl, Hap, Ilm
McGill 13					
Dy-spt	1	50	70	1100	Gl, Ilm
Sc4-b	1	50	70	1100	Gl, Ilm
With 10 wt% P2O5					
McGill 14					
Sc4-b	1	50	93	1050	Gl, Plg, Qtz, Ilm

Sc4-b + F	1	50	93	1050	Gl, Qtz, Ilm
McGill 15					
Sc4-b + F	1	50	69	1075	Gl, Fap, Unk, Qtz, Ilm
McGill 16					
Sc4-b	1	50	69	1100	Gl
Sc4-b + F	1	50	69	1100	Gl, Fap

[a] D1: duration above the liquidus before cooling (1250°C); D2: duration at the final temperature.
[b] Tf: final temperature of the experiment.
[c] Abbreviation used for the phases: Fap, fluoroapatite; Hap, Hydroxyapatite; Gl, glass (liquid); Plg, plagioclase; Cpx, clinopyroxene; Low-Ca px, Low-Ca pyroxene; Ol, olivine; Ilm, ilmenite and Unk, unknown phase.

3.3.3 Analytical techniques

The quenched experiments were mounted and polished for petrographic and electron-microprobe analyses. The electron-microprobe analyses were performed using a Cameca SX100 (Laval University, Québec City, Canada), operated with an accelerating voltage of 15kV and a 20 nA beam current. The incident-beam diameter was 5 μm on glass (where space permitted) to minimize alkali volatility under the electron beam. A focused beam (1 μm) was used in all other cases. All microprobe analyses were carried out using wavelength dispersive spectrometers (WDS). Standards used were albite for Na and Al, orthoclase for Si and K, hematite for Fe, wollastonite for Ca, olivine for Mg, $MnTiO_3$ for Ti, chlorapatite for P and apatite for F. The counting times were 20s on the peak and 10s on the background.

3.3.4 Attainment of equilibrium

Backscattered electron images did not show any zonation (Fig. 3. 1). We carried out our analyses on apatite using line-traverse on 100 μm thick thin-sections. The constancy of concentration during line-traverse and the low standard deviations on these mineral analyses (Table 3. 3) confirm that the minerals are not strongly compositionally zoned. The standard deviations (1σ) of multiple analyses on glass are low (varies between 1 to 10% but, is generally less than 2 %).

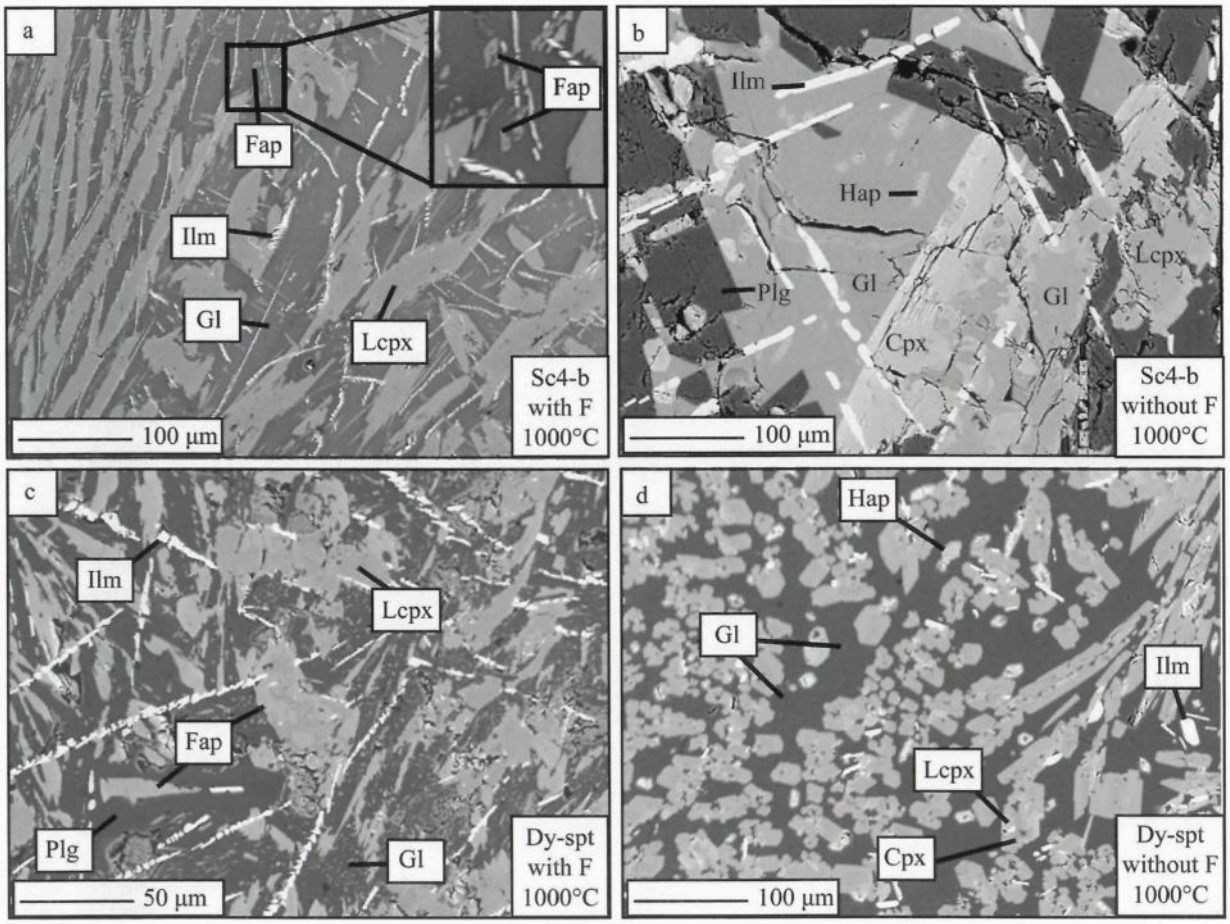

Figure 3. 1 : Backscattered electron images of the Sc4-b and Dy-spt run products. Note the absence of compositional zonation in the crystals, reflecting a close approach to equilibrium in our experiments. (a) McGill 1 with Sc4-b composition, (b) McGill 7 with Sc4-b composition, (c) McGill 1 with Dy-spt composition, (d) McGill 7 with Dy-spt composition. Abbreviations used for the phases: Fap, fluoroapatite; Hap, Hydroxyapatite; Gl, glass; Plg, plagioclase; Cpx, clinopyroxene; Lcpx, Low-Ca pyroxene and Ilm, ilmenite.

Table 3. 3. Electron microprobe analyses (wt %) of run products.

Run no.	Phase [a]	% modal [b]	number of analyses	SiO_2	TiO_2	Al_2O_3	FeO	MgO	CaO	Na_2O	K_2O	P_2O_5	F	H_2O	Total
With 5 wt% P_2O_5 With F															
McGill 1															
Dy-spt	Fap	10	6	1.69 (0.92)			1.59 (0.16)	0.41 (0.13)	47,17 (0,42)	0.07 (0.04)		40.79 (1.02)	6.79 (1.28)		102.78
	Gl	5	2	70.42 (4.75)	0.34 (0.11)	15.77 (4.39)	1.84 (0.8)	0.13 (0.03)	3.83 (3.33)	1.97 (1.72)	2.70 (0.39)	0.16 (0.13)	1.39 (0.57)		98.55
	Plg	45	5	56.37 (1.39)	0.16 (0.06)	26.33 (1.03)	0.80 (0.10)	0.06 (0.03)	9.96 (1.00)	4.75 (0.34)	0.74 (0.16)	0.08 (0.05)	0.09 (0.07)		99.34
	Low Ca px	35	10	45.25 (1.71)	1.83 (1.18)	5.72 (3.04)	27.30 (6.30)	12.85 (1.38)	4.59 (2.42)	0.22 (0.12)	0.02 (0.02)	0.34 (0.56)	0.22 (0.13)		98.35
	Ilm	5	-												
Sc4-b	Fap	5	3	5.66 (1.06)			1.50 (0.21)	0.31 (0.03)	51.41 (0.72)	0.17 (0.05)		38.87 (0.52)	4.94 (0.58)		102.92
	Gl	50	10	59.21 (0.61)	0.57 (0.04)	18.03 (0.35)	7.95 (0.52)	0.65 (0.09)	8.17 (0.29)	1.51 (0.09)	0.71 (0.04)	0.29 (0.04)	1.69 (0.22)		98.77
	Low Ca px	40	3	44.44 (0.29)	3.20 (0.18)	6.45 (0.16)	20.86 (0.61)	12.18 (0.29)	10.45 (0.14)	0.23 (0.01)		0.37 (0.06)	<0.13		98.23
	Ilm	5	-												
McGill 10															
Dy-spt	Fap	8	3	19.23 (4.24)			1.68 (0.38)	0.36 (0.08)	39.98 (3.93)	0.54 (0.37)		31.24 (1.20)	5.41 (1.14)		98.55
	Gl	10	7	69.65 (0.96)	0.64 (0.03)	14.16 (0.39)	3.61 (0.12)	0.78 (0.04)	2.84 (0.23)	1.27 (0.13)	3.95 (0.12)	0.20 (0.06)	2.40 (0.29)		99.54
	Plg	45	5	53.97 (0.30)	0.14 (0.04)	28.77 (0.38)	0.72 (0.08)	0.06 (0.02)	11.91 (0.27)	3.72 (0.09)	0.65 (0.04)	0.05 (0.02)			100.03
	Low Ca px	32	7	47.56 (0.75)	0.81 (0.16)	3.54 (0.99)	30.94 (1.51)	13.61 (0.58)	1.93 (0.23)	0.04 (0.01)	0.01 (0.00)	0.04 (0.03)	0.12 (0.08)		98.60
	Ilm	5	-												
Sc4-b	Fap	5	5	0.59 (0.17)			1.07 (0.07)	0.42 (0.02)	53.20 (0.37)	0.01 (0.01)		42.30 (0.55)	5.31 (0.85)		102.95
	Gl	70	10	56.86 (0.58)	1.28 (0.14)	16.92 (0.29)	10.09 (0.27)	1.31 (0..04)	8.41 (0.16)	2.03 (0.06)	0.60 (0.02)	0.63 (0.13)	1.59 (0.38)		99.72
	Low Ca px	20		47.88 (0.60)	1.62 (0.39)	4.58 (0.62)	24.60 (1.25)	14.88 (0.73)	5.25 (1.30)	0.13 (0.02)		0.06 (0.01)	0.04 (0.04)		99.05
	Ilm	5	-												
McGill 11															
Dy-spt	Fap	5	5	0.82 (0.62)			1.27 (0.37)	0.56 (0.08)	52.94 (0.69)	0.04 (0.04)		42.31 (0.59)	4.99 (0.51)		102.99
	Gl	90	10	46.04 (0.34)	3.49 (0.10)	15.03 (0.12)	13.89 (0.20)	4.65 (0.05)	8.26 (0.06)	2.26 (0.03)	1.10 (0.02)	2.14 (0.14)	1.27 (0.11)		98.15
	Low Ca px	3	5	47.69 (0.65)	1.40 (0.13)	6.21 (0.63)	22.05 (0.23)	17.79 (0.39)	3.39 (0.26)	0.11 (0.01)		0.06 (0.04)	< 0.07		98.80
	Ilm	2	-												

Run no.	Phase [a]	% modal [b]	number of analyses	SiO_2	TiO_2	Al_2O_3	FeO	MgO	CaO	Na_2O	K_2O	P_2O_5	F	H_2O	Total
McGill 11															
Sc4-b	Fap	3	3	1.81 (0.77)			1.41 (0.10)	0.33 (0.03)	52.79 (0.95)	0.03 (0.01)		41.71 (0.92)	5.02 (1.07)		103.10
	Gl	35	11	48.77 (0.08)	4.02 (0.15)	11.82 (0.10)	16.30 (0.35)	3.71 (0.18)	9.28 (0.11)	1.25 (0.05)	0.67 (0.03)	1.66 (0.05)	1.46 (0.51)		98.94
	Plg	25	5	53.64 (2.06)	0.12 (0.03)	29.32 (2.04)	0.82 (0.09)	0.12 (0.01)	11.70 (0.37)	4.06 (0.17)	0.19 (0.01)	0.04 (0.02)			100.04
	Low Ca px	27	5	48.93 (0.16)	0.96 (0.22)	2.34 (0.88)	27.94 (2.07)	15.41 (1.10)	3.01 (0.48)	0.04 (0.01)		0.02 (0.01)	<0.06		98.72
	Qtz	5	1	97.67	0.20	0.33	0.42	0.06	0.05	0.01		0.00			98.74
	Ilm	5	-												
McGill 12															
Dy-spt	Gl	99	10	46.35 (0.16)	3.92 (0.09)	14.05 (0.09)	14.73 (0.10)	5.43 (0.05)	8.07 (0.07)	1.85 (0.03)	1.07 (0.02)	2.18 (0.05)	0.96 (0.09)		98.62
	Ilm	1	-												
Sc4-b	Gl	100		48.08 (0.14)	4.25 (0.02)	11.44 (0.11)	15.25 (0.27)	4.63 (0.03)	9.40 (0.04)	1.82 (0.02)	0.38 (0.01)	2.48 (0.05)	1.03 (0.06)		98.78
	Ilm	Traces	-												
With 5 wt% P_2O_5 Without F															
McGill 7															
Dy-spt	Hap	10	5				1.57 (0.38)	0.36 (0.05)	52.74 (1.79)	0.08 (0.04)		42.26 (0.81)		1.76 (0.16)	98.77
	Gl	40	10	55.88 (0.72)	0.91 (0.02)	18.96 (0.16)	9.49 (0.48)	1.44 (0.04)	4.96 (0.18)	2.33 (0.08)	1.87 (0.06)	1.25 (0.07)			97.08
	Cpx	10	1	43.73	4.01	8.99	14.64	12.73	13.90	0.63	0.20	0.70	0.03		99.56
	Low Ca px	35	4	39.02 (0.77)	7.33 (0.23)	12.30 (0.42)	15.91 (0.94)	10.84 (0.43)	9.50 (0.32)	2.64 (0.13)	0.43 (0.05)	0.56 (0.11)	<0.05		98.58
	Ilm	5	-												
Sc4-b	Hap	8	4	0.87 (0.74)			1.68 (0.25)	0.24 (0.04)	53.12 (0.24)	0.11 (0.04)		42.60 (1.14)		1.79 (0.01)	100.42
	Gl	25	10	55.99 (2.24)	1.43 (0.15)	11.87 (0.34)	16.48 (1.73)	0.82 (0.10)	4.96 (0.50)	2.26 (0.09)	1.53 (0.16)	1.31 (0.22)			96.64
	Plg	25	5	58.53 (0.60)	0.08 (0.03)	25.88 (0.38)	0.48 (0.09)	0.04 (0.01)	7.62 (0.28)	7.11 (0.13)	0.19 (0.02)	0.06 (0.01)			100.01
	Cpx	12	4	46.11 (0.40)	3.52 (0.15)	6.00 (0.28)	13.80 (0.81)	11.46 (0.08)	17.56 (0.44)	0.60 (0.02)		0.37 (0.21)			99.4
	Low Ca px	20	3	48.55 (0.31)	0.58 (0.08)	1.29 (0.29)	29.15 (1.94)	12.00 (1.21)	6.95 (1.28)	0.15 (0.02)		0.03 (0.01)			98.69
	Ilm	10	-												

Run no.	Phase [a]	% modal [b]	number of analyses	SiO_2	TiO_2	Al_2O_3	FeO	MgO	CaO	Na_2O	K_2O	P_2O_5	F	H_2O	Total
McGill 8															
Dy-spt	Hap	3	3	0.38 (0.03)			2.82 (0.19)	2.92 (0.03)	46.47 (0.03)	1.10 (0.10)		43.76 (0.48)		1.81 (0.01)	99.26
	Gl	15	5	73.54 (1.49)	1.35 (0.74)	12.35 (1.23)	4.58 (0.95)	0.44 (0.12)	0.97 (0.24)	1.16 (0.58)	2.57 (0.51)	0.18 (0.04)			97.15
	Plg	27	5	60.06 (0.81)	0.14 (0.06)	24.65 (0.38)	0.86 (0.06)	0.05 (0.03)	6.35 (0.50)	7.35 (0.28)	0.56 (0.13)	0.05 (0.02)			99.52
	Cpx	15	5	43.94 (0.39)	4.29 (0.27)	6.84 (0.26)	14.65 (1.66)	10.83 (0.60)	16.21 (0.74)	0.69 (0.04)		1.28 (0.51)			98.73
	Low Ca px	35	5	47.74 (0.68)	0.65 (0.08)	0.96 (0.14)	35.92 (1.77)	7.35 (1.62)	6.55 (0.98)	0.14 (0.03)		0.05 (0.03)			99.35
	Ilm	5	-												
Sc4-b	Hap	3	5	0.94 (0.56)			5.50 (0.32)	1.83 (0.06)	45.53 (0.63)	0.46 (0.05)		43.13 (0.69)		1.79 (0.02)	99.20
	Gl	12	5	69.82 (1.70)	0.77 (0.07)	12.00 (0.30)	7.45 (1.05)	0.23 (0.02)	1.72 (0.20)	1.14 (0.20)	2.98 (0.19)	0.39 (0.04)			96.50
	Plg	40	5	57.07 (0.78)	0.17 (0.04)	26.40 (0.25)	0.99 (0.21)	0.10 (0.04)	8.50 (0.52)	6.15 (0.34)	0.70 (0.10)	0.11 (0.03)			
	Cpx	25	4	47.34 (1.39)	2.07 (0.34)	4.41 (0.78)	14.70 (1.36)	9.71 (0.62)	19.95 (0.73)	0.58 (0.07)					98.75
	Ol	15	5	32.77 (0.26)	< 0.32	0.18 (0.10)	47.62 (1.38)	17.55 (0.87)	0.52 (0.09)	0.06 (0.02)		0.74 (0.22)			99.75
	Ilm	5	-												
McGill 9															
Dy-spt	Gl	100	10	54.40 (0.26)	4.36 (0.08)	16.63 (0.13)	<0.02	6.05 (0.11)	7.69 (0.10)	6.51 (0.06)	0.66 (0.01)	2.17 (0.05)			98.50
	Ilm	Traces	-												
Sc4-b	Gl	98	10	58.94 (0.41)	5.12 (0.14)	14.32 (0.08)	0.06 (0.04)	4.74 (0.15)	7.62 (0.20)	5.22 (0.08)	0.29 (0.01)	1.80 (0.03)			98.12
	Hap	2	5	1.10 (0.79)				0.74 (0.02)	50.71 (0.90)	0.36 (0.04)		40.99 (0.91)		0.09 (0.03)	100.39
	Ilm	Traces	-												
McGill 13															
Dy-spt	Gl	100	10	52.35 (0.27)	4.40 (0.03)	16.07 (0.08)	3.43 (0.05)	6.34 (0.07)	9.38 (0.06)	3.60 (0.05)	1.12 (0.02)	2.35 (0.03)			99.06
	Ilm	Traces	-												
Sc4-b	Gl	100	10	52.90 (0.29)	4.46 (0.07)	12.70 (0.12)	4.93 (0.08)	4.93 (0.08)	10.19 (0.06)	3.06 (0.03)	0.42 (0.01)	2.55 (0.07)			98.80
	Ilm	Traces	-												

Run no.	Phase [a]	% modal [b]	number of analyses	SiO_2	TiO_2	Al_2O_3	FeO	MgO	CaO	Na_2O	K_2O	P_2O_5	F	H_2O	Total
With 10 wt% P_2O_5															
McGill 14															
Sc4-b	Gl	75	6	45.90 (1.55)	3.97 (0.21)	11.16 (0.48)	15.19 (0.44)	4.27 (0.21)	8.85 (0.40)	2.43 (0.18)	0.34 (0.04)	6.64 (0.67)			
	Plg	15	3	60.63 (0.27)	0.20 (0.03)	23.94 (0.48)	0.59 (0.17)	0.08 (0.01)	6.36 (0.26)	7.20 (0.11)	0.23 (0.02)	0.12 (0.04)			
	Qtz	5	-												
	Ilm	5	-												
Sc4-b + F	Gl	90	9	41.77 (1.43)	4.28 (0.13)	10.79 (0.34)	16.50 (0.59)	4.87 (0.23)	9.87 (0.29)	1.39 (0.08)	0.32 (0.04)	8.23 (0.59)	0.13 (0.06)		
	Qtz	5	-												
	Ilm	5	-												
McGill 15															
Sc4-b + F	Gl	70	5	51.45 (0.56)	2.41 (1.62)	15.45 (1.07)	12.68 (0.99)	1.98 (0.69)	7.21 (0.75)	1.93 (0.19)	0.46 (0.03)	5.60 (1.03)			
	Fap	10	5	0.58 (0.42)			1.58 (0.10)	0.76 (0.02)	51.58 (0.21)	0.06 (0.03)		41.77 (0.73)	4.28 (1.28)		
	Unk	10	4	43.59 (0.33)	1.45 (0.31)	5.61 (0.58)	23.23 (0.78)	13.32 (1.64)	6.40 (0.73)	0.12 (0.04)	0.08 (0.04)	5.83 (0.98)			
	Qtz	5	-												
	Ilm	5	-												
McGill 16															
Sc4-b	Gl	100		46.65 (0.15)	4.17 (0.06)	11.20 (0.12)	14.18 (0.11)	4.53 (0.05)	8.94 (0.04)	2.44 (0.16)	0.36 (0.01)	6.80 (0.10)			99.27
Sc4-b + F	Gl	99		45.84 (0.98)	4.33 (0.11)	11.80 (0.29)	14.63 (0.30)	4.67 (0.11)	8.74 (0.17)	1.69 (0.04)	0.45 (0.03)	6.66 (0.20)	0.11 (0.09)		98.91
	Fap	1		0.91 (0.85)			1.69 (0.28)	0.86 (0.11)	52.11 (0.98)	0.06 (0.02)		41.23 (1.09)	3.51 (0.05)	< 0.20	100.59

Numbers in parentheses indicate the standard deviation.

[a] Abbreviation used for the phases: Fap, fluoroapatite; Hap, Hydroxyapatite; Gl, glass (liquid); Plg, plagioclase; Cpx, clinopyroxene; Low-Ca px, Low-Ca pyroxene; Ol, olivine; Ilm, ilmenite and Unk, unknown phase.

[b] Modal percentages were determined by optical observations.

Moreover, dry experiments of similar melt fractions, durations (from 72h to 179h) and temperatures (from 1030°C to 1075°C) were previously demonstrated to reach equilibrium (Tollari et al. 2006). These lines of evidence suggest that equilibrium was achieved during the experiments.

3.4 RESULTS

3.4.1 Phase equilibria

The observed phase relations are listed in Tables 3. 2 and 3. 3 and illustrated in Fig. 3. 1 for the experiments with 5 weight percent of P_2O_5. All experiments contained glasses that correspond to residual liquids. In addition to glass, silicate, oxide and phosphate minerals are present.

The silicate minerals present are plagioclase, clinopyroxene, low-Ca pyroxene, olivine and quartz. The phosphates are fluoroapatite or hydroxyapatite. The Fe-Ti oxide is ilmenite. The absence of other oxides (magnetite) is due to the low oxygen fugacity (FMQ - 1 to - 2) of the experimentation (Toplis and Carroll, 1995). It is possible that other phases were present in the experimental charges, but were not analysed or described. This could be due to their low abundance and the fact that they did not intersect the surface exposed for electron microprobe analysis. This would explain the slight differences of composition between initial compositions and experiments which contained only glass. Contrary to the dry experiments (Tollari et al. 2006) the charges doped with 10 weight percent P_2O_5 did not contain evidence of liquid-liquid immiscibility (i.e. two glasses with different compositions or the presence of globules of glass).

3.4.2 Experiments with 5 wt% P_2O_5

- Experiments with fluorine

The appearance of the different phases is described only for the temperature studied. The first phase observed in our charges for both bulk rock compositions is ilmenite (1100°C). In the Skaergaard analogue (Sc4-b), at 1040°C ilmenite is joined by fluoroapatite, plagioclase, low-Ca pyroxene and quartz. At 1015°C and 1000°C, quartz was not observed. This is probably due to the low abundance of quartz in these runs (less than 5 % observed at 1040°C) and it is possible that quartz did not intersect the surface exposed for electron microprobe analysis. In the Sept-Îles analogue (Dy-spt), ilmenite is joined by fluoroapatite and low-Ca pyroxene at 1040°C, then by plagioclase at 1015°C. At 1000°C the assemblage is the same as at 1015°C.

- Experiments without fluorine

The first phase to appear for both bulk rock compositions is ilmenite at 1100°C. Then at 1040°C hydroxyapatite appears in Sc4-b composition followed by plagioclase, clinopyroxene and low-Ca pyroxene at 1015°C. In Dy-spt, ilmenite is joined by hydroxyapatite, plagioclase, clinopyroxene and olivine at 1015°C. At 1000°C Olivine disappears and low-Ca pyroxene appears. Plagioclase is most probably present at this temperature, but was not observed in the sample due to its low abundance (15 % at 1015°C), as discussed above for quartz.

3.4.3 Experiments with 10 wt% P_2O_5

These experiments were carried out only with the Sc4-b composition. Ten weight percent P_2O_5 was added (with and without addition of F) in an effort to provoke liquid immiscibility as observed in the low-pressure dry experiments. The first phase to appear in Sc4-b + F with 10 wt % P_2O_5 is apatite (1100°C). At 1075°C apatite is joined by an unknown phase ($Si_{1.7}Mg_{0.8}Fe_{0.7}Ca_{0.3}Al_{0.3}P_{0.2}O_6$), quartz and ilmenite. Apatite and the unknown phase were not observed at 1050°C. In Sc4-b with 10 wt % P_2O_5, but without F, we noted the absence of apatite at all studied temperatures. At 1050°C we observed plagioclase, quartz and ilmenite.

3.5 DISCUSSION

3.5.1 Effect of melt composition and pressure on crystalline phosphate saturation

- Effect of melt composition -

As summarised by Tollari et al. (2006) and Watson (1979), melt composition has an important effect on phosphate saturation. In particular SiO_2 and CaO have been found to have a major affect on the level of P_2O_5 required to saturate a magma. Alkalis also influence the amount of P_2O_5 required to achieve saturation but to a lesser extent (Bea et al. 1992). Tollari et al. (2006) worked on a ferrobasalt (a Skaergaard analogue) in a dry system thus the phosphate that crystallized was whitlockite rather than apatite. The addition of H_2O and F to our ferrobasaltic system in this study, leads to apatite crystallization and more

closely approaches terrestrial conditions. The apatite crystals appear at 1040°C for Sc4-b with and without F, and for Dy-spt at 1040°C with F and 1015°C without F.

To investigate the relationship between SiO_2, CaO and P_2O_5 in these systems, we have plotted SiO_2, CaO and P_2O_5 content in our liquid saturated in apatite in binary diagrams P_2O_5-SiO_2 (Fig. 3. 2 a) and P_2O_5-CaO (Fig. 3. 2 b). We used only our data for liquids in equilibrium with apatite to observe the effect of melt composition (SiO_2, CaO and F) on phosphate saturation. Our data show positive correlations between P_2O_5 and CaO and negative correlations between P_2O_5 and SiO_2 content in the glass. The addition of F in this system does not apparently change the relationship between these elements but does lower the concentrations of P_2O_5 necessary to cause apatite saturation.

The open symbols (F-free experiments) define trends slightly above the filled symbols (F-bearing experiments). For example in experiments with approximately 55 % SiO_2, would require 1.5 % P_2O_5 to attain saturation in an F-free system and only 0.6 % in a F-bearing system. It is difficult to discern the effect of H_2O on apatite saturation from our experimental results as H_2O was added to all runs.

- Effect of pressure -

The models of Harrison and Watson (1984) and Tollari et al. (2006) highlight the effect of melt composition and temperature on phosphate saturation. According to Tollari et al. (2006) temperature is a secondary factor compared to the effect of composition. Watson (1980) worked on apatite saturation in basic magmatic liquids at different temperatures (1165°C to 1350°C) and pressures (0.1 MPa to 2500 MPa). He concluded that apatite solubility is almost insensitive to pressure.

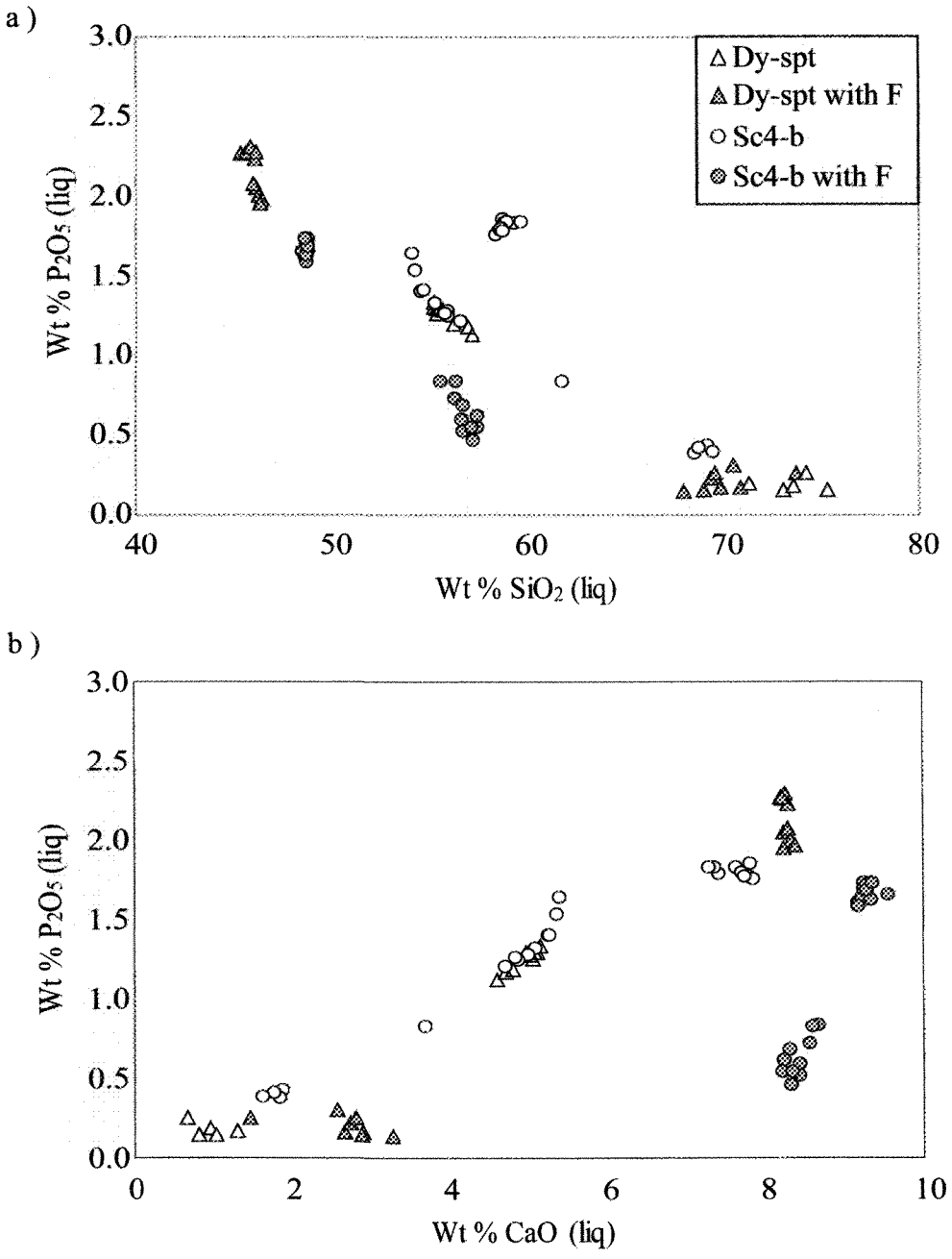

Figure 3. 2. a) a) Covariation of P_2O_5 and SiO_2 of apatite saturated liquids; b) Covariation of P_2O_5 and CaO of apatite saturated liquids.

In order to investigate the effect of pressure on phosphate saturation in ferrobasaltic systems, we compared our new results (500 MPa) with the previous results of Watson (1980) and Tollari et al. (2006) (Figs. 3. 3 a and b). Data from our experiments and experiments from Watson (1980) and Tollari et al. (2006) show a similar trend: a positive correlation between P_2O_5 and CaO and a negative correlation between P_2O_5 and SiO_2. However, the distribution of data above 10 wt. % CaO does not define a clear relationship of P_2O_5-CaO in the study of Watson (1980). The similarity in the trends from both sets of experiments run at different pressures confirms the observation of Watson (1980) that changes in pressure have only a minor effect on apatite saturation.

3.5.2 Effect of melt composition and pressure on immiscibility field

- Effect of melt composition -

In the introduction, two models were proposed to explain the origin of apatite-oxide-rich rocks: the magma becomes saturated in apatite and Fe-Ti oxide or the magma becomes saturated in an immiscible Fe-Ti-P liquid. Previous experimental studies have generated two liquid immiscibility in basaltic systems (Tollari et al. 2006). However, the immiscibility observed is not directly applicable to natural-mafic systems for two reasons: the melts in which immiscibility occurred contained no volatiles (H_2O, F or Cl), and immiscibility only occurred using starting compositions with 10 weight percent of P_2O_5.

The current experiments were to investigate whether the addition of H_2O or F to silicate melt could lead to immiscibility. Indeed, the stability of silicate melt is a function of the concentration and distribution of the oxygen species (Hess 1980).

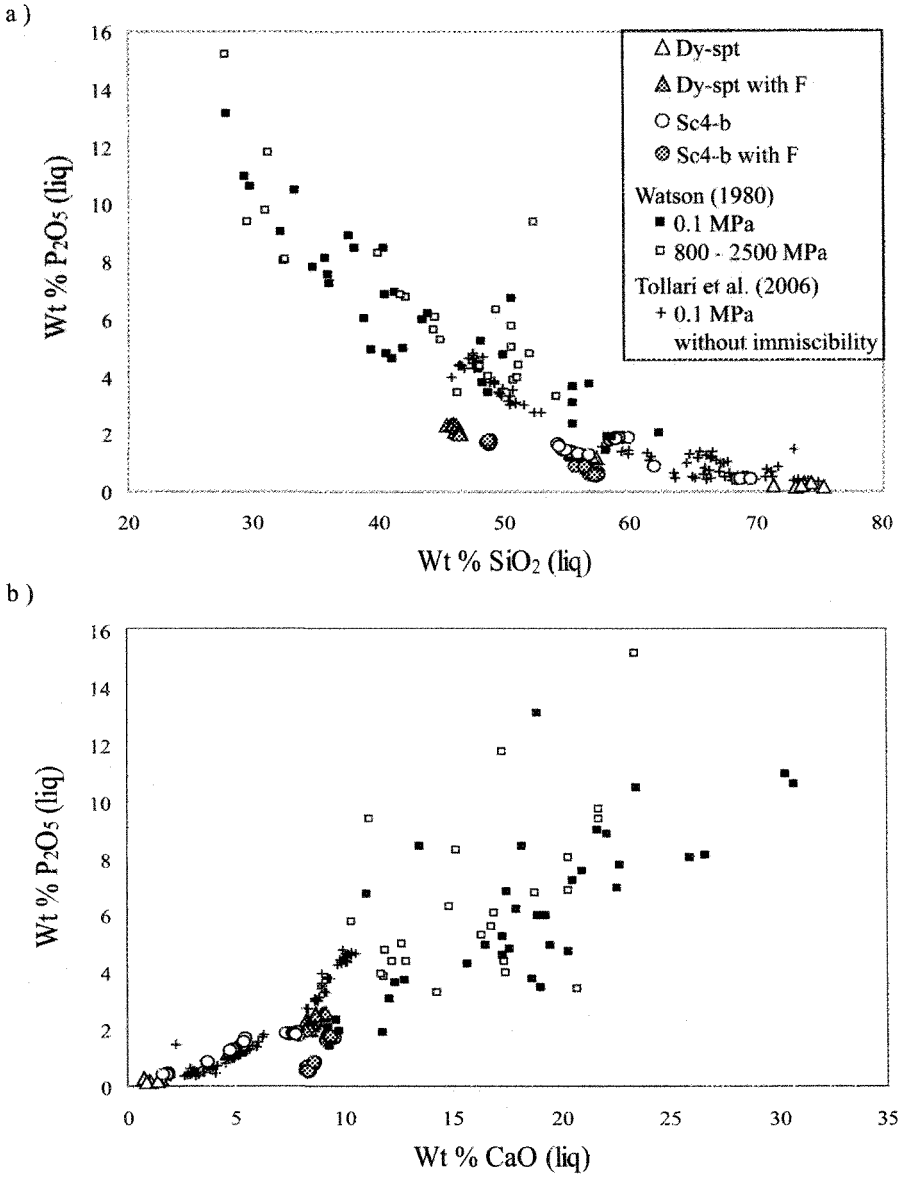

Figure 3. 3. a) Covariation of P_2O_5 and SiO_2 of apatite saturated liquids from this study and the literature. Circles: this study, black squares: data from 0.1 MPa experiments of Watson (1980), white squares: data from 800 to 2500 MPa experiments of Watson (1980) and cross symbols: data from 0.1 MPa experiments of Tollari et al. (2006); b) Covariation of P_2O_5 and CaO of apatite saturated liquids with and without F addition. Same symbols used.

The current experiments were to investigate whether the addition of H_2O or F to silicate melt could lead the immiscibility. Indeed, the stability of silicate melt is a function of the concentration and distribution of the oxygen species (Hess 1980). Addition of H_2O in a silicate melt breaks Si-O-Si bonds and causes depolymerisation of the magma; this could lead to the instability of the melt and form two liquids by immiscibility (Hess 1980; Mysen 2007; Mysen and Cody 2004; Mysen and Cody 2005). Due to the fluorine-oxygen substitution in the melt structure, F is very soluble in silicate magmas (Mysen et al. 2004). The presence of this element causes a decrease of silicate-melt activities (Manning et al. 1980) which would also suggest that it plays a role in melt polymerization.

Although we added 1 weight percent of H_2O and 1 weight percent F to our charges no immiscibility was observed. In the dry system, immiscibility was observed in experiments with similar starting compositions chose in this study (Sc4-8 and Sc4-b) to which 10 weight percent P_2O_5 was added (Tollari et al. 2006). The series of experiments with the composition Sc4-b plus 10 weight percent of P_2O_5 in the present study did not display evidence for immiscibility.

- Effect of pressure -

A second hypothesis was that the pressure can affect the stability of the magma structure and also play a role in the immiscibility. Hudon et al. (2004) studied the effect of pressure on the immiscibility field in the systems $CaO\text{-}SiO_2$, $MgO\text{-}SiO_2$, and $CaMgSi_2O_6\text{-}SiO_2$ at temperatures from 1810°C to 2000°C. They observed a decrease of the two-liquid immiscibility fields and a displacement of both towards higher temperature with an increase of pressure. These systems are not representative of a natural-mafic system due to the lack of alumina, alkalies and iron. The anhydrous experiments on natural compositions

of Tollari et al. (2006) that displayed liquid-liquid immiscibility were performed at 0.1 MPa, whereas the experiments of Watson (1980) which did not display immiscibility were carried out at 800 to 2500 MPa. Thus, it appears that pressure may, in fact, reduce the field of liquid-liquid immiscibility. However, liquid-liquid immiscibility has been observed in melts similar to natural ones at 400 MPa by Bogaerts and Schmidt (2006). These authors obtained liquid-liquid immiscibility in the system Fe_2SiO_4-$KAlSi_3O_8$-SiO_2-MgO-CaO-TiO_2-P_2O_5. To characterize the effect of pressure on the immiscibility field on this system, we compared data from 0.1 MPa experiments (Tollari et al. 2006) and 400 MPa experiments (Bogaerts and Schmidt 2006) in which immiscibility was observed (Fig. 3. 4 and 3. 5).

Figure 3. 4 is a pseudo-binary projection of the SiO_2-FeO+TiO_2+MgO+CaO+P_2O_5 system and shows the immiscibility field based upon the 400 MPa experiments of Bogaerts and Schmidt (2006) and the 0.1 MPa experiments of Tollari et al. (2006). It appears that an increase of pressure causes a decrease in the width of the immiscibility field, and temperature maximum of immiscibility seems to move towards higher temperatures with increasing pressure which is also consistent with the results of Hudon et al. (2004).

In order to better compare experimental results from different studies with each other and with natural rocks we plotted the liquid-liquid immiscibility data on the pseudo-ternary diagram of Weiblen and Roedder (1973) (Fig. 3. 5 a and b). Figure 3. 5 a) shows data from 0.1 MPa experiments (Tollari et al. 2006) and 400 MPa experiments (Bogaerts and Schmidt 2006) in the system SiO_2-TiO_2-Al_2O_3-FeO-MgO-CaO-Na_2O-K_2O-P_2O_5. These data define the maximum extent of the liquid-liquid immiscibility field for temperature between 1000°C and 1100°C at mid-to-upper crustal pressures.

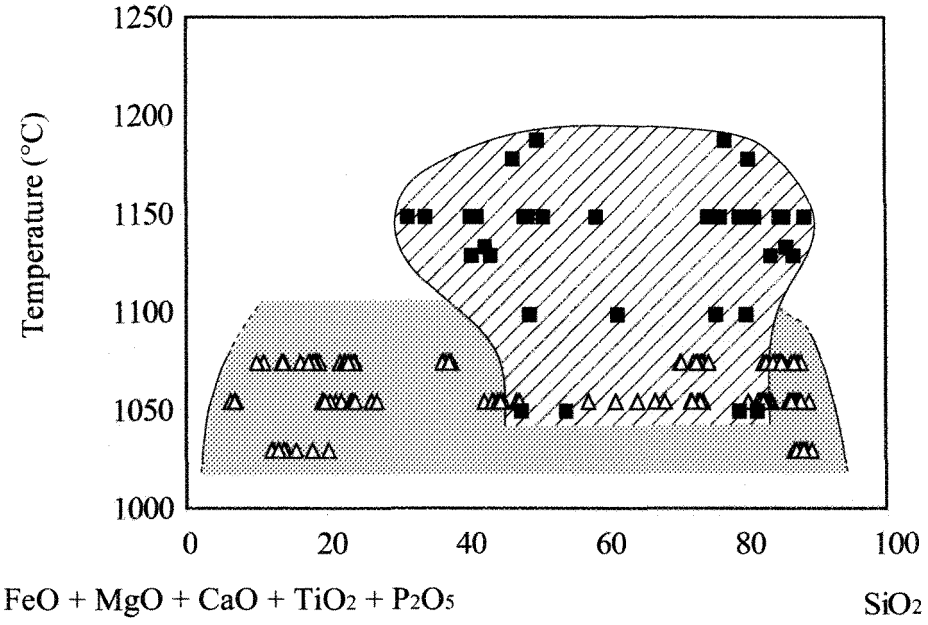

Figure 3. 4. SiO_2-FeO+TiO_2+MgO+CaO+P_2O_5 pseudo-binary phase diagram displaying the extent of liquid-liquid immiscibility. The element contents are in weight percent. Grey shaded zone corresponds 0.1 MPa experiments (Tollari et al., 2006) and hatched zone corresponds to 400 MPa experiments (Bogaerts and Schmidt, 2006).

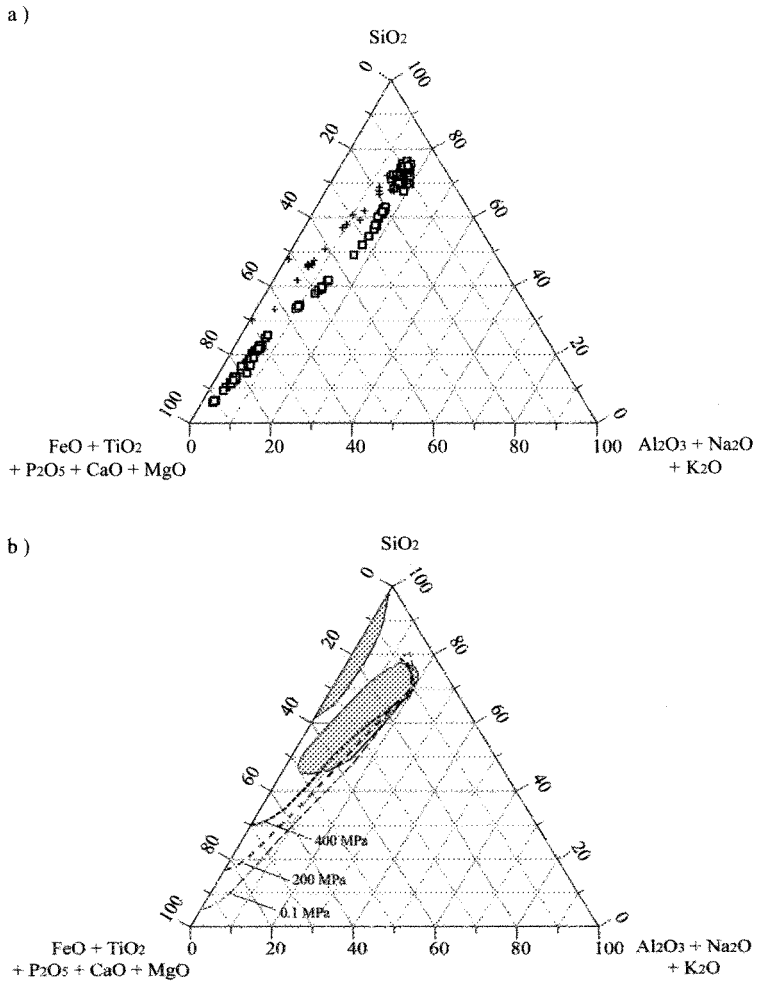

Figure 3. 5. a) Data from experiments with liquid-liquid immiscibility in the pseudoternary system SiO_2-TiO_2+FeO+P_2O_5+MgO+CaO-Al_2O_3+Na_2O+K_2O. Crosses: 400 MPa experiments (Bogaerts and Schmidt, 2006); squares: 0.1 MPa experiments (Tollari et al., 2006). b) Immiscibility fields corresponding to the previous data. Fine dotted line corresponds to 0.1 MPa experiments (Tollari et al., 2006); thick dotted line corresponds to 400 MPa (Bogaerts and Schmidt, 2006) experiments; the intermediate dotted line correspond to the extrapolated immiscibility field at 200 MPa and grey shaded zones correspond to the immiscibility fields of Roedder (1951). All compositions are recalculated on the basis of plotted oxides only.

This immiscibility field is similar in composition to the low-temperature liquid-liquid immiscibility field outlined by Roedder (1951) (Fig. 3. 5 b) based primarily upon studies of natural rocks.

In our 500 MPa experiments we did not observe any evidence of immiscibility. Plotting the melt compositions in the pseudo-ternary diagrams demonstrates that most plot outside of the field of liquid-liquid immiscibility (Fig 3. 6). However, in this projection a few of the liquids do appear to plot inside the field of liquid immiscibility even though no immiscibility was observed. We suggest that the reason for this discrepancy is that these experiments were carried out at lower temperature than the immiscibility experiments of Bogaerts and Schmidt (2006).

When these compositions are plotted in the phase diagram of the systems studied by Bogaerts and Schmidt (2006) (Fig 3. 7) it is observed that melts previously shown in the 400 MPa immiscibility field on Fig. 3. 6, could lie outside of it if the field does not extend to lower temperatures. Based on our textural observations and analyses of the experimental runs we are confident that liquids from the 500 MPa experiments on Skaergaard analogue and Intrusive Suite of Sept-Îles analogue never reached the liquid-liquid immiscibility boundary.

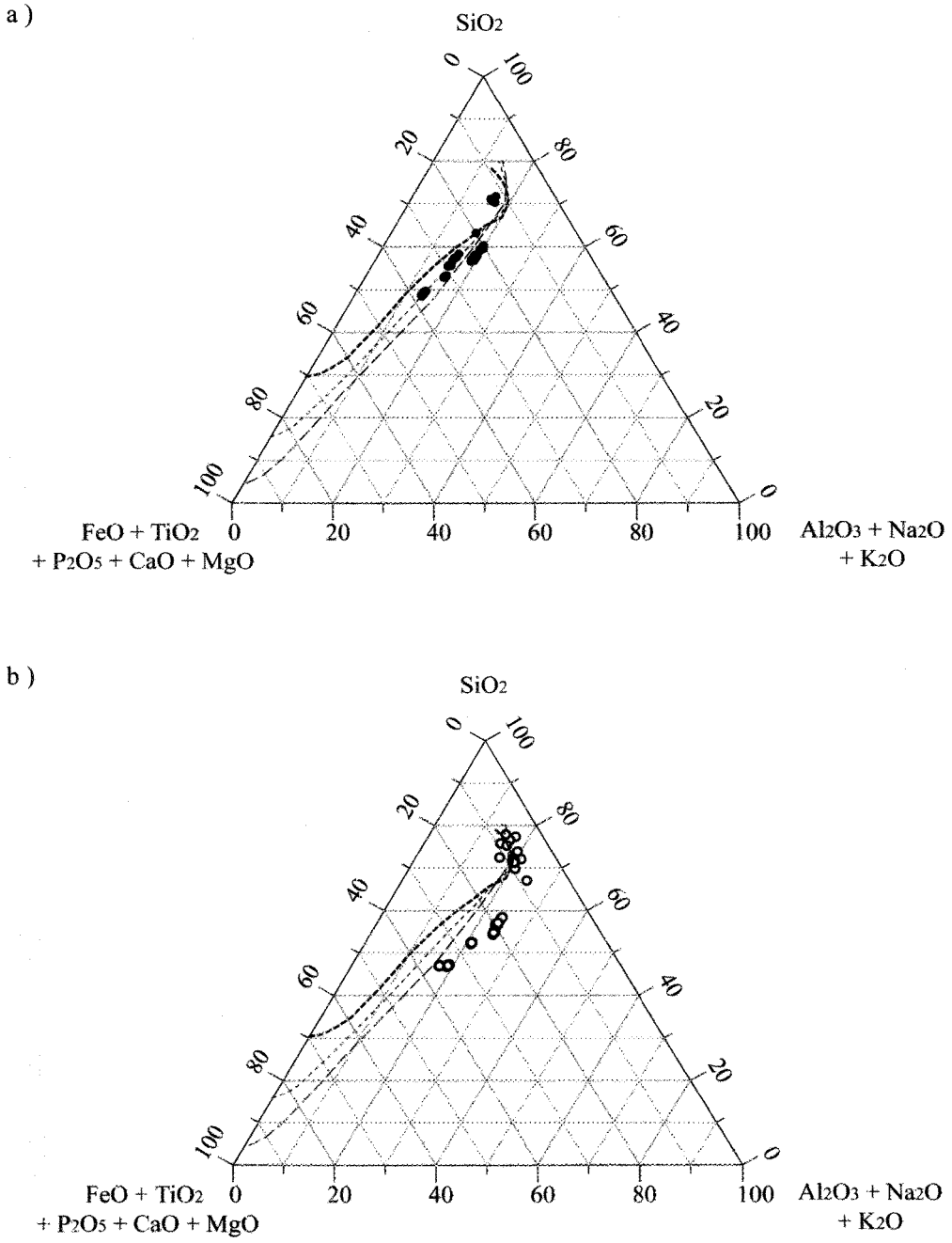

Figure 3. 6 a) Data from experiments with Sc4-b composition; b) Data from experiments with Dy-spt composition. Dotted lines from Fig. 3. 5. All compositions are recalculated on the basis of plotted oxides only.

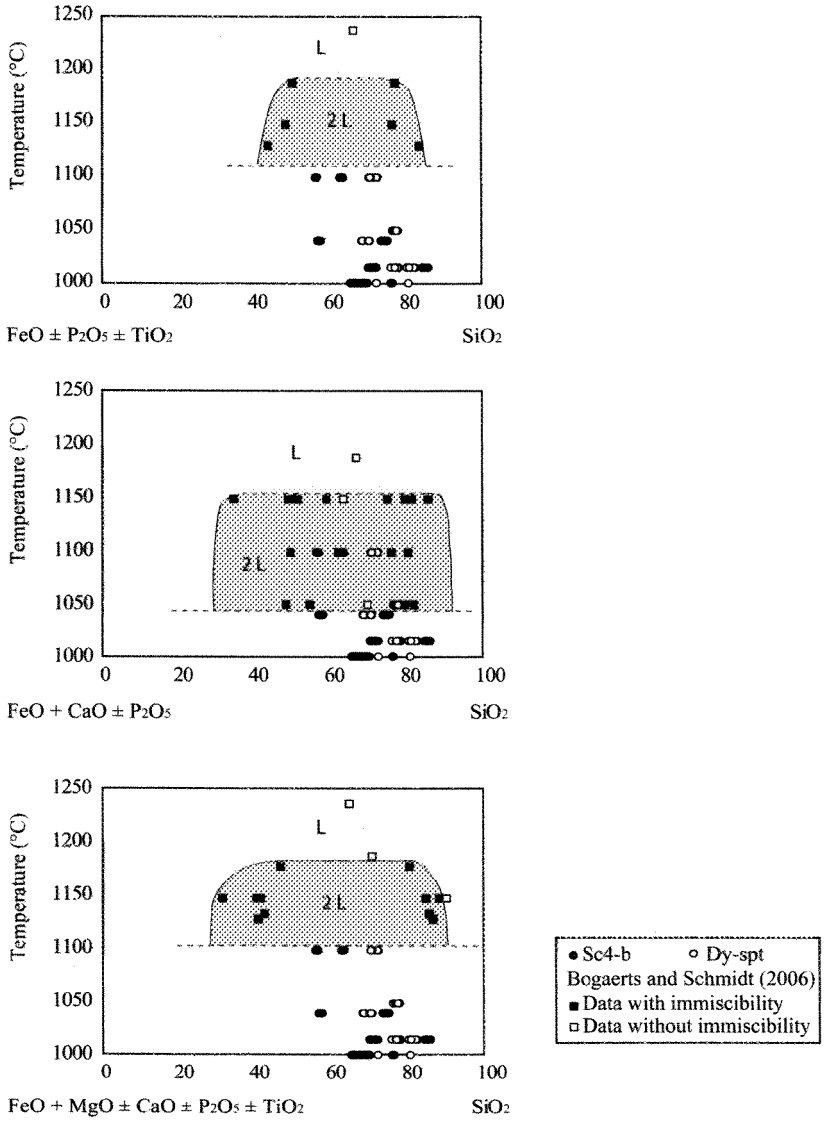

Figure 3. 7. Pseudobinary phase diagram of the three systems studied by Bogaerts and Schmidt (2006). The element contents are in weight percent. Immiscibility field (grey shaded field) defined by the 400 MPa experiments of Bogaerts and Schmidt (2006). Black square: immiscibility observed; white square: no immiscibility obtained. The experimental data obtained during this study for starting composition Sc4-b (black circles) and Dy-spt (white circles) are also plotted. In our experiments we did not observe immiscibility textures; we interpreted this to mean that the immiscibility field ends at the dotted line.

3.5.3 Implications on models of apatite-oxide-rich rocks and nelsonite formation

The formation of nelsonites is highly debated. Many previous studies have strongly argued for one or the other formation models (apatite and oxide crystallization or two liquids immiscibility). Combining the results of this study together with those of Bogaerts and Schmidt (2006) and of Tollari et al. (2006) we can now investigate the importance of these two processes by comparing phosphate saturation and liquid-liquid immiscibility surfaces with liquid lines of descent for natural mafic igneous complexes.

To this end, using data from this study and literature, we investigated the evolution of melts in two layered intrusions, the Sept-Îles Intrusive suite, Quebec, Canada and the Skaergaard complex of Greenland and also investigated the anorthositic complex of Lac St-Jean, Quebec, Canada. Using the published analyses of residual melts in these complexes (Fredette 2006; Tollari et al. submitted; Wager and Brown 1968) we plotted their liquid lines of descent the pseudo-ternary diagram SiO_2-FeO-TiO_2-MgO-CaO-P_2O_5-Al_2O_3-Na_2O-K_2O.

- The Intrusive Suite of Sept-Îles –

In the Sept-Îles Intrusive suite, the apatite-oxide-rich rocks occur in the Critical Zone (ZCR), in the upper part of the Layered Series (Cimon 1998; Higgins 2005). This zone consists from the base upwards of magnetitite, nelsonite, troctolitic-nelsonite, nelsonitic troctolite and microtroctolite. Apatite and oxides are always closely associated. Apatite is present as a euhedral mineral in all these rocks. The subdivision of the ZCR is based on the percentage of oxides present. Rocks where silicate minerals form the matrix to oxide grains

(oxides 1-33 vol %) are referred to as nelsonitic-troctolite. Rocks where the oxides form a matrix to the silicates (33 to 66 vol %) are referred to as troctolitic nelsonites and those containing more than 66 vol % oxides are referred to as nelsonite. The nelsonite has a sharp contact at its base with the massive magnetite layer and grades at its top into troctolitic-nelsonite. The depth of apatite-oxide-rich rocks formation could be estimated, based on the stratigraphy, around 2-3 Km (pressure of 100-150 MPa).

No liquid line of descent or initial magma has been proposed for the Intrusive Suite of Sept-Îles. However, mafic dykes were proposed to be the possible parental magmas to the apatite-oxide-rich rocks in this intrusion (Hounsell 2003; Tollari et al. submitted). We used the program PELE (Boudreau 1999) to simulate crystal fractionation of the dyke composition (Fig. 3. 8). The liquid line of descent obtained with PELE moves away the immiscibility field and does not intersect it before apatite saturation. This is the same behaviour we observed in our experiments.

Thus, the melt of the upper part of Intrusive Suite of Sept-Îles would be saturated in apatite and oxide during crystal fractionation and liquid-liquid immiscibility does not appear to play a role in the petrogenesis of the nelsonites.

- The Anorthositic Complex of the Lac-St-Jean –

In anorthositic complex the apatite-oxide-rich rocks are generally found as lenses (Ashwal 1993; Dymek, et al. 2001). In the Anorthositic Complex of the Lac-St-Jean, the rocks most enriched in apatite and Fe-Ti oxides are nelsonitic peridotite (Fredette 2006). The pressure of anorthositic complex formation is estimated around 500-1300 MPa (Longhi 2005).

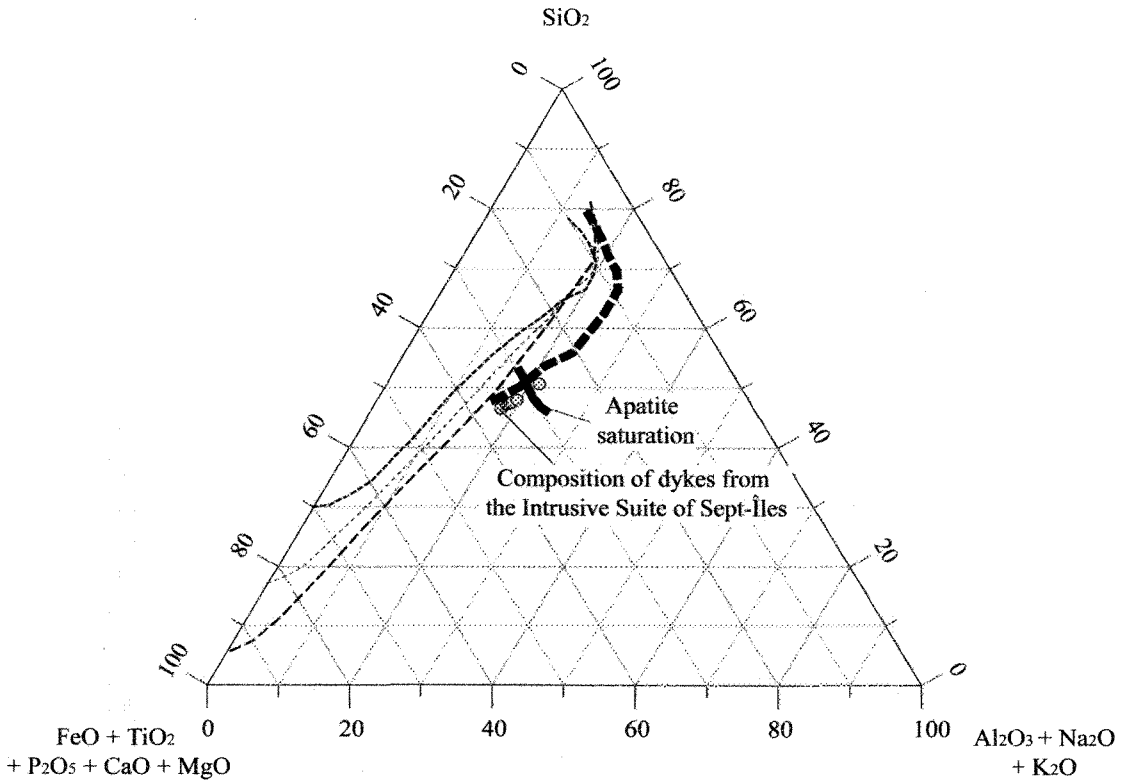

Figure 3. 8. Composition of the proposed liquid lines of descent for the Intrusive Suite of Sept-Îles (Tollari et al., submitted) calculated with PELE software (Boudreau, 1999) (Grey circles). Black-thick-dotted line is trend of data from our experiments using Dy-spt composition. Balck-thick line is apatite surface saturation in the program. Dotted lines from Fig. 3. 5. All compositions are recalculated on the basis of plotted oxides only.

Euhedral apatite can reach 25% modal abundance in these rocks and has a uniform distribution. Ferrodiorite dykes are associated with nelsonite (Fredette 2006). These rocks contain primarily plagioclase (50-60%), clinopyroxene (10-20%), biotite (7-10%), magnetite (1-5%), ilmenite (5-10%) and apatite (2-4%). The ferrodiorites are interpreted as the parental magma of apatite-oxide-rich rocks in the anorthosite complex (Fredette 2006).

A simulation of crystal fractionation, starting with an average ferrodiorite composition, was run until apatite saturation occurred at the same point of previously observed in our experiments (Fig. 3. 9). The average ferrodiorite composition is more distant from the immiscibility field than in the two other previous simulations (Skaergaard melt and mafic dykes of Sept-Îles). The trend moves away from the immiscibility field and does not cross it before apatite saturation. These observations indicate that, once again, immiscibility would not be expected to be the process that produced the apatite-oxide-rich rocks in this intrusion.

- *The Skaergaard Layered Intrusion –*

In the Skaergaard layered intrusion, apatite becomes a cumulus phase in the Upper Zone, at the boundary UZa-b (Wager 1960). The depth of apatite crystallization is unknown but it could be estimated, based on the stratigraphy, around 1.5-3 Km (pressure of 75-150 MPa). The rocks which contain apatite and Fe-Ti oxides in this part of the intrusion are ferrogabbro and not nelsonite and are composed of plagioclase, olivine, augite, magnetite ± inverted iron wollastonite and apatite. Apatite is present as a primary euhedral mineral in all rocks found above the boundary Uza.

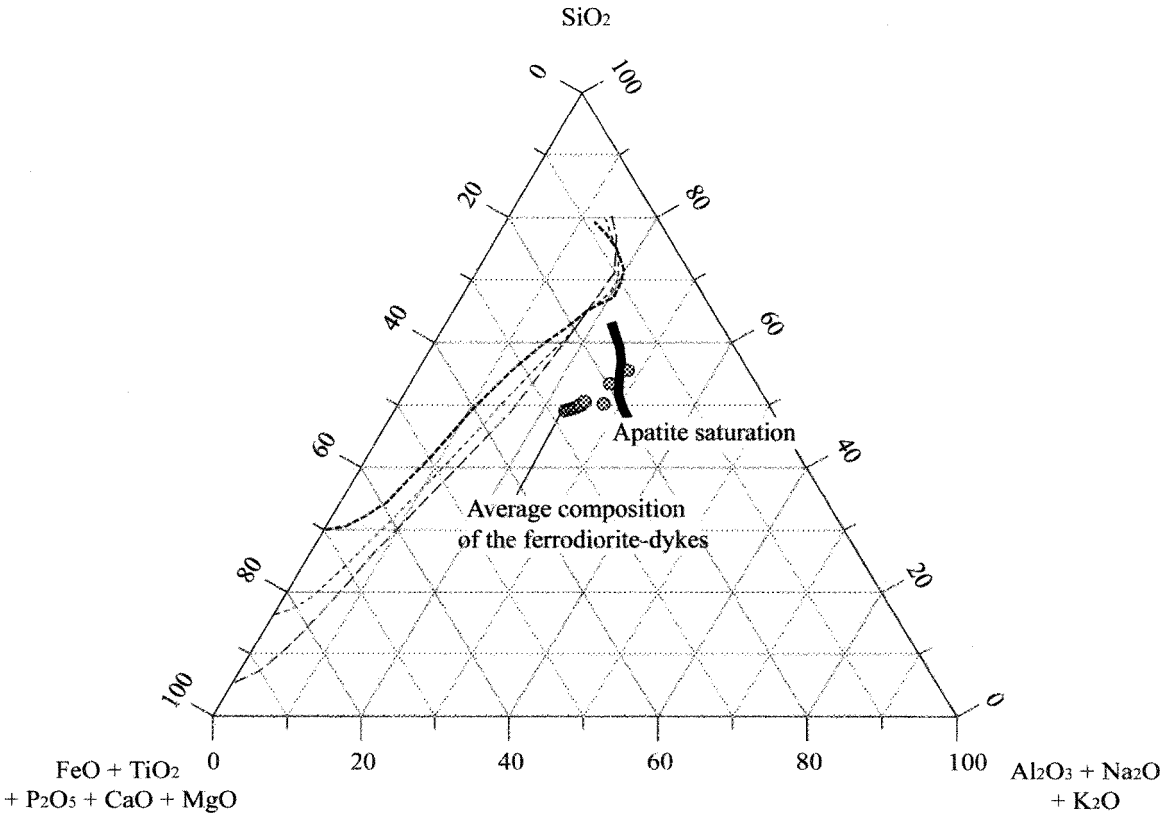

Figure 3. 9. Composition of the proposed liquid lines of descent for the average composition of the ferrodiorite dykes from the Anorthositic Complex of the Lac St-Jean calculated with PELE software (Boudreau, 1999). Black-thick line is the apatite saturation surface in the program. Dotted lines from Fig. 3. 5. All compositions are recalculated on the basis of plotted oxides only.

Many previous studies have investigated melt evolution in the Skaergaard Layered Intrusion (Brooks and Nielsen 1978; Brooks and Nielsen 1990; Hunter and Sparks 1987; Hunter and Sparks 1990a; Hunter and Sparks 1990b; Hunter and Sparks 1990c; McBirney and Naslund 1990; Morse 1990). All liquid lines of descent proposed for the upper part of this intrusion have a similar trend (Hunter and Sparks 1987; Tegner 1997; Toplis and Carroll 1995; Wager 1960), except those proposed by McBirney and Naslund (1990) and by Brooks and Nielsen (Brooks and Nielsen 1978). In this study we chose the liquid line of descent from Wager and Brown (1968) because it is representative of the general trend (decrease of SiO_2 content followed by an increase of the SiO_2 content) (Fig. 3. 10).

The liquid line of descent of the Skaergaard Intrusion moves across the diagram and reaches the apatite saturation surface without crossing the liquid-liquid immiscibility field. Moreover, the melt composition at which apatite saturation is predicted is very close to the composition we observed in our experiments. Thus our results indicate the importance of crystallization-fractionation leading to apatite saturation, not liquid-liquid immiscibility, in the Skaergaard Intrusion.

3.6 CONCLUSION

Our new data confirm earlier studies indicating that phosphate saturation in silicate melts is mainly controlled by SiO_2 and CaO; with addition of H_2O and/or F leading to the formation of apatite. In F-bearing experiments apatite saturation was attained at lower P_2O_5 concentrations than in the F-free experiments.

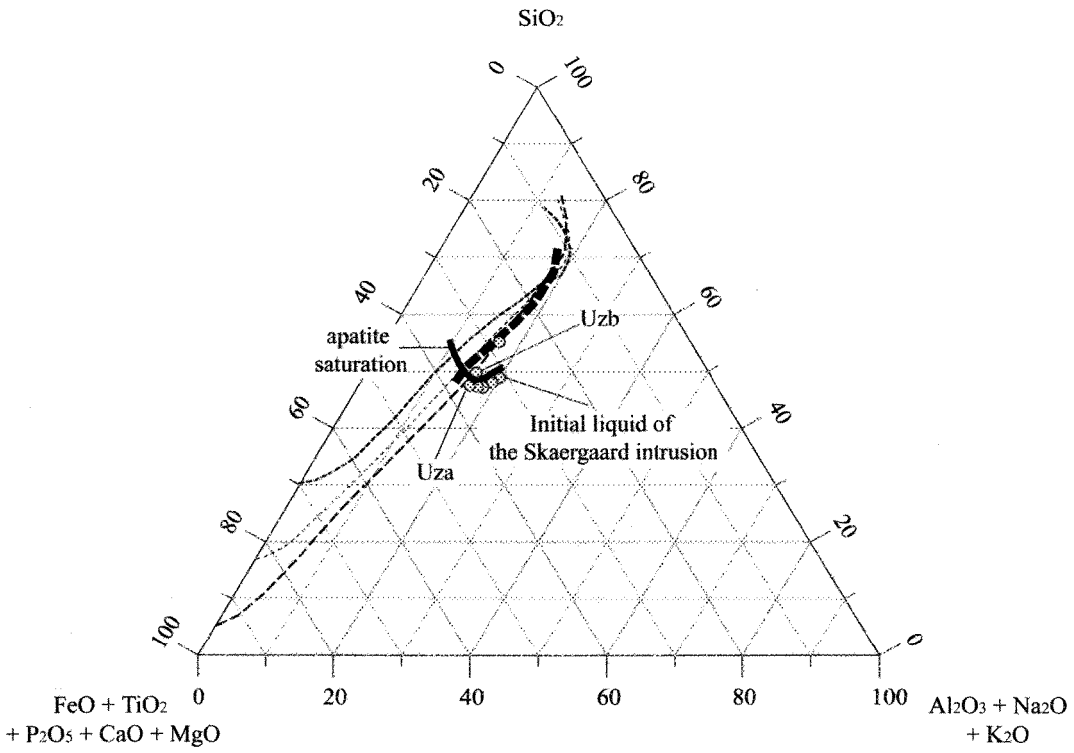

Figure 3. 10. Composition of the proposed liquid lines of descent for the Skaergaard intrusion (Grey circles) (Wager and Brown, 1968). Black-thick-dotted line is trend of data from our experiments using Sc4-b composition. Black-thick line is the apatite saturation surface. Uza, Upper Zone a = appearance of olivine; Uzb, Upper Zone b = appearance of apatite. Temperatures assumed are 1150°C (initial liquid of the Skaergaard intrusion), 1050°C (Uza) and 1000°C (Uzb). Dotted lines from Fig. 3. 5. All compositions are recalculated on the basis of plotted oxides only.

Thus, in natural terrestrial systems fluoroapatite saturation will occur before whitlockite or hydroxyapatite. The addition of F and H_2O did not lead to the formation of liquid-liquid immiscibility.

Combining our results with literature data base allowed us to determine the liquid-liquid immiscibility fields at upper to middle crustal pressures (0.1 MPa to 400 MPa) in the pseudo ternary diagram SiO_2-FeO-TiO_2-MgO-CaO-P_2O_5-Al_2O_3-Na_2O-K_2O. Pressure appears to play an important role on the extent of the liquid-liquid immiscibility field. Indeed, an increase of pressure leads to decrease in the size of the immiscibility field in this system. Our results combined with previous ones demonstrate that an increase or decrease of temperature lead to the disappearance of immiscibility fields. Indeed, the immiscibility fields in natural melt compositions exist for only a small range of melt composition and temperature.

Considering the two models for the formation of nelsonite, crystal accumulation or liquid immiscibility, we compared the liquid lines of descent for the Skaergaard Layered Intrusion, the Sept-Îles intrusive suite and the anorthositic Complex of the Lac-St-Jean. In all three cases the liquid would attain apatite saturation before becoming saturated in Fe-Ti-P liquid. Thus, our study does not support the model of immiscibility for the origin of these rocks.

ACKNOWLEGMENTS

This work was supported the Canada Research Chair in Magmatic Metallogeny to S.J.B. and an NSERC Discovery grant to D.R.B. The referees are thanked for giving up their valuable time to review this manuscript. This work has benefited from the help of

numerous people, but N.T. would like to acknowledge the special support of Ambre Luguet, Bélinda Godel and Liping Bai.

REFERENCES

Ashwal LD (1993) Anorthosites, vol. Springer, Berlin Heidelberg New York

Baker DR (2004) Piston-cylinder calibration at 400 to 500 MPa: A comparison of using water solubility in albite melt and NaCl melting. American Mineralogist 89(10):1553-1556

Barnes S-J, Maier WD, Ashwal LD (2004) Platinum-group element distribution in the Main Zone and Upper Zone of the Bushveld Complex, South Africa. Chem. Geol. 208(1-4):293-317

Bea F, Fershtater G, Corretge LG (1992) The geochemistry of phosphorus in granite rocks and the effect of aluminum. Lithos 29(1-2):43-56

Bogaerts M, Schmidt MW (2006) Experiments on silicate melt immiscibility in the system Fe_2SiO_4–$KAlSi_3O_8$–SiO_2–CaO–MgO–TiO_2–P_2O_5 and implications for natural magmas. Contribution to Mineralogy and Petrology 152:257–274

Boudreau AE (1999) PELE - a version of the MELTS software program for the PC platform. Computers & Geosciences 25:201-203

Brooks CK, Nielsen TFD (1978) Early stages in differentiation of Skaergaard magma as revealed by a closely related suite of dike rocks. Lithos 11(1):1-14

Brooks CK, Nielsen TFD (1990) The differentiation of the Skaergaard intrusion. A discussion of Hunter, R., H. and Sparks, R.,S., J., (Contribution mineralogic and petrology, 95, pp. 451-461). Contributions to Mineralogy and Petrology 104:244-247

Cimon J (1998) L'unité à apatite de rivière des rapides, Complexe de Sept îles. Localisation stratigraphique et facteurs à l'origine de sa formation. Ministère des ressources naturelles, Québec 97(5):1-32

Dymek RF, Owens BE (2001) Petrogenesis of apatite-rich rocks (nelsonites and oxide-apatite gabbronorites) associated with massif anorthosites. Economic Geology and the Bulletin of the Society of Economic Geologists 96(4):797-815

Eales HV, Cawthorn RG (1996) The Bushveld Complex. In: Cawthorn RG (ed) Layered Intrusions, vol. Elsevier, Amsterdam, pp 181-229

Emslie RF (1975) Nature and origin of anorthositic suites. Geoscience Canada 2(2):99-104

Fredette J (2006) Pétrographie, géochimie et potentiel économique en Fe-Ti-P du secteur de Lac à Paul, Parte Nord de le Suite Anorthositique du Lac-Saint-Jean, Province du Grenville, Québec. In: Sciences de la Terre, vol. Université du Québec à Chicoutimi, Chicoutimi, p 294

Frost BR (1991) Introduction to oxygen fugacity and Its petrologic importance. Reviews in Mineralogy 25:1-9

Goldberg SA (1984) Geochemical relationships between anorthosite and associated iron-rich rocks, Laramie Range, Wyoming. Contributions to Mineralogy and Petrology 87(4):376-387

Harrison TM, Watson EB (1984) The behavior of apatite during crustal anatexis - Equilibrium and kinetic considerations. Geochim. Cosmochim. Acta 48(7):1467-1477

Hess PC (1980) Polymerization model for silicate melts. In: Hargraves RB (ed) Physics of magmatic processes, vol. Princeton University Press, pp 3-48

Higgins MD (2005) A new interpretation of the structure of the Sept Iles Intrusive suite, Canada. Lithos 83(3-4):199-213

Hounsell V (2003) géochimie des dykes mafiques et composés de la suite intrusives de Sept-Îles, Québec. In: Département des Sciences de la Terre, vol. Université du Québec à Chicoutimi, Chicoutimi, p 48

Hudon P, Jung IH, Baker DR (2004) Effect of pressure on liquid-liquid miscibility gaps: A case study of the systems CaO-SiO2, MgO-SiO2, and CaMgSi2O6-SiO2. J. Geophys. Res.-Solid Earth 109(B3)

Hunter RH, Sparks RSJ (1987) The differentiation of the Skaergaard Intrusion. Contributions to Mineralogy and Petrology 95(4):451-461

Hunter RH, Sparks RSJ (1990a) The differentiation of the Skaergaard Intrusion - Reply. Contributions to Mineralogy and Petrology 104(2):248-251

Hunter RH, Sparks RSJ (1990b) The differentiation of the Skaergaard Intrusion - Reply. Contributions to Mineralogy and Petrology 104(2):251-253

Hunter RH, Sparks RSJ (1990c) The differentiation of the Skaergaard Intrusion - Reply. Contributions to Mineralogy and Petrology 104(2):253-254

Huntington HD (1979) Kiglapait Mineralogy .1. Apatite, Biotite, and Volatiles. Journal of Petrology 20(3):625-652

Jakobsen JK, Veksler IV, Tegner C, Brooks CK (2005) Immiscible iron- and silica-rich melts in basalt petrogenesis documented in the Skaergaard intrusion. Geology 33(11):885-888

Longhi J (2005) A mantle or mafic crustal source for Proterozoic anorthosites? Lithos 83(3-4):183-198

Manning DAC, Hamilton DL, Henderson CMB, Dempsey MJ (1980) The probable occurence of interstitial Al in hydrous, F-bearing and F-Free aluminosilicate melts. Contributions to Mineralogy and Petrology 75(3):257-262

McBirney AR, Naslund HR (1990) The differentiation of the Skaergaard Intrusion - a discussion. Contributions to Mineralogy and Petrology 104(2):235-240

McLelland J, Ashwal L, Moore L (1994) Composition and petrogenesis of oxide-rich, apatite-rich gabbronorites associated with Proterozoic anorthosite massifs - Examples from the Adirondack Mountains, New-York. Contributions to Mineralogy and Petrology 116(1-2):225-238

Morse SA (1980) Kiglapait mineralogy .2. Fe-Ti oxide minerals and the activities of oxygen and silica. Journal of Petrology 21(4):685-719

Morse SA (1990) The differentiation of the Skaergaard Intrusion - discussion. Contributions to Mineralogy and Petrology 104(2):240-244

Mysen BO (2007) The solution behavior of H_2O in peralkaline aluminosilicate melts at high pressure with implications for properties of hydrous melts. Geochim. Cosmochim. Acta 71(7):1820-1834

Mysen BO, Cody GD (2004) Solubility and solution mechanism of H_2O in alkali silicate melts and glasses at high pressure and temperature. Geochim. Cosmochim. Acta 68(24):5113-5126

Mysen BO, Cody GD (2005) Solution mechanisms of H_2O in depolymerized peralkaline melts. Geochim. Cosmochim. Acta 69(23):5557-5566

Mysen BO, Cody GD, Smith A (2004) Solubility mechanisms of fluorine in peralkaline and meta-aluminous silicate glasses and in melts to magmatic temperatures. Geochim. Cosmochim. Acta 68(12):2745-2769

Nabil H (2003) Genèse des dépôts de Fe-Ti-P associés aux intrusions litées (exemples: intrusion mafique de Sept-Îles, au Québec; Complexe de Duluth aux États-Unis). In: Département des Sciences de la Terre, vol. Université du Québec à Chicoutimi, Chicoutimi, p 441

Naslund HR (1983) The effect of oxygen fugacity on liquid immiscibility in iron-bearing silicate melts. American Journal of Science 283(10):1034-1059

Philpotts AR (1967) Origin of certain iron-titanium oxide and apatite rocks. Economic Geology 62(3):303-315

Roedder E (1951) Low temperature liquid immiscibility in the system K_2O-FeO-Al_2O_3-SiO_2. American Mineralogist 36:282-286

Tegner C (1997) Iron in plagioclase as a monitor of the differentiation of the Skaergaard intrusion. Contributions to Mineralogy and Petrology 128(1):45-51

Tegner C, Cawthorn RG, Kruger FJ (2006) Cyclicity in the Main and Upper Zones of the Bushveld Complex, South Africa: crystallization from a Zoned Magma Sheet. Journal of petrology:1-23

Tollari N, Barnes S-J, Nabil H, Cox RA (submitted) Trace elements concentrations in apatites from the Intrusive Suite of Sept-Îles, Canada and the Bushveld Complex, South Africa - Implications for the genesis of nelsonites.

Tollari N, Toplis MJ, Barnes S-J (2006) Predicting phosphate saturation in silicate magmas: An experimental study of the effects of melt composition and temperature. Geochim. Cosmochim. Acta 70(6):1518-1536

Toplis MJ, Carroll MR (1995) An experimental-study of the influence of oxygen fugacity on Fe-Ti oxide stability, phase-relations, and mineral-melt equilibria in ferro-basaltic systems. Journal of Petrology 36(5):1137-1170

Toplis MJ, Libourel G, Carroll MR (1994) The role of phosphorus in crystallization processes of basalt - an experimental-study. Geochim. Cosmochim. Acta 58(2):797-810

Wager LR (1960) The major element variation of the layered series of the Skaergaard Intrusion and a Re-estimation of the average composition of the Hidden Layered Series and of the successive residual magmas. Journal of Petrology 1(3):364-&

Wager LR, Brown GM (1968) Layered igneous rocks, vol. Oliver and Boyd, Edinburgh

Watson EB (1979) Apatite saturation in basic to intermediate magmas. Geophysical Research Letters 6(12):937-940

Watson EB (1980) Apatite and phosphorus in mantle source regions - an experimental-study of apatite-melt equilibria at pressures to 25-Kbar. Earth and Planetary Science Letters 51(2):322-335

Weiblen PW, Roedder E (1973) Compositional interrelationships of mare basalts from bulk chemical and melt inclusion studies. Geochimica and Cosmochimica Acta 1(4):681-703

CHAPITRE 4

TRACE ELEMENTS CONCENTRATIONS IN APATITES FROM THE SEPT-ÎLES INTRUSIVE SUITE, CANADA AND THE BUSHVELD COMPLEX, SOUTH AFRICA – IMPLICATIONS FOR THE GENESIS OF NELSONITES

N. Tollari, S-J. Barnes, R. A. Cox , H. Nabil, soumis dans Chemical Geology, 08/2007

4.1 RÉSUMÉ

Les nelsonites sont des roches formées par l'accumulation d'apatite et d'oxydes de Fe et Ti, que l'on retrouve dans les intrusions litées. Les processus à l'origine de leur formation sont encore fortement discutés. Deux principaux modèles sont proposés : le modèle de cristallisation fractionnée et celui d'immiscibilité. Nous avons analysés les éléments majeurs et traces des apatites de 14 échantillons provenant de la suite intrusive de Sept-Îles (Canada) et de la Rustenburg Layered Suite (complexe de Bushveld, Afrique du sud). Les textures des phases minérales (cristaux euhédraux) et les compositions minérales (concentrations en ETR, Cl dans l'apatite et concentration du magnésium dans l'ilménite) sont conformes au modèle de cristallisation fractionnée. Les profils des éléments traces recalculées pour les liquides parents des nelsonites de la suite intrusive de Sept-Îles sont semblables à ceux des dykes proposés pour être à l'origine des nelsonites. Nous avons

utilisé le logiciel PELE pour modéliser la cristallisation fractionnée de ces dykes jusqu'à leur saturation en apatite. Les compositions minérales modélisées et les profils d'éléments traces sont similaires aux compositions observées dans les nelsonites de Sept-Îles. Nous avons réalisés des modélisations similaires pour les roches de la Rustenburg Layered Suite et nous arrivons aux mêmes conclusions pour cette intrusion. Nos résultats soutiennent l'hypothèse selon laquelle les nelsonites, ainsi que les roches associées sont formées par cristallisation fractionnée.

4.2 INTRODUCTION

Apatite is a modally-major phase in the late stage products of layered intrusions or anorthositic complexes (Cimon 1998; Dymek and Owens 2001; Eales and Cawthorn 1996; Fredette 2006; McLelland et al. 1994; Von Gruenewaldt 1993). In such cases, the apatite can be associated with Fe-Ti oxides. These apatite-oxide-rich rocks display a wide variety of compositions and names such as grabbro-nelsonite, troctolitic-nelsonite or jotunite (Cimon 1998; Eales and Cawthorn 1996; Hargraves 1962; Higgins 2005; Huntington 1979; Philpotts 1981). Possibly the rarest rock type of this family is nelsonite (Philpotts 1967; Watson 1907). Watson (1907) introduced this term to describe dykes, composed of approximately one third apatite and two thirds Fe-Ti oxides, in the counties of Nelson and Amherst, Virginia, USA. Nelsonites commonly show homogeneous equigranular texture, and occur as dykes or layers associated with oxides such as magnetite and/or ilmenite (Dymek and Owens 2001; Kolker 1982; Philpotts 1967). Nelsonites also occur in association with alkaline, calc-alkaline volcanic and plutonic rocks (Frietsch and Perdahl 1995; Hildebrand 1986).

The origin of these Fe-Ti oxide and apatite-rich rocks is highly debated. Crystal fractionation followed by accumulation from mafic magmas has been proposed by the majority of authors (Barnes et al. 2004; Dymek and Owens 2001; Eales and Cawthorn 1996; Emslie 1975; Goldberg 1984; McLelland et al. 1994; Tegner et al. 2006) while on the other hand it has been proposed that nelsonite forms from liquid-liquid immiscibility (Jakobsen et al. 2005; Naslund 1983; Philpotts 1967). More recent experimental studies show that apatite and Fe-Ti oxides can crystallise from a mafic magma that has experienced fractional crystallisation (Tollari et al. submitted; Tollari et al. 2006). These studies suggest that accumulation of oxide and apatite on the crystal pile could therefore produce nelsonite. However, these experiments produced assemblages which correspond to gabbronorite and troctolite but not true nelsonite.

According to Dymek and Owens (2001), apatite controls many trace elements such as U, Th, Sr and Rare Earth Elements (REE). Apatite could therefore provide information on late stage melt evolution in layered intrusions as this mineral will record trace element fractionation during the magma differentiation in the upper part of the magma chamber.

Parental magma compositions were modelled using the trace element data. Trace elements in both whole-rocks and in-situ in the apatite grains in 12 nelsonites and associated apatite-oxide-rich rocks from Sept-Îles Intrusive Suite, Canada, have been determined. These data were then compared with similar analyses performed on 2 samples from the Rustenburg Layered Suite in the Bushveld Complex, South Africa. Finally, we compared our crystallization model with modeling of crystal fractionation evolution (using PELE software; Boudreau 1999) for apatite-oxide-rich rocks from Sept-Îles Intrusive Suite, Canada; and from the Rustenburg Layered Suite in the Bushveld Complex, South Africa.

4.3 SAMPLES DESCRIPTION

4.3.1 Sept-Îles Intrusive Suite

The Sept-Îles Intrusive Suite is centered 30 km to the south-west of the town of Sept-Îles in Québec. It has a diameter of 80 km and a surface area of 4000 km^2 (Fig. 4. 1). The intrusion is divided into four series: the Lower, the Layered, the Transitional (or Upper Border) and the Upper Series (Cimon 1998; Higgins 2005). Apatite and Fe-Ti oxides are present as major cumulate phases in the Layered Series (Cimon 1998; Higgins 2005; Higgins and Doig 1981). Higgins (2005) suggests that the Suite consists of several overlapping intrusions: the Sept-Îles Mafic intrusion (SIMI), which makes up the bulk of the intrusion, the Sept-Îles Border intrusion at the a margins of the SIMI, the Sept-Îles Late Gabbro intrusions, late dykes and sills, and the Pointe du Criade intrusion, which makes up part of the Upper Series. However, as there is no map outlining the exact position of the different intrusions, and thus we will use the divisions of Cimon (1998).

The rocks sampled in this study are from four boreholes (borehole numbers 1166-95-01, 1166-95-04, 1166-95-11 and 1166-95-13) from the northern portion of the complex (Fig 4. 1). The nelsonites occur in the Critical Zone (ZCR) of the Layered Series (Cimon 1998) (Fig. 4. 2). This zone, approximately 250 m thick, consists -from the base upwards- of magnetitite, nelsonite, troctolitic-nelsonite, nelsonitic troctolite and microtroctolite (Fig. 4. 2). The subdivision of the ZCR is based on the percentage of oxides. Rocks made up of 1-33 vol. % of oxide in a silicate matrix, are referred to as nelsonitic-troctolite. When the abundance of oxides increases to 33-66 vol. %, rocks are referred to as troctolitic nelsonites, and those containing > 66 vol. % oxides are referred to as nelsonites.

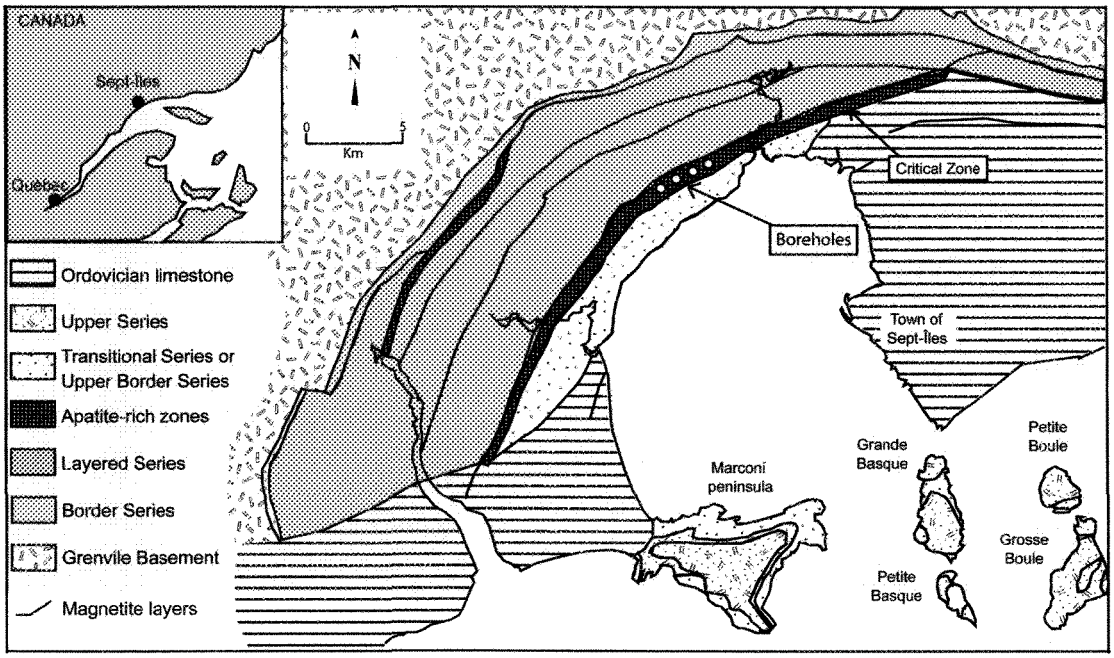

Figure 4. 1: Geological map of the Sept-Îles Intrusive Suite showing the position of the studied boreholes. (Modified after Cimon., 1998 and Higgins, 2005)

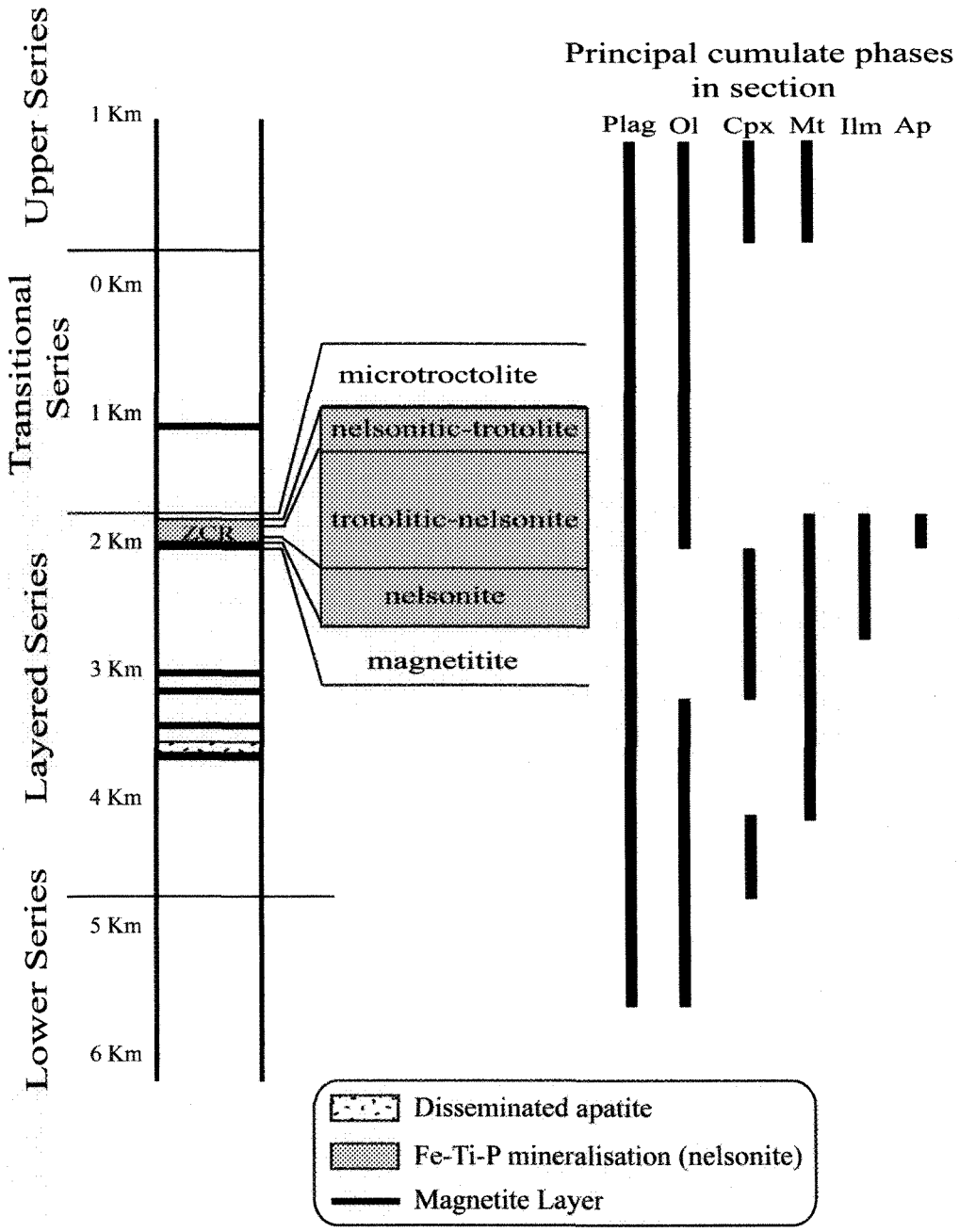

Figure 4. 2: Simplified stratigraphic section of the Sept-Îles Intrusive Suite showing position of ZCR, Critical Zone (Modified after Cimon, 2004 and Nabil, 2003) from which samples were taken. Plag = plagioclase, Ol = olivine, Cpx = clinopyroxene, Mt = magnetite, Ilm= ilmenite and Ap = apatite

The nelsonite has a sharp basal contact with the massive magnetite layer and grades at its top into troctolitic-nelsonite. The layer of nelsonite is approximately 10 m thick and the nelsonitic-troctolite and troctolitic-nelsonite are approximately 150 m thick.

Nabil (2003) and Higgins (2005) suggested that oxide saturation of those evolved magmas was initiated by contamination of the magma by roof autoliths that sank into the magma chamber and locally increased the fO_2 triggering magnetite crystallization. Consequently, Nabil (2003) modelled the whole rock composition of nelsonite and troctolitic nelsonite as cumulates of oxides and apatite plus some silicates.

- Petrography -

In the ZCR of the Sept-Îles complex, nelsonite is mainly composed of apatite (28 to 36 vol. %, Table 4. 1), ilmenite (approximately 20 to 35 vol. %) and magnetite (approximately 20 to 30 vol. %), with olivine (6 to 19 vol. %) and some plagioclase (2 to 10 vol. %). The grain size of apatite is 0.2-2 mm, magnetite and ilmenite 1-2 mm, and silicates 1-5 mm. Apatite and Fe-Ti oxide are always closely associated (Fig. 4. 3 a-b). Ilmenite and magnetite occurs as anhedral grains or as ilmenite exsolution lamellae in magnetite. Plagioclase occurs as slightly altered cumulus phase with two different forms: (1) as euhedral grains or (2) as lobed grains and is slightly altered. Olivine is lobate, fractured and partly replaced by oxides and serpentine.

The troctolitic-nelsonite is composed of 15-30 vol. % olivine (1-4 mm), 7-50 vol. % plagioclase (1-8mm) and 1-17 vol. % clinopyroxene with interstitial nelsonitic matrix composed of 6-26 vol. % of apatite (< 1-1mm), and ~14-35 vol. % of Fe-Ti oxides (~1mm) (Fig. 4. 3 c-d).

Table 4. 1: Approximate modal % of the minerals present, wt % of Mg in ilmenite and Mg number of olivine.

Sample	Rock type	Mt	Ilm	Ap	Plag	Ol	Cpx	%wt MgO ilm	Fo
Sept-Îles Intrusive Suite									
HN-99-01	nelsonitic-troctolite	9	9	8	50	20	5	*1.43*	*44*
HN-99-04	nelsonitic-troctolite	15	12	15	32	21	5	*1.54*	*52*
HN-99-13	nelsonitic-troctolite	8	6	10	45	14	17	*1.72*	*52*
HN-99-45	troctolitic-nelsonite	17	16	26	10	26	5	*1.89*	*54*
HN-99-44	troctolitic-nelsonite	15	11	17	29	26	2	*2.26*	*59*
HN-99-47	troctolitic-nelsonite	14	16	24	18	23	5	*2.33*	*59*
HN-99-21	troctolitic-nelsonite	19	16	22	17	23	3	*2.39*	*60*
HN-99-52	troctolitic-nelsonite	18	16	24	13	23	6	*2.55*	*62*
HN-99-25	nelsonite	20	20	35	3	19	3	*2.86*	*63*
HN-99-53	nelsonite	22	33	32	7	6		*3.91*	-
HN-99-29	nelsonite	27	27	28	10	8		*4.06*	*67*
HN-99-46	nelsonite	20	33	36	5	6		*4.07*	-
Rustenburg Layered Suite									
103.88	ferrodiorite	6	3	2	48	15	5	*0.07*	*6*
304.72	nelsonite	28	22	25	6		4	*0.17*	-

Mt = magnetite; Ilm = ilmenite; Ap = apatite; Plag = plagioclase; Ol = olivine and Cpx = clinopyroxene.

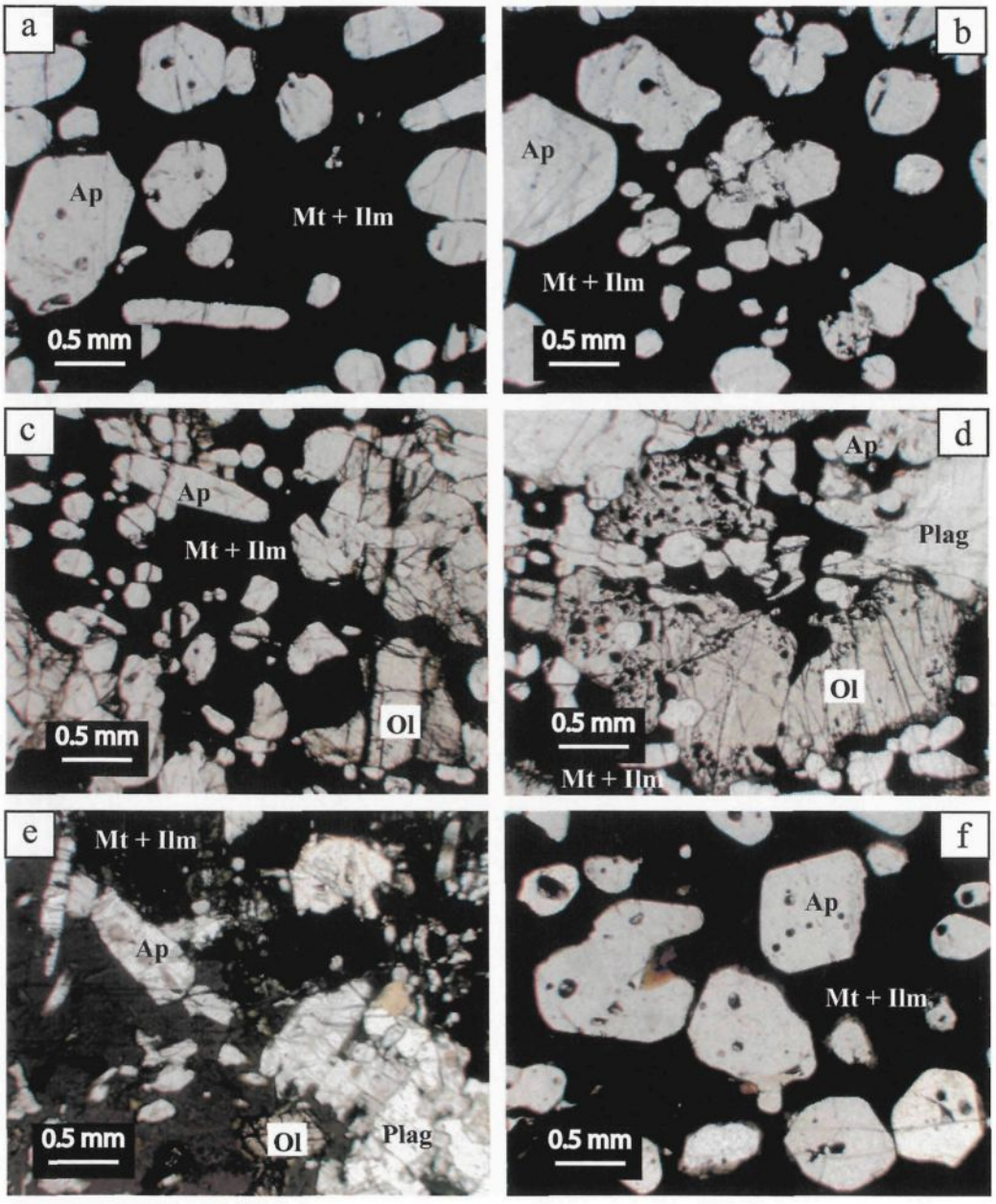

Figure 4. 3: Photomicrographs illustrating textures and mineralogy of the samples. Samples from Sept-Îles Intrusive Suite: a) HN-99-29 nelsonite; b) HN-99-46 nelsonite; c) HN-99-25 troctolitic-nelsonite and d) HN-99-13 nelsonitic-troctolite; Samples from the Rustenburg Layered Suite of the Bushveld Complex: e) 103.88 ferrodiorite; f) 304.72 nelsonite. (Ap = apatite, Mt = magnetite, Ilm = ilmenite, Plag = plagioclase, Ol = olivine).

Olivine and plagioclase occur as cumulus phases. Olivine occurs as large lobate grains, fractured and partly serpentinised and contains many oxide inclusions (Fig. 4. 3 c-d). Plagioclase occurs as euhedral grains, in some cases it is lobate with evidence of high temperature deformation features (kinks band, undulose extinction), likely resulting from compaction of the crystal pile. Apatite and Fe-Ti oxides have similar textures in the troctolitic-nelsonite to those observed in the nelsonites. Ilmenite occurs as anhedral grains or as exsolutions in magnetite, whereas magnetite is always anhedral (Fig. 4. 3 c-d).

4.3.2 Rustenburg Layered

The Bushveld Complex consists of the Rustenburg Layered Suite, the Granite and Granophyre Suite and a suite of mafic to ultramafic sills which underlie the Rustenburg Layered Suite (SACS, 1980) (Fig. 4. 4). The Rustenburg Layered Suite is divided into five zones: the Marginal, the Lower, the Critical, the Main and the Upper Zones (Hall 1932). Our samples were obtained from the Bellevue stratigraphic borehole drilled through the Upper and Main Zones on the northern limb of the complex (Fig. 4. 4). The nelsonite and nelsonitic ferrodiorite occur towards the top of the Upper Zone. The Upper Zone is divided into three subzones based on cumulate mineralogy (Von Gruenewaldt 1973). The lower 1000 m of the zone, subzone A, has plagioclase and magnetite as cumulate phases; this is overlain by the subzone B where olivine becomes a cumulate phase (subzone B). Apatite is a cumulate phase in the final 500 m of the section (subzone C). More details on the stratigraphy in the Bellevue borehole are available in Ashwal et al. (2005) and may be compared with the stratigraphy of the western limb of the complex reported by Tegner et al. (2006).

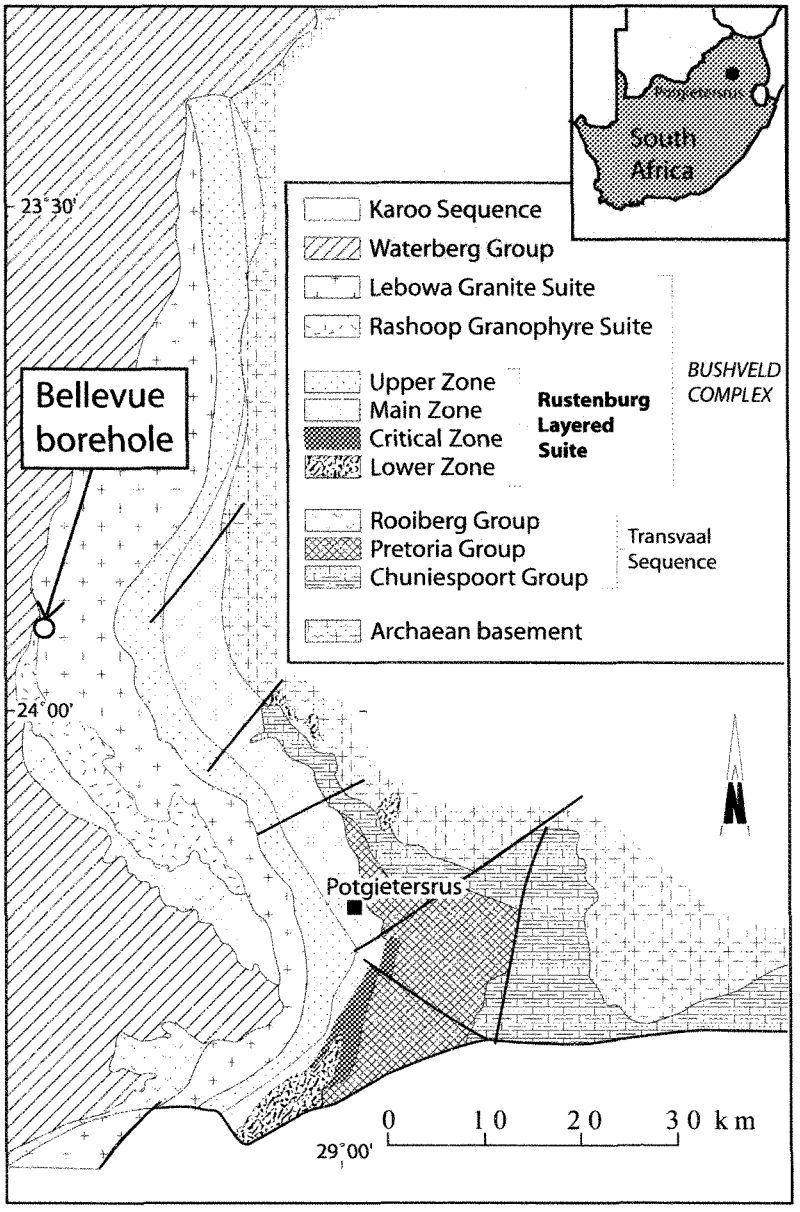

Figure 4. 4: Geological map of the Northern Limb of the Rustenburg Layered Suite of the Bushveld Complex showing the position of the Bellevue Borehole (BV-1) (Modified after Von Gruenewaldt et al., 1986 and 1989).

In the Bellevue borehole, a layer of nelsonite is present at a depth of 305 m (Fig 5) and is referred to as the R layer (Barnes et al. 2004). Our two samples are from the nelsonite and the overlying nelsonitic diorite (Fig. 4. 5). Nelsonites in similar stratigraphic positions have been reported from the Western Limb and Villa Nora sections (Reynolds 1985a; Von Gruenewaldt 1993) of the Bushveld complex. Tegner et al. (2006) reported the presence of 6 nelsonite layers in boreholes of the Western Limb.

According to Reynolds (1985b), the formation of the Bushveld nelsonite is due to crystallisation of an Fe-Ti-Mn-Ca-P-REE-rich liquid , that was immiscible with a highly evolved residual dioritic magma. Other authors considered nelsonite formation to result from crystal fractionation and accumulation (Barnes et al. 2004).

- Petrography -

The nelsonite contains mainly apatite (25 vol. %, 0.5-1 mm in diameter or length), and Fe-Ti oxides (50 vol. %), with approximately equal amounts of ilmenite and magnetite (Fig. 4. 3 f). Ilmenite occurs as anhedral grains or as exsolutions in magnetite whereas, magnetite is always anhedral. Nelsonite contains minor pyroxene (clinopyroxene and low-Ca pyroxene) (~7 vol. %), plagioclase (~6 vol. %), biotite (~6 vol. %) and amphibole (~6 vol. %). Plagioclase and pyroxene occur as cumulus phases whereas biotite and amphibole occur in veins or in fractures.

The overlying ferrodiorite consists of plagioclase (48 vol. %; 2-4 mm), olivine (15 vol. %; 1-4 mm), Fe-Ti-oxides (9 vol. %; < 1-2 mm), clinopyroxene (5 vol. %; 1-3 mm) and apatite (~2 vol. %) (Fig. 4. 3 e). In addition to these phases, there is minor K-feldspar, quartz, biotite and amphibole.

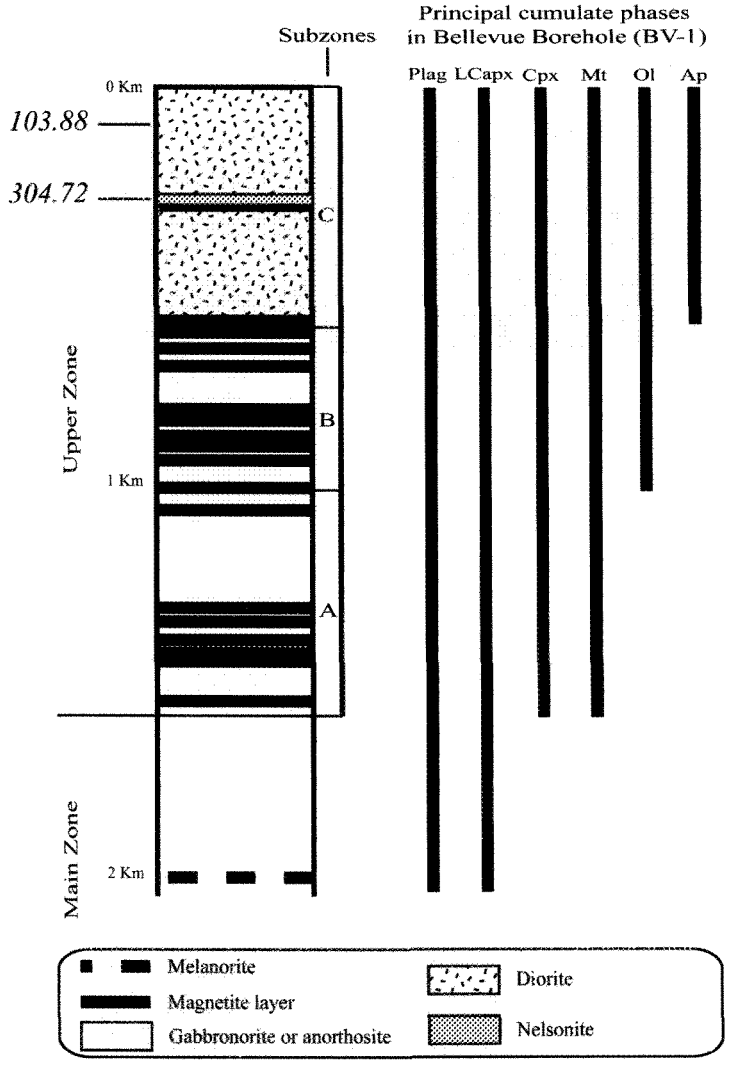

Figure 4. 5: Simplified stratigraphic section of the Bellevue Borehole (BV-1) of the Upper Zone of the northern portion of the Bushveld Complex (Modified after Ashwal et al., 2005 and Barnes et al., 2004) showing the position of the samples. Plag = plagioclase, LCapx = Low Ca pyroxene, Cpx = clinopyroxene, Mt = magnetite, Ol = olivine and Ap = apatite.

Apatite (0.1-0.2 mm in size) is observed at the grain boundaries between plagioclase, olivine and Fe-Ti oxide grains, or occurs as inclusions in clinopyroxene. Plagioclase occurs as euhedral grains, whose rims show slight alteration. Olivine and clinopyroxene are lobate, fractured and replaced by oxides and serpentine. Iron-Ti oxides consist of ilmenite and magnetite which show the same anhedral and exsolution relationships as in the previous samples.

4.4 ANALYTICAL METHOD

4.4.1 Major elements

Major elements in apatite were determined using a Cameca SX100 electron microprobe at Laval University. An accelerating voltage of 15 kV, with a beam current of 20 nA and the beam size of 1μm were used for all analyses. All microprobe analyses were carried out using wavelength dispersive spectrometry (WDS). Standards used were albite for Na and Al, orthoclase for Si and K, hematite for Fe, wollastonite for Ca, olivine for Mg, $MnTiO_3$ for Ti chloroapatite for P and apatite for F. Backscattered electron images of each apatite crystal were uniform with no apparent zonation. In each sample, 5 to 20 points were analysed.

4.4.2 Trace elements

Trace elements were determined on 100 μm thick polished sections using a New Wave Research Nd-YAG 213 nm UV laser ablation microprobe (LAM) system. The beam size was 40 μm with pulse energy of 0.17 mJ and a frequency of 20 Hz. Because the backscattered images indicate no apatite zoning with respect to major elements, line scans

were used. The line scan rate was 10 μm/s and data was collected for 50 to 60 seconds. Ablated material was carried into a Thermo X7 ICP-MS using a flow of ~1 l/min of He in the laser cell. The data were reduced using Thermo Elemental Plasma Lab "time-resolved analysis" (TA) data acquisition software allowing about 30 s for background followed by 50 to 60 s for laser ablation. All elements were measured using a 10 ms dwell time. NIST 612 glass was used for instrument calibration; Calcium was used as an internal standard to correct the ablation yield differences between and during individual analyses on both the samples and the standards. NIST 610 was used as a secondary standard.

4.5 RESULTS

4.5.1 Apatite Composition

- Major elements -

All of the apatites are fluorapatite (Table 4. 2). Fluorine contents vary from 3.49 to 4.24 wt. % for the apatites from Sept-Îles Intrusive Suite. Apatite from two samples from the Bushveld Complex contain 3.75 wt. % F. Chlorine contents vary from 0.09 to 0.17 wt. % for the apatites from Sept-Îles Intrusive Suite, but are considerably higher in the apatites of the Bushveld Complex (0.52 to 0.94 wt. %). The amount of Cl in the apatites is partly dependent on the stratigraphic position of the samples, increasing when going up the cumulate pile. In fact, in the Sept-Îles Suite, the Cl content evolves from 0.09-0.11 wt. % in the nelsonite, to 0.1-0.17 wt. % in the overlying troctolitic-nelsonite. In the Bushveld samples, the apatites of the nelsonite contain 0.5 wt. % and up to 0.9 wt. % in the olivine-ferrodiorite.

Table 4. 2 : Analyses of apatites from the Sept-Îles Intrusive Suite and from the Rustenburg Layered suite.

Sept-Îles Intrusive Suite													Rustenburg Layered Suite	
Microprobe analyses														
	HN-99-01 Nelsonitic-troctolite	HN-99-04 nelsonitic-troctolite	HN-99-13 nelsonitic-troctolite	HN-99-45 troctolitic-nelsonite	HN-99-44 troctolitic-nelsonite	HN-99-47 troctolitic-nelsonite	HN-99-21 troctolitic-nelsonite	HN-99-52 troctolitic-nelsonite	HN-99-25 nelsonite	HN-99-53 Nelsonite	HN-99-29 nelsonite	HN-99-46 nelsonite	103.88 ferrodiorite	304.72 nelsonite
n [(a)]	3	3	10	6	3	6	6	6	10	6	10	10	10	10
FeO wt %	0.12	0.28	0.19	0.16	0.11	0.20	0.10	0.16	0.19	0.17	0.15	0.15	0.36	0.27
MgO	0.00	0.12	0.35	0.02	0.08	0.06	0.02	0.06	0.06	0.12	0.08	0.12		
CaO	54.98	54.20	53.63	54.44	54.94	54.54	54.81	54.84	53.62	55.02	53.49	53.28	53.24	52.83
Na2O	0.04	0.06	0.07	0.04	0.04	0.05	0.04	0.04	0.04	0.05	0.05	0.04	0.04	0.06
P2O5	43.57	42.92	43.29	43.04	43.85	43.43	43.71	43.34	43.32	43.65	43.35	43.30	43.13	43.30
F	4.21	3.61	4.24	4.02	4.11	3.83	3.96	3.86	3.49	3.93	3.76	3.80	3.75	3.75
Cl	0.11	0.17	0.14	0.09	0.16	0.12	0.10	0.11	0.10	0.11	0.09	0.09	0.94	0.52
Total	103.04	101.36	101.91	101.81	103.29	102.23	102.74	102.41	100.82	103.05	100.97	100.78	101.46	100.73
Less O = F	1.77	1.52	1.79	1.69	1.73	1.61	1.67	1.63	1.47	1.65	1.58	1.60	1.58	1.58
Less O = Cl	0.02	0.04	0.03	0.02	0.04	0.03	0.02	0.02	0.02	0.02	0.02	0.02	0.21	0.12
Total	101.24	99.80	100.09	100.10	101.52	100.59	101.05	100.76	99.33	101.37	99.37	99.16	99.67	99.03
LA-ICPMS analyses														
n [(a)]	10	10	10	10	10	10	10	10	10	10	10	10	10	10
Sr	913	856	777	857	526	982	865	704	1087	758	855	621	367	363
Y	780	733	785	824	631	647	738	585	671	352	463	459	584	830
Zr	20.7	30.5	5.2	5.1	10.8	8.3	10.7	7.3	8.9	4.3	5	6.4	5.6	2.2
Nb	5.03	<1.31	<1.31	<1.31	<1.31	<1.31	<1.31	<1.31	<1.31	<1.31	<1.31	<1.31	<1.31	<1.31
Ba	17	38	27	21	15	24	17	12	16	10	16	10	19	13
La	601	660	747	697	370	564	496	400	479	248	320	282	1021	1142
Ce	1748	1692	2036	1934	896	1470	1101	1102	1203	781	769	695	2200	2593
Pr	276	268	290	299	139	228	185	170	197	116	154	117	267	354
Nd	1274	1142	1215	1253	685	974	902	772	940	530	718	595	948	1332
Sm	263	225	225	248	152	201	192	163	200	114	155	135	159	234
Eu	60.8	51.5	30.8	59.1	38.6	64.2	48	46.2	62.5	41.3	54.3	42.7	15.5	17.2
Gd	262	226	213	258	162	217	203	171	209	116	156	47	164	226
Tb	31.5	27	25.9	31.1	19.5	26.3	24.8	20.5	24.9	13.4	18.8	17.3	19.1	27.4
Dy	171	147	149	166	110	139	141	117	137	72	98	96	110	157
Ho	29.1	25.8	26.7	28.9	19.1	23.8	25	20.4	23.6	12.1	16.6	16.3	20.6	28.2

Er	65.5	61.3	66.7	68.9	45.6	58.4	60.1	49.7	56.4	27.6	38	37.7	51.1	68.6
Tm	7.3	7.1	7.8	7.8	5.3	6.3	7	5.8	6.4	3.1	4	4.2	6	7.9
Yb	40.7	39.2	42.5	40.5	28.2	33.2	37.6	32	35	16.5	20.8	21.9	31.8	41
Lu	5.59	5.16	5.56	5.35	3.82	4.23	5.06	4.29	4.74	2.15	2.68	2.93	4.14	5.31
Hf	0.41	0.46	<0.40	<0.40	<0.40	<0.40	<0.40	<0.40	<0.40	<0.40	<0.40	<0.40	<0.40	<0.40
Ta	0.35	<0.32	<0.32	<0.32	<0.32	<0.32	<0.32	<0.32	<0.32	<0.32	<0.32	<0.32	<0.32	<0.32
Th	14.06	9.27	3.12	7.31	5	5.62	5.52	4.76	4.87	2.25	2.84	3.24	23.78	22.86
U	4.23	2.54	0.91	1.59	1.08	1.24	0.98	1.47	1.18	0.72	0.73	0.56	7.76	6.42

[(a)] Number of analyses

We have only two samples from this complex, thus we cannot speculate about any potential trend. Stratigraphy-dependent compositional variation has also been observed both for the fosterite content of olivine and the MgO content of ilmenite, both decrease higher in the intrusion (Table 4. 1). Thus we can classify samples according to their degree of magmatic evolution.

- Trace elements -

Trace elements also show a variation with the stratigraphy position of the samples within the both intrusions. In the Sept-Îles intrusion, trace element contents of apatite increase from the bottom to the top of the section. In fact, apatites from nelsonites contain 352-671 ppm Y while apatites from the overlying trotolitic-nelsonite contain 585-785 ppm Y (Table 4. 2). The REE (except Eu), Th, U, Zr, Hf show similar enrichment. In contrast Eu, Sr and Ba have similar concentrations throughout the section. The REE contents of apatite from this intrusion are very similar to previous analyses of apatite from apatite-rich rocks associated with massif anorthosites (Dymek and Owens 2001).

The apatites from Rustenburg Layered Suite are much richer (2 or 3 times higher) in LREE, Th and U than the Sept-Îles apatites, but contain similar amounts of HREE, Zr and Hf, and much lower Sr and Eu values (2 or 3 times lower). Contrary to the observation at Sept-Îles where the REE increased in apatite up section, the ferrodiorite apatites have slightly lower REE and Y concentrations than the nelsonite apatites. As noted previously, we have only two samples from this locality this case thus, it is impossible to describe a trend

4.5.2 Mass balance

A mass balance calculation was performed in order to better understand the distribution of the trace elements in nelsonite and which elements are controlled by apatite. This mass balance calculation was done for Ca, P, Cl, Sr, Ba, REE, Hf, Ta, Th and U, as their whole-rock concentrations are available (Nabil 2003). The mass balance calculation assumes that P_2O_5 present in whole rock is 100 % concentrated in apatite. Thus the weight fraction of apatite is given by:

$$F_a = P_2O_5w / P_2O_5a$$

Where P_2O_5w = whole rock concentration of P_2O_5, and P_2O_5a = average P_2O_5 concentration of all apatite analyses (Tables 4. 2 and 4. 3).

The percentage of each element present in apatite was then calculated using the following equation

$$W^i_a = C^i_a * F_a / C^i_w * 100$$

Where W^i_a = percentage of element i present in apatite, C^i_a = Concentration of element i in apatite, C^i_w = whole rock concentration of element i in the whole rock and F_a = weight fraction of apatite.

The mass balance calculation shows that the elements may be broadly divided into 3 groups. The first group consists of the elements largely incorporated in apatite namely, REE, U, Th and Cl (≈ 75-100 %). Given the similarity of the geochemical behaviour of Y with the HREE (Arth 1976), we assume that this element belongs to this group. The second group of elements; Ca, Sr and Eu are also concentrated in apatite in the nelsonites (≈ 75-100 %), but in the silicate rocks, the proportions drop considerably (≈ 10-65 %).

Table 4. 3: Whole rock concentrations of selected elements and weight fraction of the elements in apatite

Sept-Îles Intrusive Suite													Rustenburg Layered Suite	
Sample	HN-99-01	HN-99-04	HN-99-13	HN-99-45	HN-99-44	HN-99-47	HN-99-21	HN-99-52	HN-99-25	HN-99-53	HN-99-29	HN-99-46	103.88	304.72
Rock type	nelsonitic-troctolite	nelsonitic-troctolite	Nelsonitic-troctolite	troctolitic-nelsonite	troctolitic-nelsonite	troctolitic-nelsonite	troctolitic-nelsonite	troctolitic-nelsonite	nelsonite	nelsonite	nelsonite	nelsonite	ferrodiorite	nelsonite
Whole rock [a]														
MnO (wt %)	0.48	0.43	0.3	0.47	0.45	0.42	0.38	0.39	0.39	0.43	0.39	0.37	0.36	0.25
CaO	8.36	10.48	11.62	9.67	13	13.65	12	18.54	16.66	15.99	14.46	12.83	6.52	11.42
P2O5	2.81	5.44	2.69	5.54	8.93	8.79	7.84	12.69	12.12	11.19	9.94	8.61	0.86	5.93
Cl (ppm)	99	357	85	122	506	469	277	275	561	308	186	478	2050	1899
Sr	489	270	483	305	167	311	226	214	264	201	439	166	255	221
Ba	379	240	375	121	49	142	72	20	-10	30	-10	11	381	219
La	46	84	62	85	95	121	89	95	116	78	70	83	37	162
Ce	123	206	164	228	238	300	235	413	302	344	252	222	72	360
Nd	80	128	96	135	163	186	148	186	209	169	159	138	38	178
Sm	20	29	20	32	39	42	34	47	47	40	34	35	7	35
Eu	7.3	7.7	4.2	8.3	10.6	12.9	9.2	18	14.6	15.9	12.7	9.7	2.6	3
Tb	2.6	4	2.8	4.5	5.9	6.1	4.8	6.3	6.5	5.3	4.6	5.2	1.1	4.6
Yb	3.4	5.7	5.1	5.4	7.1	7	6.3	7.2	8.1	5.7	4.9	7	2.8	6.9
Lu	0.5	0.8	0.7	0.7	1	0.9	0.9	0.9	1.1	0.8	0.6	0.9	0.5	0.9
Hf	2.3	2.9	1.8	1.7	3.7	4.3	2.8	3.3	3	2.6	2.1	2.7	3.4	4.8
Ta	2.8	3.3	1.7	3	4.4	6.3	3.8	0.6	4.2	0.4	0.4	0.3	0.6	3.8
Th	1	1.4	0.3	1	1.7	1.3	1	1	1.2	0.9	0.5	1.1	6.1	10.1
U	0.35	0.47	0.1	0.32	0.4	0.35	0.28	0.32	0.28	0.37	0.14	0.44	1.3	2.9
Element [b]	Wt fraction of element in apatite (W^i_a)													
MnO	1.1	1.6	1.1	1.6	2.9	2.9	2	2.9	5.5	3.1	2.7	3.7	0.6	4.6
CaO	42	64	29	70	85	79	80	82	91	87	85	84	16	63
Cl	72	35	102	105	61	43	65	42	45	92	111	96	9	38
Sr	12	40	10	36	65	64	69	84	115	97	45	85	3	22
Ba	0.3	2	0.4	2.2	6.5	3.4	4.2	21.6	-	8.5	-	14.2	0.1	0.8

La	85	99	74	104	80	95	101	95	116	82	105	87	55	96
Ce	93	103	77	109	78	100	85	99	112	59	70	49	61	99
Nd	103	112	79	119	87	107	110	112	126	81	104	94	49	103
Sm	87	96	70	99	80	97	102	92	119	75	103	85	44	92
Eu	54	84	46	92	75	101	95	95	120	67	98	70	12	78
Tb	79	85	57	89	68	88	94	79	107	66	93	80	34	82
Yb	77	86	52	97	82	97	108	91	122	75	97	90	23	81
Lu	73	79	47	94	79	94	105	95	120	71	98	100	18	79
Hf	1.2	2.0	0.4	0.8	0.7	0.9	0.9	0.7	1.0	0.5	1.1	0.5	0.1	0.3
Ta	0.8	0.1	0.1	0.1	0.3	0.1	0.2	2.8	0.2	1.3	0.5	0.5	0.1	0.1
Th	91	83	65	94	61	88	100	86	114	65	130	95	8.0	31
U	78	68	57	64	56	72	63	66	118	50	120	51	12	30

[a] Whole rock analyses are from Nabil (2003).

[b] Major elements determined by XRF at the Ontario Geological Survey. Trace elements determined by INAA at Université du Québec à Chicoutimi using the method of Bedard and Barnes (2002).

This reflects the presence of cumulate plagioclase in these rock and the fact that these elements are also concentrated in plagioclase (Drake and Weill 1975). The third group of elements consists of Mn, Ba, Hf and Ta. For these elements the proportion present in apatite is very low (generally < 3 %). Due to the similarity of the geochemical behaviour of Zr with Hf and Nb with Ta, one would expect that the proportion of Zr and Nb accommodated in apatite to be low. Manganese, Nb, Ta, Hf and Zr partition into Fe-Ti oxides (Arth 1976; Nash and Crecraft 1985; Pearce and Norry 1979). Thus, the behaviour of these elements is probably controlled by Fe-Ti oxides.

4.5.3 Mantle normalized trace elements patterns elements compatible with apatites

In this section, we used only the trace elements controlled by apatite, i. e. the first and second group (REE, U, Th, Y, Sr and Eu).

- Sept-Îles Intrusive suite -

The mantle-normalized concentration patterns of the apatites from the Sept-Îles Intrusion are LREE-enriched (La/Lu_N = 12-13, N primitive-mantle normalized after McDonough and Sun,(1995)) with large negative Sr, U and Th anomalies (Fig. 4. 6). Rare earth element and Y concentrations in nelsonite span over 1-2 orders of magnitude (~30 - 1200 X the mantle), while U, Th and Sr show less variable contents (20-300 X the mantle) (Fig. 4. 6). The negative Sr, U and Th anomalies reflect the lower compatibility of these elements into apatite compared to REE (e.g. D_{La} = 5-12 and D_{Sr} = 1.1-1.3) (Bedard 2001; Prowatke and Klemme 2006; Watson and Green 1981).

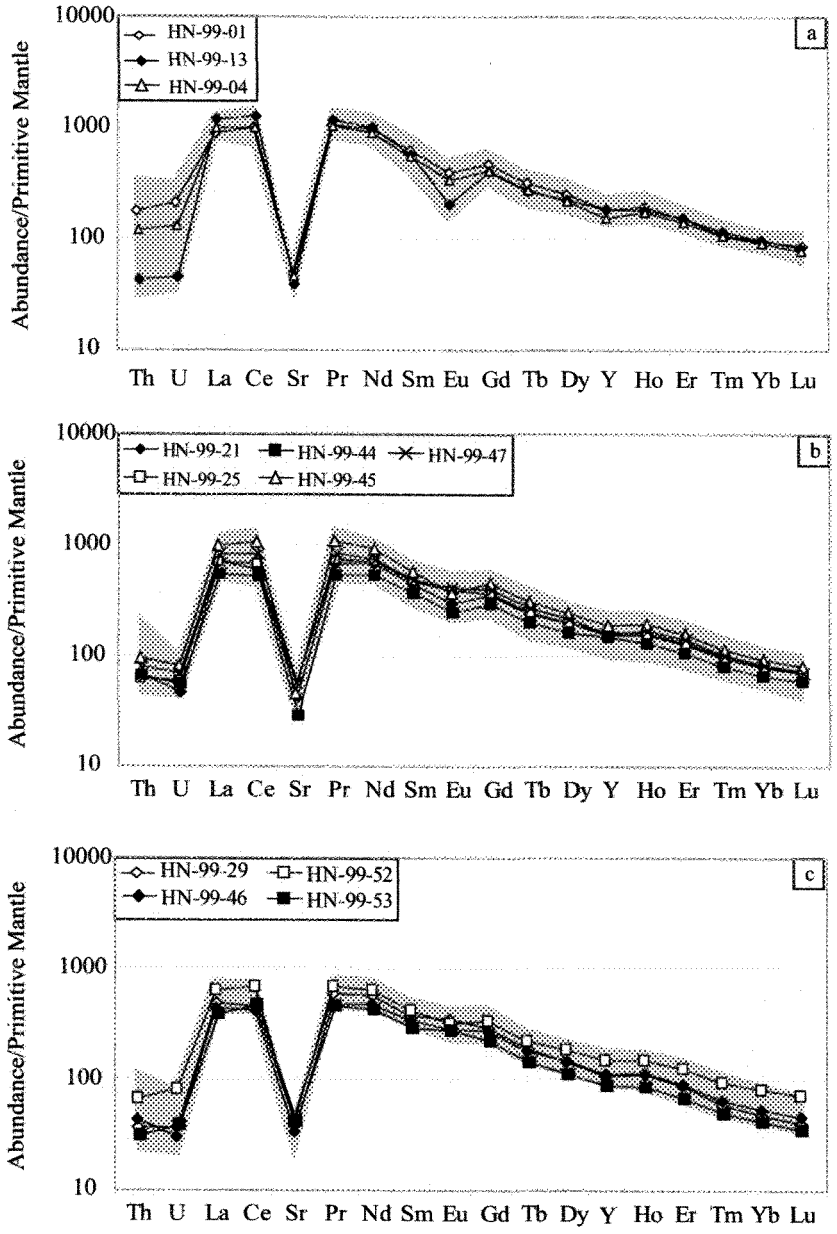

Figure 4. 6: Spider diagram of apatites from Sept-Îles Intrusive suite. a) Nelsonitic-troctolite with negative Eu anomaly, b) troctolitic-nelsonite and c) nelsonite. Lines correspond to the average compositions and grey zones correspond to the range of all data. Primitive mantle values are from McDonough and Sun (1995).

The apatites from the nelsonites show no Eu anomalies (Eu/Eu* ~ 1) (Fig. 4. 6 c), while apatites from the nelsonitic troctolite show slight negative anomalies (Eu/Eu* = 0.7) (Fig. 4. 6 b). In the uppermost unit, the nelsonitic-troctolite apatites have more pronounced negative anomalies (Eu/Eu* = 0.43) (Fig. 4. 6 a). Furthermore, the Sr anomaly increases up section from Sr/Sr* 0.04 to 0.08. The absence of Eu anomalies in the nelsonite apatites suggests that the liquid from which it crystallized did not contain a significant Eu anomaly, i.e. the liquid hadn't crystallized sufficient plagioclase to become Eu-depleted at the time of apatite crystallization. The presence of a negative Eu anomaly and the increase in the size of the Sr anomaly in the overlying nelsonitic troctolite suggests that plagioclase crystallized during the formation of the unit thereby depleting the magma in both elements.

The concentrations of elements controlled by apatite are greater in the samples higher in the stratigraphy (Table 4. 2 and 4. 3). For example, the La in the apatites from nelsonites is ~ 500 times higher than the mantle concentration and La in the nelsonitic troctolite is ~ 1000 times higher than the mantle concentration. Given that the partition coefficients of LREE into apatite in a mafic system are of the order of 10, the amount of apatite extracted from the melt must have been much less 10 % of the total solids to permit the LREE enrichment in the magma.

- Rustenburg Layered Suite -

The overall shape of the mantle normalized patterns for the Bushveld apatites is similar to those of Sept Îles apatites with a strong enrichment of LREE (La/Lu_N = 22.3 in the nelsonite) and large negative Th, U, Sr and Eu anomalies (Fig. 4. 7). The concentrations of Sr and Eu are lower (20 and 100 times the mantle content, respectively) while the concentrations of the other trace elements are higher than in the Sept-Îles apatites (Fig. 4. 7).

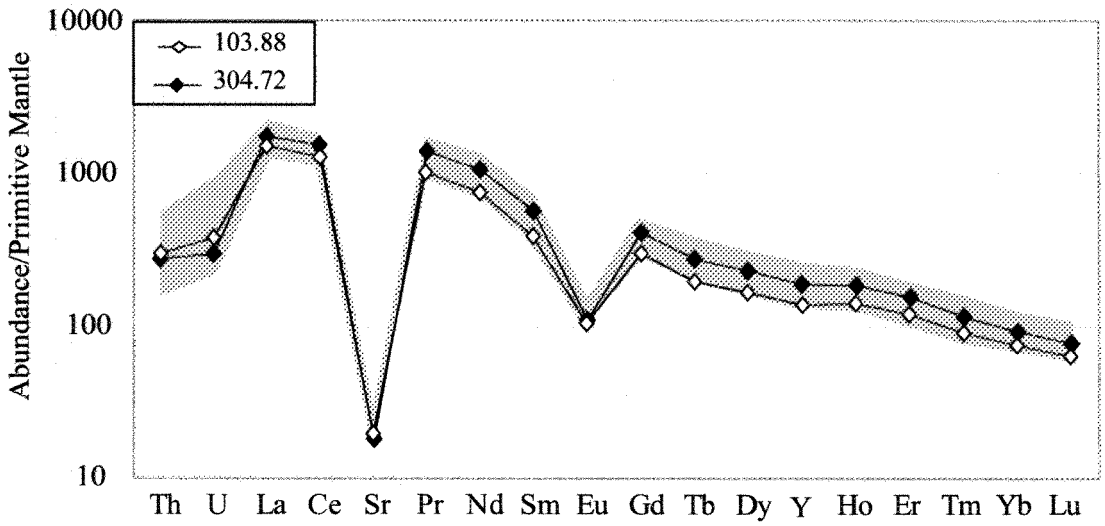

Figure 4. 7: Spider diagram of apatites from the Rustenburg Layered Suite of the Bushveld Complex. Sample 103.88 ferrodiorite and 304.2 nelsonite. Lines correspond to the average compositions and grey zone corresponds to the range of all data. Primitive mantle values are from McDonough and Sun (1995).

Consequently, the Sr and Eu anomalies are larger (Sr/Sr* = 0.011, Eu/Eu* = 0.23 in nelsonite). As in the Sept-Îles Intrusive Suite, the degree of REE fractionation increases up the section (La/Lu_N = 26 at the top). However, in contrast to the Sept-Îles apatites, the U, Th, REE and Y contents of the apatite do not increase between the two samples. The REE and Y range from ~70 to ~2200 times higher than the mantle concentration for the apatites in nelsonite and from ~60 to ~1600 for the apatites from ferrodiorite (Fig. 4. 7).

4.6 DISCUSSION

4.6.1 Apatite Composition

For both major elements and trace elements, apatite composition varies with stratigraphic position of the samples within the Sept-Îles intrusion. According to Mathez and Webster (2005), chlorine becomes enriched in fractionated magmas. This, together with the evolution of Mg contents in ilmenite and olivine, suggests that magma of the Sept-Îles intrusions is becoming more fractionated towards the top of the intrusion. We made the assumption that magma of the Bushveld complex is becoming more fractionated towards the top of the intrusion too.

- Mass balance and inversion -

The mass balance calculation indicates that most of the REE, U, Th, Cl, Ca and Sr, are present in apatite (≈ 75-100 %) and, thus, apatite controls the behaviour of these elements (Table 4. 3). An estimate of the composition of the liquids from which the apatites crystallized may be obtained by inversion of these element concentrations using the equation: $C_l=C_{ap}/D$

Where C_l= concentration of the element in the liquid, C_{ap}= concentration of the element in apatite and D = partition coefficient (Table 4. 4).

Figure 4. 8 shows the primitive mantle (PM)-normalized-calculated trace patterns for parental magmas of nelsonite from Sept-Îles Intrusive suite and from the Rustenburg Layered Suite. The partition coefficients used to this calculation are from Bedard (2001), Watson and Green (1981) and Prowatke and Klemme (2006). These profiles correspond to LREE-enriched melts (La_N 80–150 times the primitive mantle content and Lu_N 8–17 times the primitive mantle content). The patterns are broadly parallel, however the calculated magma in equilibrium with the apatites of the nelsonite from Rustenburg Layered Suite is enriched in Th and U compared to the magma in equilibrium with the Sept-Îles apatites. The former is slightly enriched in LREE and depleted in HREE. The pronounced negative Eu and Sr anomalies observed in this pattern are likely due to the extensive crystallization of plagioclase in the Upper Zone (Barnes et al. 2004; Eales and Cawthorn 1996; Maier and Barnes 1998). Comparatively, the calculated parental magma of the Sept-Îles Intrusive Suite shows a smaller negative Sr anomaly.

The inversion modeling suggests that the Bushveld magma was more evolved than the Sept-Îles magma at the time of nelsonite formation. This interpretation is also supported by additional evidences such as the higher Mg content in ilmenite and Mg # of olivine in the Sept-Îles rocks and the presence of phases such as amphibole and biotite and higher concentration of incompatible trace elements (e.g. U, Th, Cl, Zr, Hf and Ba) in the Bushveld apatites, and by the stratigraphic position. Moreover, the evolution of the apatite composition up the intrusions also supports the idea that the Sept-Îles parental magma was more primitive and that nelsonites are also more primitive than the troctolitic-nelsonites.

Table 4. 4: Estimate compositions of the liquids from which the apatites from the Sept-Îles Intrusive Suite and the Rustenburg Layered suite crystallized.

Samples	Locality	Th	U	La	Ce	Sr	Pr	Nd	Sm	Eu	Gd	Tb	Dy	Ho	Y	Er	Tm	Yb	Lu
Concentration in apatite																			
HN-99-25	Sept-Îles Intrusive suite	4.9	1.2	479	1203	1087	197	940	200	62.5	209.3	24.9	137	23.6	671	56.4	6.40	35.0	4.74
HN-99-29	Sept-Îles Intrusive Suite	2.8	0.73	320	769	855	154	718	155	54.3	155.8	18.8	98.5	16.6	463	38.0	4.04	20.8	2.68
HN-99-46	Sept-Îles Intrusive Suite	3.2	0.56	282	695	621	117	595	135	42.7	146.6	17.3	95.9	16.3	459	37.7	4.19	21.9	2.93
HN-99-53	Sept-Îles Intrusive Suite	2.3	0.72	248	781	758	116	530	114	41.3	115.9	13.4	72.1	12.1	352	27.6	3.05	16.5	2.15
304.72	Rustenburg Layered Suite	22.9	6.4	1142	2593	363	354	1332	234	17.2	226.0	27.4	157	28.2	830	68.6	7.91	41.0	5.31
Partition coefficient (a)		**1.6**	**1.8**	**3.37**	**7**	**1.3**	**9**	**11**	**12**	**9.6**	**10**	**9**	**8.3**	**7**	**7**	**6**	**5**	**4**	**4**
Concentration in calculated liquid																			
HN-99-25	Sept-Îles Intrusive suite	3.04	0.66	142	172	836	22	85	17	6.51	20.9	2.77	16.53	3.37	96	9.40	1.28	8.76	1.19
HN-99-29	Sept-Îles Intrusive Suite	1.78	0.41	95	110	658	17	65	13	5.65	15.6	2.09	11.86	2.37	66	6.33	0.81	5.21	0.67
HN-99-46	Sept-Îles Intrusive Suite	2.03	0.31	84	99	478	13	54	11	4.45	14.7	1.92	11.56	2.33	66	6.28	0.84	5.48	0.73
HN-99-53	Sept-Îles Intrusive Suite	1.41	0.40	74	112	583	13	48	10	4.30	11.6	1.48	8.69	1.72	50	4.60	0.61	4.14	0.54
304.72	Rustenburg Layered Suite	14.29	3.57	339	370	279	39	121	19	1.79	22.6	3.05	18.86	4.03	119	11.44	1.58	10.24	1.33

[(a)] partition coefficients from Bedard (2001), Watson and Green (1981) and Prowatke and Klemme (2006).

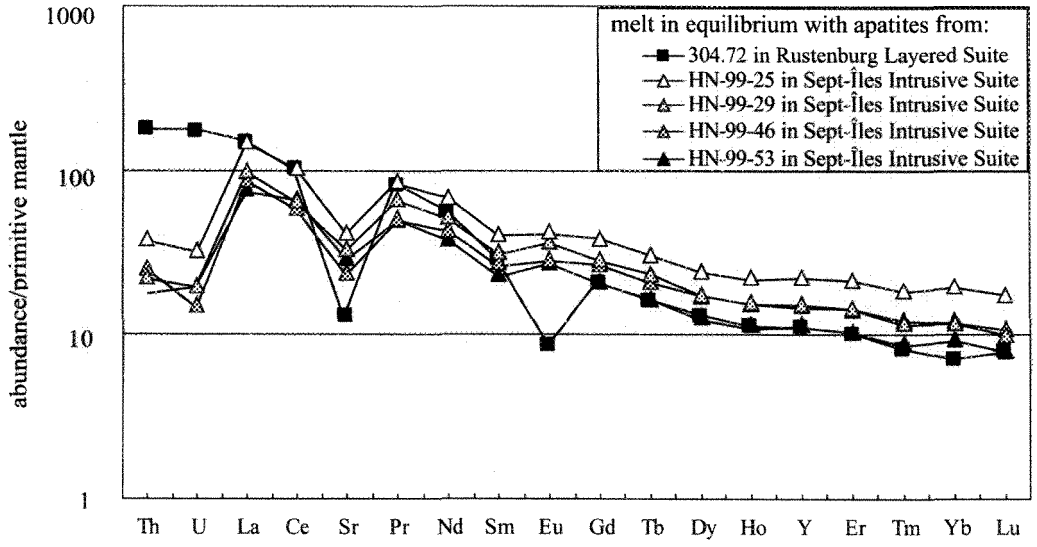

Figure 4. 8: Calculated normalized traces elements patterns of the melts in equilibrium with apatite from nelsonite in the Rustenburg Layered Suite of the Bushveld Complex (304.72) and in the Sept-Îles Intrusive Suite (HN-99-53, HN-99-46, HN-99-29 and HN-99-25). Partition coefficient values are from Watson and Green (1981), Bédard (2001) and Prowatke and Klemme (2006).

4.6.2 Implications for parental magma of nelsonite

- Sept-Îles Intrusive suite -

Hounsell (2003) reported the composition of mafic dykes associated with the Sept-Îles Intrusive Suite. The most common dykes (group B dykes) have the composition of a diorite (Table 4. 5). A mafic liquid of this composition would have olivine, plagioclase and clinopyroxene on the liquidus, which is consistent with the cumulate mineralogy of the Layered Series in the Sept-Îles Intrusive Suite (Fig. 4. 2).

We have modeled crystal fractionation of a liquid with the composition of the dykes using the PELE program (Boudreau 1999). The pressure chosen was 300 MPa and the oxygen buffer was set to FMQ. Pressures between 100 MPa and 400 MPa produced a crystallization sequence similar to that observed but 300 MPa approximated most closely the observed proportions. After ≈ 15% fractional crystallisation Fe-Ti oxide joins plagioclase, Ca-rich pyroxene and olivine and after ≈ 15% more fractional crystallisation apatite is on the liquidus (Table 4. 5). The composition of olivine (Fo_{60}) and clinopyroxene (Di_{75}) from the model approximates the compositions of these phases in the nelsonitic-troctolites, troctolitic-nelsonites and nelsonites (e.g. clinopyroxene Di_{71}-Di_{76}; olivine Fo_{50}-Fo_{63} in troctolitic-nelsonite*)*. The equation of Tollari et al. (2006), modified to account of the presence of alkalis (Bea et al. 1992) is in agreement with PELE and predicts that apatite saturation is possible for this composition. As shown by figure 4. 9 a, the calculated composition of the magma in equilibrium with the apatites in the nelsonites from Sept-Îles overlaps the compositions of the initial dykes. As outlined above, the melt would have undergone ≈ 30% fractionation before apatite crystallisation.

Table 4. 5: Modeling of the evolution of proposed parental magma for nelsonite from Sept-Îles Intrusive Suite

	Average composition of B-group dykes (a)	Liquid composition at apatite saturation (b)		Wt. % of each mineral extracted before apatite saturation (c)	Composition of cumulate phase at the time of apatite saturation
Liquid composition					
SiO_2 (wt%)	46.21	48.79	**Ol**	**6.63**	fo: 0.60
TiO_2	4.29	3.14	**Hem-Ilm**	**3.57**	ilm: 0.96
Al_2O_3	14.03	15.19	**Mt-Usp**	**1.02**	mt: 0.33
Fe_2O_3	15.96	12.81	**Cpx**	**6.99**	di: 0.75
MnO	0.21	0.31	**Plag**	**10.37**	an: 0.67
MgO	5.04	2.66	**Apatite**	**0.26**	
CaO	8.79	7.69	**Total**	**28.92**	
Na_2O	3.47	4.33			
K_2O	1.25	1.76			
P_2O_5	0.70	0.83			
LOI	1.37	1.92			
Total	100.59	100.00			
Th (ppm)	2.70	3.87			
U	0.73	1.04			
La	33.92	51.08			
Ce	80.88	118.23			
Sr	438.67	359.35			
Pr	11.08	15.66			
Nd	51.05	72.12			
Sm	11.83	16.43			
Eu	3.63	4.56			
Gd	11.44	15.81			
Tb	1.71	2.37			
Dy	9.28	13.05			
Ho	1.75	2.48			
Y	49.28	69.53			
Er	4.33	6.21			
Tm	0.62	0.90			
Yb	3.71	5.44			
Lu	0.54	0.81			

(a) Average composition of B-group dykes. Major elements from Hounsell (2003) and trace elements from this study.

(b) Liquid at apatite saturation after 25 % fractionation of average composition of B-group dykes and apatite saturation.

(c) Phases present when apatite appears on liquidus. Modeling of crystal fractionation with PELE software, a P.C. version of MELTS . Pressure used during modeling is 3 kb and the oxygen buffer was FMQ. (hem = hemoilmenite; ilm = ilmenite; mt = magnetite; usp = ulvospinel).

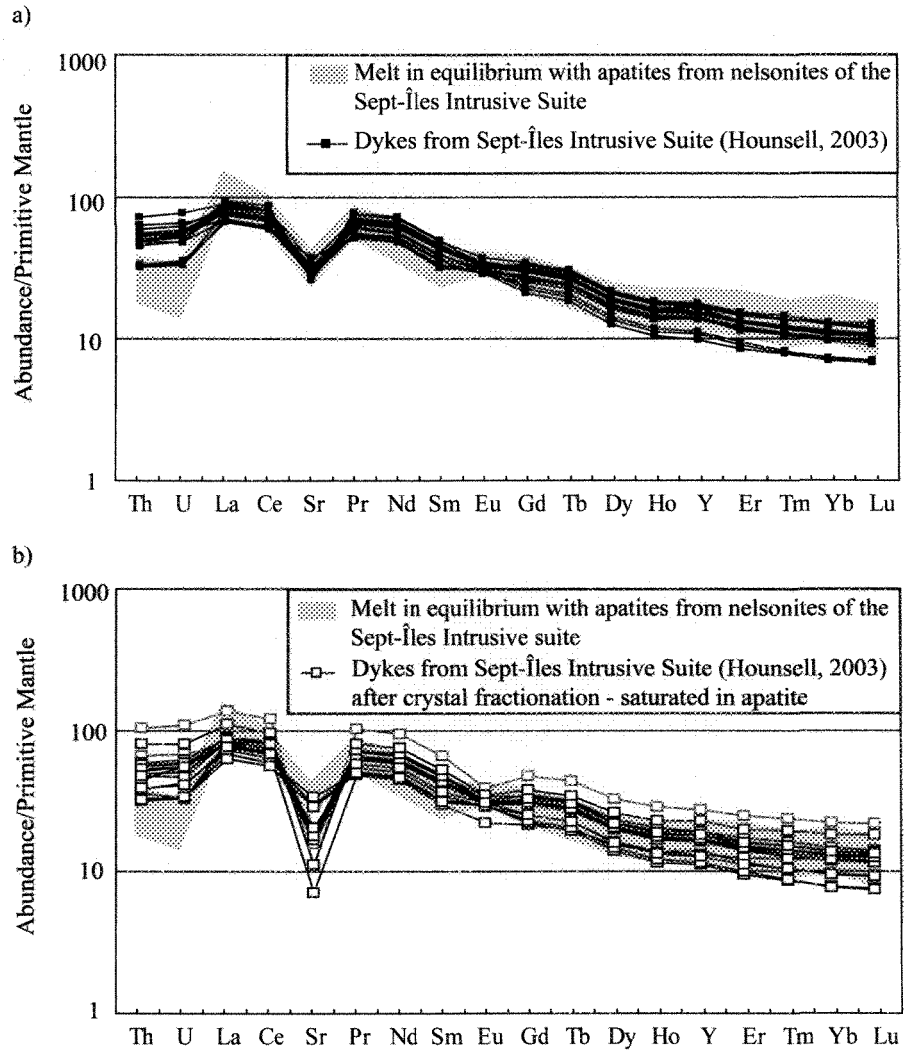

Figure 4. 9: Calculated normalized trace element patterns of the melts in equilibrium with apatite from nelsonite in the Sept-Îles Intrusive Suite (HN-99-53, HN-99-46, HN-99-29 and HN-99-25) and, a) patterns of the mafic dykes proposed to be parental magma for the nelsonites (analyses from Hounsell (2003) and this study) and b) patterns of the mafic dykes after saturation in apatite by crystal fractionation (≈ 15-30% of crystallisation). PELE software is used to do the modeling of crystal fractionation (Boudreau, 1999). Partition coefficient values are from Watson and Green (1981), Bédard (2001) and Prowatke and Klemme (2006).

The trace element compositions of the melt, at the time of apatite saturation estimated using PELE software (figure 4. 9 b), are similar to those recalculated from apatite by inversion (Table 4. 4).

- Rustenburg Layered Suite -

On the basis of their geochemical composition, the dykes and sills of the Bushveld Complex, thought to represent the magmas that formed the complex, may be divided into two groups. The first group (B-1) are basaltic andesites of boninitic composition (Curl 2001). The second group (B-2 and B-3) have the composition of tholeiitic basalts (Fig. 4. 10 a) (Curl 2001).

B-1 magmas show PM-normalized trace element patterns broadly similar to those calculated for the magma from which the apatite crystallized. It however does not show negative Sr and Eu anomalies (Fig. 4. 10 a). A fractionated B-1 magma with such trace element composition could then be the magma from which the apatite crystallized. However, B-1 contains very little P_2O_5 (Table 4. 6) and even after 95 % fractionation apatite does not appear on the liquidus. Furthermore, the B-1 magma does not crystallize olivine, while olivine is a cumulus phase in this part of the Upper Zone. Thus the evolved B-1 magma can not be the parental magma of the nelsonite. Because it does not show enrichment in LREE, U and Th and has positive Sr and Eu anomalies, the B-3 magma is unlikely to be the magma from which the nelsonite formed (Fig. 4. 10 a). On the other hand, the trace element pattern of the B-2 magma is similar to the apatite pattern except that it does not display the Th and U enrichment that the calculated apatite-saturated magma shows (Fig. 4. 10 a).

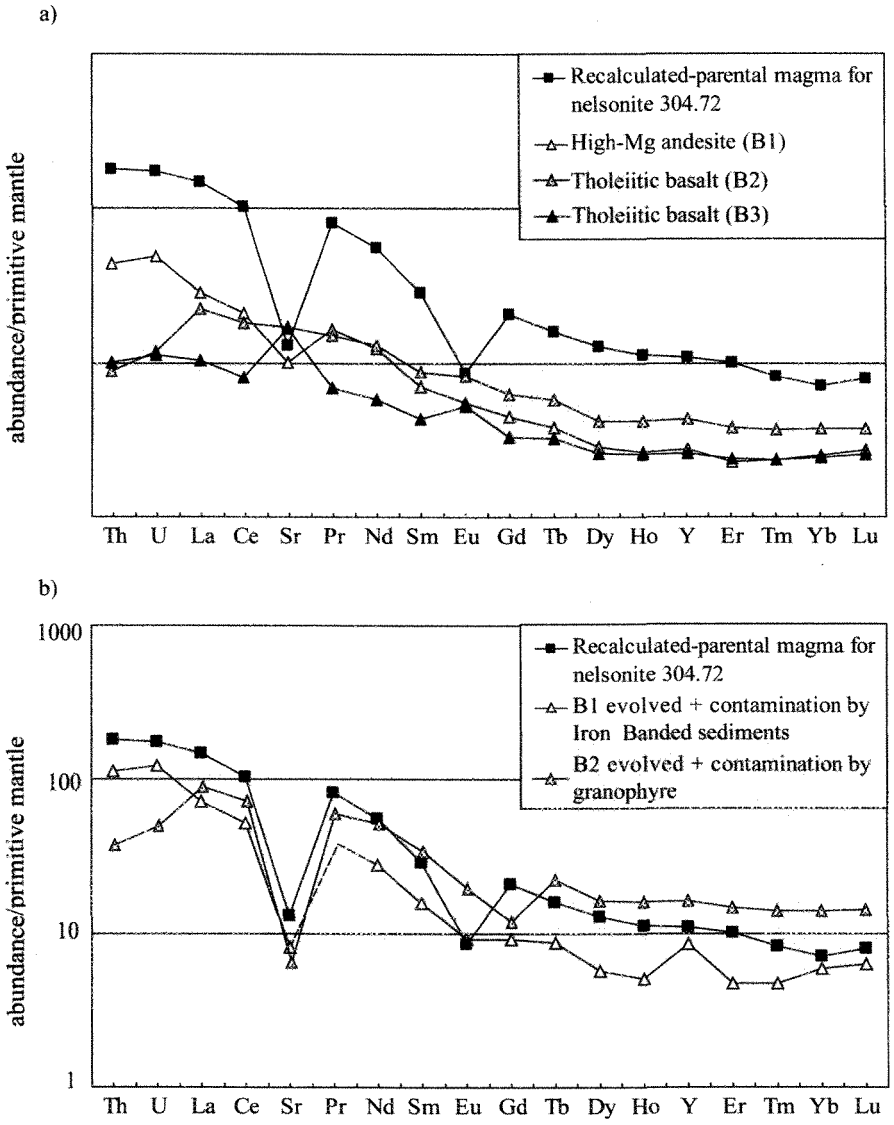

Figure 4. 10: Calculated trace elements patterns for melts in equilibrium with apatite from nelsonite from the Rustenburg Layered Suite of the Bushveld Complex a) versus B1, B2 and B3 (proposed Bushveld Complex parental magmas); b) versus B1 after cristal fractionation and contamination by Iron Banded sediments from Transvaal (Beukes et al., 1990 and Pele software modeling) and B2 after cristal fractionation and contamination by granophyre (Royer 2001). Partition coefficient values are from Watson and Green (1981), Bédard (2001) and Prowatke and Klemme (2006).

Table 4. 6: Modeling of the evolution of proposed parental magma for nelsonite from Rustenburg layered Suite

	B-1 [a]	B-2 [a]	B-3 [a]	Granophyre [b]	Ironstone [c]	B-2 at apatite saturation [d]	B-1 after crystal fractionation and contamination [e]
SiO_2 (wt. %)	55.85	51.20	51.58	69.22	48.73	67.38	77.46
TiO_2	0.34	0.70	0.41	0.43	0.04	0.24	0.00
Al_2O_3	11.93	15.42	16.14	13.55	0.04	12.06	9.71
Fe_2O_3	10.48	12.18	10.40	3.84	35.80	5.74	2.20
MnO	0.18	0.19	0.18	0.01	0.00	0.81	0.69
MgO	11.57	7.23	7.68	0.52	2.98	0.26	0.03
CaO	6.56	10.44	11.08	1.13	10.99	4.59	3.69
Na_2O	1.67	1.87	1.76	3.35	0.13	3.06	1.48
K_2O	0.99	0.29	0.31	7.18	0.00	1.24	2.13
P_2O_5	0.08	0.15	0.04	0.10	0.30	0.64	0.59
LOI	0.10	0.04	0.12	0.02	0.05	4.29	2.70
Total	99.75	99.70	99.70	99.24	99.06	100.31	100.00
Th (ppm)	3.51	0.70	0.80	27.23	0.02	2.87	8.87
U	1.01	0.24	0.23	8.43	0.10	0.98	2.52s
La	18.24	14.44	6.68	62.73	3.20	55.39	46.3
Ce	35.33	30.47	13.58	109.59	3.96	116.49	87.4
Sr	202.64	341.31	338.36	116.22	30.00	125.90	161.18
Pr	4.23	3.86	1.75	-	-	14.88	-
Nd	15.69	16.28	7.24	31.00	0.00	62.78	34.92
Sm	2.83	3.55	1.74	6.19	0.46	13.44	6.33
Eu	0.84	1.27	0.81	0.74	0.19	2.92	1.41
Gd	2.44	3.39	1.80	-	0.00	6.29	4.93
Tb	0.34	0.52	0.29	0.96	0.11	1.94	0.78
Dy	1.92	2.83	1.75	4.61	0.00	10.63	3.81
Ho	0.39	0.62	0.38	1.68	0.00	2.31	0.75
Y	11.84	18.42	11.08	0.00	13.00	68.46	36.62
Er	1.00	1.66	1.04	-	0.00	6.24	2.08
Tm	0.16	0.25	0.16	-	0.00	0.93	0.32
Yb	1.11	1.64	1.07	3.81	0.56	6.04	2.59
Lu	0.18	0.25	0.17	0.55	0.10	0.92	0.42

[a] Composition from Curl (2001)
[b] Composition based on granophyres from Royee (2001).
[c] Composition based on the sample 8 from the borehole CN-109 (Beukes and Klein 1990).
[d] Modeling of crystal fractionation with PELE 6.01 software, a P.C. version of MELTS (Boudreau 1999); until obtaining apatite saturation. B-2 after 76 % fractionation.
(e) Modeling of crystal fractionation with PELE 6.01 software, a P.C. version of MELTS (Boudreau 1999); until obtaining apatite saturation. B-1, after 75 % fractionation and 40 % contamination. Pressure used during modeling is 3Kb and the oxygen buffer was FMQ.

PELE simulation of crystal fractionation of this magma shows that after 76 % crystal fractionation, this liquid would be saturated in apatite with the phase assemblage similar to that observed in the rocks; Fe-Ti oxide, plagioclase, olivine (Fo_{22}) and clinopyroxene. The equation of Tollari et al. (2006) confirms that this liquid would be saturated in apatite. The trace element pattern of this liquid is similar to that of the magma calculated to be in equilibrium with the apatite, with large negative Sr and Eu anomalies, because of the extensive plagioclase crystallization (Fig. 4. 10 b). However, the U and Th concentrations are much lower in the magma derived from the B-2 liquid than the U and Th concentrations recalculated from the apatite (Th = 14.29, U= 3.57 in calculated magma; Th = 2.87, U= 0.98 in B-2).

The apatite-bearing rocks of the Bushveld are found in the upper 500 m of the intrusion, where there are many crustal xenoliths and numerous granophyres (Ashwal et al. 2005; Royer 2001). There are in fact granitic veins within the 10 m nelsonite layer. The trace element patterns of the granophyres from the Bushveld show a strong enrichment in Th and U (Fig. 4. 10 b). This suggests that the magma in this zone may have been contaminated by melts derived from the xenoliths, and this could be the source of the high U and Th concentrations in the apatite. We may also consider that B-1 magma could have experienced contamination. In the case of the B-1 magma, the "missing" ingredient was the P_2O_5. Among the host rock types of the Bushveld Complex (Beukes and Klein 1990; Eales and Cawthorn 1996), a potential contaminant containing P_2O_5 is the banded iron formation that forms part of the Transvaal Supergroup sediments. The PELE simulation of an AFC process, in which the magma experienced a total of ~40 % contamination, shows that apatite would be on the liquidus after approximately 75 % crystal fractionation (Fig. 4. 10 b and Table 4. 6). Contamination process was already suggested in the Bushveld Complex on

the base of variable Ti contents and variable but radiogenic Sr_i isotopic signatures (Cawthorn 1996; Eales and Cawthorn 1996; Kruger 1994).

The mineral assemblage at the time of saturation is Fe-oxide, plagioclase, clinopyroxene and quartz. The Fe-oxide contains a much lower Ti content than the observed Fe-oxide and the olivine is more Fo rich than the observed olivine. The trace element patterns are quasi parallels than the trace element patterns calculated for the magma in equilibrium with the apatite.

We suggest that the apatite and iron oxide could have formed from either the B-1 magma contaminated with banded iron formation or the B-2 contaminated with granophyre (~15 % of contamination).

4.6.3 Models of nelsonite formation - Crystal fractionation and accumulation

This study shows that crystal fractionation of a specific mafic magma could lead to troctolitic nelsonite formation with minerals of the composition matching those of the natural samples in the case of the Sept-Îles Intrusive suite and ferrodiorite of the Rustenburg Layered Suite.

In the upper part of layered intrusions, the fractionated magma has a high content of Fe, Ti and P. The high content of Fe and Ti leads to saturation in Fe-Ti oxides (Fig 4. 11). The high phosphate contents and Fe-Ti oxide saturation trigger saturation in apatite (Toplis et al. 1994), and apatite and Fe-Ti oxides crystallize almost simultaneously. Because of density difference, the liquid and the crystals separate (Wager and Brown 1968) and the interstitial liquid is expelled because of the weight of the crystal pile and compaction.

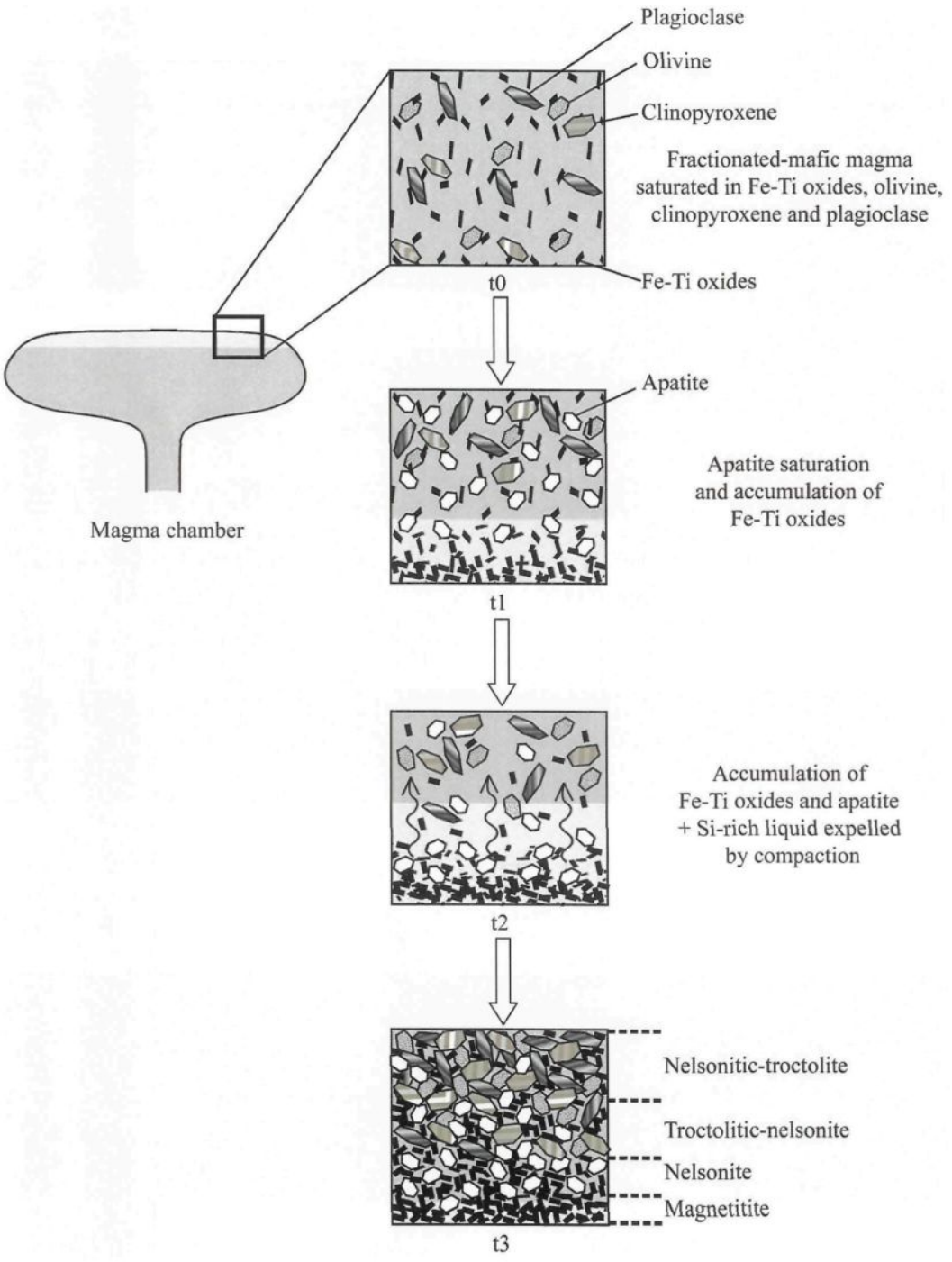

Figure 4. 11: Formation model of the nelsonites and associated rocks by crystal fractionation and accumulation in the upper part of the layered intrusions. (t0 = initial time, t1, t2 and t3 = cooling history of magma).

The resulting cumulate rocks occur as layer forms which contain primary apatite and Fe-Ti oxides (the nelsonites). The weakness of this model is that modeling suggests clinopyroxene and apatite to be on the liquidus at the same time. These two minerals have a similar density and thus separating them by crystal settling, to form the nelsonites, seems unlikely. However, the new experimental work of Tollari et al. (submitted) showed that hydroxyapatite crystallizes just before clinopyroxene from ferrobasalt of the composition similar to the Sept-Îles dykes (hydroxyapatite 1040°C, clinopyroxene 1015°C) and in F-bearing runs clinopyroxene crystallization was suppressed by the crystallization of fluoroapatite.

4.7 CONCLUSIONS

Our results indicate that apatite controls REE, U, Th, Cl, Ca, and Sr budget in nelsonites. Composition in those trace elements was recalculated for the parental magmas of apatite-oxide-rich rocks from the Sept-Îles Intrusive suite and, from the Rustenburg Layered Suite. Comparison of these recalculated trace element composition with those of the natural rocks proposed to be the parental magmas of the Sept-Îles and Bushveld intrusions, indicate that the troctolitic-nelsonite from Sept-Îles Intrusive suite could be formed by crystal fractionation of a magma similar to the composition of the marginal diorite dykes followed by oxide and apatite saturation. The crystal settling of these phases could lead to a series of layers in magnetitite, nelsonite and troctolitic-nelsonite. In the case of the Bushveld Complex approximately 75 % of fractionation of a high Mg basalt (B1) combined with 40 % contamination by Banded Iron formation of the Transvaal, or ≈ 75 % of fractionation of the tholeiitic basalt (B2) combined with 15 % contamination by granophyre, will bring

apatite and oxide onto the liquidus. Our study shows that crystal fractionation could explain the formation of troctolitic-nelsonite but, an additional crystal accumulation step must be considered to explain rocks only containing apatite and Fe-Ti oxides.

Acknowledgements

This work was supported financially by a Canada Research Chair grant to S.J.B. This work has benefited from the help of numerous people and N.T. would like to acknowledge the support of Bélinda Godel, Fabien Solgadi, Nicolas Vinet and Marc Choquette for his help during microprobe analyses in the Laboratoire de Microanalyses de Laval, Québec City.

References

Arth, J.G., 1976. Behaviour of trace elements during magmatic processes - a summary of theoretical models and ther allications. Journal of Ressources of the U.S. Geological Survey, 4: 41-47.

Ashwal, L.D., Webb, S.J. and Knoper, M.W., 2005. Magmatic stratigraphy in the Bushveld Northern Lobe: continuous geophysical and mineralogical data from the 2950 m Bellevue drillcore. South African Journal of Geology, 108(2): 199-232.

Barnes, S.-J., Maier, W.D. and Ashwal, L.D., 2004. Platinum-group element distribution in the Main Zone and Upper Zone of the Bushveld Complex, South Africa. Chemical Geology, 208(1-4): 293-317.

Bea, F., Fershtater, G. and Corretge, L.G., 1992. The geochemistry of phosphorus in granite rocks and the effect of aluminum. Lithos, 29(1-2): 43-56.

Bedard, J.H., 2001. Parental magmas of the Nain Plutonic Suite anorthosites and mafic cumulates: a trace element modelling approach. Contributions to Mineralogy and Petrology, 141(6): 747-771.

Bedard, L.P. and Barnes, S.J., 2002. A comparison of the capacity of FA-ICP-MS and FA-INAA to determine platinum-group elements and gold in geological samples. Journal of Radioanalytical and Nuclear Chemistry, 254(2): 319-329.

Beukes, N.J. and Klein, C., 1990. Geochemistry and sedimentology of a facies transition - from microbanded to granular iron-formation - in the Early Proterozoic Transvaal Supergroup, South-Africa. Precambrian Research, 47(1-2): 99-139.

Boudreau, A.E., 1999. PELE - a version of the MELTS software program for the PC platform. Computers & Geosciences 25: 201-203.

Cawthorn, R.G., 1996. Layered Intrusions. Elsevier, Amsterdam, 531 pp.

Cimon, J., 1998. L'unité à apatite de rivière des rapides, Complexe de Sept îles. Localisation stratigraphique et facteurs à l'origine de sa formation. Ministère des ressources naturelles, Québec, 97(5): 1-32.

Curl, E.A., 2001. Parental magmas of the Bushveld Complex, South Africa. Ph.D. Thesis, Monash University, Australia, 140 pp.

Drake, M.J. and Weill, D.F., 1975. Partition of Sr, Ba, Ca, Y, Eu2+, Eu3+, and other ree between plagioclase feldspar and magmatic liquid - experimental study. Geochimica et Cosmochimica Acta, 39(5): 689-712.

Dymek, R.F. and Owens, B.E., 2001. Petrogenesis of apatite-rich rocks (nelsonites and oxide-apatite gabbronorites) associated with massif anorthosites. Economic Geology and the Bulletin of the Society of Economic Geologists, 96(4): 797-815.

Eales, H.V. and Cawthorn, R.G., 1996. The Bushveld Complex. In: R.G. Cawthorn (Editor), Layered Intrusions. Elsevier, Amsterdam, pp. 181-229.

Emslie, R.F., 1975. Nature and origin of anorthositic suites. Geoscience Canada, 2(2): 99-104.

Fredette, J., 2006. Pétrographie, géochimie et potentiel économique en Fe-Ti-P du secteur de Lac à Paul, Parte Nord de le Suite Anorthositique du Lac-Saint-Jean, Province du Grenville, Québec. classic Thesis, Université du Québec à Chicoutimi, Chicoutimi, 294 pp.

Frietsch, R. and Perdahl, J.-H., 1995. Rare earth elements in apatite and magnetite in Kiruna-type iron ores and some other iron types. Ore Geology Reviews, 9: pp. 489-510.

Goldberg, S.A., 1984. Geochemical relationships between anorthosite and associated iron-rich rocks, Laramie Range, Wyoming. Contributions to Mineralogy and Petrology, 87(4): 376-387.

Hall, A.L., 1932. The Bushveld Igneous Complex in the central Transvaal. Geological Society, South Africa Memoir 28: 544.

Hargraves, R.B., 1962. Petrology of the Allard Lake anorthosite suite, Quebec. In: A.E.J. Engel, James H. L. and B.F. Leonard (Editors), Petrologic Studies. Geological Society of America, Buddington, pp. 163-189.

Higgins, M.D., 2005. A new interpretation of the structure of the Sept Iles Intrusive suite, Canada. Lithos, 83(3-4): 199-213.

Higgins, M.D. and Doig, R., 1981. The Sept-Iles Anorthosite Complex - Field relationships, geochronology, and petrology. Canadian Journal of Earth Sciences, 18(3): 561-573.

Hildebrand, R.S., 1986. Kiruna-type deposits: Their origin and relationship to intermediate subvolcanis plutons in the Great Bear magmatic zone, Northwest Canada. Economic Geology, 81: pp. 640-659.

Hounsell, V., 2003. géochimie des dykes mafiques et composés de la suite intrusives de Sept-Îles, Québec. projet de fin d'études Thesis, Université du Québec à Chicoutimi, Chicoutimi, 48 pp.

Huntington, H.D., 1979. Kiglapait Mineralogy .1. Apatite, Biotite, and Volatiles. Journal of Petrology, 20(3): 625-652.

Jakobsen, J.K., Veksler, I.V., Tegner, C. and Brooks, C.K., 2005. Immiscible iron- and silica-rich melts in basalt petrogenesis documented in the Skaergaard intrusion. Geology, 33(11): 885-888.

Kolker, A., 1982. Mineralogy and geochemistry of Fe-Ti oxide and apatite (nelsonite) deposits and evaluation of the liquid immiscibility hypothesis. Economic Geology, 77(5): 1146-1158.

Kruger, F.J., 1994. the Sr-isotopic stratigraphy of the western Bushveld Complex. South Africa Journal of Geology, 97: 393-398.

Maier, W.D. and Barnes, S.J., 1998. Concentrations of rare earth elements in silicate rocks of the Lower, Critical and Main Zones of the Bushveld Complex. Chemical Geology, 150(1-2): 85-103.

Mathez, E.A. and Webster, J.D., 2005. Partitioning behaviour of chlorine and fluorine in the system apatite-silicate melt-fluid. Geochimica et Cosmochimica Acta, 69(5): 1275-1286.

McDonough, W.F. and Sun, S.S., 1995. The composition of the earth. Chemical Geology, 120(3-4): 223-253.

McLelland, J., Ashwal, L. and Moore, L., 1994. Composition and petrogenesis of oxide-rich, apatite-rich gabbronorites associated with Proterozoic anorthosite massifs - Examples from the Adirondack Mountains, New-York. Contributions to Mineralogy and Petrology, 116(1-2): 225-238.

Nabil, H., 2003. Genèse des dépôts de Fe-Ti-P associés aux intrusions litées (exemples: intrusion mafique de Sept-Îles, au Québec; Complexe de Duluth aux États-Unis). Ph. D. Thesis, Université du Québec à Chicoutimi, Chicoutimi, 441 pp.

Nash, W.P. and Crecraft, H.R., 1985. Partition coefficients for trace elements in silicic magmas. Geochimica and Cosmochimica Acta, 49: 2309-2322.

Naslund, H.R., 1983. The effect of oxygen fugacity on liquid immiscibility in iron-bearing silicate melts. American Journal of Science, 283(10): 1034-1059.

Pearce, J.A. and Norry, M.J., 1979. Petrogenetic implications of Ti, Zr, Y and Nb variations in volcanic rocks. Contributions to Mineralogy and Petrology, 69: 33-47.

Philpotts, A.R., 1967. Origin of certain iron-titanium oxide and apatite rocks. Economic Geology, 62(3): 303-315.

Philpotts, A.R., 1981. A model for the generation of massif-type anorthosites. Canadian Mineralogist, 19: 233-253.

Prowatke, S. and Klemme, S., 2006. Trace element partitioning between apatite and silicate melts. Geochimica et Cosmochimica, 70: 4513-4527.

Reynolds, I.M., 1985a. Contrasted mineralogy and textural relationships in the uppermost titaniferous magnetite layers of the Bushveld Complex in the Bierkraal Area North of Rustenburg. Economic Geology, 80(4): 1027-1048.

Reynolds, I.M., 1985b. The nature and origin of titaniferous magnetite-rich layers in the Upper Zone of the Bushveld Complex - a review and synthesis. Economic Geology, 80(4): 1089-1108.

Royer, R., 2001. Les roches encaissantes du complexe du Bushveld et la contamination possible des magmas andésite basaltique (B1) et basalte tholéiitique (B2). projet de fin d'études Thesis, Université du Québec à Chicoutimi, Chicoutimi, 34 pp.

Tegner, C., Cawthorn, R.G. and Kruger, F.J., 2006. Cyclicity in the Main and Upper Zones of the Bushveld Complex, South Africa: crystallization from a Zoned Magma Sheet. Journal of petrology: 1-23.

Tollari, N., Baker, D.R. and Barnes, S.J., submitted. Experimental study on the effect of pressure and fluorine on silicate melt crystallization - implications on the evolution of layered intrusions.

Tollari, N., Toplis, M.J. and Barnes, S.-J., 2006. Predicting phosphate saturation in silicate magmas: An experimental study of the effects of melt composition and temperature. Geochimica et Cosmochimica Acta, 70(6): 1518-1536.

Toplis, M.J., Libourel, G. and Carroll, M.R., 1994. The role of phosphorus in crystallization processes of basalt - an experimental-study. Geochimica et Cosmochimica Acta, 58(2): 797-810.

Von Gruenewaldt, G., 1973. The Main and Upper Zones of the Bushveld Complex in the Roossenekal area, eastern Transvaal. Transactions Geological Society of South Africa, 76: 207-227.

Von Gruenewaldt, G., 1993. Ilmenite-apatite enrichments in the Upper Zone of the Bushveld Complex: A major titanium-rock phosphate resource. International Geology Review, 35: 987-1000.

Wager, L.R. and Brown, G.M., 1968. Layered igneous rocks. Oliver and Boyd, Edinburgh.

Watson, E.B. and Green, T.H., 1981. Apatite liquid partition-coefficients for the rare-earth elements and strontium. Earth and Planetary Science Letters, 56(DEC): 405-421.

Watson, T.L., 1907. Mineral resources of Virginia, J. P. Bell Company, Lynchburg.

CHAPITRE 5

RÉSUMÉ ET CONCLUSIONS

L'objectif principal de ce travail de recherche était de définir les facteurs influençant la saturation des minéraux phosphatés dans les magmas mafiques. Des études antérieures ont permis de mettre en avant certains facteurs compositionnels tel que la silice (Harrison and Watson 1984) ou les alcalins (Bea et al. 1992), ainsi que l'effet de la température (Harrison and Watson 1984) dans des magmas basiques à intermédiaires. Cette étude, quand à elle, est axée sur les systèmes mafiques.

Comme cela a déjà été dit, les roches riches en apatite et oxydes de Fe et Ti se retrouvent principalement dans la partie supérieures des intrusions litées mafiques (Cimon 1998; Eales and Cawthorn 1996; Morse 1980; Wager and Brown 1968) ou associées à des complexes anorthositiques (Dymek and Owens 2001; Fredette 2006).

L'apatite présente un double intérêt. En plus de nous renseigner sur les conditions qui régnaient dans la chambre magmatique lors de sa cristallisation (température, pression, $fO2$), elle peut nous permettre de mieux comprendre les processus à l'origine d'un type peu commun de roche, les nelsonites, qui se composent d'1/3 apatite et de 2/3 oxyde de Fe et Ti. Deux modèles sont proposés pour expliquer la formation de ce type de roche : Dans le premier modèle l'apatite et les oxydes cristallisent à partir d'un magma mafique évolué et s'accumulent pour former des lits nelsonitiques (Barnes et al. 2006; Eales and Cawthorn 1996; Emslie 1975; Goldberg 1984; McLelland et al. 1994; Tegner et al. 2006). Le second

modèle suggère que les nelsonites soient le produit de l'immiscibilité de deux liquides (Jakobsen et al. 2005; Naslund 1976; Philpotts 1967).

Dans les paragraphes suivant je reviendrais sur nos principaux résultats. Je décrirais leurs implications sur la saturation de l'apatite dans les magmas mafiques et je conclurais sur l'application de nos résultats à des systèmes naturels. Finalement, je décrirais le modèle de formation des nelsonites favorisé par les résultats de cette étude.

5.1 CRISTALLISATION DES MINÉRAUX PHOSPHATÉS DANS LES MAGMAS SILICATÉS

Dans les roches naturelles qui nous intéressent, les minéraux phosphatés sont étroitement liés aux oxydes de Fe et Ti. Nous avons donc réalisé une série d'expériences à une atmosphère afin de tester l'influence de la teneur en Fe et de l'état d'oxydation sur la saturation en minéraux phosphatés dans des systèmes magmatiques.

Ces expériences démontrent que ni le contenu en Fe, ni l'état d'oxydation du système joue un rôle significatif sur la saturation en phosphate. Nos résultats indiquent cependant que la teneur en SiO_2 et en CaO contrôle la quantité nécessaire de P_2O_5 pour provoquer la saturation en minéraux phosphaté. La température apparaît comme étant un facteur secondaire. L'étroite relation entre ces différents facteurs et la concentration en P_2O_5 nécessaire pour provoquer la cristallisation d'un minéral phosphaté (apatite ou whitlockite) est résumée par l'équation suivante :

$$M_{P_2O_5}^{liq-sat} = \exp\left[T\left(\frac{-0.8579}{139.00 - M_{SiO_2}^{liq}} + 0.0165\right) - 3.3333\ln\left(M_{CaO}^{liq}\right)\right]$$

Dans cette équation M représente la concentration molaire et T la température en K. Cette équation est valide à travers un éventail très large de composition et de température (par exemple valable de 10 à 80% molaire de SiO_2 et pour des températures allant de ≈ 800 à 1400°C). Cependant, tout comme le modèle de Harrison et Watson (1984), notre modèle nécessite un facteur de correction pour les compositions alcalines (Bea et al. 1992) (Na_2O + K_2O > 3 % poids semble être la limite). Cette équation permet d'illustrer les effets relatifs de chacun des facteurs mis en évidence. Ainsi, le facteur compositionnel prédomine sur le facteur thermique.

Le but principal de cette première série d'expériences était de considérer l'effet de la fugacité d'oxygène sur la saturation des phosphates et des oxydes de Fe et Ti. C'est pourquoi elles ont étaient réalisées à 0.1 MPa et qu'aucun volatile tel que F et H_2O n'a été ajouté aux compositions initiales. L'absence de volatiles explique le fait que le phosphate qui a cristallisé était de la whitlockite et non de l'apatite.

Un ajout de F et de H_2O peut potentiellement changer la structure du magma silicaté et ainsi influencer le moment de la saturation en apatite et an oxydes de Fe et Ti. C'est pour cette raison que nous avons réalisé une deuxième série d'expériences (Chapitre 3). En utilisant la même composition ferrobasaltique que lors des premières mais en y ajoutant de H_2O et/ou du F. De plus, nous avons utilisé une seconde composition plus alcaline (analogue de dykes provenant de la Suite Intrusive de Sept-Îles (Hounsell 2003)).

Cette fois-ci nous avons cristallisé de l'apatite à la place de la whitlockite. Nos nouvelles données confirment nos précédents résultats concernant l'effet de SiO_2 et de CaO sur la saturation des minéraux phosphatés. De plus, l'ajout de F au système affecte la saturation d'apatite, qui se produit à des concentrations plus faible en SiO_2 et plus élevées en CaO que dans un système hydraté sans F.

La quantité de P_2O_5 nécessaire pour saturer un magma mafique en un minéral phosphaté dépend donc principalement de la teneur en SiO_2 et en CaO de ce magma. La température et le F sont des facteurs secondaires malgré le fait que le F est nécessaire à la cristallisation de fluoroapatite.

5.2 CHAMPS D'IMMISCIBILITÉ DANS LES SYSTÈMES MAFIQUES

Dans nos premières expériences nous avons travaillé avec des liquides de compositions ferrobasaltiques semblables au magma de Skaergaard auxquels nous avons ajouté 5 et 10 % poids de P_2O_5 (Chapitre 2). Dans les expériences contenant 10 % poids de P_2O_5 nous avons observé des évidences texturales d'immiscibilité. Cette immiscibilité n'est cependant pas directement applicable à un système naturel. En effet, la plupart des magmas basaltiques contiennent seulement entre 0.2 et 1 % poids de P_2O_5. Cependant, ces données sont très intéressantes puisqu'en les combinant avec les données de Bogaerts et Schmidt (2006) nous avons pu définir deux champs d'immiscibilité de deux liquides. Ces champs d'immiscibilité sont stables pour des pressions correspondantes à la croûte supérieure à moyenne (0.1 MPa à 400 MPa) dans le système SiO_2-FeO-TiO_2-MgO-CaO-P_2O_5-Al_2O_3-Na_2O-K_2O. La comparaison de l'étendue de ces deux champs d'immiscibilité indique que la pression joue un rôle important sur l'ampleur du champ. En effet, une augmentation de

pression mène à une diminution importante du champ d'immiscibilité de ce système (Fig 3. 4). Les champs d'immiscibilité ne sont pas uniquement sensibles à la pression. En effet, l'immiscibilité de deux liquides existe pour une gamme de composition, de pression et de température donnée.

5.3 APPLICATIONS AUX ROCHES NATURELLES

Nous avons appliqué nos résultats à différents exemples naturels tel que la Suite Intrusive de Sept-Îles, la Rustenburg Layered Suite du complexe du Bushveld, l'intrusion litée de Skaergaard et le complexe anorthositique du Lac-St-Jean, afin de déterminer quels processus sont à l'origine des roches riches en apatite et en oxydes de Fe et Ti.

- *Immiscibilité de deux liquides –*

Nos données ajoutées à celles de Bogaerts et Schmidt (2006) nous ont permis de définir l'extension des champs d'immiscibilité de deux liquides dans des systèmes mafiques en fonction de la température et de la pression.

Connaissant les deux modèles de formation proposés pour les roches riches en apatites et oxydes de Fe et Ti et nelsonitiques nous voulions vérifier si les magmas de certaines intrusions et complexes anorthositiques traversaient les champs d'immiscibilité de deux liquides avant de saturer en apatite. Pour cela nous avons comparé les trajectoires d'évolutions des magmas de la suite intrusive de Sept-Îles, du complexe anorthositique du Lac-St-Jean et de l'intrusion litée de Skaergaard (Figs 3. 8, 3. 9 et 3. 10).

Dans les cas de la suite intrusive de Sept-Îles et du complexe anorthositique du Lac-St-Jean nous avons utilisé le programme PELE (Boudreau 1999) pour modéliser l'évolution

des roches proposée comme étant possiblement à l'origine des nelsonites (respectivement dykes mafiques (Hounsell 2003) et ferrodiorite (Fredette 2006)). Dans le cas de l'intrusion litée de Skaergaard nous avons utilisés les liquides recalculés par Wager et Brown (1968). Dans les trois cas étudiés les trajectoires des liquides ne croisent pas les champs d'immiscibilité avant la saturation en apatite. Il semble donc peu probable que les nelsonites (ou les roches riches en apatite et en oxydes de Fe et Ti) soit le produit de l'immiscibilité de deux liquides.

- *Cristallisation fractionnée et accumulation* –

Puisque nos observations précédentes ne soutiennent pas le modèle d'immiscibilité de deux liquides, nous avons voulu vérifier dans quelle mesure le modèle de cristallisation fractionnée suivit par l'accumulation des cristaux d'apatite et d'oxyde de Fe et Ti était applicable à nos échantillons (Chapitre 4).

L'apatite est un minéral dans lequel on retrouve en grande quantité certains éléments traces tels que U, Th, Sr et ETR (Toplis and Dingwell 1996). Grâce à cette caractéristique ce minéral peut enregistrer les variations de ces différents éléments dans la pile magmatique et par conséquent, nos donner de précieuses informations sur la composition des liquides au cours de la différentiation du magma dans la chambre magmatique.

Afin de tester le modèle de cristallisation fractionnée nous avons analysé les éléments majeurs et traces des apatites contenues dans douze échantillons de roches riches en apatite et oxydes de Fe et Ti de la suite intrusive de Sept-Îles. Nous avons, par la suite, comparé ces résultats avec ceux obtenus lors de l'analyse de deux échantillons de la Rustenburg Layered Suite dans le complexe du Bushveld. Afin de vérifier quels éléments

sont principalement contrôlés par l'apatite nous avons fait un bilan de masse. Il apparaît que, dans les nelsonites, l'apatite contrôle les Terres Rares, l'U, le Th, le Cl, le Ca, et le Sr. Puisque l'apatite contrôle ces élément nous avons pu, grâce aux coefficients de partage de Bedard (2001) et de Watson et Green (1981), recalculé la composition du magma parent des nelsonites des deux intrusions étudiées (Fig 4. 8). Dans les deux cas, les profils d'éléments traces normalisés au manteau primitif, correspondent à des compositions magmatiques évoluées. Nous avons ensuite comparé le profil recalculé pour la suite intrusive de Sept-Îles avec celui de roches proposées pour être les magmas parents des nelsonites (Dykes mafiques de Hounsell 2003). Ces dykes ne contiennent pas d'apatite, nous avons donc modélisé leur cristallisation fractionnée à l'aide du programme PELE (Boudreau 1999). Les résultats de cette modélisation indiquent qu'il est possible de cristalliser des nelsonite troctolitiques à partir des compositions de ces dykes. De plus, les profils d'éléments traces au moment de la saturation en apatite de ces dykes sont similaires aux profils recalculés précédemment (Fig 4. 9). En impliquant la séparation par densité dans la pile magmatique il est possible d'expliquer la formation de la séquence de roches que l'on retrouve dans la zone critique de la suite intrusive de Sept-Îles (magnetitite, nelsonite et troctolitic-nelsonite).

Dans le cas de la Rustenburg Layered Suite aucune roche n'est proposée pour être le magma parent des nelsonites, nous avons donc utilisé les liquides proposés comme magma initiaux de l'intrusion (B-1 et B-2 de Hamer et Sharpe (1985)). Après 76 % de cristallisation le profil d'éléments traces de B-2 est quasi parallèle au profil recalculé. Il montre cependant une anomalie négative en U et Th. B1, quant à lui, ne contient pas assez de P_2O_5 (même après 90 % de cristallisation) pour obtenir la saturation en apatite. Il a donc fallut lors de la modélisation fractionnée de ces deux magmas impliquer une contamination

par des roches encaissantes (granophyre pour B-2 et Banded Iron formation du Transvaal pour B-1) (Fig 4. 10). Il faut cependant garder à l'esprit que dans le cas de B-1 40% de contamination sont nécessaires d'après les modélisations. Un tel volume de contamination a des implications majeures sur les variations des rapports isotopiques ainsi que sur la composition magmatique. B-2 contaminé par un granophyre reste donc l'hypothèse là plus probable.

Après ces modélisations il apparaît donc possible que les troctolites nelsonitiques et les ferrodiorites soient le résultat de la cristallisation fractionnée. La formation des nelsonite peut s'expliquer par la chute de l'apatite et des oxydes de Fe et Ti par densité dans la pile magmatique.

5.4 IMPLICATIONS SUR LES MODÈLES DE FORMATION DES NELSONITES

L'ensemble de nos résultats expérimentaux ainsi que nos modélisations et nos observations pétrographiques tendent à favoriser le modèle de cristallisation fractionnée suivit par l'accumulation de l'apatite et des oxydes de Fe et Ti pour expliquer la formation des nelsonites. Le paragraphe suivant a pour but de décrire en détail ce modèle de formation (Fig 1. 13).

Dans la partie supérieure des intrusions litées ou des complexes anorthositiques le magma fractionné a des concentrations élevées en Fe, Ti et P. La teneur élevée en Fe et Ti provoque la saturation en oxydes du magma tandis que les concentration élevées en P cause la saturation en apatite (Toplis et al. 1994). L'apatite et les oxydes de Fe et Ti cristallisent donc presque simultanément. Le liquide résiduel et les cristaux formés se séparent en raison de leur différence de densité. En effet, le liquide riche en silice étant plus léger que les

cristaux d'apatite et d'oxydes va « flotter » alors que les minéraux formés vont chuter dans la pile magmatique (Wager and Brown 1968). En raison du poids de la pile de cristaux, le liquide résiduel interstitiel est expulsé progressivement avec l'accumulation. Il se forme progressivement des couches qui contiennent principalement de l'apatite et des oxydes de Fe et Ti (nelsonites).

Malgré ces résultats, ce modèle a une faiblesse. Les simulations numériques suggèrent que le clinopyroxène et l'apatite soient sur le liquidus en même temps. Ces deux minéraux ont des densités très proches. Il est donc difficile d'expliquer leur séparation dans la pile magmatique. Cependant, les travaux expérimentaux traités dans le chapitre 3 montrent qu'un ajout de F à notre basalte synthétique permet de supprimer la cristallisation de clinopyroxène. Le programme PELE ne prend pas en considération le F dans ces modélisations ce qui expliquerait la présence calculée du clinopyroxène sur le liquidus avec l'apatite.

À la lumière des résultats présentés dans cette thèse le modèle proposé pour expliquer la formation des nelsonites, aussi bien dans la partie supérieure des intrusions litées que dans les complexes anorthositiques, est le modèle de cristallisation fractionnée et d'accumulation. Il serait cependant intéressant d'approfondir certains points. Par exemple, faire une étude plus complète de l'ordre de cristallisation des différentes phases minérales dans ce type de roche afin de mieux comprendre les relations apatite-clinopyroxène. Dans le même but une étude expérimentale reconstituant l'effet de la gravité sur la chute et la séparation des cristaux dans la pile magmatique permettrait de dire si il est physiquement possible de former des couches principalement constituées d'apatite et d'oxydes de Fe et Ti. D'un autre côté, il serait aussi intéressant de quantifier les coefficients de partage de divers éléments (traces et majeurs) entre l'apatite et les deux liquides immiscibles présent

dans les expérience de Tollari et al., (2006). Ceci permettrait de modéliser l'évolution de ces liquides et de vérifier si il est possible de cristalliser une nelsonite à partir du liquides riche en Fe, Ti et P.

Référence

Barnes, S.-J. and Cox, R.A. 2006. Platinum-group element, gold, silver and base metal distribution in compositionally zoned sulfide droplets from the Medvezky CreekMine, Noril'sk, Russia. Contribution to Mineralogy and Petrology. **152**: 187-200

Bea, F., Fershtater, G., and Corretge, L.G. 1992. The geochemistry of phosphorus in granite rocks and the effect of aluminum. Lithos. **29**: 43-56.

Bedard, J.H. 2001. Parental magmas of the Nain Plutonic Suite anorthosites and mafic cumulates: a trace element modelling approach. Contributions to Mineralogy and Petrology. **141**: 747-771.

Bogaerts, M., and Schmidt, M.W. 2006. Experiments on silicate melt immiscibility in the system Fe_2SiO_4–$KAlSi_3O_8$–SiO_2–CaO–MgO–TiO_2–P_2O_5 and implications for natural magmas. Contribution to Mineralogy and Petrology. **152**: 257–274.

Boudreau, A.E. 1999. PELE - a version of the MELTS software program for the PC platform. Computers & Geosciences. **25**: 201-203.

Cimon, J. 1998. L'unité à apatite de rivière des rapides, Complexe de Sept îles. Localisation stratigraphique et facteurs à l'origine de sa formation. In Proceedings of the 33rd forum on the Geology of industrial minerals--Actes du 33 ème forum sur la Geologie des mineraux industriels Special Volume. Canadian Institute of Mining and Metallurgy, Canada, **50**: 75-96.

Dymek, R.F., and Owens, B.E. 2001. Petrogenesis of apatite-rich rocks (nelsonites and oxide-apatite gabbronorites) associated with massif anorthosites. Economic Geology, **96**: 797-815.

Eales, H.V., and Cawthorn, R.G. 1996. The Bushveld Complex. In Layered Intrusions. Edited by Cawthorn R.G.. Elsevier, Amsterdam. p. 181-229.

Emslie, R.F. 1975. Nature and origin of anorthositic suites. Geoscience Canada. **2**: 99-104.

Fredette, J. 2006. Pétrographie, géochimie et potentiel économique en Fe-Ti-P du secteur de Lac à Paul, Parte Nord de le Suite Anorthositique du Lac-Saint-Jean, Province du Grenville, Québec. Mémoire de maîtrise ès sciences, Université du Québec à Chicoutimi, Chicoutimi.

Goldberg, S.A. 1984. Geochemical relationships between anorthosite and associated iron-rich rocks, Laramie Range, Wyoming. Contributions to Mineralogy and Petrology. **87**: 376-387.

Harmer, R.E., and Sharpe, M.R. 1985. Field relations and strontium isotope systematics of the marginal rocks of the Eastern Bushveld Complex. Economic Geology. **80**: 813-837.

Harrison, T.M., and Watson, E.B. 1984. The behavior of apatite during crustal anatexis - Equilibrium and kinetic considerations. Geochimica et Cosmochimica Acta. **48**: 1467-1477.

Hounsell, V. 2003. Géochimie des dykes mafiques et composés de la suite intrusives de Sept-Îles, Québec. Projet de fin d'études, Université du Québec à Chicoutimi, Chicoutimi.

Jakobsen, J.K., Veksler, I.V., Tegner, C., and Brooks, C.K. 2005. Immiscible iron- and silica-rich melts in basalt petrogenesis documented in the Skaergaard intrusion. Geology. **33**: 885-888.

McLelland, J., Ashwal, L., and Moore, L. 1994. Composition and petrogenesis of oxide-rich, apatite-rich gabbronorites associated with Proterozoic anorthosite massifs -

Examples from the Adirondack Mountains, New-York. Contributions to Mineralogy and Petrology. **116**: 225-238.

Morse, S.A. 1980. Kiglapait mineralogy .2. Fe-Ti oxide minerals and the activities of oxygen and silica. Journal of Petrology. **21**: 685-719.

Naslund, H.R. 1976. Liquid immiscibility in the system KAl-Si3O8-NaAlSi3O8-FeO-Fe2O3 and its applications to natural magmas. Carnegie Institution of Washington, Year Book. **75**: 592-596.

Philpotts, A.R. 1967. Origin of certain iron-titanium oxide and apatite rocks. Economic Geology. **62**: 303-315.

Tegner, C., Cawthorn, R.G., and Kruger, F.J. 2006. Cyclicity in the Main and Upper Zones of the Bushveld Complex, South Africa: crystallization from a Zoned Magma Sheet. Journal of petrology: 1-23.

Tollari, N., Toplis, M.J., and Barnes, S.-J. 2006. Predicting phosphate saturation in silicate magmas: An experimental study of the effects of melt composition and temperature. Geochimica et Cosmochimica Acta. **70**: 1518-1536.

Toplis, M.J., and Dingwell, D.B. 1996. The variable influence of P2O5 on the viscosity of melts of differing alkali/aluminium ratio: Implications for the structural role of phosphorus in silicate melts. Geochimica et Cosmochimica Acta. **60**: 4107-4121.

Toplis, M.J., Dingwell, D.B., and Libourel, G. 1994. The effect of phosphorus on the iron redox ratio, viscosity, and density of an evolved ferro-basalt. Contributions to Mineralogy and Petrology. **117**: 293-304.

Wager, L.R., and Brown, G.M. 1968. Layered igneous rocks. Oliver and Boyd, Edinburgh.

Watson, E.B., and Green, T.H. 1981. Apatite liquid partition-coefficients for the rare-earth elements and strontium. Earth and Planetary Science Letters. **56**: 405-421.

ANNEXES

ANNEXES 1

ANALYSES MICROSONDE DES LIQUIDES RÉSIDUELS

– EXPÉRIENCES DU CHAPITRE 2 -

Annexe 1.1 : expérience 2 – liquides résiduels - 1054°C et 0,1 MPa

sc4b5	%pds oxydes									
échantillon	**SiO_2**	**TiO_2**	**Al_2O_3**	**FeO**	**MgO**	**CaO**	**Na_2O**	**K_2O**	**P_2O_5**	**Total**
sc4b51	47,91	4,71	11,14	14,73	4,75	9,98	2,28	0,53	4,53	100,55
sc4b52	47,55	4,75	11,26	14,92	4,77	9,95	2,26	0,54	4,79	100,79
sc4b53	48,34	4,75	10,84	14,72	4,89	10,05	2,31	0,53	4,66	101,08
sc4b56	47,93	4,48	11,29	14,42	4,58	10,09	1,81	0,55	4,47	99,63
sc4b57	47,56	4,58	11,15	14,53	4,51	10,33	2,20	0,49	4,73	100,07
sc4b58	47,19	4,60	11,32	14,69	4,69	10,30	2,08	0,53	4,63	100,02
sc4b59	47,53	4,52	11,17	14,62	4,64	10,15	1,99	0,51	4,59	99,72
sc4b510	47,28	4,60	11,28	14,54	4,68	10,50	2,01	0,48	4,65	100,02
moyenne	**47,66**	**4,62**	**11,18**	**14,65**	**4,69**	**10,17**	**2,12**	**0,52**	**4,63**	**100,24**
écart-type	**0,38**	**0,10**	**0,15**	**0,15**	**0,12**	**0,19**	**0,18**	**0,02**	**0,10**	
sc4b10										
échantillon	**SiO_2**	**TiO_2**	**Al_2O_3**	**FeO**	**MgO**	**CaO**	**Na_2O**	**K_2O**	**P_2O_5**	**Total**
liquide2										
sc4b1021	38,29	3,23	10,04	15,94	8,62	9,49	1,41	0,18	13,05	100,26
sc4b103	42,17	2,95	11,06	15,09	7,51	9,20	1,64	0,25	10,98	100,85
sc4b104	42,16	3,03	11,38	15,56	7,38	9,05	1,41	0,18	9,98	100,13
sc4b105	39,25	3,08	10,29	16,12	8,23	9,72	1,44	0,21	11,57	99,91
sc4b106	39,20	3,18	10,56	16,10	8,71	9,52	1,33	0,20	11,58	100,38
sc4b107	40,24	3,13	10,79	15,38	8,22	9,50	1,39	0,20	11,07	99,91
sc4b108	40,22	3,08	10,63	16,24	8,44	8,98	1,47	0,20	11,18	100,43
sc4b109	39,50	3,14	10,92	15,87	8,46	9,21	1,54	0,18	11,21	100,02
moyenne	**40,13**	**3,10**	**10,71**	**15,79**	**8,20**	**9,33**	**1,45**	**0,20**	**11,33**	**100,24**
écart-type	**1,40**	**0,09**	**0,43**	**0,41**	**0,49**	**0,26**	**0,10**	**0,02**	**0,86**	
liquide1										
sc4b1025	61,81	1,89	13,34	8,26	3,34	4,72	2,41	0,69	3,20	99,66
sc4b1023	62,44	1,68	13,48	7,95	3,09	4,67	2,33	0,65	3,41	99,69
sc4b1024	62,15	1,79	13,40	7,83	3,21	4,62	2,35	0,68	3,54	99,57
sc4b1022	60,92	1,86	13,26	8,25	3,42	4,91	2,34	0,63	3,80	99,38
sc4b1029	61,06	1,78	13,41	8,36	3,34	4,80	2,44	0,67	3,83	99,67
sc4b1030	57,58	1,97	13,73	8,99	3,99	5,47	2,61	0,55	4,74	99,61
moyenne	**60,99**	**1,83**	**13,44**	**8,27**	**3,40**	**4,86**	**2,41**	**0,64**	**3,75**	**99,60**
écart-type	**1,78**	**0,10**	**0,16**	**0,41**	**0,31**	**0,31**	**0,11**	**0,05**	**0,54**	
sc485										
échantillon	**SiO_2**	**TiO_2**	**Al_2O_3**	**FeO**	**MgO**	**CaO**	**Na_2O**	**K_2O**	**P_2O_5**	**Total**
liquide										
sc4856	67,63	2,79	12,25	5,34	1,69	4,60	2,17	1,06	1,00	98,54
sc4855	67,37	2,72	12,47	5,92	1,65	4,78	2,11	1,11	1,02	99,14
sc48512	67,91	2,84	11,68	6,69	1,68	4,72	2,04	1,05	1,04	99,64
sc4857	66,99	2,81	12,15	6,85	1,78	5,06	2,34	1,04	1,08	100,09
sc48511	65,50	2,96	11,79	8,01	1,93	5,38	2,25	0,92	1,20	99,95
sc48510	66,52	2,84	11,76	7,29	1,71	4,92	2,24	1,00	1,20	99,48
sc4851	66,20	2,98	11,61	7,77	1,80	5,44	2,05	0,99	1,28	100,11
sc4859	64,83	3,16	11,81	7,78	2,01	5,58	2,14	0,97	1,33	99,62
sc4854	66,67	3,00	11,84	7,75	1,94	5,24	2,21	0,97	1,38	101,00

sc4853	65,62	3,06	11,76	7,68	1,81	5,39	1,85	0,98	1,40	99,57
moyenne	**66,52**	**2,92**	**11,91**	**7,11**	**1,80**	**5,11**	**2,14**	**1,01**	**1,19**	**99,71**
écart-type	**1,00**	**0,14**	**0,28**	**0,90**	**0,13**	**0,34**	**0,14**	**0,05**	**0,15**	
Sc4810										
échantillon	**SiO_2**	**TiO_2**	**Al_2O_3**	**FeO**	**MgO**	**CaO**	**Na_2O**	**K_2O**	**P_2O_5**	**Total**
liquide 1										
sc48101	20,82	1,75	3,94	13,06	17,06	14,88	0,67	0,08	28,08	100,34
sc48102	21,62	1,90	4,14	13,36	17,72	13,25	0,82	0,07	27,69	100,56
sc481010	23,17	2,01	4,65	12,73	15,69	16,86	0,81	0,12	26,49	102,53
sc481017	25,47	2,31	4,81	12,70	16,26	13,65	0,93	0,10	24,71	100,93
sc481020	22,95	2,15	4,60	12,48	16,39	14,32	0,89	0,05	26,95	100,78
moyenne	**22,80**	**2,02**	**4,43**	**12,87**	**16,62**	**14,59**	**0,82**	**0,08**	**26,79**	**101,03**
écart-type	**1,77**	**0,22**	**0,37**	**0,34**	**0,78**	**1,42**	**0,10**	**0,03**	**1,31**	
liquide 2										
sc48101	68,96	0,89	12,77	3,83	4,56	2,90	1,32	1,15	1,78	98,16
sc48103	70,42	1,04	11,69	4,66	2,83	3,16	0,74	1,23	2,84	98,60
sc48107	71,07	1,11	11,82	4,54	2,49	2,77	0,86	1,22	1,96	97,84
moyenne	**70,15**	**1,01**	**12,09**	**4,34**	**3,29**	**2,95**	**0,97**	**1,20**	**2,19**	**98,20**
écart-type	**1,08**	**0,12**	**0,59**	**0,45**	**1,11**	**0,20**	**0,31**	**0,04**	**0,56**	

Annexe 1.2 : expérience 3 – liquides résiduels - 1075°C et 0,1 MPa

sc4b5 %pds oxydes										
échantillon	**SiO_2**	**TiO_2**	**Al_2O_3**	**FeO**	**MgO**	**CaO**	**Na_2O**	**K_2O**	**P_2O_5**	**Total**
liquide										
sc4b55	46,94	4,68	10,88	15,52	5,62	9,89	2,18	0,49	4,30	100,49
sc4b56	46,53	4,87	10,78	15,33	4,77	10,11	2,08	0,52	4,43	99,41
sc4b57	46,48	4,88	10,89	15,40	4,47	10,16	2,08	0,51	4,35	99,22
moyenne	**46,65**	**4,81**	**10,85**	**15,42**	**4,95**	**10,05**	**2,12**	**0,51**	**4,36**	**99,71**
écart-type	**0,25**	**0,11**	**0,06**	**0,09**	**0,60**	**0,14**	**0,06**	**0,02**	**0,07**	
sc4b10										
échantillon	**SiO_2**	**TiO_2**	**Al_2O_3**	**FeO**	**MgO**	**CaO**	**Na_2O**	**K_2O**	**P_2O_5**	**Total**
liquide1										
sc4b1016	17,47	2,13	4,11	11,66	18,05	15,59	0,61	0,09	29,81	99,53
sc4b1017	17,79	2,00	4,04	12,44	18,75	14,11	0,67	0,07	28,93	98,80
sc4b1018	17,96	1,99	4,15	12,15	17,56	15,10	0,79	0,11	29,06	98,88
sc4b1019	17,43	2,09	3,95	12,54	17,75	14,69	1,01	0,14	29,99	99,59
sc4b1020	16,78	1,84	4,04	10,98	17,96	16,02	0,88	0,06	31,00	99,57
sc4b1021	16,98	2,05	3,99	12,27	17,73	14,87	0,75	0,09	30,35	99,07
sc4b1022	18,07	2,01	4,40	11,74	17,31	15,30	0,79	0,09	29,29	99,00
sc4b1023	17,68	2,12	4,19	12,58	17,36	15,08	0,94	0,09	29,79	99,83
moyenne	**17,52**	**2,03**	**4,11**	**12,04**	**17,81**	**15,10**	**0,81**	**0,09**	**29,78**	**99,28**
écart-type	**0,45**	**0,09**	**0,14**	**0,55**	**0,46**	**0,58**	**0,13**	**0,03**	**0,69**	
liquide2										
sc4b1029	67,30	1,02	12,59	4,17	1,95	2,45	0,84	1,58	1,45	93,34
sc4b1032	67,94	1,04	12,76	4,04	2,06	2,58	0,91	1,52	1,56	94,41
sc4b1034	68,00	1,07	12,53	4,15	2,08	2,37	0,77	1,39	1,47	93,83
moyenne	**67,75**	**1,05**	**12,63**	**4,12**	**2,03**	**2,47**	**0,84**	**1,49**	**1,49**	**93,86**
écart-type	**0,39**	**0,03**	**0,12**	**0,07**	**0,07**	**0,11**	**0,07**	**0,10**	**0,06**	
sc485										
échantillon	**SiO_2**	**TiO_2**	**Al_2O_3**	**FeO**	**MgO**	**CaO**	**Na_2O**	**K_2O**	**P_2O_5**	**Total**
liquide										
sc48514	59,48	2,78	11,64	8,30	2,29	5,91	2,37	0,86	1,40	95,03
sc48515	61,53	2,54	11,66	7,87	2,15	5,37	2,18	0,88	1,34	95,51
sc48516	61,79	2,53	11,87	7,69	2,09	5,26	2,21	1,01	1,22	95,66
sc48517	57,84	2,91	11,81	8,91	2,49	6,02	2,04	0,80	1,58	94,40
sc48518	58,49	2,81	11,69	8,36	2,44	6,21	2,06	0,83	1,75	94,64
sc48519	59,21	2,77	11,75	8,39	2,45	6,22	1,21	0,85	1,84	94,68
sc48520	60,03	2,66	11,71	8,00	2,31	5,58	2,19	0,87	1,31	94,65
sc48521	61,64	2,53	11,75	7,48	2,06	5,10	2,24	0,96	1,11	94,86
moyenne	**60,00**	**2,69**	**11,73**	**8,13**	**2,28**	**5,71**	**2,06**	**0,88**	**1,44**	**94,93**
écart-type	**1,51**	**0,15**	**0,08**	**0,46**	**0,17**	**0,44**	**0,36**	**0,07**	**0,26**	
sc4810										
échantillon	**SiO_2**	**TiO_2**	**Al_2O_3**	**FeO**	**MgO**	**CaO**	**Na_2O**	**K_2O**	**P_2O_5**	**Total**
liquide1										
sc481013	21,99	1,23	4,94	10,68	20,16	12,11	0,86	0,07	25,91	97,95
sc481014	21,76	1,68	4,83	11,14	20,01	12,73	0,76	0,10	25,26	98,26
sc481015	22,77	1,63	4,85	10,62	19,87	12,21	0,85	0,08	25,46	98,33
sc481016	22,46	1,96	4,56	10,49	17,59	14,01	0,81	0,07	25,65	97,59

sc481017	20,94	1,71	4,27	11,18	18,63	15,02	0,82	0,07	26,03	98,66
sc481018	21,35	1,94	4,30	10,48	18,25	14,63	0,89	0,07	26,66	98,57
sc481020	21,01	1,81	4,56	10,73	17,03	14,50	0,70	0,10	26,08	96,52
moyenne	**21,75**	**1,71**	**4,62**	**10,76**	**18,79**	**13,60**	**0,81**	**0,08**	**25,86**	**97,98**
écart-type	**0,70**	**0,24**	**0,27**	**0,29**	**1,25**	**1,22**	**0,07**	**0,01**	**0,46**	
liquide2										
sc481022	68,40	0,98	12,37	3,72	2,01	2,41	2,89	1,32	1,41	95,51
sc481023	67,64	1,01	12,61	3,84	2,54	2,71	2,05	1,28	1,58	95,26
sc481025	67,54	1,02	12,25	3,88	2,75	2,97	1,92	1,30	2,01	95,63
sc481026	67,00	1,14	12,32	4,25	2,68	2,95	2,46	1,21	1,95	95,95
sc481027	67,25	1,05	12,56	3,87	2,70	2,98	2,19	1,23	2,01	95,83
sc481028	68,83	1,00	12,49	3,88	2,47	2,67	2,29	1,27	1,46	96,35
moyenne	**67,78**	**1,03**	**12,44**	**3,91**	**2,52**	**2,78**	**2,30**	**1,27**	**1,74**	**95,76**
écart-type	**0,70**	**0,06**	**0,14**	**0,18**	**0,27**	**0,23**	**0,34**	**0,04**	**0,28**	

Annexe 1.3 : expérience 4 – liquides résiduels - 1056°C et 0,1 MPa

sc4b5	%pds oxydes									
échantillon	**SiO_2**	**TiO_2**	**Al_2O_3**	**FeO**	**MgO**	**CaO**	**Na_2O**	**K_2O**	**P_2O_5**	**Total**
liquide										
sc4b511	49,32	4,45	11,51	15,33	4,40	9,24	2,17	0,68	3,83	100,91
sc4b512	49,76	4,30	11,54	15,13	4,34	8,97	2,20	0,67	3,43	100,34
sc4b513	49,96	4,33	11,31	15,12	4,40	8,95	2,18	0,64	3,60	100,48
sc4b514	50,55	4,24	11,53	14,31	4,30	9,13	2,22	0,66	3,33	100,26
sc4b515	49,22	4,19	11,46	15,13	4,48	9,28	2,09	0,61	3,78	100,23
sc4b516	49,22	4,60	10,89	15,19	4,44	9,32	2,21	0,65	3,80	100,30
sc4b517	47,65	4,65	10,34	16,35	4,50	9,70	1,98	0,58	4,28	100,04
sc4b518	47,52	4,58	10,67	16,36	4,38	9,83	1,94	0,55	4,45	100,26
sc4b519	50,71	4,30	10,98	14,95	3,90	8,95	2,09	0,67	3,55	100,10
sc4b57	45,86	4,19	10,58	16,39	4,08	8,95	1,83	0,65	3,96	96,49
moyenne	**48,98**	**4,38**	**11,08**	**15,43**	**4,32**	**9,23**	**2,09**	**0,64**	**3,80**	**99,94**
écart-type	**1,53**	**0,18**	**0,45**	**0,70**	**0,19**	**0,32**	**0,13**	**0,04**	**0,36**	
sc4b10										
échantillon	**SiO_2**	**TiO_2**	**Al_2O_3**	**FeO**	**MgO**	**CaO**	**Na_2O**	**K_2O**	**P_2O_5**	**Total**
liquide1										
sc4b107	34,64	3,81	7,77	20,56	8,37	10,07	1,29	0,20	12,96	99,66
sc4b108	34,67	3,73	7,79	20,69	7,97	10,27	1,24	0,25	12,84	99,43
sc4b109	34,96	3,81	8,01	20,54	8,30	10,31	1,25	0,25	12,78	100,20
sc4b1010	34,84	3,77	8,02	20,36	8,39	10,21	1,33	0,22	13,03	100,16
sc4b1011	34,19	3,80	7,78	21,02	8,53	10,30	1,27	0,18	13,46	100,52
sc4b1012	34,09	3,76	7,63	20,80	8,38	10,33	1,25	0,22	13,35	99,81
sc4b1013	34,03	3,85	7,81	20,43	8,51	10,53	1,31	0,21	13,05	99,74
sc4b1014	33,65	3,77	7,61	20,22	8,68	10,43	1,24	0,19	13,83	99,61
moyenne	**34,38**	**3,79**	**7,80**	**20,58**	**8,39**	**10,31**	**1,27**	**0,21**	**13,16**	**99,89**
écart-type	**0,46**	**0,04**	**0,15**	**0,25**	**0,21**	**0,14**	**0,04**	**0,03**	**0,36**	
liquide2										
sc4b1015	61,94	1,94	13,30	8,93	2,84	4,36	1,47	1,29	2,84	98,91
sc4b1016	61,61	1,93	13,32	9,12	1,92	4,33	1,49	1,27	2,89	97,89
sc4b1017	61,20	2,00	13,57	9,42	2,84	4,46	1,57	1,31	3,16	99,53
sc4b1018	59,05	2,05	13,32	10,06	2,60	4,85	1,61	1,18	3,71	98,41
sc4b1019	59,66	2,03	13,15	10,01	3,19	4,65	1,39	1,16	3,38	98,62
sc4b1020	62,07	1,91	13,15	9,35	2,35	4,28	1,57	1,32	2,84	98,84
sc4b1021	63,13	1,86	13,52	8,63	2,64	4,19	1,54	1,29	2,84	99,63
sc4b1022	61,12	1,97	13,55	9,16	2,50	4,51	1,50	1,23	3,07	98,60
moyenne	**61,22**	**1,96**	**13,36**	**9,33**	**2,61**	**4,45**	**1,52**	**1,26**	**3,09**	**98,80**
écart-type	**1,32**	**0,06**	**0,17**	**0,50**	**0,38**	**0,22**	**0,07**	**0,06**	**0,31**	
sc485										
échantillon	**SiO_2**	**TiO_2**	**Al_2O_3**	**FeO**	**MgO**	**CaO**	**Na_2O**	**K_2O**	**P_2O_5**	**Total**
liquide										
sc48525	67,67	1,74	11,75	5,44	1,02	3,20	1,81	1,47	0,54	94,63
sc48526	68,23	1,64	11,86	5,15	0,96	3,12	1,67	1,42	0,40	94,46
sc48527	68,14	1,72	11,54	5,44	1,00	3,08	1,67	1,59	0,52	94,70
sc48528	65,98	1,78	11,75	6,66	1,21	3,74	1,61	1,47	0,60	94,80
sc48521	68,74	1,75	11,61	5,29	0,93	3,05	2,00	1,49	0,58	95,44

sc48522	69,09	1,63	11,55	5,32	0,93	2,99	1,59	1,48	0,58	95,16
sc48523	70,06	1,66	11,28	4,95	0,91	2,84	1,77	1,57	0,43	95,46
moyenne	**68,27**	**1,70**	**11,62**	**5,47**	**0,99**	**3,14**	**1,73**	**1,50**	**0,52**	**94,95**
écart-type	**1,27**	**0,06**	**0,19**	**0,56**	**0,10**	**0,28**	**0,14**	**0,06**	**0,08**	

sc4810

échantillon	**SiO_2**	**TiO_2**	**Al_2O_3**	**FeO**	**MgO**	**CaO**	**Na_2O**	**K_2O**	**P_2O_5**	**Total**
liquide2										
sc481026	68,83	1,42	11,46	3,75	1,12	1,82	1,13	1,50	1,59	92,60
sc481027	66,61	0,98	15,06	3,66	1,09	3,36	1,75	1,29	1,38	95,18
sc481028	68,19	1,03	12,63	3,77	1,03	1,98	0,94	1,40	1,26	92,24
sc48104	69,27	0,96	11,79	3,48	1,29	1,83	0,72	1,37	1,74	92,45
moyenne	**68,22**	**1,10**	**12,74**	**3,66**	**1,13**	**2,25**	**1,14**	**1,39**	**1,49**	**93,12**
écart-type	**1,17**	**0,22**	**1,63**	**0,13**	**0,11**	**0,75**	**0,44**	**0,09**	**0,21**	
liquide3										
sc481033	13,17	2,06	3,51	15,87	14,32	15,87	0,80	0,07	33,37	99,03
sc481034	15,76	1,65	3,57	16,85	15,07	14,87	0,66	0,08	30,52	99,01
sc481036	13,58	1,53	2,99	17,24	17,83	12,88	0,66	0,09	32,85	99,64
moyenne	**14,17**	**1,75**	**3,36**	**16,65**	**15,74**	**14,54**	**0,71**	**0,08**	**32,25**	**99,23**
écart-type	**1,39**	**0,28**	**0,32**	**0,71**	**1,85**	**1,52**	**0,08**	**0,01**	**1,52**	

Annexe 1.4 : expérience 5 – liquides résiduels - 1056°C et 0,1 MPa

sc4b5	%pds oxydes									
échantillon	**SiO_2**	**TiO_2**	**Al_2O_3**	**FeO**	**MgO**	**CaO**	**Na_2O**	**K_2O**	**$P2O_5$**	**Total**
liquide										
sc4b526	63,66	1,29	10,80	4,80	0,85	2,86	0,33	1,74	0,65	86,97
sc4b527	63,71	1,07	13,64	4,63	0,80	4,04	0,98	1,67	0,49	91,04
sc4b528	65,34	1,27	11,68	5,25	1,01	2,91	0,78	2,01	0,50	90,72
sc4b529	66,52	1,28	11,47	5,03	1,00	2,83	0,75	2,03	0,46	91,36
sc4b531	66,22	1,30	11,14	4,95	0,91	2,67	0,72	1,99	0,43	90,33
moyenne	**65,09**	**1,24**	**11,75**	**4,93**	**0,91**	**3,06**	**0,71**	**1,89**	**0,51**	**90,09**
écart-type	**1,35**	**0,10**	**1,11**	**0,23**	**0,09**	**0,56**	**0,24**	**0,17**	**0,08**	
sc4b10										
échantillon	**SiO_2**	**TiO_2**	**Al_2O_3**	**FeO**	**MgO**	**CaO**	**Na_2O**	**K_2O**	**P_2O_5**	**Total**
liquide 1										
sc4b1019	72,29	0,78	12,69	3,89	1,69	2,10	0,84	2,01	1,27	97,56
sc4b1020	72,09	0,78	12,79	3,61	1,58	2,04	1,04	2,01	1,07	97,02
sc4b1021	72,00	0,77	12,69	3,97	1,60	1,97	0,77	2,00	0,93	96,72
sc4b1022	71,75	0,71	13,40	3,96	1,49	2,34	1,06	1,91	1,01	97,63
sc4b1023	72,63	0,73	12,76	3,96	1,47	1,78	0,88	2,03	0,97	97,21
sc4b1025	72,11	0,73	12,87	4,05	1,58	2,00	0,88	1,82	1,05	97,08
moyenne	**72,15**	**0,75**	**12,87**	**3,91**	**1,57**	**2,04**	**0,91**	**1,96**	**1,05**	**97,20**
écart-type	**0,30**	**0,03**	**0,27**	**0,16**	**0,08**	**0,18**	**0,11**	**0,08**	**0,12**	
liquide2										
sc4b1028	19,13	1,74	4,05	14,43	15,29	14,64	0,73	0,16	26,39	96,56
sc4b1029	18,53	1,61	3,83	13,51	15,54	15,73	0,72	0,13	27,31	96,91
sc4b1030	18,03	1,49	4,20	13,66	15,60	15,52	0,86	0,12	27,23	96,69
sc4b1031	18,33	1,56	3,92	14,97	16,18	13,99	0,86	0,14	27,21	97,15
sc4b1032	18,41	1,57	3,91	14,32	16,05	15,17	0,79	0,08	27,46	97,77
moyenne	**18,49**	**1,59**	**3,98**	**14,18**	**15,73**	**15,01**	**0,79**	**0,12**	**27,12**	**97,01**
écart-type	**0,41**	**0,09**	**0,14**	**0,60**	**0,37**	**0,70**	**0,07**	**0,03**	**0,42**	
sc485										
échantillon	**SiO_2**	**TiO_2**	**Al_2O_3**	**FeO**	**MgO**	**CaO**	**Na_2O**	**K_2O**	**P_2O_5**	**Total**
liquide										
sc48516	73,41	2,01	12,31	2,17	0,72	1,73	0,24	1,15	0,46	94,18
sc48518	75,00	1,28	11,48	2,66	0,77	1,92	0,47	1,26	0,37	95,21
moyenne	**74,21**	**1,64**	**11,90**	**2,41**	**0,75**	**1,83**	**0,35**	**1,20**	**0,41**	**94,70**
écart-type	**1,13**	**0,51**	**0,59**	**0,35**	**0,04**	**0,14**	**0,16**	**0,08**	**0,06**	
sc4810										
échantillon	**SiO_2**	**TiO_2**	**Al_2O_3**	**FeO**	**MgO**	**CaO**	**Na_2O**	**K_2O**	**P_2O_5**	**Total**
liquide1										
sc481018	7,02	0,66	1,43	13,53	18,11	17,15	0,91	0,05	39,56	98,41
sc481027	6,22	1,85	1,24	12,34	17,05	18,76	0,64	0,05	37,91	96,04
sc481029	6,90	1,25	1,20	13,08	17,99	17,63	0,81	0,04	38,10	97,01
moyenne	**6,71**	**1,26**	**1,29**	**12,98**	**17,72**	**17,85**	**0,79**	**0,04**	**38,52**	**97,15**
écart-type	**0,43**	**0,59**	**0,12**	**0,60**	**0,58**	**0,83**	**0,14**	**0,01**	**0,90**	
liquide 2										
sc481020	71,35	1,07	13,56	3,08	1,39	2,71	1,08	1,32	2,13	97,69
sc481023	72,56	0,92	12,55	3,19	1,42	2,02	1,04	1,47	2,10	97,28

sc481025	72,87	0,85	12,72	3,07	1,31	2,43	1,16	1,42	1,86	97,68
moyenne	**72,26**	**0,95**	**12,94**	**3,11**	**1,37**	**2,39**	**1,09**	**1,40**	**2,03**	**97,55**
écart-type	**0,81**	**0,11**	**0,54**	**0,07**	**0,06**	**0,34**	**0,06**	**0,07**	**0,15**	

Annexe 1.5 : expérience 6 – liquides résiduels - 1055°C et 0,1 MPa

sc4b5 %pds oxydes										
échantillon	**SiO_2**	**TiO_2**	**Al_2O_3**	**FeO**	**MgO**	**CaO**	**Na_2O**	**K_2O**	**P_2O_5**	**Total**
liquide										
sc4b53	50,91	3,59	10,87	16,64	3,01	8,61	2,16	0,80	3,10	99,69
sc4b54	50,39	3,70	11,07	16,83	2,88	8,79	1,95	0,77	3,13	99,49
sc4b55	49,79	3,77	10,73	17,41	3,06	9,05	1,81	0,69	3,31	99,61
sc4b56	49,56	3,91	9,88	17,76	3,07	8,95	2,07	0,68	3,47	99,35
sc4b57	51,63	3,53	10,16	16,83	2,88	8,59	1,94	0,81	3,00	99,36
sc4b58	50,46	3,62	9,98	17,77	2,84	8,74	1,91	0,78	3,01	99,11
sc4b59	52,42	3,50	10,55	16,15	2,57	8,27	1,87	0,83	2,76	98,91
sc4b510	52,94	3,35	10,83	16,19	2,58	8,23	1,88	0,79	2,74	99,52
moyenne	**51,01**	**3,62**	**10,51**	**16,95**	**2,86**	**8,65**	**1,95**	**0,77**	**3,06**	**99,38**
écart-type	**1,22**	**0,17**	**0,45**	**0,64**	**0,20**	**0,30**	**0,12**	**0,06**	**0,25**	
sc4b10										
échantillon	**SiO_2**	**TiO_2**	**Al_2O_3**	**FeO**	**MgO**	**CaO**	**Na_2O**	**K_2O**	**P_2O_5**	**Total**
liquide										
sc4b1014	69,00	1,45	12,75	6,42	1,71	2,57	0,91	1,74	1,51	98,07
sc4b1015	69,50	1,47	12,77	6,47	1,72	2,67	0,97	1,70	1,48	98,76
sc4b1016	70,05	1,35	12,78	5,93	1,48	2,51	0,87	1,80	1,33	98,11
sc4b1017	70,27	1,36	13,08	6,27	1,49	2,44	1,18	1,88	1,35	99,32
sc4b1018	68,67	1,50	12,49	6,26	1,51	2,62	0,97	1,68	1,67	97,36
sc4b1019	67,72	1,19	15,48	5,63	1,32	4,17	1,59	1,44	1,26	99,81
sc4b1020	69,16	1,39	13,04	6,20	1,50	2,51	1,04	1,71	1,49	98,03
moyenne	**69,19**	**1,39**	**13,20**	**6,17**	**1,53**	**2,79**	**1,08**	**1,71**	**1,44**	**98,49**
écart-type	**0,86**	**0,10**	**1,03**	**0,29**	**0,14**	**0,61**	**0,25**	**0,14**	**0,14**	
sc485										
échantillon	**SiO_2**	**TiO_2**	**Al_2O_3**	**FeO**	**MgO**	**CaO**	**Na_2O**	**K_2O**	**P_2O_5**	**Total**
liquide										
sc48510	70,79	2,17	11,64	5,46	0,86	3,47	0,81	1,19	0,53	96,90
sc48511	70,99	2,17	11,63	5,43	1,01	3,59	0,89	1,22	0,78	97,72
sc48512	71,46	2,06	12,15	5,32	0,94	3,43	0,98	1,22	0,54	98,11
sc48513	71,90	2,12	11,60	4,80	0,92	3,50	0,81	1,28	0,90	97,82
moyenne	**71,28**	**2,13**	**11,75**	**5,25**	**0,93**	**3,50**	**0,87**	**1,23**	**0,69**	**97,64**
écart-type	**0,49**	**0,05**	**0,27**	**0,31**	**0,06**	**0,07**	**0,08**	**0,04**	**0,18**	
sc4810										
échantillon	**SiO_2**	**TiO_2**	**Al_2O_3**	**FeO**	**MgO**	**CaO**	**Na_2O**	**K_2O**	**P_2O_5**	**Total**
liquide										
sc481025	70,72	0,90	12,01	3,40	1,39	2,03	0,85	1,32	2,29	94,90
sc481026	72,64	1,09	13,34	3,40	0,97	2,26	1,87	1,39	1,26	98,20
sc481027	70,89	0,87	14,87	2,86	0,95	3,46	1,59	1,17	1,40	98,07
sc481028	72,83	0,92	11,95	3,08	1,00	1,57	0,79	1,48	1,28	94,92
sc481029	72,07	0,88	12,97	3,46	1,30	2,37	1,00	1,34	1,96	97,33
sc481030	71,22	1,03	12,64	3,04	1,14	1,96	1,11	1,40	1,57	95,11
moyenne	**71,73**	**0,95**	**12,96**	**3,21**	**1,12**	**2,27**	**1,20**	**1,35**	**1,63**	**96,42**
écart-type	**0,91**	**0,09**	**1,08**	**0,24**	**0,18**	**0,64**	**0,43**	**0,11**	**0,41**	

Annexe 1.6 : expérience 7 – liquides résiduels - 1032°C et 0,1 MPa

sc4b5 %pds oxydes										
échantillon	**SiO_2**	**TiO_2**	**Al_2O_3**	**FeO**	**MgO**	**CaO**	**Na_2O**	**K_2O**	**P_2O_5**	**Total**
liquide										
sc4b55	64,59	1,50	11,18	11,40	0,88	4,87	1,37	1,90	1,00	98,69
sc4b56	66,47	1,40	11,47	9,61	0,77	4,09	1,36	2,02	0,73	97,92
sc4b58	67,28	1,40	11,64	9,28	0,74	3,87	1,34	2,02	0,68	98,25
sc4b515	69,41	1,36	11,56	7,42	0,67	3,20	0,98	2,06	0,45	97,10
sc4b516	69,40	1,33	11,80	7,66	0,71	3,40	1,00	2,09	0,51	97,90
sc4b517	66,08	1,57	11,10	9,89	0,85	4,46	1,39	1,86	0,85	98,04
moyenne	**67,20**	**1,43**	**11,46**	**9,21**	**0,77**	**3,98**	**1,24**	**1,99**	**0,70**	**97,98**
écart-type	**1,92**	**0,09**	**0,27**	**1,49**	**0,08**	**0,63**	**0,19**	**0,09**	**0,21**	
sc4b10										
échantillon	**SiO_2**	**TiO_2**	**Al_2O_3**	**FeO**	**MgO**	**CaO**	**Na_2O**	**K_2O**	**P_2O_5**	**Total**
liquide1										
sc4b107	12,20	2,48	2,96	22,91	11,71	14,91	0,42	0,10	31,72	99,41
sc4b1012	12,77	2,27	3,34	23,41	10,94	14,13	0,74	0,18	31,18	98,95
sc4b1015	13,72	2,79	2,81	23,33	10,50	13,84	0,63	0,13	30,14	97,89
sc4b1016	11,74	1,40	3,05	22,56	11,52	14,75	0,60	0,15	32,84	98,61
sc4b1017	13,47	1,94	3,35	22,10	11,03	14,84	0,71	0,16	30,78	98,38
moyenne	**12,78**	**2,17**	**3,10**	**22,86**	**11,14**	**14,50**	**0,62**	**0,14**	**31,33**	**98,65**
écart-type	**0,83**	**0,53**	**0,24**	**0,55**	**0,48**	**0,48**	**0,12**	**0,03**	**1,02**	
liquide2										
sc4b1022	73,19	0,91	12,79	4,06	0,75	1,29	0,70	2,60	1,14	97,43
sc4b1023	71,46	1,13	13,12	4,80	0,88	1,58	0,73	2,54	1,26	97,49
sc4b1024	68,95	1,10	12,38	4,32	0,76	1,37	0,70	2,49	1,05	93,12
sc4b1027	71,38	0,96	12,84	4,14	0,83	1,54	0,85	2,45	1,32	96,29
sc4b1028	72,92	0,93	12,73	4,21	0,82	1,52	0,82	2,47	1,44	97,86
sc4b1029	72,88	0,99	12,89	4,46	0,74	1,32	0,80	2,68	1,11	97,86
sc4b1030	72,24	0,96	13,18	4,25	0,72	1,36	0,70	2,58	1,19	97,18
moyenne	**71,86**	**0,99**	**12,85**	**4,32**	**0,78**	**1,43**	**0,76**	**2,54**	**1,22**	**96,75**
écart-type	**1,47**	**0,09**	**0,27**	**0,25**	**0,06**	**0,12**	**0,06**	**0,08**	**0,13**	
sc485										
échantillon	**SiO_2**	**TiO_2**	**Al_2O_3**	**FeO**	**MgO**	**CaO**	**Na_2O**	**K_2O**	**P_2O_5**	**Total**
liquide										
sc48517	73,10	2,59	11,75	0,51	0,49	2,20	0,44	1,46	1,47	94,02
sc4810										
échantillon	**SiO_2**	**TiO_2**	**Al_2O_3**	**FeO**	**MgO**	**CaO**	**Na_2O**	**K_2O**	**P_2O_5**	**Total**
liquide1										
sc481022	19,99	1,06	4,38	11,56	13,89	16,73	1,13	0,39	33,46	102,58
sc481024	15,31	1,26	4,62	12,63	14,67	17,63	1,56	0,22	34,36	102,26
moyenne	**17,65**	**1,16**	**4,50**	**12,10**	**14,28**	**17,18**	**1,34**	**0,31**	**33,91**	**102,42**
écart-type	**3,31**	**0,15**	**0,17**	**0,76**	**0,55**	**0,63**	**0,31**	**0,12**	**0,63**	
liquide2										
sc481025	73,06	0,83	12,71	2,45	0,94	1,73	1,29	1,86	1,50	96,37
sc481026	71,82	0,83	11,41	2,68	1,65	1,77	0,98	1,96	2,42	95,52
sc481029	71,80	0,75	12,65	2,42	1,07	2,23	1,14	1,86	2,02	95,93
moyenne	**72,23**	**0,80**	**12,26**	**2,52**	**1,22**	**1,91**	**1,14**	**1,89**	**1,98**	**95,94**

écart-type	**0,72**	**0,05**	**0,74**	**0,14**	**0,38**	**0,28**	**0,16**	**0,06**	**0,46**

ANNEXES 2

ANALYSES MICROSONDE DES LIQUIDES RÉSIDUELS

– EXPÉRIENCES DU CHAPITRE 3 -

Annexe 2.1 : expérience McGill 7 – 1000°C et 500 MPa – composition SC4-b avec 5% P_2O_5

McGill 7	%pds oxydes										
échantillon	**SiO_2**	**TiO_2**	**Al_2O_3**	**FeO**	**MgO**	**CaO**	**Na_2O**	**K_2O**	**P_2O_5**	**F**	**Total**
verre 9	54,65	1,50	11,58	18,05	0,88	5,26	2,33	1,42	1,40	0,06	97,12
verre 10	54,22	1,70	11,38	17,71	0,98	5,41	2,37	1,44	1,64	0,08	96,91
verre 11	61,91	1,13	12,67	11,98	0,65	3,71	2,18	1,94	0,83	0,00	97,00
verre 12	55,39	1,43	11,77	17,11	0,84	5,10	2,20	1,46	1,32	0,00	96,60
verre 13	54,82	1,51	11,77	17,23	0,88	5,28	2,27	1,46	1,41	0,06	96,67
verre 14	54,35	1,52	11,89	17,41	0,89	5,36	2,43	1,43	1,53	0,00	96,81
verre 15	56,01	1,44	11,70	16,79	0,81	5,00	2,26	1,50	1,28	0,00	96,79
verre 16	55,99	1,35	11,91	16,62	0,75	4,89	2,18	1,52	1,25	0,01	96,46
verre 17	55,84	1,37	12,01	16,15	0,77	4,85	2,19	1,55	1,26	0,00	95,99
verre 18	56,70	1,36	12,05	15,77	0,74	4,72	2,16	1,59	1,21	0,03	96,33
moyenne	**55,99**	**1,43**	**11,87**	**16,48**	**0,82**	**4,96**	**2,26**	**1,53**	**1,31**	**0,02**	**96,67**
écart-type	**2,24**	**0,15**	**0,34**	**1,73**	**0,10**	**0,50**	**0,09**	**0,16**	**0,22**	**0,03**	

Annexe 2.2 : expérience McGill 8 – 1015°C et 500 MPa – composition SC4-b avec 5% P_2O_5

McGill 8	%pds oxydes										
échantillon	**SiO_2**	**TiO_2**	**Al_2O_3**	**FeO**	**MgO**	**CaO**	**Na_2O**	**K_2O**	**P_2O_5**	**F**	**Total**
verre 2	69,31	0,84	11,60	8,11	0,25	1,90	1,20	2,92	0,43	0,01	96,57
verre 3	68,62	0,84	11,90	8,15	0,24	1,87	1,19	2,98	0,38	0,00	96,16
verre 4	68,85	0,76	12,40	8,00	0,23	1,79	1,37	3,25	0,41	0,01	97,07
verre 5	69,54	0,68	12,19	7,30	0,20	1,64	1,13	3,03	0,39	0,00	96,10
moyenne	**69,08**	**0,78**	**12,02**	**7,89**	**0,23**	**1,80**	**1,22**	**3,05**	**0,40**	**0,01**	**96,48**
écart-type	**0,42**	**0,08**	**0,35**	**0,40**	**0,02**	**0,12**	**0,10**	**0,15**	**0,02**	**0,01**	

Annexe 2.3 : expérience McGill 9 – 1040°C et 500 MPa – composition SC4-b avec 5% P_2O_5

McGill 9	%pds oxydes										
échantillon	**SiO_2**	**TiO_2**	**Al_2O_3**	**FeO**	**MgO**	**CaO**	**Na_2O**	**K_2O**	**P_2O_5**	**F**	**Total**
verre 11	58,60	5,15	14,30	0,03	4,79	7,80	5,10	0,29	1,77	0,00	97,82
verre 12	58,81	5,21	14,28	0,05	4,95	7,81	5,19	0,28	1,85	0,00	98,43
verre 13	58,45	5,30	14,30	0,01	4,94	7,85	5,14	0,29	1,75	0,09	98,11
verre 14	58,93	5,13	14,28	0,09	4,70	7,65	5,26	0,29	1,82	0,00	98,13
verre 15	58,70	4,89	14,50	0,06	4,66	7,42	5,37	0,27	1,79	0,00	97,66
verre 16	59,45	5,06	14,35	0,09	4,56	7,37	5,28	0,30	1,82	0,00	98,28
verre 17	59,82	4,90	14,38	0,04	4,45	7,28	5,18	0,30	1,83	0,01	98,19
verre 18	59,02	5,28	14,24	0,00	4,80	7,63	5,23	0,30	1,83	0,03	98,36
verre 19	58,77	5,09	14,26	0,09	4,78	7,71	5,29	0,30	1,79	0,00	98,09
verre 20	58,86	5,18	14,35	0,11	4,77	7,74	5,18	0,27	1,77	0,01	98,23
moyenne	**58,94**	**5,12**	**14,32**	**0,06**	**4,74**	**7,62**	**5,22**	**0,29**	**1,80**	**0,01**	**98,13**
écart-type	**0,41**	**0,14**	**0,08**	**0,04**	**0,15**	**0,20**	**0,08**	**0,01**	**0,03**	**0,03**	

Annexe 2.4 : expérience McGill 10 – 1015°C et 500 MPa – composition SC4-b avec 5% P_2O_5 + F

McGill 10	%pds oxydes										
Échantillon	**SiO_2**	**TiO_2**	**Al_2O_3**	**FeO**	**MgO**	**CaO**	**Na_2O**	**K_2O**	**P_2O_5**	**F**	**Total**
verre 39	57,34	1,33	16,82	10,02	1,28	8,32	1,97	0,60	0,46	1,98	100,10
verre 40	56,84	1,56	16,68	10,45	1,32	8,43	2,00	0,58	0,52	1,75	100,12
verre 41	56,41	1,42	16,59	10,35	1,36	8,56	1,92	0,58	0,72	1,56	99,47
verre 42	55,68	1,42	16,60	10,31	1,35	8,66	2,02	0,56	0,83	1,69	99,13
verre 43	57,53	1,24	16,62	10,02	1,31	8,23	2,00	0,63	0,62	1,69	99,88
verre 44	57,55	1,18	17,24	9,80	1,29	8,20	2,13	0,62	0,54	1,55	100,10
verre 45	56,77	1,19	17,00	9,54	1,29	8,42	2,04	0,62	0,59	1,69	99,14
verre 46	56,81	1,13	17,23	10,13	1,25	8,30	2,05	0,61	0,68	1,66	99,84
verre 47	57,22	1,15	17,27	10,16	1,29	8,35	2,06	0,59	0,54	0,57	99,20
verre 48	56,43	1,23	17,20	10,10	1,36	8,59	2,08	0,59	0,83	1,77	100,17
Moyenne	**56,86**	**1,28**	**16,92**	**10,09**	**1,31**	**8,41**	**2,03**	**0,60**	**0,63**	**1,59**	**99,71**
écart-type	**0,58**	**0,14**	**0,29**	**0,27**	**0,04**	**0,16**	**0,06**	**0,02**	**0,13**	**0,38**	

Annexe 2.5 : expérience McGill 11 – 1040°C et 500 MPa – composition SC4-b avec 5% P_2O_5 + F

McGill 11	%pds oxydes										
échantillon	**SiO_2**	**TiO_2**	**Al_2O_3**	**FeO**	**MgO**	**CaO**	**Na_2O**	**K_2O**	**P_2O_5**	**F**	**Total**
verre 8	48,86	3,92	11,80	16,55	3,71	9,23	1,32	0,68	1,65	1,55	99,27
verre 1	48,72	3,99	11,92	16,27	3,67	9,17	1,26	0,68	1,61	1,34	98,64
verre 2	48,85	3,99	11,88	16,29	3,82	9,24	1,28	0,65	1,73	1,69	99,42
verre 3	48,58	4,27	11,95	16,73	3,79	9,23	1,28	0,67	1,64	1,62	99,76
verre 4	48,76	4,11	11,86	15,88	3,72	9,24	1,22	0,66	1,69	1,67	98,81
verre 5	48,75	3,79	11,79	16,37	3,70	9,28	1,18	0,67	1,71	1,36	98,60
verre 6	48,79	4,01	11,73	16,49	3,67	9,17	1,24	0,70	1,58	1,62	98,99
verre 7	48,82	4,08	11,72	16,28	3,41	9,55	1,21	0,68	1,66	1,54	98,94
verre 8	48,80	4,22	11,64	16,65	3,40	9,33	1,19	0,70	1,62	0,00	97,55
verre 9	48,83	3,91	11,83	16,29	3,91	9,28	1,31	0,61	1,68	1,87	99,52
verre 10	48,69	3,88	11,90	15,49	4,00	9,35	1,26	0,64	1,73	1,82	98,74
Moyenne	**48,77**	**4,02**	**11,82**	**16,30**	**3,71**	**9,28**	**1,25**	**0,67**	**1,66**	**1,46**	**98,93**
écart-type	**0,08**	**0,15**	**0,10**	**0,35**	**0,18**	**0,11**	**0,05**	**0,03**	**0,05**	**0,51**	

Annexe 2.6 : expérience McGill 12 – 1100°C et 500 MPa – composition SC4-b avec 5% P_2O_5 + F

McGill 12	%pds oxydes										
échantillon	**SiO_2**	**TiO_2**	**Al_2O_3**	**FeO**	**MgO**	**CaO**	**Na_2O**	**K_2O**	**P_2O_5**	**F**	**Total**
verre 92	47,96	4,27	11,55	15,49	4,64	9,29	1,85	0,38	2,52	1,02	98,97
verre 93	47,86	4,27	11,34	15,37	4,58	9,39	1,84	0,38	2,45	1,06	98,53
verre 94	47,91	4,26	11,48	14,80	4,65	9,40	1,81	0,38	2,45	1,11	98,27
verre 95	48,27	4,25	11,25	15,20	4,61	9,44	1,84	0,38	2,45	1,01	98,70
verre 96	48,09	4,24	11,44	15,35	4,58	9,43	1,84	0,37	2,55	1,08	98,96
verre 97	48,13	4,27	11,44	15,08	4,63	9,39	1,78	0,38	2,56	1,10	98,77
verre 98	48,16	4,27	11,57	15,57	4,69	9,44	1,82	0,36	2,41	0,91	99,21
verre 99	48,00	4,21	11,46	15,32	4,64	9,39	1,81	0,40	2,50	0,98	98,70
verre 100	48,16	4,27	11,56	15,48	4,63	9,37	1,82	0,36	2,45	1,01	99,11
verre 101	48,23	4,24	11,33	14,83	4,63	9,41	1,82	0,37	2,50	0,99	98,34
moyenne	**48,08**	**4,25**	**11,44**	**15,25**	**4,63**	**9,40**	**1,82**	**0,38**	**2,48**	**1,03**	**98,75**
écart-type	**0,14**	**0,02**	**0,11**	**0,27**	**0,03**	**0,04**	**0,02**	**0,01**	**0,05**	**0,06**	

Annexe 2.7 : expérience McGill 13 – 1100°C et 500 MPa – composition SC4-b avec 5% P_2O_5

McGill 13	%pds oxydes										
échantillon	**SiO_2**	**TiO_2**	**Al_2O_3**	**FeO**	**MgO**	**CaO**	**Na_2O**	**K_2O**	**P_2O_5**	**F**	**Total**
verre 72	53,11	4,43	12,76	7,22	4,89	10,11	3,08	0,42	2,60	0,09	98,71
verre 73	53,25	4,47	12,78	7,62	4,96	10,24	3,10	0,41	2,49	0,04	99,37
verre 74	52,96	4,39	12,72	7,54	5,04	10,24	3,00	0,43	2,48	1,32	100,12
verre 75	53,01	4,54	12,73	7,26	4,89	10,12	3,07	0,42	2,50	0,09	98,64
verre 76	53,30	4,38	12,82	7,72	4,94	10,15	3,06	0,40	2,66	0,09	99,50
verre 77	52,54	4,47	12,42	7,78	4,89	10,20	3,04	0,43	2,60	0,02	98,39
verre 78	52,44	4,45	12,62	7,58	4,94	10,22	3,07	0,41	2,50	0,26	98,48
verre 79	52,98	4,61	12,76	7,66	5,07	10,18	3,05	0,44	2,50	0,00	99,24
verre 80	52,65	4,46	12,76	7,66	4,88	10,15	3,06	0,43	2,66	0,00	98,71
verre 81	52,80	4,40	12,63	7,77	4,79	10,31	3,04	0,43	2,54	0,02	98,72
moyenne	**52,90**	**4,46**	**12,70**	**7,58**	**4,93**	**10,19**	**3,06**	**0,42**	**2,55**	**0,19**	**98,99**
écart-type	**0,29**	**0,07**	**0,12**	**0,20**	**0,08**	**0,06**	**0,03**	**0,01**	**0,07**	**0,40**	

Annexe 2.8 : expérience McGill 1 – 1000°C et 500 MPa – composition Dy-Spt avec 5% P_2O_5 + F

McGill 1	%pds oxydes										
échantillon	**SiO_2**	**TiO_2**	**Al_2O_3**	**FeO**	**MgO**	**CaO**	**Na_2O**	**K_2O**	**P_2O_5**	**F**	**Total**
verre 39	73,78	0,41	12,66	2,40	0,15	1,48	0,76	2,98	0,25	1,79	96,68
verre 41	67,06	0,26	18,87	1,27	0,11	6,19	3,19	2,43	0,07	0,98	100,43
moyenne	**70,42**	**0,34**	**15,77**	**1,84**	**0,13**	**3,83**	**1,97**	**2,70**	**0,16**	**1,39**	**98,55**
écart-type	**4,75**	**0,11**	**4,39**	**0,80**	**0,03**	**3,33**	**1,72**	**0,39**	**0,13**	**0,57**	

Annexe 2.9 : expérience McGill 4 – 1050°C et 500 MPa – composition Dy-Spt avec 5% P_2O_5

McGill 4	%pds oxydes										
échantillon	**SiO_2**	**TiO_2**	**Al_2O_3**	**FeO**	**MgO**	**CaO**	**Na_2O**	**K_2O**	**P_2O_5**	**F**	**Total**
verre 21	51,62	4,53	12,29	9,07	5,01	8,92	1,32	0,30	2,49	0,00	95,54
verre 22	51,44	4,30	12,06	9,27	5,00	8,94	1,27	0,30	2,50	0,07	95,15
verre 23	50,35	4,26	12,00	9,61	4,98	9,00	1,37	0,30	2,49	0,03	94,40
verre 24	49,96	4,35	12,85	9,83	4,84	9,00	1,40	0,29	2,55	0,00	95,07
verre 25	50,74	4,43	12,08	9,37	4,90	9,12	1,42	0,30	2,58	0,00	94,92
verre 76	51,69	4,26	12,35	9,12	4,97	8,66	1,30	0,32	2,29	0,00	94,96
verre 77	51,79	4,29	12,34	8,88	4,94	8,68	1,25	0,30	2,29	0,00	94,76
verre 78	51,91	4,33	12,24	9,01	4,99	8,68	1,26	0,31	2,31	0,06	95,10
verre 79	51,39	4,20	11,96	9,18	4,88	8,50	1,33	0,31	2,22	0,01	93,98
verre 80	52,43	4,13	12,48	8,91	4,97	8,45	1,24	0,31	2,14	0,02	95,09
verre 81	52,86	4,15	12,50	8,52	4,78	8,27	1,18	0,32	1,94	0,00	94,50
verre 82	53,16	4,26	12,71	8,19	4,91	8,21	1,17	0,31	1,98	0,06	94,97
verre 83	51,71	4,60	13,02	8,35	5,26	8,44	1,32	0,31	2,23	0,09	95,34
verre 84	50,90	4,96	12,79	8,35	5,39	8,64	1,29	0,28	2,53	0,00	95,11
verre 85	51,06	4,91	12,49	8,42	5,35	8,68	1,33	0,30	2,49	0,00	95,01
moyenne	**51,53**	**4,40**	**12,41**	**8,94**	**5,01**	**8,68**	**1,30**	**0,30**	**2,34**	**0,02**	**94,93**
écart-type	**0,87**	**0,25**	**0,32**	**0,49**	**0,18**	**0,27**	**0,07**	**0,01**	**0,21**	**0,03**	

Annexe 2.10 : expérience McGill 7 – 1000°C et 500 MPa – composition Dy-Spt avec 5% P_2O_5

McGill 7	%pds oxydes										
échantillon	**SiO_2**	**TiO_2**	**Al_2O_3**	**FeO**	**MgO**	**CaO**	**Na_2O**	**K_2O**	**P_2O_5**	**F**	**Total**
verre 29	55,28	0,90	19,08	9,70	1,46	5,12	2,22	1,82	1,30	0,00	96,87
verre 30	55,27	0,95	18,89	10,02	1,46	5,15	2,39	1,81	1,34	0,00	97,27
verre 31	55,48	0,93	19,15	9,72	1,45	5,08	2,35	1,80	1,29	0,04	97,29
verre 32	55,47	0,91	18,60	9,85	1,45	5,07	2,28	1,84	1,26	0,04	96,77
verre 33	55,76	0,92	18,86	9,74	1,49	5,02	2,21	1,84	1,28	0,00	97,12
verre 34	55,50	0,92	19,09	9,66	1,49	5,01	2,44	1,83	1,30	0,00	97,24
verre 35	55,47	0,92	18,97	9,67	1,44	4,97	2,35	1,87	1,29	0,00	96,95
verre 36	56,28	0,90	18,97	9,13	1,40	4,82	2,33	1,93	1,19	0,00	96,95
verre 37	57,01	0,90	19,00	8,67	1,40	4,72	2,29	1,95	1,18	0,00	97,11
verre 38	57,26	0,89	19,02	8,69	1,35	4,61	2,40	1,97	1,13	0,02	97,33
moyenne	**55,88**	**0,91**	**18,96**	**9,49**	**1,44**	**4,96**	**2,33**	**1,87**	**1,25**	**0,01**	**97,09**
écart-type	**0,72**	**0,02**	**0,16**	**0,48**	**0,04**	**0,18**	**0,08**	**0,06**	**0,07**	**0,02**	

Annexe 2.11 : expérience McGill 8 – 1015°C et 500 MPa – composition Dy-Spt avec 5% P_2O_5

McGill 8	%pds oxydes										
échantillon	**SiO_2**	**TiO_2**	**Al_2O_3**	**FeO**	**MgO**	**CaO**	**Na_2O**	**K_2O**	**P_2O_5**	**F**	**Total**
verre 6	71,36	2,64	11,48	6,04	0,51	0,97	1,39	3,38	0,19	0,10	98,05
verre 7	74,31	0,93	12,48	4,00	0,36	0,69	0,95	2,53	0,25	0,00	96,49
verre 8	73,09	0,80	14,43	3,95	0,32	1,04	2,06	2,60	0,15	0,00	98,43
verre 9	75,36	1,14	11,89	3,88	0,40	0,83	0,65	1,97	0,14	0,01	96,27
verre 10	73,60	1,24	11,49	5,06	0,60	1,32	0,74	2,40	0,17	0,00	96,61
moyenne	**73,54**	**1,35**	**12,35**	**4,58**	**0,44**	**0,97**	**1,16**	**2,57**	**0,18**	**0,02**	**97,17**
écart-type	**1,49**	**0,74**	**1,23**	**0,95**	**0,12**	**0,24**	**0,58**	**0,51**	**0,04**	**0,04**	

Annexe 2.12 : expérience McGill 9 – 1040°C et 500 MPa – composition Dy-Spt avec 5% P_2O_5

McGill 9	%pds oxydes										
échantillon	**SiO_2**	**TiO_2**	**Al_2O_3**	**FeO**	**MgO**	**CaO**	**Na_2O**	**K_2O**	**P_2O_5**	**F**	**Total**
verre 1	54,46	4,28	16,71	0,02	6,23	7,81	6,58	0,67	2,18	0,07	99,01
verre 2	54,42	4,33	16,69	0,05	6,17	7,79	6,47	0,67	2,19	0,00	98,78
verre 3	54,23	4,35	16,40	0,01	6,02	7,77	6,58	0,67	2,13	0,00	98,16
verre 4	54,28	4,19	16,58	0,00	6,09	7,75	6,58	0,66	2,17	0,00	98,33
verre 5	54,50	4,39	16,54	0,03	6,09	7,61	6,48	0,68	2,21	0,07	98,60
verre 6	54,75	4,46	16,52	0,00	5,93	7,65	6,47	0,64	2,14	0,00	98,55
verre 7	54,52	4,39	16,82	0,04	5,97	7,59	6,53	0,67	2,22	0,00	98,76
verre 8	53,81	4,48	16,55	0,05	6,15	7,77	6,56	0,65	2,20	0,00	98,21
verre 9	54,62	4,40	16,68	0,02	5,96	7,59	6,43	0,65	2,25	0,00	98,59
verre 10	54,37	4,37	16,80	0,00	5,92	7,56	6,45	0,66	2,08	0,00	98,22
moyenne	**54,40**	**4,36**	**16,63**	**0,02**	**6,05**	**7,69**	**6,51**	**0,66**	**2,17**	**0,01**	**98,52**
écart-type	**0,26**	**0,08**	**0,13**	**0,02**	**0,11**	**0,10**	**0,06**	**0,01**	**0,05**	**0,03**	

Annexe 2.13 : expérience McGill 10 – 1015°C et 500 MPa – composition Dy-Spt avec 5% P_2O_5 + F

McGill 10	%pds oxydes										
échantillon	**SiO_2**	**TiO_2**	**Al_2O_3**	**FeO**	**MgO**	**CaO**	**Na_2O**	**K_2O**	**P_2O_5**	**F**	**Total**
verre 1	70,93	0,65	14,23	3,53	0,74	2,67	1,04	3,73	0,17	2,63	100,31
verre 2	70,55	0,63	14,21	3,50	0,82	2,58	1,28	4,02	0,30	2,67	100,56
verre 3	69,43	0,58	14,16	3,69	0,84	2,75	1,30	4,09	0,23	1,87	98,93
verre 4	69,93	0,66	14,10	3,76	0,74	2,91	1,24	3,93	0,16	2,60	100,02
verre 5	68,02	0,69	14,88	3,72	0,75	3,28	1,47	3,94	0,14	2,56	99,44
verre 6	69,07	0,64	14,03	3,60	0,74	2,89	1,30	4,03	0,15	2,23	98,67
verre 7	69,62	0,64	13,54	3,47	0,80	2,81	1,30	3,94	0,26	2,28	98,65
moyenne	**69,65**	**0,64**	**14,16**	**3,61**	**0,78**	**2,84**	**1,27**	**3,95**	**0,20**	**2,40**	**99,51**
écart-type	**0,96**	**0,03**	**0,39**	**0,12**	**0,04**	**0,23**	**0,13**	**0,12**	**0,06**	**0,29**	

Annexe 2.14 : expérience McGill 11 – 1040°C et 500 MPa – composition Dy-Spt avec 5% P_2O_5 + F

McGill 11	%pds oxydes										
échantillon	**SiO_2**	**TiO_2**	**Al_2O_3**	**FeO**	**MgO**	**CaO**	**Na_2O**	**K_2O**	**P_2O_5**	**F**	**Total**
verre 21	45,33	3,44	14,96	13,63	4,66	8,20	2,26	1,10	2,26	1,32	97,15
verre 22	45,67	3,49	15,00	13,69	4,66	8,19	2,23	1,08	2,27	1,16	97,43
verre 23	45,90	3,62	14,94	14,01	4,69	8,25	2,30	1,13	2,30	1,28	98,40
verre 24	46,09	3,59	15,03	13,76	4,59	8,28	2,23	1,09	2,23	1,05	97,95
verre 25	46,13	3,66	14,83	14,09	4,73	8,21	2,28	1,12	2,27	1,39	98,72
verre 26	46,19	3,40	15,20	13,66	4,60	8,23	2,30	1,08	2,05	1,32	98,02
verre 27	46,04	3,53	15,25	13,86	4,71	8,28	2,25	1,13	2,07	1,22	98,33
verre 28	46,28	3,39	14,98	14,06	4,64	8,32	2,22	1,09	2,00	1,22	98,20
verre 29	46,44	3,37	15,05	14,01	4,61	8,37	2,28	1,12	1,97	1,40	98,60
verre 30	46,37	3,43	15,05	14,14	4,60	8,22	2,27	1,11	1,95	1,38	98,52
moyenne	**46,04**	**3,49**	**15,03**	**13,89**	**4,65**	**8,26**	**2,26**	**1,10**	**2,14**	**1,27**	**98,13**
écart-type	**0,34**	**0,10**	**0,12**	**0,20**	**0,05**	**0,06**	**0,03**	**0,02**	**0,14**	**0,11**	

Annexe 2.15 : expérience McGill 12 – 1100°C et 500 MPa – composition Dy-Spt avec 5% P_2O_5 + F

McGill 12	%pds oxydes										
échantillon	**SiO_2**	**TiO_2**	**Al_2O_3**	**FeO**	**MgO**	**CaO**	**Na_2O**	**K_2O**	**P_2O_5**	**F**	**Total**
verre 82	46,39	3,97	14,05	14,71	5,46	8,15	1,89	1,04	2,19	1,09	98,93
verre 83	46,47	3,81	14,04	14,67	5,41	8,13	1,85	1,06	2,20	0,92	98,56
verre 84	46,47	3,84	14,16	14,93	5,39	7,95	1,86	1,09	2,26	1,09	99,04
verre 85	46,65	4,02	13,99	14,64	5,47	8,15	1,86	1,06	2,15	1,08	99,06
verre 86	46,07	3,93	14,03	14,71	5,39	8,04	1,78	1,07	2,13	0,87	98,01
verre 87	46,35	3,99	13,97	14,74	5,51	8,12	1,87	1,08	2,23	0,87	98,72
verre 88	46,17	3,90	13,90	14,69	5,48	8,05	1,84	1,09	2,18	0,91	98,21
verre 89	46,28	3,91	14,16	14,83	5,36	8,01	1,86	1,05	2,24	0,90	98,60
verre 90	46,33	3,93	14,13	14,81	5,45	7,99	1,88	1,05	2,15	0,95	98,67
verre 91	46,36	3,90	14,03	14,60	5,38	8,09	1,81	1,08	2,11	0,88	98,23
moyenne	**46,35**	**3,92**	**14,05**	**14,73**	**5,43**	**8,07**	**1,85**	**1,07**	**2,18**	**0,96**	**98,60**
écart-type	**0,16**	**0,06**	**0,09**	**0,10**	**0,05**	**0,07**	**0,03**	**0,02**	**0,05**	**0,09**	

Annexe 2.16 : expérience McGill 13 – 1100°C et 500 MPa – composition Dy-Spt avec 5% P_2O_5

McGill 13	%pds oxydes										
échantillon	**SiO_2**	**TiO_2**	**Al_2O_3**	**FeO**	**MgO**	**CaO**	**Na_2O**	**K_2O**	**P_2O_5**	**F**	**Total**
verre 62	52,41	4,42	16,18	3,41	6,45	9,37	3,62	1,12	2,33	0,21	99,51
verre 63	52,53	4,41	16,18	3,50	6,41	9,36	3,67	1,14	2,37	0,00	99,56
verre 64	51,68	4,38	15,98	3,52	6,24	9,47	3,53	1,14	2,38	0,02	98,33
verre 65	52,28	4,45	16,13	3,39	6,38	9,34	3,64	1,10	2,36	0,01	99,07
verre 66	52,42	4,37	16,04	3,39	6,35	9,32	3,54	1,12	2,32	0,00	98,88
verre 67	52,48	4,40	16,00	3,39	6,28	9,37	3,64	1,10	2,30	0,06	99,02
verre 68	52,28	4,45	16,04	3,37	6,28	9,45	3,55	1,10	2,37	0,22	99,10
verre 69	52,75	4,35	16,11	3,49	6,29	9,43	3,67	1,10	2,36	0,07	99,63
verre 70	52,36	4,44	15,96	3,47	6,37	9,45	3,57	1,12	2,41	0,00	99,15
verre 71	52,36	4,39	16,08	3,41	6,34	9,28	3,58	1,13	2,34	0,00	98,91
moyenne	**52,35**	**4,40**	**16,07**	**3,43**	**6,34**	**9,38**	**3,60**	**1,12**	**2,35**	**0,06**	**99,11**
écart-type	**0,27**	**0,03**	**0,08**	**0,05**	**0,07**	**0,06**	**0,05**	**0,02**	**0,03**	**0,09**	

Annexe 2.17 : expérience McGill 14 – 1050°C et 500 MPa – composition SC4-b avec 10% P_2O_5

McGill 14	%pds oxydes										
échantillon	**SiO_2**	**TiO_2**	**Al_2O_3**	**FeO**	**MgO**	**CaO**	**Na_2O**	**K_2O**	**P_2O_5**	**F**	**Total**
verre 38	46,23	4,19	10,66	15,47	4,37	8,68	2,31	0,35	6,17	0,00	98,43
verre 39	48,11	3,86	11,48	14,70	4,02	8,21	2,46	0,39	5,55	0,00	98,78
verre 40	43,99	4,22	10,53	15,68	4,54	9,31	2,50	0,29	7,30	0,10	98,45
verre 41	44,35	3,87	11,42	15,59	4,35	9,23	2,44	0,32	7,19	0,00	98,75
verre 42	45,86	3,67	11,74	14,71	4,34	8,87	2,71	0,33	6,62	0,04	98,89
verre 45	46,84	4,02	11,10	15,01	4,01	8,80	2,17	0,40	6,98	0,14	99,47
moyenne	**45,90**	**3,97**	**11,16**	**15,19**	**4,27**	**8,85**	**2,43**	**0,34**	**6,64**	**0,05**	**98,79**
écart-type	**1,55**	**0,21**	**0,48**	**0,44**	**0,21**	**0,40**	**0,18**	**0,04**	**0,67**	**0,06**	

Annexe 2.18 : expérience McGill 14F – 1050°C et 500 MPa – composition SC4-b avec 10% P_2O_5 + F

McGill 14F	%pds oxydes										
échantillon	**SiO_2**	**TiO_2**	**Al_2O_3**	**FeO**	**MgO**	**CaO**	**Na_2O**	**K_2O**	**P_2O_5**	**F**	**Total**
verre 52	42,83	4,15	11,20	16,09	4,68	9,67	1,39	0,33	7,66	0,13	98,12
verre 54	42,80	4,29	11,10	16,27	4,69	9,64	1,45	0,36	7,87	0,13	98,59
verre 55	41,52	4,27	10,78	16,54	4,96	9,91	1,38	0,34	8,26	0,08	98,03
verre 56	40,62	4,44	10,45	17,14	5,01	10,13	1,35	0,28	8,81	0,05	98,27
verre 57	40,77	4,32	10,55	16,58	4,91	9,98	1,33	0,30	8,47	0,21	97,43
verre 58	42,77	4,11	10,96	15,59	4,65	9,64	1,47	0,37	7,92	0,24	97,70
verre 59	44,08	4,13	11,18	15,93	4,60	9,48	1,51	0,38	7,35	0,07	98,70
verre 60	40,99	4,35	10,61	16,97	5,07	10,06	1,38	0,28	8,48	0,13	98,32
verre 61	39,54	4,45	10,27	17,38	5,26	10,37	1,27	0,27	9,25	0,12	98,18
moyenne	**41,77**	**4,28**	**10,79**	**16,50**	**4,87**	**9,87**	**1,39**	**0,32**	**8,23**	**0,13**	**98,15**
écart-type	**1,43**	**0,13**	**0,34**	**0,59**	**0,23**	**0,29**	**0,08**	**0,04**	**0,59**	**0,06**	

Annexe 2.19 : expérience McGill 15F – 1075°C et 500 MPa – composition SC4-b avec 10% P_2O_5 + F

McGill 15F	%pds oxydes										
échantillon	**SiO_2**	**TiO_2**	**Al_2O_3**	**FeO**	**MgO**	**CaO**	**Na_2O**	**K_2O**	**P_2O_5**	**F**	**Total**
verre 21	52,08	0,89	15,64	12,00	1,57	7,44	2,09	0,47	6,93	0,01	99,11
verre 26	51,38	3,37	15,16	12,51	1,64	7,30	2,09	0,50	5,69	0,00	99,64
verre 28	51,93	1,67	15,33	11,86	1,91	8,01	1,86	0,43	5,99	0,00	98,98
verre 29	51,16	4,77	14,08	12,72	1,60	7,36	1,97	0,47	5,25	0,00	99,37
verre 30	50,73	1,32	17,04	14,34	3,19	5,97	1,64	0,44	4,13	0,00	98,78
moyenne	**51,45**	**2,41**	**15,45**	**12,68**	**1,98**	**7,21**	**1,93**	**0,46**	**5,60**	**0,00**	**99,18**
écart-type	**0,56**	**1,62**	**1,07**	**0,99**	**0,69**	**0,75**	**0,19**	**0,03**	**1,03**	**0,00**	

Annexe 2.20 : expérience McGill 16F – 1100°C et 500 MPa – composition SC4-b avec 10% P_2O_5

McGill 16	%pds oxydes										
échantillon	**SiO_2**	**TiO_2**	**Al_2O_3**	**FeO**	**MgO**	**CaO**	**Na_2O**	**K_2O**	**P_2O_5**	**F**	**Total**
verre 11	46,36	4,33	11,51	4,64	8,65	14,73	1,68	0,47	6,69	0,04	99,10
verre 12	46,44	4,27	11,60	4,63	8,64	14,91	1,73	0,48	6,62	0,19	99,50
verre 13	46,64	4,34	11,42	4,57	8,65	14,32	1,67	0,46	6,65	0,20	98,91
verre 15	46,40	4,13	11,63	4,56	8,66	14,31	1,70	0,46	6,56	0,07	98,48
verre 17	46,55	4,30	11,87	4,57	8,54	14,29	1,75	0,49	6,32	0,00	98,68
verre 18	45,62	4,39	12,05	4,74	8,81	14,59	1,70	0,46	6,57	0,21	99,12
verre 19	44,58	4,43	12,16	4,80	8,90	14,93	1,63	0,43	6,91	0,01	98,77
verre 20	44,12	4,48	12,12	4,83	9,06	14,99	1,65	0,41	6,94	0,17	98,76
moyenne	**45,84**	**4,33**	**11,80**	**4,67**	**8,74**	**14,63**	**1,69**	**0,45**	**6,66**	**0,11**	**98,91**
écart-type	**0,98**	**0,11**	**0,29**	**0,11**	**0,17**	**0,30**	**0,04**	**0,03**	**0,20**	**0,09**	

Annexe 2.21 : expérience McGill 16 – 1100°C et 500 MPa – composition SC4-b avec 10% P_2O_5

McGill 16F	%pds oxydes										
échantillon	**SiO_2**	**TiO_2**	**Al_2O_3**	**FeO**	**MgO**	**CaO**	**Na_2O**	**K_2O**	**P_2O_5**	**F**	**Total**
verre 1	46,45	4,15	11,25	14,35	4,57	8,88	2,49	0,37	6,91	0,17	99,59
verre 2	46,45	4,12	11,33	14,30	4,44	8,89	2,49	0,36	6,62	0,33	99,33
verre 3	46,48	4,22	11,10	14,18	4,57	8,97	2,52	0,36	6,88	0,00	99,27
verre 4	46,69	4,22	11,19	14,01	4,47	8,94	2,47	0,36	6,82	0,00	99,16
verre 5	46,69	4,26	11,28	14,23	4,54	8,99	2,03	0,34	6,84	0,01	99,21
verre 6	46,77	4,12	11,02	14,17	4,53	8,92	2,48	0,36	6,74	0,13	99,25
verre 7	46,72	4,22	11,32	14,13	4,59	8,91	2,54	0,36	6,70	0,19	99,66
verre 9	46,83	4,15	11,31	14,18	4,59	8,96	2,49	0,36	6,78	0,05	99,68
verre 10	46,75	4,09	11,04	14,05	4,50	9,00	2,49	0,35	6,91	0,07	99,24
moyenne	**46,65**	**4,17**	**11,20**	**14,18**	**4,53**	**8,94**	**2,44**	**0,36**	**6,80**	**0,11**	**99,38**
écart-type	**0,15**	**0,06**	**0,12**	**0,11**	**0,05**	**0,04**	**0,16**	**0,01**	**0,10**	**0,11**	